

# Performance Analysis of Free Space Optical Communication Channel with Transmit and Receive Diversity

Thesis submitted

by

**AKINCHAN DAS**

University Registration No.: 1011707006 of 2017

Doctor of Philosophy (Engineering)

Department of Electronics and Telecommunication Engineering

Faculty Council of Engineering and Technology

Jadavpur University

Kolkata, India

Year 2023

JADAVPUR UNIVERSITY  
KOLKATA - 700 032, INDIA

INDEX NO. 196/17/E

Title of the Thesis:

**Performance Analysis of Free Space Optical Communication Channel with Transmit and Receive Diversity**

Name, Designation and Institution of the Supervisors:

**1. Dr. Chayanika Bose**

Ex-Professor

Department of ETCE, Jadavpur University

188, Raja S C Mallik Road, Jadavpur, Kolkata-700032

**2. Dr. Aniruddha Chandra**

Associate Professor

Department of ECE, NIT Durgapur

M. G. Road, A-Zone, Durgapur, West Bengal, 713209

## List of Publications

### International Journals:

1. **A. Das**, B. Bag, C. Bose and A. Chandra “Performance analysis of FSO links employing a transmit and receive diversity-based operating system under Málaga turbulence channels with pointing errors”, *Optics Continuum*, 1(2), 366–387, Feb. 2022 [\[link\]](#)
2. **A. Das**, B. Bag, C. Bose and A. Chandra “Free space optical links over Málaga turbulence channels with transmit and receive diversity”, *Optics Communications*, 456, 124591, Feb. 2020 [\[link\]](#)
3. **A. Das**, B. Bag, C. Bose and A. Chandra “Performance analysis of MIMO FSO link with Alamouti coding and switch-and-examine combining” *Photonic Network Communications*, 36(3), 350-360, Aug. 2018 [\[link\]](#)
4. B. Bag, **A. Das**, C. Bose and A. Chandra (2020) “Improving the performance of a DF relay-aided FSO system with an additional source-relay mmWave RF backup” *IEEE/OSA Journal of Optical Communications and Networking*, 12(12), 390–402, Dec. 2020 [\[link\]](#)
5. B. Bag, **A. Das**, I. S. Ansari, A. Prokeš, C. Bose and A. Chandra “Performance Analysis of hybrid FSO systems using FSO/RF-FSO link adaptation” *IEEE Photonics Journal*, 10(3), 1–17, Jun. 2018 [\[link\]](#)
6. B. Bag, **A. Das**, A. Chandra and C. Bose “Capacity analysis for Rayleigh / Gamma-Gamma mixed RF/FSO link with fixed-gain AF relay” *IEICE Transactions on Communications*, E100-B(10), 1747–1757, Apr. 2017 [\[link\]](#)

### Book Chapters:

1. B. Bag, **A. Das**, A. Chandra and R. Róka ”Performance Analysis of FSO Links in Turbulent Atmosphere”, *Design, Implementation, and Analysis of Next Generation Optical Networks: Emerging Research and Opportunities*, IGI Global, Ch-4, 100–156, ISBN: 9781522597674, Jul. 2019 [\[link\]](#)

---

## List of Presentations in National/ International/ Conference / Workshops:

1. **A. Das**, B. Bag, C. Bose and A. Chandra “ABER of an FSO Link in Gamma-Gamma Turbulence with SSK and SEC”, Proc. *2021 IEEE 93rd Vehicular Technology Conference (VTC2021-Spring)*, Helsinki, Finland, Apr. 2021, 1–5 [\[link\]](#)
2. **A. Das**, B. Bag and A. Chandra “BER of MIMO FSO link with Alamouti coding and SEC”, Proc. *IEEE International Conference on Wireless Communications, Signal Processing and Networking (WiSPNET)*, Chennai, India, Mar. 2017, 1823–1827 [\[link\]](#)
3. **A. Das**, B. Bag and A. Chandra “Performance analysis of fixed gain AF relay assisted mixed RF-FSO links”, Proc. *2<sup>nd</sup> International Conference on Opto-Electronics and Applied Optics 2015 (IEEE OPTRONIX-2015)*, University of British Columbia; Canada, Oct. 2015, 1–4 [\[link\]](#)
4. **A. Das**, B. Bag and A. Chandra “End-to-end performance analysis of relayed FSO transmissions over Gamma-Gamma fading channels using STBC”, Proc. *International Conference on Opto-Electronics and Applied Optics, IEM OPTRONIX*, Kolkata, India, Dec. 2014, 1–5, [\[link\]](#)
5. B. Bag, **A. Das**, C. Bose and A. Chandra, “Link quality of a RF-assisted relayed FSO system under turbulence, pointing error and fading”, Proc. *IEEE 4<sup>th</sup> International Conference on Computer, Electrical & Communication Engineering (ICCECE)*, Techno India University, India, Jan. 2020, 1–6 [\[link\]](#)
6. B. Bag, **A. Das**, C. Bose and A. Chandra, “Hybrid FSO/RF-FSO systems over generalized Málaga distributed channels with pointing errors”, Proc. *IEEE 27<sup>th</sup> European Signal Processing Conference (EUSIPCO)*, Coruña, Spain, Sep. 2019, 1–5 [\[link\]](#)
7. B. Bag, **A. Das** and A. Chandra, “Capacity analysis for Rayleigh/Gamma-Gamma mixed RF/FSO relayed transmission”, Proc. *IEEE International Conference on Wireless Communications, Signal Processing and Networking (WiSPNET)*, Chennai, India, Mar. 2017, 1828–1832 [\[link\]](#)
8. B. Bag, **A. Das** and A. Chandra, “Performance Analysis of dual-hop AF relaying FSO System using Alamouti scheme over G-G fading channel”, Proc. *12<sup>th</sup> International Conference on Fiber Optics and Photonics, Optical Society of America*, IIT Kharagpur, India, Dec. 2014, 1–5 [\[link\]](#)

---

# PROFORMA - 1

## “Statement of Originality”

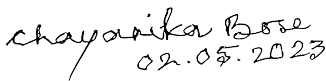
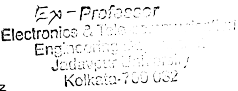


I Akinchan Das registered on 11<sup>th</sup> Aug, 2017 do hereby declare that this thesis entitled “Performance Analysis of Free Space Optical Communication Channel with Transmit and Receive Diversity” contains literature survey and original research work done by the undersigned candidate as part of Doctoral studies.

All information in this thesis have been obtained and presented in accordance with existing academic rules and ethical conduct. I declare that, as required by these rules and conduct, I have fully cited and referred all materials and results that are not original to this work.

I also declare that I have checked this thesis as per the “Policy on Anti Plagiarism, Jadavpur University, 2023”, and the level of similarity as checked by iThenticate software is 0%.

Signature of Candidate:   
Date : 02.05.2023

Certified by Supervisor(s):  
(Signature with date, seal)

-   
02.05.2023  

-   
02/05/23  


---

## PROFORMA - 2

### CERTIFICATE FROM THE SUPERVISORS

This is to certify that the thesis entitled “**Performance Analysis of Free Space Optical Communication Channel with Transmit and Receive Diversity**” submitted by Akinchan Das, who got his name registered on 11<sup>th</sup> August, 2017 for the award of Ph.D.(Engg.) degree of Jadavpur University is absolutely based upon his own work under the supervision of Dr. Chayanika Bose and Dr. Aniruddha Chandra and that neither her/his thesis nor any part of the thesis has been submitted for any degree/ diploma or any other academic award anywhere before.

1. Dr. Chayanika Bose  
Ex-Professor  
Department of ETCE, Jadavpur University

*chayanika Bose*  
02.05.2023

Ex-Professor  
Electronics & Telecommunication Engg.  
Department of ETCE,  
Jadavpur University,  
Kolkata-700 032

---

Signature of the Supervisor and date with Office Seal

2. Dr. Aniruddha Chandra  
Associate Professor  
Department of ECE, NIT Durgapur

*Aniruddha Chandra*  
02/05/22

Dr. ANIRUDDHA CHANDRA  
Associate Professor  
Department of Electronics & Communication Engg.  
National Institute of Technology  
Durgapur-713209, India

---

Signature of the Supervisor and date with Office Seal

---

## ACKNOWLEDGEMENTS

I am deeply obliged to many good-wishers who have contributed to smoothly completing this thesis. First of all, I would like to express my sincere gratitude to my thesis supervisors **Dr. Chayanika Bose** *Ex-Professor in the Department of Electronics and Telecommunication Engineering at Jadavpur University, Kolkata.* and **Dr. Aniruddha Chandra** *Associate Professor in the Department of Electronics and Communication Engineering at National Institute of Technology, Durgapur.* I am thankful for their guidance, caring, and grooming toward completing my Ph.D. work. So I would like to thank them for their support, valuable suggestions, and continuous mentoring during this journey.

I would also like to thank my co-author, Dr. Banibrata Bag, for his valuable assistance in my various research work. I also want to express my heartiest thank to Dr. Imran Shafique Ansari, Lecturer at the school of engineering at the University of Glasgow, United Kingdom, for his helpful suggestions in my research work.

I also acknowledge all the faculty members of the Department of Electronics and Communication Engineering at Haldia Institute of Technology and all other well-wishers for their continuous encouragement and moral support to complete my Ph.D. work.

Finally, a special thanks go to my beloved wife, Moumita Jana, my daughter Ashmi Das and all my family members. Thank you all for supporting me with every step of this remarkable journey.

*Akinchan Das.*

AKINCHAN DAS

---

## ABSTRACT

Beyond fifth generation (B5G) cellular operators around the globe are considering free space optical (FSO) systems, owing to their high capacity feature, as an alternative to the fixed backhaul radio-frequency (RF) links. One of the major challenges for FSO is the line-of-sight (LOS) requirement, stemming from the fact that light signals are focused, and their propagation is highly directional. Even a minuscule drift of transmitter or receiver causes misalignment; resulting in a situation that is commonly known as *pointing error*. The other major challenge is the turbulence induced by random fluctuations of the medium. The scintillation changes the irradiance in a random fashion leading to *atmospheric turbulence*. The similarity of the turbulence effects with RF multipath fading inspired the FSO link designers to explore the already established fading mitigation techniques; the most popular of them is undoubtedly the receiver and /or transmitter diversity scheme. Utilizing either *transmitter diversity*, or *receiver diversity*, or *both* leads to different FSO communication system architectures: multiple-input-single-output (MISO) FSO, single-input-multiple-output (SIMO) FSO and multiple-input-multiple-output (MIMO) FSO.

The following stages have been accomplished in the proposed research work. At first, we have incorporated the transmitter diversity technique, namely the Alamouti *space-time-block-coding* (STBC) scheme, into a primary single-input-single-output (SISO) FSO link to construct a MISO FSO system. Next, a SIMO FSO link has been modeled by incorporating a *switch-and-examine-combining* (SEC) receiver diversity scheme into the SISO FSO link. Finally, we have integrated both transmitter and receiver diversity schemes in the single FSO link to build up an STBC-SEC MIMO FSO communication system and compare all measuring metrics with the rest of the other FSO communication systems. Besides, another MIMO FSO communication system has been designed using *space shift keying* (SSK) transmitter diversity scheme along with selection combining (SC) receiver diversity scheme and compared the resultant outcome with previously mentioned MIMO FSO systems. Generalized Málaga and gamma-gamma statistical distributions have been considered to analyze the turbulent channel, and the effect of pointing errors in the FSO communication system has also been considered during analytical derivations. In this thesis, we have provided the system outcome based on standard performance metrics of the communication system, such as *outage probability* (OP), *average bit error rate* (ABER), and *average capacity*. The analysis leads to a better understanding of how diversity can help in mitigating the two fundamental challenges, atmospheric turbulence and pointing error. The degree of improvement varies across topologies, and although, in general, a topology of higher complexity (i.e. higher number of transmitter or receiver chains) offers larger improvement, there exists no clear single winner. Rather, the degree of improvement has an uncorrelated nature across the metrics. Thus, before employing such diversity techniques, a detailed study of environmental and design factors are necessary to attain optimal results.



# Contents

<b>Acknowledgements</b>	<b>vi</b>
<b>Abstract</b>	<b>vii</b>
<b>Contents</b>	<b>viii</b>
<b>List of Figures</b>	<b>xii</b>
<b>List of Tables</b>	<b>xv</b>
<b>Abbreviations</b>	<b>xix</b>
<b>Symbols</b>	<b>xxi</b>
<b>1 Introduction</b>	<b>1</b>
1.1 History behind FSO communication . . . . .	1
1.2 Pros and Cons of FSO communication . . . . .	4
1.2.1 Advantages of FSO communication . . . . .	4
1.2.2 Limitations of FSO communication . . . . .	7
1.3 Applications of FSO communication . . . . .	10
1.3.1 Current scenarios . . . . .	11
1.4 Motivation of research . . . . .	11
1.5 Literature review with prior work . . . . .	12
1.6 Thesis objective . . . . .	14
1.7 Thesis layout . . . . .	15
<b>2 FSO Communication System Design and Channel Characterization</b>	<b>17</b>
2.1 Introduction . . . . .	17
2.2 Organization . . . . .	18
2.3 An FSO system design . . . . .	18
2.4 Some fundamental parameters associated with FSO link design . . . . .	21
2.4.1 Geometrical loss . . . . .	21
2.4.2 Aperture averaging . . . . .	22
2.4.3 Scattering and absorption . . . . .	23

2.4.4	Refractive index and scintillation . . . . .	24
2.4.5	Pointing error . . . . .	26
2.5	Statistical channel models for FSO link . . . . .	29
2.5.1	Moderate-to-strong AT in absence of pointing error . . . . .	30
2.5.1.1	PDF under gamma-gamma distribution . . . . .	30
2.5.1.2	CDF under gamma-gamma distribution . . . . .	32
2.5.1.3	MGF under gamma-gamma distribution . . . . .	32
2.5.2	Generalised AT in absence of pointing error . . . . .	33
2.5.2.1	PDF under Málaga distribution . . . . .	33
2.5.2.2	CDF under Málaga distribution . . . . .	34
2.5.2.3	MGF under Málaga distribution . . . . .	35
2.5.3	Moderate-to-strong AT in presence of pointing error . . . . .	35
2.5.3.1	PDF under gamma-gamma distribution . . . . .	36
2.5.3.2	CDF under gamma-gamma distribution . . . . .	37
2.5.3.3	MGF under gamma-gamma distribution . . . . .	38
2.5.4	Generalised AT in presence of pointing error . . . . .	38
2.5.4.1	PDF under Málaga distribution . . . . .	38
2.5.4.2	CDF under Málaga distribution . . . . .	39
2.5.4.3	MGF under Málaga distribution . . . . .	40
2.6	Diversity model . . . . .	40
2.6.1	Transmit diversity . . . . .	40
2.6.1.1	Alamouti space time block code . . . . .	41
2.6.1.2	Spatial shift keying . . . . .	43
2.6.2	Receive diversity . . . . .	44
2.6.2.1	Switch-and-examine combining . . . . .	45
2.6.2.2	Selection combining . . . . .	47
2.7	Performance metrics . . . . .	48
2.7.1	Outage probability . . . . .	48
2.7.2	Average bit error rate . . . . .	49
2.7.3	Average capacity . . . . .	49
2.8	Numerical results and discussion for SISO FSO link . . . . .	50
2.9	Chapter summary . . . . .	66
<b>3</b>	<b>Performance Analysis of FSO Communication Channel with Alamouti Transmit Diversity</b> . . . . .	<b>67</b>
3.1	Introduction . . . . .	68
3.2	Organization . . . . .	68
3.3	Performance analysis with Alamouti STBC . . . . .	68
3.3.1	Gamma-Gamma turbulence in absence of pointing error . . . . .	69
3.3.1.1	Outage probability . . . . .	70
3.3.1.2	Average bit error rate . . . . .	70
3.3.1.3	Average capacity . . . . .	71

3.3.2	Gamma-Gamma turbulence in presence of pointing error . . .	72
3.3.3	Málaga turbulence in absence of pointing error . . . . .	72
3.3.4	Málaga turbulence in presence of pointing error . . . . .	73
3.4	Numerical results and discussion for MISO FSO link . . . . .	74
3.5	Chapter summary . . . . .	88
<b>4</b>	<b>Performance Analysis of FSO Communication Channel with SEC Receive Diversity</b>	<b>89</b>
4.1	Introduction . . . . .	90
4.2	Organization . . . . .	90
4.3	Gamma-Gamma turbulence in absence of pointing error . . . . .	90
4.3.1	Outage probability . . . . .	91
4.3.2	Average bit error rate . . . . .	93
4.3.3	Average capacity . . . . .	94
4.4	Gamma-Gamma turbulence in presence of pointing error . . . . .	95
4.4.1	Outage probability . . . . .	95
4.4.2	Average bit error rate . . . . .	96
4.4.3	Average capacity . . . . .	97
4.5	Málaga turbulence in absence of pointing error . . . . .	98
4.5.1	Outage probability . . . . .	98
4.5.2	Average bit error rate . . . . .	99
4.5.3	Average capacity . . . . .	100
4.6	Málaga turbulence in presence of pointing error . . . . .	101
4.6.1	Outage probability . . . . .	102
4.6.2	Average bit error rate . . . . .	103
4.6.3	Average capacity . . . . .	104
4.7	Numerical results and discussion for SIMO FSO link . . . . .	104
4.8	Chapter summary . . . . .	170
<b>5</b>	<b>Performance Analysis of FSO Communication Channel with Alamouti Transmit and SEC Receive Diversity</b>	<b>171</b>
5.1	Introduction . . . . .	172
5.2	Organization . . . . .	172
5.3	Performance analysis with Alamouti STBC and SEC . . . . .	173
5.3.1	Gamma-Gamma turbulence in absence of pointing error . . .	175
5.3.2	Gamma-Gamma turbulence in presence of pointing error . . .	175
5.3.3	Málaga turbulence in absence of pointing error . . . . .	176
5.3.4	Málaga turbulence in presence of pointing error . . . . .	177
5.4	Numerical results and discussion for MIMO FSO link . . . . .	177
5.5	Chapter summary . . . . .	204

<b>6</b>	<b>Performance Analysis of FSO Communication Channel with SSK Transmit diversity and SC Receive Diversity</b>	<b>205</b>
6.1	Introduction . . . . .	206
6.2	Organization . . . . .	206
6.3	Performance analysis with SSK . . . . .	207
6.3.1	Gamma-Gamma turbulence in absence of pointing error . . .	207
6.3.2	Gamma-Gamma turbulence in presence of pointing error . . .	209
6.3.3	Málaga turbulence in absence of pointing error . . . . .	209
6.3.4	Málaga turbulence in presence of pointing error . . . . .	210
6.4	Performance analysis with SSK and SC . . . . .	211
6.4.1	Gamma-Gamma turbulence in absence of pointing error . . .	211
6.4.2	Gamma-Gamma turbulence in presence of pointing error . . .	215
6.4.3	Málaga turbulence in absence of pointing error . . . . .	215
6.4.4	Málaga turbulence in presence of pointing error . . . . .	216
6.5	Numerical results and discussion for SSK based MIMO FSO link . . .	217
6.6	Chapter summary . . . . .	229
<b>7</b>	<b>Summary of Results and Future Works</b>	<b>230</b>
7.1	Summary of results . . . . .	230
7.2	Future works . . . . .	235
	<b>Appendices</b>	<b>237</b>
<b>A</b>	<b>Channel Characterisation with Alamouti STBC</b>	<b>237</b>
<b>B</b>	<b>Closed-form Expression of BER using MGF</b>	<b>239</b>
<b>C</b>	<b>Closed-form PDF for GG Turbulence with SSK</b>	<b>241</b>
<b>D</b>	<b>PDF of GG Turbulence with SSK in Presence of Pointing Error</b>	<b>244</b>
<b>E</b>	<b>Closed-form Expression for <math>\mathcal{J}_1</math> and <math>\mathcal{J}_2</math></b>	<b>246</b>
<b>F</b>	<b>Closed-form Expression for <math>\mathcal{P}_1</math> and <math>\mathcal{P}_2</math></b>	<b>249</b>
<b>G</b>	<b>MATLAB Code for Monte Carlo simulation of a turbulent channel</b>	<b>253</b>
	<b>Bibliography</b>	<b>255</b>

# List of Figures

1.1	Classification of the optical wireless communication system. . . . .	2
1.2	A typical free space optical communication system. . . . .	3
2.1	A schematic diagram of a typical FSO communication system. . . . .	19
2.2	Receiver aperture in (a) absence and (b) presence of pointing error. . .	27
2.3	The Alamouti STBC with two transmitters and one receiver. . . . .	41
2.4	A typical SSK system with $N_t$ transmitters and a single receiver. . . .	43
2.5	The classical multi-branch switch-and-examine combining. . . . .	45
2.6	The classical selection combining technique. . . . .	47
2.8	Outage Probability of the single FSO link under different atmospheric turbulence condition in the absence and presence of pointing error regime. . . . .	57
2.9	Average bit error rate of the single FSO link under different atmo- spheric turbulence condition in the absence and presence of pointing error regime. . . . .	61
2.10	Average capacity of the single FSO link under different atmospheric turbulence condition in the absence and presence of pointing error regime. . . . .	65
3.1	Alamouti STBC-based $2 \times 1$ MISO FSO communication system. . . . .	69
3.2	Outage Probability of the MISO FSO link employing Alamouti STBC scheme at the transmitter end with different atmospheric turbulence conditions in the absence and presence of pointing error. . . . .	79
3.3	Average bit error rate of the MISO FSO link employing Alamouti STBC scheme at the transmitter end with different atmospheric tur- bulence condition in the absence and presence of pointing error. . . . .	83
3.4	Average capacity of the MISO FSO link employing Alamouti STBC scheme at the transmitter end with different atmospheric turbulence condition in the absence and presence of pointing error. . . . .	87
4.1	The SEC-based SIMO FSO communication system using one transmit antenna and $N_r$ receiver antennas. . . . .	91

---

4.2	Outage Probability of the SIMO FSO link employing switch and examine combining scheme at the receiver end with Gamma-Gamma distribution using different atmospheric turbulence conditions in the absence of pointing error. . . . .	109
4.3	Outage Probability of the SIMO FSO link employing switch and examine combining scheme in the receiver end with Gamma-Gamma distribution using different atmospheric turbulence conditions in the presence of pointing error. . . . .	113
4.4	Outage Probability of the SIMO FSO link employing switch and examine combining scheme in the receiver end with Málaga distribution using different atmospheric turbulence condition in the absence of pointing error. . . . .	117
4.5	Outage Probability of the SIMO FSO link employing switch and examine combining scheme at the receiver end with Málaga distribution using different atmospheric turbulence conditions in the presence of pointing error. . . . .	121
4.6	Average bit error rate of the SIMO FSO link employing switch and examine combining scheme in the receiver end with Gamma-Gamma distribution using different atmospheric turbulence conditions in the absence of pointing error. . . . .	128
4.7	Average bit error rate of the SIMO FSO link employing switch and examine combining scheme at the receiver end with Gamma-Gamma distribution using different atmospheric turbulence condition in the presence of pointing error. . . . .	135
4.8	Average bit error rate of the SIMO FSO link employing switch and examine combining scheme at the receiver end with Málaga distribution using different atmospheric turbulence condition in the absence of pointing error. . . . .	141
4.9	Average bit error rate of the SIMO FSO link employing switch and examine combining scheme at the receiver end with Málaga distribution using different atmospheric turbulence conditions in the presence of pointing error. . . . .	147
4.10	Average capacity of the SIMO FSO link employing switch and examine combining scheme at the receiver end with Gamma-Gamma distribution using different atmospheric turbulence condition in the absence of pointing error. . . . .	153
4.11	Average capacity of the SIMO FSO link employing switch and examine combining scheme at the receiver end with Gamma-Gamma distribution using different atmospheric turbulence condition in the presence of pointing error. . . . .	158

4.12	Average capacity of the SIMO FSO link employing switch and examine combining scheme in the receiver end with Málaga distribution using different atmospheric turbulence condition in the absence of pointing error. . . . .	163
4.13	Average capacity of the SIMO FSO link employing switch and examine combining scheme at the receiver end with Málaga distribution using different atmospheric turbulence conditions in the presence of pointing error. . . . .	168
5.1	A $2 \times N_r$ MIMO FSO system with Alamouti STBC and SEC. . . . .	173
5.2	Average bit error rate of the MIMO FSO link employing Alamouti STBC at the transmitter end and switch and examine combining scheme at the receiver end, with Gamma-Gamma distribution using different atmospheric turbulence conditions in the absence of pointing error. . . . .	184
5.3	Average bit error rate of the MIMO FSO link employing Alamouti STBC at the transmitter end and switch and examine combining scheme at the receiver end with Gamma-Gamma distribution using different atmospheric turbulence condition in the presence of pointing error. . . . .	191
5.4	Average bit error rate of the MIMO FSO link employing Alamouti STBC at the transmitter end and switch and examine combining scheme at the receiver end with Málaga distribution using different atmospheric turbulence condition in the absence of pointing error. . . . .	197
5.5	Average bit error rate of the MIMO FSO link employing Alamouti STBC at the transmitter end and switch and examine combining scheme at the receiver end with Málaga distribution using different atmospheric turbulence condition in the presence of pointing error. . . . .	203
6.1	SSK-SC $2 \times N_r$ MIMO FSO communication system. . . . .	212
6.2	Average bit error rate of the MISO FSO link employing SSK scheme at the transmitter end with different atmospheric turbulence conditions in the absence and presence of pointing error regime. . . . .	222
6.3	Average bit error rate of the SSK-SC-FSO based MIMO FSO link employing SSK scheme at the transmitter end and selection combining at the receiver end with different atmospheric turbulence conditions in the absence and presence of pointing error regime. . . . .	227

# List of Tables

1.1	Attenuation loss ( $\alpha$ ) due to atmospheric turbulence . . . . .	8
2.1	Scattering coefficient for various weather conditions . . . . .	24
2.2	Pointing Error Setting Parameters . . . . .	28
3.1	Fading distribution parameters for numerical analysis and simulation	74
3.2	Summary of the equations used for figures, Fig. 3.2 to Fig. 3.4. . . . .	75
4.1	Summary of the equations used for figures, Fig. 4.2 to Fig. 4.5. . . . .	105
4.2	Summary of the equations used for figures, Fig. 4.6 to Fig. 4.9. . . . .	122
4.3	Optimum switching threshold of $1 \times N_r$ SIMO FSO system in the absence of pointing error with $N_r = 2, 3, 4, 5$ and $6$ for different average SNR with turbulence parameter $\alpha_t = 2.20$ and $\beta_t = 0.65$ . . . . .	123
4.4	Optimum switching threshold of $1 \times 4$ SIMO FSO system in the absence of pointing error with different average SNR for different turbulence parameter. . . . .	124
4.5	Optimum switching threshold of $1 \times N_r$ SIMO FSO system in the presence of pointing error ( $\xi = 0.5607$ ) with $N_r = 2, 3, 4, 5$ and $6$ for different average SNR with turbulence parameter $\alpha_t = 2.20$ and $\beta_t = 0.65$ . . . . .	129
4.6	Optimum switching threshold of $1 \times 4$ SIMO FSO system in the presence of pointing error ( $\xi = 0.5607$ ) with different average SNR for different turbulence parameter. . . . .	130
4.7	Optimum switching threshold of $1 \times N_r$ SIMO FSO system in the absence of pointing error with $N_r = 2, 3, 4, 5$ and $6$ for different average SNR with turbulence parameter $\alpha_t = 2.29$ and $\beta_t = 1$ . . . . .	136
4.8	Optimum switching threshold of $1 \times 4$ SIMO FSO system in the absence of pointing error with different average SNR for different turbulence parameters. . . . .	137
4.9	Optimum switching threshold of $1 \times N_r$ SIMO FSO system in the presence of pointing error ( $\xi = 0.5607$ ) with $N_r = 2, 3, 4, 5$ and $6$ for different average SNR with turbulence parameter $\alpha_t = 2.29$ and $\beta_t = 1$ . . . . .	142



4.10	Optimum switching threshold of $1 \times 4$ SIMO FSO system in the presence of pointing error ( $\xi = 0.5607$ ) with different average SNR for different turbulence parameter. . . . .	143
4.11	Comparison of ABER for different FSO communication systems under Gamma-Gamma statistical distribution with pointing error ( $\xi = 0.5607$ ) for turbulence parameters $\alpha_t = 4.20$ and $\beta_t = 2.72$ . . . . .	148
4.12	Summary of the equations used for figures, Fig. 4.10 to Fig. 4.13. . . . .	148
4.13	Optimum switching threshold of $1 \times N_r$ SIMO FSO system in the absence of pointing error with $N_r = 2, 3, 4, 5$ and $6$ for different average SNR with turbulence parameter $\alpha_t = 2.20$ and $\beta_t = 0.65$ . . . . .	149
4.14	Optimum switching threshold of $1 \times 4$ SIMO FSO system in the absence of pointing error with different average SNR for different turbulence parameters. . . . .	149
4.15	Optimum switching threshold of $1 \times N_r$ SIMO FSO system in the presence of pointing error ( $\xi = 0.5607$ ) with $N_r = 2, 3, 4, 5$ and $6$ for different average SNR with turbulence parameter $\alpha_t = 2.20$ and $\beta_t = 0.65$ . . . . .	154
4.16	Optimum switching threshold of $1 \times 4$ SIMO FSO system in the presence of pointing error ( $\xi = 0.5607$ ) with different average SNR for different turbulence parameter. . . . .	154
4.17	Optimum switching threshold of $1 \times N_r$ SIMO FSO system in the absence of pointing error with $N_r = 2, 3, 4, 5$ and $6$ for different average SNR with turbulence parameter $\alpha_t = 2.29$ and $\beta_t = 1$ . . . . .	159
4.18	Optimum switching threshold of $1 \times 4$ SIMO FSO system in the absence of pointing error with different average SNR for different turbulence parameters. . . . .	159
4.19	Optimum switching threshold of $1 \times N_r$ SIMO FSO system in the presence of pointing error ( $\xi = 0.5607$ ) with $N_r = 2, 3, 4, 5$ and $6$ for different average SNR with turbulence parameter $\alpha_t = 2.29$ and $\beta_t = 1$ . . . . .	164
4.20	Optimum switching threshold of $1 \times 4$ SIMO FSO system in the presence of pointing error ( $\xi = 0.5607$ ) with different average SNR for different turbulence parameter. . . . .	164
4.21	Comparison of Average capacity for different FSO communication systems under Gamma-Gamma statistical distribution without pointing error for turbulence parameters $\alpha_t = 4.20$ and $\beta_t = 2.72$ . . . . .	169
4.22	Comparison of Average capacity for different FSO communication systems under Gamma-Gamma statistical distribution with pointing error ( $\xi = 0.5607$ ) for turbulence parameters $\alpha_t = 4.20$ and $\beta_t = 2.72$ . . . . .	169
5.1	Summary of the equations used for figures, Fig. 5.2 to Fig. 5.5. . . . .	178

5.2	Optimum switching threshold of $2 \times N_r$ SIMO FSO system in the absence of pointing error with $N_r = 2, 3, 4, 5$ and $6$ for different average SNR with turbulence parameter $\alpha_t = 2.20$ and $\beta_t = 0.65$ . . . . .	179
5.3	Optimum switching threshold of $2 \times 4$ MIMO FSO system in the absence of pointing error with different average SNR for different turbulence parameter $(\alpha_t, \beta_t)$ . . . . .	180
5.4	Optimum switching threshold of $2 \times N_r$ MIMO FSO system in the presence of pointing error ( $\xi = 0.5607$ ) with $N_r = 2, 3, 4, 5$ and $6$ for different average SNR with turbulence parameter $\alpha_t = 2.20$ and $\beta_t = 0.65$ . . . . .	186
5.5	Optimum switching threshold of $2 \times 4$ MIMO FSO system in the presence of pointing error ( $\xi = 0.5607$ ) with different average SNR for different turbulence parameter. . . . .	187
5.6	Optimum switching threshold of $2 \times N_r$ MIMO FSO system in the absence of pointing error with $N_r = 2, 3, 4, 5$ and $6$ for different average SNR with turbulence parameter $\alpha_t = 2.29$ and $\beta_t = 1$ . . . . .	192
5.7	Optimum switching threshold of $2 \times 4$ MIMO FSO system in the absence of pointing error with different average SNR for different turbulence parameters. . . . .	193
5.8	Optimum switching threshold of $2 \times N_r$ MIMO FSO system in the presence of pointing error ( $\xi = 0.5607$ ) with $N_r = 2, 3, 4, 5$ and $6$ for different average SNR with turbulence parameter $\alpha_t = 2.29$ and $\beta_t = 1$ . . . . .	198
5.9	Optimum switching threshold of $2 \times 4$ MIMO FSO system in the presence of pointing error ( $\xi = 0.5607$ ) with different average SNR for different turbulence parameter. . . . .	199
5.10	Comparison of ABER for different FSO communication system under Málaga statistical distribution without pointing error for $\alpha_t = 2.29$ and $\beta_t = 1$ . . . . .	204
5.11	Comparison of ABER for different FSO communication system under Málaga statistical distribution with pointing error ( $\xi = 0.5607$ ) for turbulence parameters $\alpha_t = 2.29$ and $\beta_t = 1$ . . . . .	204
6.1	Summary of the equations used for figures, Fig. 6.2 to Fig. 6.3. . . . .	217
6.2	Comparison of ABER for different FSO communication system under Gamma-Gamma statistical distribution with pointing error ( $\xi = 0.8565$ ) for turbulence parameters $\alpha_t = 2.20$ and $\beta_t = 0.65$ . . . . .	228
6.3	Comparison of ABER for different FSO communication system under Málaga statistical distribution with pointing error ( $\xi = 0.8565$ ) for turbulence parameters $\alpha_t = 2.29$ and $\beta_t = 1$ . . . . .	228

---

7.1	Comparison of performance metrics for different diversity aided FSO communication systems under Gamma-Gamma turbulence ( $\alpha_t = 4.20$ , $\beta_t = 2.72$ ) in the absence and presence of pointing error ( $\xi = 0.5607$ ) for SNR = 30 dB . . . . .	231
7.2	Comparison of ABER for different MIMO FSO communication systems under Gamma-Gamma statistical distribution without and with ( $\xi = 0.5607$ ) pointing error for $\alpha_t = 4.20$ , $\beta_t = 2.72$ , and average SNR = 30 dB . . . . .	235

# Abbreviations

<b>Abbreviation</b>	<b>Description</b>
<b>ABER</b>	<b>A</b> verage <b>B</b> it <b>E</b> rror <b>R</b> ate
<b>AT</b>	<b>A</b> tmospheric <b>T</b> urbulence
<b>AWGN</b>	<b>A</b> dditive <b>W</b> hite <b>G</b> aussian <b>N</b> oise
<b>BER</b>	<b>B</b> it <b>E</b> rror <b>R</b> ate
<b>CDF</b>	<b>C</b> umulative <b>D</b> ensity <b>F</b> unction
<b>E/O</b>	<b>E</b> lectrical to <b>O</b> ptical converter
<b>erfc</b>	complementary error function
<b>FSO</b>	<b>F</b> ree- <b>S</b> pace <b>O</b> ptics
<b>FSOC</b>	<b>F</b> ree- <b>S</b> pace <b>O</b> ptical <b>C</b> ommunication
<b>FSP</b>	<b>F</b> ree- <b>S</b> pace <b>P</b> hotonics
<b>GG</b>	<b>G</b> amma- <b>G</b> amma
<b>ICI</b>	<b>I</b> nter <b>C</b> hannel <b>I</b> nterference
<b>i.i.d.</b>	<b>I</b> ndependent and <b>I</b> dentically <b>D</b> istributed
<b>IM/DD</b>	<b>I</b> ntensity <b>M</b> odulation/ <b>D</b> irect <b>D</b> etection
<b>LASER</b>	<b>L</b> ight <b>A</b> mplification by <b>S</b> timulated <b>E</b> mission of <b>R</b> adiation
<b>LED</b>	<b>L</b> ight- <b>E</b> mitting <b>D</b> iode
<b>LOS</b>	<b>L</b> ine of <b>S</b> ight
<b>MGF</b>	<b>M</b> oment <b>G</b> enerating <b>F</b> unction
<b>MIMO</b>	<b>M</b> ulti <b>I</b> nput <b>M</b> ulti <b>O</b> utput
<b>MISO</b>	<b>M</b> ulti <b>I</b> nput <b>S</b> ingle <b>O</b> utput
<b>NLOS</b>	<b>N</b> on- <b>L</b> ine of <b>S</b> ight

---

<b>O/E</b>	<b>O</b> ptical to <b>E</b> lectrical converter
<b>OOK</b>	<b>O</b> n <b>O</b> ff <b>K</b> eying
<b>OP</b>	<b>O</b> utage <b>P</b> robability
<b>OWC</b>	<b>O</b> ptical <b>W</b> ireless <b>C</b> ommunication
<b>PDF</b>	<b>P</b> robability <b>D</b> ensity <b>F</b> unction
<b>QoS</b>	<b>Q</b> uality of <b>S</b> ervice
<b>RF</b>	<b>R</b> adio <b>F</b> requency
<b>RV</b>	<b>R</b> andom <b>V</b> ariable
<b>SC</b>	<b>S</b> election <b>C</b> ombining
<b>SEC</b>	<b>S</b> witch-and- <b>E</b> xamine <b>C</b> ombiner
<b>SIMO</b>	<b>S</b> ingle <b>I</b> nput <b>M</b> ulti <b>O</b> utput
<b>SISO</b>	<b>S</b> ingle <b>I</b> nput <b>S</b> ingle <b>O</b> utput
<b>SM</b>	<b>S</b> patial <b>M</b> odulation
<b>SNR</b>	<b>S</b> ignal to <b>N</b> oise <b>R</b> atio
<b>SSC</b>	<b>S</b> witch-and- <b>S</b> tay <b>C</b> ombining
<b>SSK</b>	<b>S</b> pace <b>S</b> hift <b>K</b> eying
<b>STBC</b>	<b>S</b> pace <b>T</b> ime <b>B</b> lock <b>C</b> ode
<b>wop</b>	<b>W</b> ith <b>O</b> ut <b>P</b> ointing
<b>wp</b>	<b>W</b> ith <b>P</b> ointing

# Symbols

$A_0$	pointing error constant parameter
$a$	Receiver aperture diameter size
$C_n^2$	Refractive index parameter
$E(\cdot)$	Statistical expectation function
$E_i(-\cdot)$	negative exponential integral
$erfc(\cdot)$	The complementary error function
$\exp(\cdot)$	The exponential function
$F_0$	Phase front radius
$F_X(x)$	Cumulative density function of variable X
$f_X(x)$	Probability density function of variable X
$G_{pq}^{mn}[\cdot]$	The Meijer G-function with parameters m, n, p, and q
$h_{ij}$	Channel fading coefficient
$k$	optical wave number
$K_\nu(\cdot)$	The modified Bessel function of second kind with order $\nu$
$\log_2(\cdot)$	The logarithm function with base 2
$\ln(\cdot)$	Natural logarithm function
$\mathcal{M}(\cdot)$	Moment generating function of the variables
${}_p\tilde{F}_q$	The generalized hypergeometric function
$w_0$	Beam waist radius
$w_z$	Beam waist radius at distance z
$\alpha_t$	Turbulence parameter

---

$\beta_t$	Turbulence parameter
$\Gamma(\cdot)$	The Euler's Gamma function
$\gamma$	Instantaneous SNR
$\gamma_0$	Switching threshold SNR
$\gamma_{th}$	Threshold SNR
$\bar{\gamma}$	Average SNR
$\xi$	Pointing error
$\lambda$	Transmitted beam wavelength
$\sigma_x^2$	Rytov variance

# Chapter 1

## Introduction

### 1.1 History behind FSO communication

Free Space Optical (FSO) communication is a wireless information transmission technology in which information is transmitted through the atmospheric medium by the propagation of light. The idea of carrying data through the air medium by a modulated light signal is an old technology. In the eighth century BC, the optical data transmission technique was first established with the help of the fire-signaling method by the Greek people to send information from one point to another, such as alarms, calls for help, or some announcements of certain events. This transmission method was not very popular due to its technological limitation. Some American and Indian people used smoke signals to transmit information for the same reason by 150 BC. During 1790-1794, French naval navigators used the optical telegraph, which was made based on a chain of semaphores. In 1810, Carl Friedrich Gauss invented a new optical device constructed by a couple of mirrors called the heliograph, a device frequently used for military purposes during the end of the 19th century and early 20th century. Graham Bell experimentally established the first wireless optical communication. In 1880 Alexander Graham Bell demonstrated the “photophone” communication, which was modulated by the sunlight. The photophone is



a telecommunication device that allows speech transmission on a light beam. After that, improvements in this mode of communication remain more-or-less insignificant due to some technological restrictions [1], which were eliminated once LASER was realized in the early 1960s.

The classification of the optical wireless communication (OWC) system is presented in Fig. 1.1. It indicates FSO communication, also called free space photonics (FSP), is one of the prime OWCs.

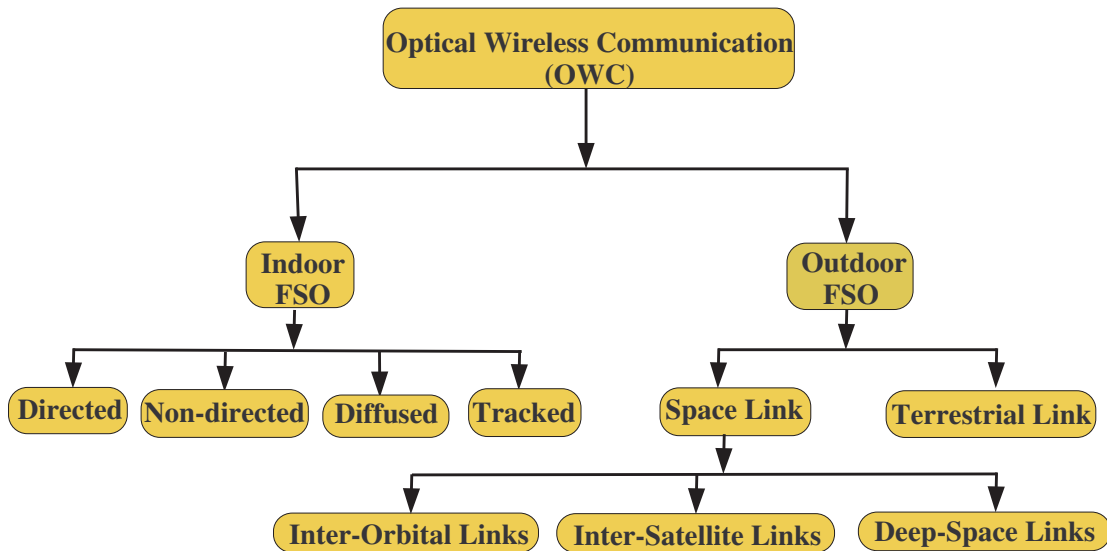


FIGURE 1.1: Classification of the optical wireless communication system.

The FSO communication is a promising solution for next-generation wireless connection due to its unique features. In the case of an optical fiber communication system, a transmission link between the sender and the user must be set up for data transmission. But, FSO communication uses air as a medium to establish serial

connectivity instead of using a guided medium. It utilizes a 350-1550 nm optical wavelength band and contributes an attractive data transmission rate of up to 30 Gbps with large bandwidth.

A typical FSO communication system is presented in Fig. 1.2. The fundamental FSO communication link (SISO FSO) commonly consists of one transmitter as a source (S) and a single receiver as a destination (D). Generally, at the source end, a LASER or LED is used to carry the digital information by transmitting the narrow-band optical beam. At the destination, usually, a telescope is used to receive this optical beam. Other blocks in the communication chain are discussed in detail in Section 2.3.



FIGURE 1.2: A typical free space optical communication system.

## 1.2 Pros and Cons of FSO communication

The FSO communication system is an emerging wireless broadband technology with enormous advantages over traditional radio frequency (RF) and optical fiber communication systems. Its easy installation, massive bandwidth, complete communication cycle with low bit error rate (BER), high data transmission rate during the data transfer period, secure data transmission, freedom from the licensed spectrum, and others make it suitable for serving internet facilities globally in the future. The advantages of an FSO system and its associated limitations are discussed in the following two sub-sections.

The system is free from a licensed spectrum, which means the technology does not require any license agreement from regulatory bodies or the government to use the spectrum. In addition, the technology offers immunity to RF-induced electromagnetic interference, which is a major problem for traditional RF link in the 4G wireless communication system. Compared to a typical optical fiber communication system, the installation process here is much simpler, and the associated cost is minimal. These advantages ensure that the system may be used as an ad-hoc network in various places like any disaster area, battlefield, earthquake area, and many more. Besides, the additional application area of the system is in space communication, designing a Local Area Network (in a small city, offices, or an academic campus environment), surveillance, etc.

### 1.2.1 Advantages of FSO communication

- **Low Power:** A link between transmitter and receiver is established through narrowband optical beam generated by optical sources like LED or LASER [2]. Both optical sources consume very little electric power to produce the optical signal, leading to a minimum power requirement for data transmission.

- **Easy Installation:** Optical fiber communication system installation is quite time-consuming. It involves a series of steps like laying the optical fiber into the ground, joining the slicing fiber, checking fiber bending, etc. But, installation of an FSO system is much simpler; the average installation time is approximately half an hour. This ensures that the system can be used as an ad-hoc network in various places like any disaster area, battlefield, earthquake area, and many more. Besides, the system is useful in augmenting the capacity of existing infrastructure based networks as well.
- **Low-Cost:** The overall cost of an optical fiber system is too high due to the use of optical fiber and its expensive installation. The cost of RF-dependent wireless communication systems is also high due to the use of the licensed frequency spectrum. On the other hand, the FSO communication system is free from a licensed spectrum, which means the technology does not require any license agreement from regulatory bodies or the government to use the spectrum [3].

Thus, low power requirement, simple architecture, easy installation, and use of the free unguided medium all these factors make the FSO communication system much more economical than any traditional communication system. Another essential issue of low cost is the high reliability of the system as indicated by its high mean time between failures (MTBF), which is more than one decade.

- **Secure Data Transmission:** FSO technology offers immunity to electromagnetic interference, which is the major problem for traditional RF links in the 4G wireless communication system. FSO system uses Line-of-Sight (LOS) technology to transfer the information by propagating a highly directional narrow band optical beam. Such a beam, obtained from a LASER, provides the link and makes it challenging to extract the information from it. At the transmitter side, the divergence angle is too small, only about one milliradian (1 mard = 0.05373 degrees); traveling waves are also immune to different

types of electromagnetic interference. Thus, data becomes more secure during transmission, and no additional data encryption is required.

- **Simple Last-Mile or Last-Leg Communication:** The word last mile is widely used in the telecommunication industry to define the link between the central servers or exchanges to the end users' premises. In densely populated and mountainous areas, providing a high-speed internet connection through wired communication to the last retail customer is pretty challenging due to the complicated and expensive installation of wired communications. The last mile or last leg problem can be resolved in such crucial situations by useful FSO links.
- **High Data Transmission Rate:** The FSO communication system yields an excellent data transmission rate for uplink and downlink transmission. In very recent technology, nearly 2.5 Gbps to 10 Gbps data rates with link distances up to 4 Km are being provided. In the modern FSO communication system, with additional wavelength division multiplexing schemes, the transmission rate may be increased up to 1.6 Tbit/s by transmitting 160 different baseband signals in a single period.
- **Low Bit Error Rate:** With the LOS data transfer protocol and narrowband optical beam during a data transfer period, the path loss of the system becomes very nominal. At the receiving terminal, the photodetector receives an almost correct version of the transmitted optical signal from the communication channel. As a result, the BER remains low and provides improved system performance.

Despite plentiful advantages, the quality of service (QoS) of the system strongly depends on the atmospheric environment. Atmospheric turbulence, flying object, and various air molecules present in the communication channel appear as significant obstacles to the propagating optical signal. Random fluctuation in the refractive

index of air also affects the LOS link. As a result, the amount of power loss increases with the traveling distance, a phenomenon called the path loss of the system. The transceiver module of the system naturally lies on top of the high-rise building or tower. The transceiver module may undergo shifts from its original position due to natural hazards like earthquakes, thunderstorms, tornados, and many more natural calamities. In such a situation, the direct LOS link is disturbed due to misalignment between the transmitter and receiver terminals. This phenomenon is called the pointing error of the system. This problem can be mitigated using transmitter and receiver diversity techniques.

### 1.2.2 Limitations of FSO communication

- **Atmospheric Loss:** Atmosphere being the communication medium influences the QoS of an FSO communication system in various ways

**Physical Obstructions:** In an FSO system, full duplex communication is accomplished with the LOS principle by transmitting a narrow band, low-power optical signal between the transceiver terminals. The traveling optical signal gets interrupted by distinct obstacles, viz. birds, kites, high-rise buildings, and tall trees present in the medium. To reach the receiver, the signal also suffers from fading [4]. Thus, the original information of the sender is partially, or in worst cases, totally lost within the channel, detoreating the overall performance of the FSO system.

**Absorption and Scattering:** Absorption and scattering of the optical signal are two crucial components by which the transmission rate frequently fluctuates through the communicating link of the system. They strongly depend on atmospheric conditions like heavy rainfall, drizzle, thunderstorm, heavy wind, fog, and the presence of different gas ions, high-energy photons, etc. Currently, (350 - 1550) nm wavelength band is used in modern FSO communication systems to carry the message signal. The beam

TABLE 1.1: Attenuation loss ( $\alpha$ ) due to atmospheric turbulence

Atmospheric Turbulence	Visibility (Km)	$\alpha$ (dB/Km)
Very clear air	50	0.0647
Clear air	20	0.2208
Haze	6	0.7360
Light fog	2	4.2850
Moderate fog	0.6	25.5160
Heavy fog	0.3	125

waist radius in the horizontal direction of transmitting optical beam is quite small (a few micrometers) compared to the sizes of raindrops and various types of fog particles. Water molecules and gas ions cause absorption, while fog and high-energy photons [5] [6] cause scattering of the optical signal. At the time of data transmission, the LOS link is more affected by raindrops and fog molecules of larger diameters. The amount of attenuation loss under various atmospheric conditions [7, 8] is displayed in TABLE 1.1.

**Scintillation:** The optical signal may suffer an additional loss due to a phenomenon called scintillation. The characteristics of air particles, like the electron, alpha particle, ion, or high-energy photon, change frequently due to atmospheric temperature fluctuation. The traveling wave undergoes collisions with such particles and loses its energy. The amplitude of the transmitted signal thus also fluctuates. Random fluctuation in the refractive index of air and affects the LOS link. As a result, the amount of power loss increases with the traveling distance, a phenomenon called the path loss of the system.

Thus, the amplitude of the transmitted signal fluctuates all through the link, delivering a poor version of the original signal at the receiver section.

- **Geometrical loss:** The internal loss of the system is commonly known as geometrical loss. Usually, the geometrical loss is comprised of different component losses arising from the diameter of the transmitter and receiver, the divergence angle at the transceiver, the radius of the transmitted optical beam, link distance between the transceiver. The amount of geometrical loss of an FSO system is commonly [9] [10] measured by the ratio of the receiver aperture and the area of the received optical beam. The transceiver module of the system is installed at the top of the high-rise building or tower. It may undergo shifts from its original position due to natural hazards like earthquakes, thunderstorms, tornados, and many more natural calamities, and such misalignment between the transmitter and receiver terminals cause fading. This phenomenon is called the pointing error of the system.
- **Background Noise:** Background noise is basically a kind of external noise that appeared due to the presence of various visible light sources like sunlight, moonlight and others. At the receiver terminal, photodetector receives the transmitted optical beam and produces the desired low DC power. But the photodetector also receives light from other background sources and converges them to electrical energy. Thus, the detector generates a DC superimposed with an AC (noise) at the receiver output and causes the poor signal to noise ratio (SNR) [11]. Such background noise deteriorates the performance of a digital transmission system by increasing its BER.

The above limitations can be mitigated by incorporating transmitter and receiver diversity in a basic FSO system. With an embedded diversity scheme, FSO becomes an excellent candidate for beyond-5G (B5G) wireless communication system.



## 1.3 Applications of FSO communication

FSO communication system is widely applied in the modern telecommunication industry worldwide.

- **Wireless Broadband:** Due to its massive bandwidth and excellent data transmission rate during the communication period, the network provider may use it for wireless broadband connection. Also, it is more economical than traditional RF links due to its licence free operation.
- **Backup Link:** The system can provide a backup link for high-speed point-to-point communication by replacing costly optical fiber in the telecommunication domain.
- **Enterprise Connection:** Simple architecture and easy installation of the FSO communication system make it useful for a LAN connection by interconnecting the buildings, offices, and other properties within a small area.
- **Military Purpose:** Being a secure data communication technique, the system is most appropriate for defense applications due to its additional attractive features like easy deployment, gigantic transmission rate, and extensive bandwidth.
- **UAV Design:** An Unmanned Aerial Vehicle (UAV) requires high-speed data transmission to support its expensive data handling purposes. An FSO communication system can efficiently satisfy the primary requirement of a UAV system.
- **Difficult Terrains:** An FSO communication system can make a data bridge between difficult locations, for example, at different points in rugged terrains, railway tracks, inside the river, busy streets, etc.

### 1.3.1 Current scenarios

In 2000 the FSO technology was first commercially launched to organize some events at the XXVII Olympiad in Sydney. Next, the link between the telecommunication satellite ARTEMIS and Earth observation satellite SPOT-4 was successfully established using a semiconductor laser. European Space Agency (ESA) demonstrated a bidirectional optical inter-satellite communication link with [12] the Japanese Space Exploration Agency (JAXA) for the first time in 2005. In December 2006, TerraSAR, the Earth observation satellite, was launched by the German Aerospace Center (GAC) with a maximum data rate of 6.5 Gbps and a link distance of 10000 km. OPALS, a spacecraft developed by NASA in December 2014 [13], established an uplink between space-to-ground communication with a 50 Mbps data rate, which works even the signal power is hampered by cloud turbulence.

Cable-free, a British startup company, offered wireless broadband connectivity with a 10 Gbps data transmission rate for outdoor wireless applications. A US-based startup company, Collinear, installed an HFSO system with an exclusive backhaul design to establish the connection between the existing RF link and the FSO communication system. In 2020, Department of Electrical Engineering at Pennsylvania State University, started investigating the FSO communication system for vehicle-to-everything (V2X) communication, robotic navigation, as well as underwater communication [14]. Director of the Center for Quantum Devices (CQD) at Northwestern University, reported that FSO system architecture could mitigate atmospheric turbulence by embedded MIMO configuration and spatial multiplexing techniques.

## 1.4 Motivation of research

As the RF spectrum is crowded, 5G wireless communication and internet-of-things (IoT) may use mm-wave to expand its capacity. It also has limitations, like spectrum sharing, spectrum licensing, interference from the cloud wave, etc., and most

importantly, is not economical. Thus, designing the 5G wireless communication system needs appropriate planning to incorporate the FSO link with existing RF architecture.

In such a system, an FSO communication link will replace an RF link and form the backbone of a future 5G wireless communication system. For the past few years [15], the system has been in use in various wireless communication domains, which reveals that the system calls for a lot of research, primarily in the domain of system architecture design. Coding for error detection and correction, transmitting and receiving diversity, advanced modulation schemes, and FSO network topologies are examples of some design algorithms excessively used for the last few decades to get a turbulence-immune FSO system.

To improve overall QoS, researchers are motivated to find methods for protecting the traveling optical beam from atmospheric turbulence and natural hazards and design a unique architecture for minimizing fading in the FSO communication system. In particular, employing the transmitter and receiver diversity in an FSO system with SIMO, MISO, and MIMO configurations can suppress the effect of natural turbulence and enhance the overall performance of the system.

## 1.5 Literature review with prior work

Depending on the degree of severity of weather conditions, atmospheric turbulence is broadly classified as weak, moderate, and strong. Researchers tried various techniques to mitigate the turbulence effect caused by the atmosphere and natural hazards. In [16], authors reported the performance of an FSO communication system with IM/DD OOK modulation technique, where Log-Normal distribution was considered to represent the weak atmospheric turbulence, and examined the average BER [17, 18] for coded FSO links. Gamma Gamma statistical distribution [19] is a popular method used to represent moderate and robust turbulence conditions.

Performance analysis of the system was made by Uysal et al.; adapting the Gamma Gamma distribution model for intense turbulence [20]. In [21], authors used rectangular quadrature modulation technique and Gamma Gamma distribution. In [22, ch.(8)][23], Málaga distribution was considered for the analysis of system behavior under strong and moderate turbulence conditions.

Various distributions like Rice-Nakagami, gamma shadowed-Rician, K, homodyned-K, exponential or Gamma-Rician, appropriate for modeling the channel under different weather conditions, can be obtained from Málaga distribution. The effect of pointing errors on the system performance metrics was studied in [24, 25]. Málaga distribution was used in [26, 27, 28] for similar investigations. Jose Maria Garrido-Balsells [29] et al. demonstrated Generalized-K distribution for atmospheric optical channels to examine the system performance. In [30] the capacity of the FSO link was estimated considering the Gamma Gamma distribution model and OOK signaling.

For better performance, different diversity techniques were investigated at the transmitter terminal of the system. Siavash M. Alamouti [31] introduced a simple transmit diversity technique, which is named Alamouti space-time block code (STBC). Adapting that coding, Simon and Vilarotter [32] determined the bit error probability with the use of IM/DD OOK and unipolar pulse-position modulation (PPM). Coherent and differential space-time code were used in [33, 34], and the average BER for the multiple numbers of transmitting antennas were estimated. PPM and space-time code were used in a MIMO FSO system, and symbol error rate (SER) for a different number of transmit antennas were studied in [35]. Authors employed selection transmit diversity with K distribution and examined the average BER for a MISO FSO system with OOK modulation in [36]. Various types of transmitter diversity techniques were examined in [37] under weak atmospheric turbulence conditions. MIMO FSO system performance analysis based on the performance metrics, viz average BER, average capacity, and outage probability, were reported in [38, 39, 40, 41, 42], where Gamma Gamma and K statistical distribution model considered for strong

atmospheric turbulent medium. A mathematical framework for calculating the average capacity of the system using Gamma Gamma distribution in the presence of pointing error was reported in [43]. In [44], authors characterized a MIMO FSO system experiencing Gamma Gamma fading and pointing error in terms of BER. In [45], switch-and-examine combining receiver diversity was employed in the system, and the outage performance of the system with a link subjected to Gamma Gamma turbulence was presented. The average BER of an FSO communication with the heterodyne detection technique, in the presence of pointing error, was described in [46]. Spatial Modulation (SM), a low complexity transmit diversity technique, was used by R. Mesleh et al [47]. Abaza and his team members adopted SSK transmission diversity, a particular case of SM for OWC over 'negative exponential' turbulence condition, and examined the system BER [48]. Salehiomran and Salehi [49] used spatial heterodyning optical code division multiple access (O-CDMA) techniques in the FSO communication system. The SSK modulation technique was used in the MIMO FSO system, and the system BER under various turbulence conditions was reported in [50] [51].

## 1.6 Thesis objective

The main objective of this thesis is to develop architectures for FSO communication systems employing transmitter and receiver diversity techniques in order to improve the QoS determined through various performance metrics of the system. In particular, the thesis objectives are as follows:

- Characterization of the turbulent channel of a single FSO link modeled by either Gamma-Gamma or generalized Málaga statistical distribution in the absence or presence of misalignment fading and examination of the performance of the same.

- Designing a MISO FSO communication system with the transmitter diversity technique and examining its performance for Málaga and Gamma-Gamma turbulence conditions without and with the pointing error impairment.
- Investigation of a SIMO FSO system with receiver diversity under Gamma-Gamma and general Málaga turbulent conditions with and without the pointing error.
- Estimation of performance metrics for a MIMO FSO system with both the transmitter diversity and receiver diversity under the combined effect of atmospheric turbulence and misalignment fading.
- Derivation of the mathematical framework for each resultant metric for all FSO topologies discussed above under various turbulence conditions in the presence of pointing error.
- Validation of all analytical results obtained in the above cases with Monte-Carlo simulation results.

## 1.7 Thesis layout

The thesis contains seven chapters, including the present introductory one, which presents the fundamentals of FSO communication, advantages and limitations of an FSO system research motivation, and objective. The rest of the thesis is outlined as follows:

Chapter 2, provides the channel characterization of the FSO communication system and discusses the necessary parameters related to the link design. It describes some statistical distributions appropriate for characterizing the communication link with atmospheric turbulence that causes random fluctuation in the amplitude of the propagating optical beam. In addition, it elaborates on various transmit and receive diversity techniques to handle the problem of signal fading. It also presents different

---

performance metrics for a single FSO link under two channel distributions in the presence of a pointing error.

In Chapter 3, we investigate the MISO FSO link incorporating the Alamouti STBC transmitter diversity under atmospheric turbulence modeled by two different statistical distributions and with pointing errors.

In Chapter 4, the performance of a SIMO FSO link with Switch and Examine Combining (SEC), a receiver diversity is examined in terms of ABER, OP, and average capacity under the influence of pointing error.

Chapter 5 presents the study of a MIMO FSO communication system with the transmitter and receiver diversity techniques in the absence and presence of misalignment fading impairments for different degrees of atmospheric turbulence (AT) severity. For this particular MIMO FSO link, the Alamouti STBC type transmits diversity and SEC type receiver diversity schemes are used.

In Chapter 6, we have incorporated spatial shift keying (SSK) transmit diversity scheme and selection combining (SC) receiver diversity scheme to set up a MIMO FSO communication link. Analytical results are derived for the proposed system under different weather conditions and compared with those for other FSO schemes.

The Final Chapter, Chapter 7, summarizes the results obtained in the thesis. It ends with the future scopes of research in this field of wireless communication.

# Chapter 2

## FSO Communication System Design and Channel Characterization

### 2.1 Introduction

The overall performance of an FSO communication system mainly depends on the architectural setup of the optical transceiver module and the characteristics of the communication link. The transceiver section comprises of optoelectronic devices like LED /LASER, photodetector, optoelectronics modulator /demodulator, optical amplifier, and many other components, while the performance of each of them will influence that of the overall system.

Atmospheric turbulence is one of the main critical hazards that appear during data transmission through free space between the transceiver terminals. It causes random fluctuation in the amplitude and phase of the traveling waves, thus leading to fluctuations in the received signal power level leading to random fading effects.



However, the influence of atmospheric turbulence can be mitigated by employing some fading mitigation techniques like diversity and aperture averaging at the transceiver terminals. Recently, the transmitter and receiver diversity techniques appear to be more popular.

## 2.2 Organization

In this chapter, we have started our discussion with the design procedure of an FSO communication system and some necessary physical factors associated with the FSO link through Section 2.3 to Section 2.4. The overview of the misalignment fading with its analytical framework has been explained in Section 2.4.5. Different statistical distributions have been studied in Section 2.5 to consider the effect of misalignment fading into the system. Various types of transmitter and receiver diversity schemes have been studied under the diversity model section Section 2.6, where the Alamouti STBC, spatial shift keying technique for transmitter diversity, and the SEC and SC techniques for receiver diversity have been described. Next, Section 2.7 defines the performance metrics like OP, ABER, and average capacity, which are strongly relevant to indices of the QoS of any communication system. Numerical results and discussion of the SISO FSO link have been analyzed in Section 2.8, and finally, the chapter concludes with the summary presented in Section 2.9.

## 2.3 An FSO system design

The schematic diagram of a typical FSO communication system in Fig. 2.1 presents the internal architecture of the transceiver module that comprises of distinct transmitter and receiver sections.

The optical transmitter section consists of optical sources, optoelectronic modulators, optical amplifiers, and transmitting antennas. In the transmitter section,

different operations are carried out before transmitting the modulated version of the input signal. The operations are as follows:

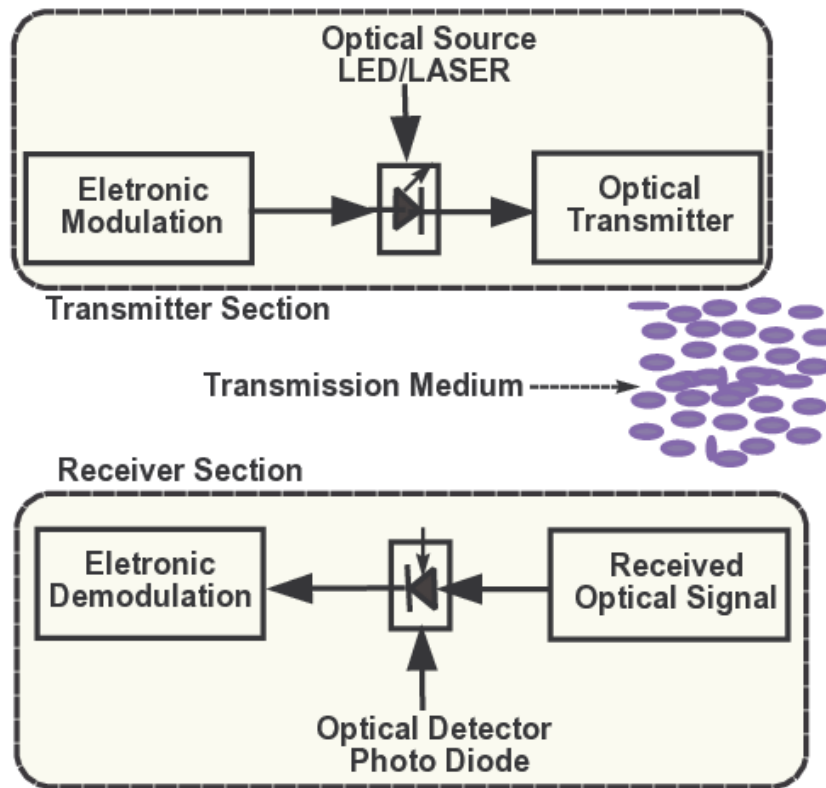


FIGURE 2.1: A schematic diagram of a typical FSO communication system.

- **Electronic Modulator:** The baseband signal is modulated by one of the modulation schemes - On-Off Keying (OOK), Pulse-Position Modulation (PPM), Quadrature-Amplitude Modulation (QAM), etc, chosen according to the user specification.
- **Electrical to Optical (E/O) Converter:** Next, the electronic modulated signal is further modulated with the optical signal by the optical modulator. Optical sources like LED or LASER are excessively used to generate optical signals. Erbium-doped fiber amplifiers (EDFA), semiconductor optical amplifiers (SOA), and Raman fiber amplifiers (RFA) may be used for the purpose [52]. Some commercial optical modulator examples include iXBlue's MPZ-LN

and MPX-LN amplifier series with the MPX-LN-0.1 series specifically being used for optical signals of 780 nm to 2000 nm wavelengths.

Type of Amplifier	Wavelength range
SOA (Semiconductor optical amplifier)	750 nm-1650 nm
EDFA (Erbium-doped fibre amplifier)	980 nm-1610 nm
RFA (Raman fibre amplifier)	1260 nm-1650 nm

- **Optical Transmitter:** Finally, the resultant modulated optical beam is amplified by an optical amplifier and transmitted through the free space by transmitting antennas.

A sequence of reverse processes takes place at the receiver section to recover the original information sent from the transmitter. The optical receiver module contains a photodetector, optoelectronic demodulator, receiver antenna array, and related equipment. The signal-recovering process is discussed below:

- **Optical Receiver:** The optical receiver section is equipped with array of telescopes that made of by photo detectors or photo transistors which receives the optical beam from the channel.
- **Optical to Electrical (O/E) Converter:** The O/E signal converter transforms the received optical wave to the electrical domain. Such O/E conversion is accomplished by a photodetector which is basically either a photodiode or phototransistor. The electrical signal available at the photodetector output yields the electronic modulated wave.
- **Demodulation:** A demodulator extracts the original information from the modulated wave. It employs an appropriate demodulation technique depending on the type of electronic modulation carried out at the transmitter section.

## 2.4 Some fundamental parameters associated with FSO link design

A few essential factors related to the FSO communication system that must be considered during the physical setup of an FSO link are discussed below:

### 2.4.1 Geometrical loss

A narrow-band optical beam is transmitted through the free space from the transmitter antenna to carry the input message to the receiver. During the traveling period, beam divergence takes place, and the transmitted optical beam width increases with the link distance [53]. Such a phenomenon is known as beam spreading. At the receiver side, the such divergent light beam can not be collected efficiently by an antenna of insufficient aperture. But, a too-wide receiver aperture causes noise generation from the ambient optical signal, resulting in internal losses. The internal loss, technically called geometrical loss of the system, is defined as the ratio of the area of the receiver aperture ( $A_r$ ) and that of the beam at the receiver plane ( $A_b$ ), and is mathematically expressed as [10]

$$L = \frac{A_r}{A_b} = \left[ \frac{D_R}{\{D_T + (R\theta)\}} \right]^2 \quad (2.1)$$

and the geometrical power loss in dB is derived as

$$L_{dB} = \frac{A_r}{A_b} = 20 \log \left[ \frac{D_R}{\{D_T + (R\theta)\}} \right] \quad (2.2)$$

where  $D_R$  and  $D_T$  represents respectively the radius of the receiver and transmitter aperture,  $R$  is the link distance, and  $\theta$  the divergence angle of the transmitted optical beam in milliradians. For the terralink laser communication system, the geometrical

loss increases from 15 to 33 dB with the channel length variation from 1 to 8 Km [54]

## 2.4.2 Aperture averaging

Aperture averaging is a technique [55] to reduce the influence of atmospheric turbulence that causes fading in the transmitted optical beam. In this approach, a receiver of a larger aperture is used which collects all incident (strong and weak) signal components. This eventually raises the average signal level with reduced degrees of fluctuation [56]. A parameter called aperture averaging factor (A) [57] is typically used to estimate the fading reduction, and is defined as [58]

$$A = \frac{\sigma_I^2(D)}{\sigma_I^2(0)} \quad (2.3)$$

where  $\sigma_I^2(D)$  represents the degrees of intensity fluctuation for a receiver aperture of diameter ( $D$ ) and  $\sigma_I^2(0)$  is that for a point receiver (i.e.,  $D = 0$ ). Intuitively,  $A < 1$ , i.e. the aperture averaged scintillation will be less than that of a point receiver, as a larger receiver will average out the fluctuations over the whole aperture and the scintillated irradiance decreases with increasing aperture size.

The aperture averaging factor for weak turbulence is approximated as

$$A \approx \left[ 1 + 1.062 \left( \frac{D^2 k}{4L} \right) \right]^{-\frac{7}{6}} \quad (2.4)$$

where  $D$  is the receiver aperture size,  $L$  is the channel length,  $k(= 2\pi/\lambda)$  is called the optical wave number,  $\lambda$  being the wavelength of the transmitted optical beam. In the presence of receiver diversity use of aperture averaging [59] at the receiver section can produce a noticeable improvement in BER. On the other hand, the averaging aperture effect may increase the background noise and, therefore, degrade the SNR of the system. Thus, an optimum receiver diameter is to be chosen for any weather

condition and misalignment environment scenario to yield low BER with reasonable SNR [60].

### 2.4.3 Scattering and absorption

Scattering and absorption are critical factors that reduce the power of narrow-band optical beams during their propagation through the atmosphere. Both phenomena occur due to interaction with the air particle in the atmosphere.

When the traveling optical beam interacts with the molecules like carbon dioxide, ozone, water vapor, hydrogen, etc., present in the communication medium, it causes power loss of the beam. The phenomenon is called absorption. The absorption coefficient significantly depends on the size and density of the gas molecule present in the medium [61]. The amount of power loss due to absorption also depends on the wavelength of the transmitted optical wave. The FSO system typically uses a (690 - 1550) nm wavelength band for communication purposes due to the existence of a low absorption window in this wavelength band. Nevertheless, the 1550 nm wavelength is the best choice for FSO communication as it suffers the least absorption in the strong atmospheric turbulence and thus provides the best link availability [62].

On the other hand, the scattering of a light beam is associated with the redirection of the light from its actual path by collision with another particle in the propagation medium [63]. On the basis of the radius ( $r$ ) of the scattering particle and wavelength ( $\lambda$ ) of light, scattering is classified into three types: Rayleigh ( $r < \lambda$ ), Mie ( $r \leq \lambda$ ), and Geometrical scattering ( $r \gg \lambda$ ). The overall atmospheric attenuation is the sum of the absorption and scattering attenuation defined by Beer-Lambert law as [64, 65]

$$\tau(\lambda, L) = \frac{P(\lambda, L)}{P(\lambda, 0)} = \exp[-\gamma(\lambda)L] \quad (2.5)$$

TABLE 2.1: Scattering coefficient for various weather conditions

Weather Condition	Visibility	Scattering coefficient
Dense fog	< 50m	> 78.2
Thick fog	50m to 200m	78.2 to 19.6
Moderate fog	200m to 500m	19.6 to 7.82
Light fog	500m to 1km	7.82 to 3.91
Thin fog	1km to 2km	3.91 to 1.96
Haze	2km to 4km	1.96 to 0.954
Light haze	4km to 10km	0.954 to 0.391
Clear	10km to 20km	0.391 to 0.196
Very clear	20km to 50km	0.196 to 0.078
Extreme clear	> 50km	0.0141

where,  $\tau(\lambda, L)$  is the total atmospheric transmittance,  $P(\lambda, 0)$  and  $P(\lambda, L)$  indicates the signal power at the transmitter and at the L from the transmitter respectively, and  $\gamma(\lambda)$  is the attenuation coefficient per unit length. However, the attenuation coefficient is composed of scattering and absorption terms, and is typically expressed as

$$\gamma(\lambda) = \alpha_m(\lambda) + \alpha_a(\lambda) + \beta_m(\lambda) + \beta_a(\lambda) \quad (2.6)$$

where,  $\alpha_m(\lambda)$  and  $\alpha_a(\lambda)$  are the molecular and aerosol absorption coefficients, while  $\beta_m(\lambda)$  and  $\beta_a(\lambda)$  are the molecular and aerosol scattering coefficients respectively. The scattering coefficients get significantly influenced by various atmospheric turbulence. TABLE 2.1 presents the scattering coefficients under various weather conditions like rain, fog, and haze [66].

#### 2.4.4 Refractive index and scintillation

When an optical beam propagates through the turbulent medium, it experiences temporal and spatial intensity fluctuation due to small temperature variations along the transmission path. This phenomenon is known as scintillation and appears [67]

due to thermal inhomogeneities present in the atmosphere. Atmospheric eddies result in an increase in air pocket temperature [68], called the Fresnel zone. In this zone, the density of the air pocket and its temperature cause of scintillation, leading to fluctuations in refractive index, called optical turbulence. For long-haul communication, the transmitted optical beam gets very much affected by scintillation and generates irradiant fluctuation in the received signal traveling near the earth's surface [69]. The unit-less parameter, scintillation, is proportional to Rytov variance, which can be expressed for plane wave as [70]  $\sigma_x^2 = 1.23C_n^2 k^{7/6} L^{11/6}$ , where  $C_n^2$  is the altitude-dependent refractive index structure constant,  $k$  is the optical wave number, and  $L$  indicates the channel distance. However, Rytov variance represents the scintillation index only for weak fluctuation; otherwise, it is considered as the measure of the strength of the optical turbulence. Different values of Rytov variance classify optical turbulence into three categories [71]. For weak optical turbulence  $\sigma_x^2 < 1$ , condition for moderate optical turbulence is  $\sigma_x^2 \approx 1$ , and  $\sigma_x^2 > 1$  indicates the strong optical turbulence region.  $\sigma_x^2$  increases with both increasing  $C_n^2$  and link distance and decreasing wavelength of the transmitted optical beam. Commonly, as an FSO communication system employs a narrow-band optical beam, the plane wave structure is more appropriate than the spherical structure.

The value of  $C_n^2$  typically lies between  $10^{-17}m^{-2/3}$  and  $10^{-13}m^{-2/3}$  to represent distinct (weak, moderate, and strong) atmospheric turbulence region. Hufnagle-Valley model is used to describe its altitude dependents as [72]

$$C_n^2(h) = 0.00594 \left(\frac{v}{27}\right)^2 (10^{-5}h)^{10} \exp\left(\frac{h}{1000}\right) + \left(2.7 \times 10^{-6} \times \exp\left(\frac{-h}{1500}\right)\right) + A \exp\left(\frac{-h}{1000}\right) \quad (2.7)$$

where  $v$  is the velocity of wind (m/s),  $h$  is altitude (m), and  $A$  is the minimal value of  $C_n^2(h)$  at the ground surface ( $h = 0$ ). In general,  $C_n^2 = 10^{-17}m^{-2/3}$  for weak atmospheric turbulence and  $C_n^2 = 10^{-13}m^{-2/3}$  for strong turbulence. An average value of  $10^{-15}m^{-2/3}$ , is often taken for moderate atmospheric turbulence.



### 2.4.5 Pointing error

Some natural hazards like heavy wind load, thermal expansion by building hardware material, and weak earthquakes cause the building to sway, which may give rise to the misalignment between the transceiver terminals of the system. This phenomenon is called the pointing error. Even a minor pointing error may produce a high impact on the performance of an FSO communication system and, therefore, deserves careful consideration during the link design. The traveling beam may be redirected both horizontally and vertically from its original location due to building sway [73]. The statistical characteristics of the building sway are derived from an independent Gaussian distribution model for both elevation (vertical) and azimuth (horizontal) angles. [74, 75]

The pointing error is composed of mainly two factors: boresight and jitter variance. The boresight is the steady displacement between the center of the beam and that of the detector due to thermal expansion, while the jitter is a random component arising from building sway and vibration. Typically, for TerraLink laser communication, the limiting value of boresight error should lie within (0.5 - 0.3) mrad [54], and for terrestrial FSO communication link, that for jitter variation is 0.3 mrad [76]. The authors in [77] considered boresight errors of 0.03906 m, 0.07812 m, and 0.11719 m to represent respectively the weak, average, and strong boresight, and standard deviations of 0.0332 m, 0.0664 m and 0.0996 m to represent respectively the low, medium, and substantial jitter for outdoor FSO link.

The different research articles reported the influences of pointing errors on the performance of an FSO communication system. The statistical model of the pointing error dependent on the detector aperture size at the receiver side, optical beam width, and standard jitter variation were presented in [24]. The normalized distribution of the transmitted Gaussian beam intensity at link distance  $Z$  from the

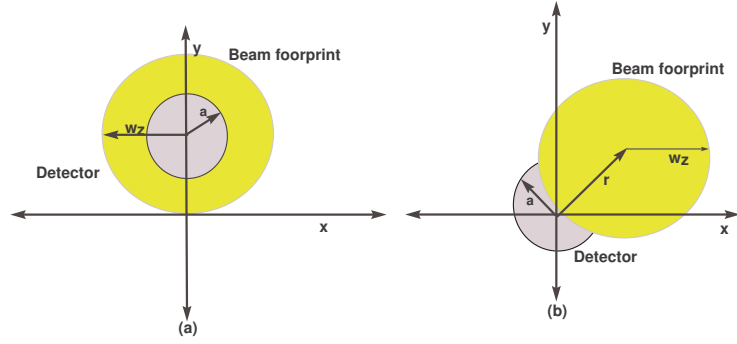


FIGURE 2.2: Receiver aperture in (a) absence and (b) presence of pointing error.

transmitter terminal is represented by [78]

$$I_{beam}(\rho; Z) = \frac{2}{\pi w_Z^2} \exp\left(-\frac{2\|\rho\|^2}{w_Z^2}\right) \quad (2.8)$$

where  $\rho$  represents the radial vector from the center of the beam and  $w_Z$  is the beam waist radius at link distance  $Z$ . The beam waist radius of the propagating beam in free space can be approximated as [24]

$$w_Z \approx w_0 \left[ 1 + \epsilon \left( \frac{\lambda Z}{\pi w_0^2} \right)^2 \right]^{\frac{1}{2}} \quad (2.9)$$

where  $w_0$  indicates the beam waist radius at zero link distance ( $Z = 0$ ),  $\epsilon = (1 + 2w_0^2/\rho_0^2(Z))$ , with  $\rho_0(Z)$  is defined as coherence length and is given by  $\rho_0(Z) = (0.55C_n^2 k^2 Z)^{-3/5}$ , assuming a circular detector aperture with radius ' $a$ ' and the Gaussian beam profile at the receiver terminal  $I_{beam}$ , shown in Fig. 2.2. The resultant attenuation due to geometrical spreading loss with pointing error ' $r$ ' can be expressed as

$$I_p(r; Z) = \int_{\mathcal{A}} I_{beam}(\rho - r; Z) d\rho \quad (2.10)$$

where  $I_p$  is function of power collected by the detector, and  $\mathcal{A}$  represents the size

TABLE 2.2: Pointing Error Setting Parameters

Symbol	Parameter	Value
Z	Link Distance	1000 m
$\lambda$	Wavelength	1550 nm
a	Radius of receiver aperture	5 cm
$w_0$	Beam waist radius	2 cm
$C_n^2$	Refractive index parameter	$3 \times 10^{-14} \text{ m}^{-2/3}$
$F_0$	Phase front radius	-10 m

of the detector. In the presence of a pointing error,  $I_p$  is also a function of radial displacement and the angle at the detector. Due to the symmetrical beam shape and detector size, the resultant  $I_p(r; Z)$  only depends on the radial distance  $r = \|r\|$  and can be written approximately as

$$I_p(r; Z) \approx A_0 \exp\left(-\frac{2r^2}{w_{Zeq}^2}\right) \quad (2.11)$$

where  $A_0$ , a constant parameter, defines the pointing loss, and mathematically can be expressed as  $A_0 = erf(v)$ ,  $erf(\cdot)$  being the error function. The parameter  $v$  is function of both the detector aperture radius ( $a$ ) and beam waist ( $w_Z$ ) as  $v = \frac{\sqrt{\pi}a}{\sqrt{2}w_Z}$ . The parameter  $w_{Zeq}$  is the equivalent beam radius at the receiver end, and is function of link distance  $Z$  and the beam waist radius ( $w_Z$ ), as  $w_{Zeq} = \frac{(w_Z^2 \sqrt{\pi} erf(v))}{(2v \exp(-v^2))}$ .  $w_Z$  can have another simple mathematical expression [26, 25],  $w_Z = w_0((\Theta_0 + \Lambda_0)(1 + 1.63\sigma_R^{12/5}\Lambda_1))^{1/2}$ , where  $\Theta_0 = 1 - \frac{Z}{F_0}$ ,  $\Lambda_1 = \frac{\Lambda_0}{\Theta_0^2 + \Lambda_1^2}$ ,  $\Lambda_0 = \frac{2Z}{kw_0^2}$ ,  $F_0$  is known as radius of curvature, and  $\sigma_R$  indicates the Rytov variance at a link distance of  $Z$  meters.

Assuming that the elevation and azimuth displacement due to building sway are independent and identically distributed (i.i.d), the pointing error caused by the radial displacement model follows the Rayleigh distribution model with PDF given as [74].

$$f_r(r) = \frac{r}{\sigma_s^2} \exp\left(-\frac{r^2}{\sigma_s^2}\right), \quad r > 0 \quad (2.12)$$

where  $\sigma_s^2$  represents the jitter standard variance at the receiver end. Combining (2.10) and (2.11), the PDF of  $I_p$  can be derived as [24]

$$f_{I_p}(I_p) = \frac{\xi^2}{A_0^{\xi^2}} I_p^{\xi^2-1}, 0 \leq I_p \leq A_0 \quad (2.13)$$

where  $\xi = w_{zeq}/2\sigma_s$  indicates the ratio between an equivalent beam radius of the receiver terminal and pointing error displacement standard deviation at the receiver terminal.

## 2.5 Statistical channel models for FSO link

Depending on the severity of the atmospheric turbulence, the communication channel is primarily classified into three distinct categories: weak, moderate, and high atmospheric turbulence. Various statistical distributions are usually employed to describe the channel characteristics of the FSO communication system under the different degrees of atmospheric turbulence conditions [79, 80, 81, 82]. Authors in [83, 84, 85] considered the Log-normal statistical distribution to model the channel under weak atmospheric turbulence conditions. The GG distribution model was employed to illustrate the channel features for moderate to strong atmospheric turbulence [86, 87]. A new and more general statistical distribution, known as Málaga distribution, was used to characterize the broader range of atmospheric turbulence medium [88, 89]. In addition, the overall link performance of the FSO system may get affected due to the effect of pointing errors. Thus, defining a generalized statistical distribution that can represent different atmospheric turbulence, and with the associated pointing error effect, is necessary.

This section will represent different statistical distributions and will describe the important functions, probability density function (PDF), cumulative density function (CDF), and moment generating function (MGF) in the absence and presence of pointing error to characterize the FSO link.

### 2.5.1 Moderate-to-strong AT in absence of pointing error

The atmospheric turbulence causes thermal inhomogeneities in the free space and is the main obstacle for an FSO link. The thermal inhomogeneities in the air lead to random fluctuations in the refractive index through the propagation path. Thus, the amplitude of the optical beam also fluctuates, and finally, the receiving unit collects the faded signal. It is challenging to describe the irradiance fluctuation of the signal by statistical distribution technique under an atmospheric turbulence environment. However, research works represented in the last few years [70] reveal that in order to model the turbulent channel, the Log-normal distribution suits for weak turbulence, while the GG distribution is for moderate-to-strong turbulence. The irradiance sample of the optical wave  $I_a$  has been defined by the product of two mutually independent Gamma RV [90, 91]  $I_x$  and  $I_y$ , such as  $I_a = I_x \times I_y$ , where  $I_x$  and  $I_y$  indicate the large scale and small scale eddies respectively.

#### 2.5.1.1 PDF under gamma-gamma distribution

The PDF for the irradiance ( $I_a$ ) of the optical beam can be represented by Gamma-Gamma statistical distribution as [43]

$$f_{I_a}(I_a) = \frac{2(\alpha_t \beta_t)^{\frac{(\alpha_t + \beta_t)}{2}}}{\Gamma(\alpha_t) \Gamma(\beta_t)} (I_a)^{\frac{(\alpha_t + \beta_t)}{2} - 1} K_{\alpha_t - \beta_t} \left( 2\sqrt{\alpha_t \beta_t I_a} \right) \quad (2.14)$$

where  $K_{\alpha_t - \beta_t}(\cdot)$  indicates the modified Bessel function of the second kind of order  $\alpha_t - \beta_t$ , and  $\Gamma(\cdot)$  is known as gamma function. The term  $\alpha_t$  and  $\beta_t$  denote the atmospheric turbulence parameters, and their numeral depends on the strength of the turbulence. They are linked together to develop the scintillation index ( $SI$ ) that measures the severity of the turbulence and is described as [39]

$$S.I. \triangleq \frac{E(I_a)^2}{[E(I_a)]^2} - 1 = \frac{1}{\alpha_t} + \frac{1}{\beta_t} + \frac{1}{\alpha_t \beta_t} \quad (2.15)$$

Furthermore, the scale parameter  $\alpha_t$  and the shape parameter  $\beta_t$  are correlated with another physical factor. For plane-wave optical radiation, these two parameters are obtained as follows [92]

$$\alpha_t = \left[ \exp \left[ \frac{0.49\sigma_R^2}{\left(1 + 1.11\sigma_R^{\frac{12}{5}}\right)^{\frac{7}{6}}} \right] - 1 \right]^{-1} \quad (2.16)$$

$$\beta_t = \left[ \exp \left[ \frac{0.51\sigma_R^2}{\left(1 + 0.69\sigma_R^{\frac{12}{5}}\right)^{\frac{5}{6}}} \right] - 1 \right]^{-1} \quad (2.17)$$

where  $\sigma_R^2$  is the Rytov variance defined earlier.

However, the PDF of the GG distribution is described in terms of the instantaneous electrical SNR ( $\gamma$ ), and average electrical SNR ( $\bar{\gamma}$ ) as [93]

$$f_\gamma(\gamma) = \frac{(\alpha_t\beta_t)^{\frac{(\alpha_t+\beta_t)}{2}}}{\Gamma(\alpha_t)\Gamma(\beta_t)\sqrt{\gamma\bar{\gamma}}} \left(\sqrt{\frac{\gamma}{\bar{\gamma}}}\right)^{\frac{(\alpha_t+\beta_t)}{2}} K_{\alpha_t-\beta_t} \left(2\sqrt{\alpha_t\beta_t}\sqrt{\frac{\gamma}{\bar{\gamma}}}\right) \quad (2.18)$$

where  $\gamma = \eta^2 I_a^2 / N_0$  and  $\bar{\gamma} = \eta[E(I_a)]^2 / N_0$ ,  $\eta$  denotes the optical-to-electrical conversion ratio. We may rewrite the above equation using the Meijer's G form of  $K_\nu(x)$  [94, Eq.(8.4.23.1)] as

$$f_\gamma(\gamma) = \frac{(\alpha_t\beta_t)^{\frac{(\alpha_t+\beta_t)}{2}}}{2\Gamma(\alpha_t)\Gamma(\beta_t)(\bar{\gamma})^{\frac{(\alpha_t+\beta_t)}{4}}} (\gamma)^{\frac{(\alpha_t+\beta_t)}{4}-1} G_{0\ 2}^{2\ 0} \left[ \alpha_t\beta_t\sqrt{\frac{\gamma}{\bar{\gamma}}} \middle| \begin{matrix} - \\ \frac{\alpha_t-\beta_t}{2}, \frac{\beta_t-\alpha_t}{2} \end{matrix} \right] \quad (2.19)$$

where,  $K_\nu(2\sqrt{x}) = \frac{1}{2}G_{0\ 2}^{2\ 0} \left[ x \middle| \begin{matrix} - \\ \frac{\nu}{2}, -\frac{\nu}{2} \end{matrix} \right]$ , and  $G[\cdot]$  is the Meijer's G function defined in [95, Eq.(9.301)].

### 2.5.1.2 CDF under gamma-gamma distribution

Consider  $Y$  be a RV and  $f_Y(y)$  its PDF, then CDF of the variable  $Y$ , is described as  $F_Y(y) = Pr(Y \leq y) = \int_0^y f_Y(y)dy$ . Using (2.18), the integral form of CDF may then be presented as

$$F_\gamma(\gamma) = \frac{(\alpha_t \beta_t)^{\frac{(\alpha_t + \beta_t)}{2}}}{2\Gamma(\alpha_t)\Gamma(\beta_t)(\bar{\gamma})^{\frac{(\alpha_t + \beta_t)}{4}}} \int_0^\gamma (\gamma)^{\frac{(\alpha_t + \beta_t)}{4} - 1} G_{0\ 2}^{2\ 0} \left[ \alpha_t \beta_t \sqrt{\frac{\gamma}{\bar{\gamma}}} \middle| \begin{matrix} - \\ \frac{\alpha_t - \beta_t}{2}, \frac{\beta_t - \alpha_t}{2} \end{matrix} \right] d\gamma \quad (2.20)$$

Next, with the help of [96, Eq.(26)], the closed-form equation of the CDF can be rewritten as

$$F_\gamma(\gamma) = \frac{(\alpha_t \beta_t)^{\frac{(\alpha_t + \beta_t)}{2}}}{\Gamma(\alpha_t)\Gamma(\beta_t)(\bar{\gamma})^{\frac{(\alpha_t + \beta_t)}{4}}} (\gamma)^{\frac{(\alpha_t + \beta_t)}{4} - 1} G_{1\ 3}^{2\ 1} \left[ \alpha_t \beta_t \sqrt{\frac{\gamma}{\bar{\gamma}}} \middle| \begin{matrix} 1 - \frac{\alpha_t + \beta_t}{2} \\ \frac{\alpha_t - \beta_t}{2}, \frac{\beta_t - \alpha_t}{2}, -\frac{\alpha_t + \beta_t}{2} \end{matrix} \right] \quad (2.21)$$

### 2.5.1.3 MGF under gamma-gamma distribution

The MGF of a RV  $\gamma$  is,  $\mathcal{M}_\gamma(s) = E\{\exp(-s\gamma)\} = \int_0^\infty \exp(-s\gamma)f_\gamma(\gamma)d\gamma$ , where  $E(\cdot)$  is the statistical expectation function and  $f_\gamma(\gamma)$  is the PDF. Employing (2.18), the MGF can be expressed as [97]

$$\mathcal{M}_\gamma(s) = \frac{(\alpha_t \beta_t)^{\frac{(\alpha_t + \beta_t)}{2}}}{2\Gamma(\alpha_t)\Gamma(\beta_t)(\bar{\gamma})^{\frac{(\alpha_t + \beta_t)}{4}}} \int_0^\infty \exp(-s\gamma) (\gamma)^{\frac{(\alpha_t + \beta_t)}{4} - 1} \times G_{0\ 2}^{2\ 0} \left[ \alpha_t \beta_t \sqrt{\frac{\gamma}{\bar{\gamma}}} \middle| \begin{matrix} - \\ \frac{\alpha_t - \beta_t}{2}, \frac{\beta_t - \alpha_t}{2} \end{matrix} \right] d\gamma \quad (2.22)$$

Applying the link between  $\exp(\cdot)$  and Meijer's G function [94, Eq.(8.4.3.1)],  $\exp(-x) = G_{0\ 1}^1\ 0 \left[ x \middle| \cdot \right]$ , the equation (2.21) may be rewritten as

$$\mathcal{M}_\gamma(s) = \frac{(\alpha_t \beta_t)^{\frac{(\alpha_t + \beta_t)}{2}}}{2\Gamma(\alpha_t)\Gamma(\beta_t)(\bar{\gamma})^{\frac{(\alpha_t + \beta_t)}{4}}} \int_0^\infty (\gamma)^{\frac{(\alpha_t + \beta_t)}{4} - 1} G_{0\ 1}^1\ 0 \left[ s\gamma \middle| \cdot \right] \times G_{0\ 2}^{2\ 0} \left[ \alpha_t \beta_t \sqrt{\frac{\gamma}{\bar{\gamma}}} \middle| \begin{matrix} - \\ \frac{\alpha_t - \beta_t}{2}, \frac{\beta_t - \alpha_t}{2} \end{matrix} \right] d\gamma \quad (2.23)$$

Finally, with the help of [94, Eq.(2.24.1.1)], the closed-form of the MGF (2.22) can be represented as

$$\mathcal{M}_\gamma(s) = \frac{(\alpha_t \beta_t)^{\frac{(\alpha_t + \beta_t)}{2}}}{4\pi \Gamma(\alpha_t) \Gamma(\beta_t) (\bar{\gamma})^{\frac{(\alpha_t + \beta_t)}{4}}} (s)^{-\frac{\alpha_t + \beta_t}{4}} G_{1\ 4}^{4\ 1} \left[ \frac{\alpha_t^2 \beta_t^2}{16 \bar{\gamma} s} \middle| \begin{matrix} 1 - \frac{\alpha_t + \beta_t}{4} \\ \frac{\alpha_t - \beta_t}{4}, \frac{\alpha_t - \beta_t + 2}{4}, \frac{\beta_t - \alpha_t}{4}, \frac{\beta_t - \alpha_t + 2}{4} \end{matrix} \right] \quad (2.24)$$

## 2.5.2 Generalised AT in absence of pointing error

The Málaga statistical distribution has been proposed by A. Jurado-Navas et al. in 2012 [27]. It is a novel and most generalized distribution to characterize the received irradiance fluctuation of an unbounded plane and spherical optical wave-front propagating through the medium having all possible degrees of turbulence. The main advantage of the Málaga distribution is its easy, mathematically tractable closed-form equation valid in a wide range (weak-to-strong) of turbulence regimes. This distribution, therefore, received significant attention in the research community for modeling any turbulence condition. In addition, different statistical distribution models can be developed by employing this particular distribution technique.

### 2.5.2.1 PDF under Málaga distribution

The PDF of the Málaga distribution for the received irradiance ( $I_a$ ) can be represented as [23]

$$f_{I_a}(I_a) = \mathcal{A} \sum_{k_t=1}^{\beta_t} a_k(I_a)^{\frac{\alpha_t + k_t}{2} - 1} k_{\alpha_t - k_t} \left( 2 \sqrt{\frac{\alpha_t \beta_t I_a}{g_t \beta_t + \bar{\Omega}_t}} \right) \quad (2.25)$$

where,  $\mathcal{A} \triangleq \frac{2(\alpha_t)^{\frac{\alpha_t}{2}}}{(g_t)^{1 + \frac{\alpha_t}{2}} \Gamma(\alpha_t)} \left( \frac{g_t \beta_t}{g_t \beta_t + \bar{\Omega}_t} \right)^{\beta_t + \frac{\alpha_t}{2}}$ ,  $a_k \triangleq \binom{\beta_t - 1}{k_t - 1} \frac{(g_t \beta_t + \bar{\Omega}_t)^{1 - \frac{k_t}{2}}}{(k_t - 1)!} \left( \frac{\bar{\Omega}_t}{g_t} \right)^{k_t - 1} \left( \frac{\alpha_t}{\beta_t} \right)^{\frac{k_t}{2}}$ , and  $\bar{\Omega}_t = \Omega_t + 2b_0 \rho_t + 2\sqrt{2b_0 \rho_t \Omega_t} \cos(\Phi_A - \Phi_B)$ . The parameters  $\alpha_t$ ,  $\beta_t$ ,  $g_t$  and  $\Omega_t$  are fading parameters associated with the atmospheric turbulence conditions [28].  $\alpha_t$  is a positive parameter related to an adequate number of the large-scale



scattering process;  $\beta_t$  is the fading parameter and is usually a natural number;  $g_t$  denotes the average power of the scattered component received by off-axis eddies, which is related to both average powers of the total scatter components ( $2b_0$ ) and the amount of scattering ( $\rho_t$ ). The value of the amount of scattering typically lies between 0 and 1.  $\Omega_t$  represents average power of the LOS components.  $K_v(\cdot)$  is the  $v^{\text{th}}$  order modified Bessel function of the second kind, and  $\Phi_A$  and  $\Phi_B$  are the scatter components of the deterministic phases of the LOS and the coupled to LOS factors respectively.

By a simple power transform process the above PDF expression can be presented in another form that involves the instantaneous electrical SNR ( $\gamma$ ) and average electrical SNR ( $\bar{\gamma}$ ) of the FSO link as follows.

$$f_\gamma(\gamma) = \frac{\mathcal{A}}{2} \sum_{k_t=1}^{\beta_t} a_k \frac{(\gamma)^{\frac{\alpha_t+k_t}{4}-1}}{(\bar{\gamma})^{\frac{\alpha_t+k_t}{4}}} K_{\alpha_t-k_t} \left( \mathcal{B} \sqrt{\alpha_t \beta_t} \sqrt{\frac{\gamma}{\bar{\gamma}}} \right) \quad (2.26)$$

Next, replacing the equivalent Meijer's G function of the 2<sup>nd</sup> order modified Bessel K function [94, Eq.(8.4.23.1)] in the above equation, (2.25), it becomes

$$f_\gamma(\gamma) = \frac{\mathcal{A}}{4} \sum_{k_t=1}^{\beta_t} a_k \frac{(\gamma)^{\frac{\alpha_t+k_t}{4}-1}}{(\bar{\gamma})^{\frac{\alpha_t+k_t}{4}}} G_{0 \ 2}^{2 \ 0} \left[ \frac{\mathcal{B}^2 \alpha_t \beta_t}{4} \sqrt{\frac{\gamma}{\bar{\gamma}}} \middle| \begin{matrix} - \\ \frac{\alpha_t-k_t}{2}, \frac{k_t-\alpha_t}{2} \end{matrix} \right] \quad (2.27)$$

where,  $\mathcal{B} = \frac{2}{\sqrt{g_t \beta_t + \Omega_t}}$ .

### 2.5.2.2 CDF under Málaga distribution

Employing the above form of PDF (2.27), the integral form of the CDF,  $F_\gamma(\gamma)$  can be expressed as

$$F_\gamma(\gamma) = \frac{\mathcal{A}}{4} \sum_{k_t=1}^{\beta_t} \frac{a_k}{(\bar{\gamma})^{\frac{\alpha_t+k_t}{4}}} \int_0^\gamma (\gamma)^{\frac{\alpha_t+k_t}{4}-1} G_{0 \ 2}^{2 \ 0} \left[ \frac{\mathcal{B}^2 \alpha_t \beta_t}{4} \sqrt{\frac{\gamma}{\bar{\gamma}}} \middle| \begin{matrix} - \\ \frac{\alpha_t-k_t}{2}, \frac{k_t-\alpha_t}{2} \end{matrix} \right] d\gamma \quad (2.28)$$

Now, using [96, Eq.(26)], the closed-form equation of the CDF can be obtained as

$$F_\gamma(\gamma) = \frac{\mathcal{A}}{2} \sum_{k_t=1}^{\beta_t} \frac{a_k}{(\bar{\gamma})^{\frac{\alpha_t+k_t}{4}}} (\gamma)^{\frac{\alpha_t+k_t}{4}} G_{1\ 3}^{2\ 1} \left[ \frac{\mathcal{B}^2 \alpha_t \beta_t}{4} \sqrt{\frac{\gamma}{\bar{\gamma}}} \middle| \begin{matrix} 1 - \frac{\alpha_t+k_t}{2} \\ \frac{\alpha_t-k_t}{2}, \frac{k_t-\alpha_t}{2}, -\frac{\alpha_t+k_t}{2} \end{matrix} \right] \quad (2.29)$$

### 2.5.2.3 MGF under Málaga distribution

Using (2.27) and the mathematical definition of MGF [97], the corresponding MGF ( $\mathcal{M}_\gamma(s)$ ) can be expressed as [98]

$$\mathcal{M}_\gamma(s) = \frac{\mathcal{A}}{4} \sum_{k_t=1}^{\beta_t} \frac{a_k}{(\bar{\gamma})^{\frac{\alpha_t+k_t}{4}}} \int_0^\infty (\gamma)^{\frac{\alpha_t+k_t}{4}-1} \exp(-s\gamma) G_{0\ 2}^{2\ 0} \left[ \frac{\mathcal{B}^2 \alpha_t \beta_t}{4} \sqrt{\frac{\gamma}{\bar{\gamma}}} \middle| \begin{matrix} - \\ \frac{\alpha_t-k_t}{2}, \frac{k_t-\alpha_t}{2} \end{matrix} \right] d\gamma \quad (2.30)$$

Now, using Meijer's G function of  $\exp(\cdot)$  [94, Eq.(8.4.3.1)], as  $\exp(-x) = G_{0\ 1}^1\ 0 \left[ x \middle| \cdot \right]$ , the above equation (2.30) may be rewritten as

$$\mathcal{M}_\gamma(s) = \frac{\mathcal{A}}{4} \sum_{k_t=1}^{\beta_t} \frac{a_k}{(\bar{\gamma})^{\frac{\alpha_t+k_t}{4}}} \int_0^\infty (\gamma)^{\frac{\alpha_t+k_t}{4}-1} G_{0\ 1}^1\ 0 \left[ s\gamma \middle| \cdot \right] G_{0\ 2}^{2\ 0} \left[ \frac{\mathcal{B}^2 \alpha_t \beta_t}{4} \sqrt{\frac{\gamma}{\bar{\gamma}}} \middle| \begin{matrix} - \\ \frac{\alpha_t-k_t}{2}, \frac{k_t-\alpha_t}{2} \end{matrix} \right] d\gamma \quad (2.31)$$

Next, with the help of [94, Eq.(2.24.1.1)], the closed-form of the equation (2.31) for MGF can be presented as

$$\mathcal{M}_\gamma(s) = \frac{\mathcal{A}}{8\pi} \sum_{k_t=1}^{\beta_t} \frac{a_k}{(\bar{\gamma})^{\frac{\alpha_t+k_t}{4}}} (s)^{-\frac{\alpha_t+k_t}{4}} G_{1\ 4}^{4\ 1} \left[ \frac{\mathcal{B}^4 \alpha_t^2 \beta_t^2}{256 \bar{\gamma} s} \middle| \begin{matrix} 1 - \frac{\alpha_t+k_t}{4} \\ \frac{\alpha_t-k_t}{4}, \frac{\alpha_t-k_t+2}{4}, \frac{k_t-\alpha_t}{4}, \frac{k_t-\alpha_t+2}{4} \end{matrix} \right] \quad (2.32)$$

### 2.5.3 Moderate-to-strong AT in presence of pointing error

The atmospheric turbulence results in pointing errors in the system. The received signal, in the presence of a pointing error, can be obtained from the product of three individual parameters such as  $I = I_a I_l I_p$ , where  $I_a$  is the irradiance fluctuation

of the transmitted optical beam,  $I_l$  is the amount of path loss due to atmospheric turbulence, and  $l_p$  is the pointing error coefficients. The atmospheric path loss does abide by the Beer-Lambert law. The amount of path loss for channel length  $x$  can be expressed as [99]  $I_l(x) = \exp(-\mu x)$ , where  $\mu$  is the linear attenuation coefficient, defined by  $\mu = \sigma C$ , with  $C$  the concentration of molecules present in the medium,  $\sigma$  the scattering coefficient. The pointing error coefficient is determined based on [25, Eq. (9)]. The channel characterization due to the combined effect of moderate-strong atmospheric turbulence and pointing error is made by some mathematical derivation:

### 2.5.3.1 PDF under gamma-gamma distribution

The unconditional PDF of the FSO link associated with atmospheric turbulence and the pointing error effect can be described using (2.13) and (2.14) for moderate-to-strong turbulence conditions as

$$f_I(I) = \int f_{I|a}(I|a) f_{I_a}(I_a) dI_a \quad (2.33)$$

where,  $f_{I|a}(I|a)$  is the joint conditional probability. It significantly depends on the misalignment fading and may be expressed as

$$f_{I|a}(I|a) = \frac{\xi^2}{A_0^{\xi^2} I_a I_l} \left( \frac{I}{I_a I_l} \right)^{\xi^2-1}, 0 \leq I \leq I_a I_l A_0 \quad (2.34)$$

using (2.34) in (2.33), the PDF becomes

$$f_I(I) = \int_{\frac{I}{I_l A_0}}^{\infty} \frac{\xi^2}{A_0^{\xi^2} I_a I_l} \left( \frac{I}{I_a I_l} \right)^{\xi^2-1} f_{I_a}(I_a) dI_a \quad (2.35)$$

We have considered GG statistical distribution to characterize the moderate-strong atmospheric turbulence condition.  $f_{I_a}$  in (2.35) can be replaced by (2.34) and the

above equation becomes

$$f_I(I) = \frac{2\xi^2(\alpha_t\beta_t)^{\frac{(\alpha_t+\beta_t)}{2}}}{(A_0I_l)^{\xi^2}\Gamma(\alpha_t)\Gamma(\beta_t)}(I)^{\xi^2-1} \int_{\frac{I}{I_l A_0}}^{\infty} (I_a)^{\frac{(\alpha_t+\beta_t)}{2}-\xi^2-1} K_{\alpha_t-\beta_t} \left(2\sqrt{\alpha_t\beta_t I_a}\right) dI_a \quad (2.36)$$

Next, with the help of [94, Eq.(8.4.23.1),Eq.(2.24.2.3)] and after some mathematical manipulation (2.36), the PDF can be expressed as [43][44]

$$f_I(I) = \frac{\xi^2\alpha_t\beta_t}{A_0I_l\Gamma(\alpha_t)\Gamma(\beta_t)} G_{1\ 3}^{3\ 0} \left[ \frac{\alpha_t\beta_t I}{A_0I_l} \middle| \begin{matrix} \xi^2 \\ \xi^2-1, \alpha_t-1, \beta_t-1 \end{matrix} \right] \quad (2.37)$$

The above equation (2.37) can be expressed in terms of the end-to-end average electrical SNR ( $\bar{\gamma}$ ) and instantaneous electrical SNR ( $\gamma$ ) of the system as

$$f_\gamma(\gamma) = \frac{\xi^2}{2\gamma\Gamma(\alpha_t)\Gamma(\beta_t)} G_{1\ 3}^{3\ 0} \left[ \alpha_t\beta_t \mathcal{K} \sqrt{\frac{\gamma}{\bar{\gamma}}} \middle| \begin{matrix} \xi^2+1 \\ \xi^2, \alpha_t, \beta_t \end{matrix} \right] \quad (2.38)$$

where,  $\mathcal{K}$  is defined as  $\frac{\xi^2}{\xi^2+1}$ , and  $\xi$  is related with pointing error as discussed earlier. When the numeral value of  $\xi \rightarrow \infty$ , the influence of the pointing error can be ignored and the performance of the system depends only on the atmospheric turbulence.

### 2.5.3.2 CDF under gamma-gamma distribution

Using (2.38), the corresponding CDF, may be represented as

$$F_\gamma(\gamma) = \frac{\xi^2}{2\Gamma(\alpha_t)\Gamma(\beta_t)} \int_0^\gamma \gamma^{-1} G_{1\ 3}^{3\ 0} \left[ \alpha_t\beta_t \mathcal{K} \sqrt{\frac{\gamma}{\bar{\gamma}}} \middle| \begin{matrix} \xi^2+1 \\ \xi^2, \alpha_t, \beta_t \end{matrix} \right] d\gamma \quad (2.39)$$

The closed-form of which can be expressed, with the help of [96, Eq.(26)], as

$$F_\gamma(\gamma) = \frac{\xi^2}{\Gamma(\alpha_t)\Gamma(\beta_t)} G_{2\ 4}^{3\ 1} \left[ \alpha_t\beta_t \mathcal{K} \sqrt{\frac{\gamma}{\bar{\gamma}}} \middle| \begin{matrix} 1, \xi^2+1 \\ \xi^2, \alpha_t, \beta_t, 0 \end{matrix} \right] \quad (2.40)$$

### 2.5.3.3 MGF under gamma-gamma distribution

For FSO link under atmospheric turbulence represented by the Gamma-Gamma distribution and in presence of pointing error, MGF can be expressed using (2.38) as

$$\mathcal{M}_\gamma(s) = \frac{\xi^2}{2\Gamma(\alpha_t)\Gamma(\beta_t)} \int_0^\infty \gamma^{-1} \exp(-s\gamma) G_{1\ 3}^{3\ 0} \left[ \alpha_t \beta_t \mathcal{K} \sqrt{\frac{\gamma}{\bar{\gamma}}} \middle| \begin{matrix} \xi^2+1 \\ \xi^2, \alpha_t, \beta_t \end{matrix} \right] d\gamma \quad (2.41)$$

Using [95, Eq.(2.24.3.1)], the corresponding closed-form expression of the above function can be represented as

$$\mathcal{M}_\gamma(s) = \frac{\xi^2 (2)^{(\alpha_t + \beta_t)}}{8\pi \Gamma(\alpha_t) \Gamma(\beta_t)} G_{3\ 6}^{6\ 1} \left[ \frac{\alpha_t^2 \beta_t^2 \mathcal{K}^2}{16 \bar{\gamma} s} \middle| \begin{matrix} 1, \frac{\xi^2+1}{2}, \frac{\xi^2+2}{2} \\ \frac{\xi^2}{2}, \frac{\xi^2+1}{2}, \frac{\alpha_t}{2}, \frac{\alpha_t+1}{2}, \frac{\beta_t}{2}, \frac{\beta_t+1}{2} \end{matrix} \right] \quad (2.42)$$

## 2.5.4 Generalised AT in presence of pointing error

Here, the Málaga distribution model is employed to characterize the irradiance fluctuation that arises from the impact of atmospheric turbulence, and the important functions of PDF, CDF, and MGF under the combined influence of atmospheric turbulence and misalignment fading are described.

### 2.5.4.1 PDF under Málaga distribution

The PDF under Málaga distribution to represent atmospheric turbulence, in presence of the pointing error, becomes, using (2.25) and (2.35) as

$$f_I(I) = \frac{(I)^{\xi^2-1} \xi^2}{(A_0 I_l)^{\xi^2}} \mathcal{A} \sum_{k_t=1}^{\beta_t} a_k \int_{\frac{I}{I_l A_0}}^\infty (I_a)^{\frac{\alpha_t+k_t}{2} - \xi^2 - 1} k_{\alpha_t - k_t} \left( 2 \sqrt{\frac{\alpha_t \beta_t I_a}{g_t \beta_t + \bar{\Omega}_t}} \right) dI_a \quad (2.43)$$

Now, used [94, Eq.(8.4.23.1),Eq.(2.24.2.3)] and after some mathematical calculation, the above equation (2.43) can be expressed as [28] [100]

$$f_I(I) = \frac{\xi^2 \mathcal{A}}{2I} \sum_{k_t=1}^{\beta_t} b_k G_{1 \ 3}^{3 \ 0} \left[ \frac{\alpha_t \beta_t}{g_t \beta_t + \bar{\Omega}_t} \frac{I}{I_l A_0} \middle| \xi^2, \alpha_t, k_t \right]^{\xi^2+1} \quad (2.44)$$

where,  $b_k$  is defined as  $b_k = a_k \left[ \frac{\alpha_t \beta_t}{g_t \beta_t + \bar{\Omega}_t} \right]^{-(\alpha_t + k_t)/2}$ , and  $A_0$  is the pointing error constant. Eq.(2.43) can further be expressed by the instantaneous SNR ( $\gamma$ ) and average SNR ( $\bar{\gamma}$ ) of the system as

$$f_\gamma(\gamma) = \frac{\xi^2 \mathcal{A}}{4\gamma} \sum_{k_t=1}^{\beta_t} b_k G_{1 \ 3}^{3 \ 0} \left[ \mathcal{B} \sqrt{\frac{\gamma}{\bar{\gamma}}} \middle| \xi^2, \alpha_t, k_t \right]^{\xi^2+1} \quad (2.45)$$

where  $\mathcal{B} = \xi^2 \alpha_t \beta_t (g_t + \bar{\Omega}) / \{(\xi^2 + 1)(g_t \beta_t + \bar{\Omega})\}$ .

#### 2.5.4.2 CDF under Málaga distribution

Following the same procedure done in case of finding the CDF of GG with pointing error, the CDF, under the combined influence of the turbulence represented by Málaga distribution and the misalignment fading, can be described (2.45) as

$$F_\gamma(\gamma) = \frac{\xi^2 \mathcal{A}}{4} \sum_{k_t=1}^{\beta_t} b_k \int_0^\gamma (\gamma)^{-1} G_{1 \ 3}^{3 \ 0} \left[ \mathcal{B} \sqrt{\frac{\gamma}{\bar{\gamma}}} \middle| \xi^2, \alpha_t, k_t \right]^{\xi^2+1} d\gamma \quad (2.46)$$

By using [96, Eq.(26)], the closed-form expression of the above equation can be developed as

$$F_\gamma(\gamma) = \frac{\xi^2 \mathcal{A}}{2} \sum_{k_t=1}^{\beta_t} b_k G_{2 \ 4}^{3 \ 1} \left[ \mathcal{B} \sqrt{\frac{\gamma}{\bar{\gamma}}} \middle| 1, \xi^2+1, \xi^2, \alpha_t, k_t, 0 \right] \quad (2.47)$$

### 2.5.4.3 MGF under Málaga distribution

The integral form of MGF can be derived with the help of its mathematical definition and (2.45) as

$$\mathcal{M}_\gamma(s) = \frac{\xi^2 \mathcal{A}}{4} \sum_{k_t=1}^{\beta_t} b_k \int_0^\infty (\gamma)^{-1} \exp(-s\gamma) G_{1 \ 3}^{3 \ 0} \left[ \mathcal{B} \sqrt{\frac{\gamma}{\bar{\gamma}}} \middle| \begin{matrix} \xi^2+1 \\ \xi^2, \alpha_t, k_t \end{matrix} \right] d\gamma \quad (2.48)$$

Now, using [94, eq. (2.24.3.1)] in the above equation, we may derive the closed-form of the estimated MGF as

$$\mathcal{M}_\gamma(s) = \frac{\xi^2 \mathcal{A}}{8\pi} \sum_{k_t=1}^{\beta_t} b_k (2)^{\alpha_t + \beta_t - 1} G_{3 \ 6}^{6 \ 1} \left[ \frac{\mathcal{B}^2}{16s\bar{\gamma}} \middle| \begin{matrix} 1, \frac{\xi^2+1}{2}, \frac{\xi^2+2}{2} \\ \frac{\xi^2}{2}, \frac{\xi^2+1}{2}, \frac{\alpha_t}{2}, \frac{\alpha_t+1}{2}, \frac{k_t}{2}, \frac{k_t+1}{2} \end{matrix} \right] \quad (2.49)$$

## 2.6 Diversity model

The diversity technique is employed extensively to mitigate the effect of atmospheric turbulence on the FSO communication system. It can be achieved using single or multiple beams and apertures at either or both transceiver terminals. A separation of  $\frac{\lambda}{2}$ , where  $\lambda$  is the wavelength of the propagation wave, should be maintained between the source and/ or destination apertures so that they are uncorrelated and contribute to diversity gain. Diversity schemes, when implemented, give rise to different link combinations like single-input-multiple-output (SIMO), multiple-input-single-output (MISO), and multiple-input-multiple-output (MIMO).

### 2.6.1 Transmit diversity

The transmit diversity scheme is used to send the same information from the transmitter by transmitting multiple beams through a MISO arrangement. Various transmit diversity techniques have been employed to develop the MISO FSO communication system [101, 58]. The two transmit diversity techniques used in this thesis

will be discussed here.

### 2.6.1.1 Alamouti space time block code

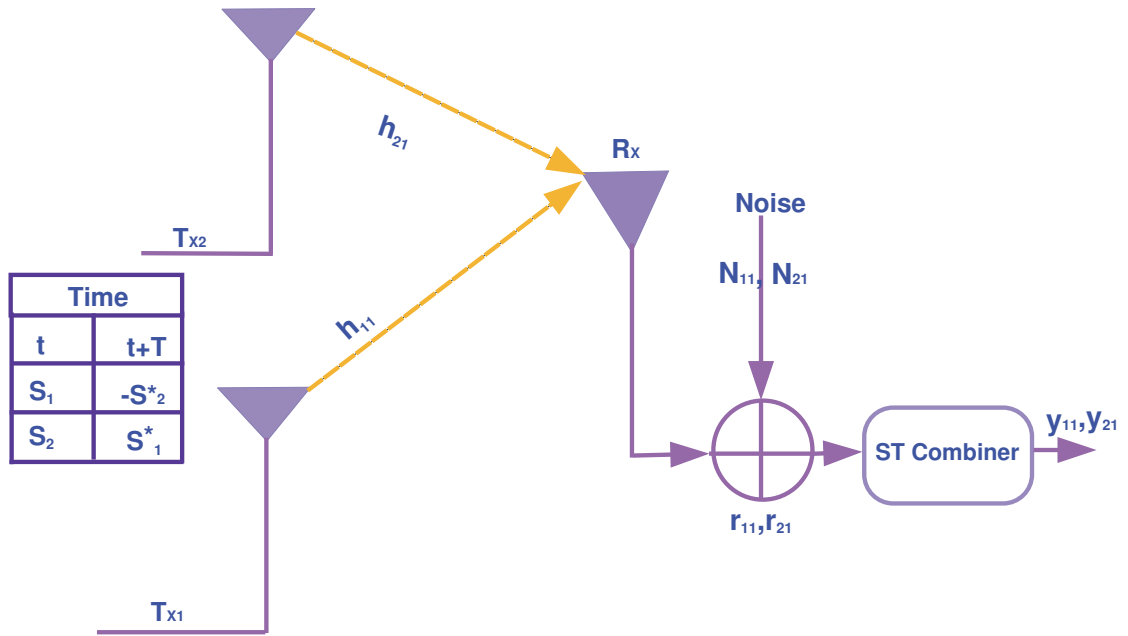


FIGURE 2.3: The Alamouti STBC with two transmitters and one receiver.

It is a classical two-beam transmit diversity scheme that uses a transmitter antenna and a single receiver antenna. The scheme is established on three fundamental functions: Information is encoded and transmitted in the sequence of encoded information symbols in the transmitter section. At the receiver end, the combiner combines the symbols of the incoming signal. The maximum likelihood detection technique is implemented at the receiver as the decision rule. The main advantage of the system is that it does not need any bandwidth expansion and feedback from the receiver terminal.

Fig. 2.3 presents that the Alamouti STBC scheme with two transmit antennas ( $T_{X1}$  and  $T_{X2}$ ) and one receiving antenna ( $R_X$ ). According to the scheme, two symbols are transmitted simultaneously by  $T_{X1}$  and  $T_{X2}$  at a given period. If  $\{s_1, s_2\}$  be



two successive baseband information symbols to be transmitted, during the first time slot  $T_{X_1}$  transmits symbol  $s_1$  and  $T_{X_2}$  transmits the symbol  $s_2$ ; in the next time slot,  $T_{X_1}$  transmits  $-s_2^*$  symbol and  $T_{X_2}$  transmits  $s_1^*$ , where  $(\cdot)^*$  indicates the complex conjugate of the symbol [31].

At the receiver terminal, the received signals ( $R_X$ ) appearing over these two-time intervals can be expressed as follows:

$$r_{11} = h_{11}s_1 + h_{21}s_2 + N_{11} \quad (2.50a)$$

$$r_{21} = -h_{11}s_2^* + h_{21}s_1^* + N_{21} \quad (2.50b)$$

where,  $h_{11}$  and  $h_{21}$  are the channel gain coefficients between transmitter and receiver antenna for  $T_{X_1}$  and  $T_{X_2}$  transmitter antennas respectively. Each signal is affected by zero-mean Gaussian noise; <sup>1</sup>  $N_{11}$  and  $N_{12}$ , indicate the degrees of noise for the first and second-time slot, respectively, with variance  $N_0$ . The noise is assumed to be statistically independent of the channel fading. The space-time (ST) combiner attached to  $R_X$  antenna branch decodes the received signal using Alamouti decoders and produces an output pair as follows

$$y_{11} = \hat{h}_{11}^* r_{11} + \hat{h}_{21} r_{21}^* \quad (2.51a)$$

$$y_{21} = -\hat{h}_{21} r_{21}^* + \hat{h}_{11}^* r_{11} \quad (2.51b)$$

where  $\hat{h}_{11}$  and  $\hat{h}_{21}$  are the estimate of  $h_{11}$  and  $h_{21}$  respectively. It may be noted that channel state information (CSI) is not required at transmitter for the Alamouti scheme. The estimation of channel coefficients ( $\hat{h}_{ij}$ ) at the receiver is generally performed with the help of periodic pilot symbol transmission.

---

<sup>1</sup>In optical systems the dominate noise we encounter is signal spontaneous emission beat noise. However, the presence of optical band pass filter before the optical pre-amplifier section in the receiver makes the noise band limited and such a noise can be approximated with a Gaussian distribution.

### 2.6.1.2 Spatial shift keying

The spatial shift keying (SSK) scheme is a particular type of spatial modulation (SM), where a train of message bits is mapped into an SSK encoder block (see Fig. 2.4) and locates the particular transmitter antenna number by which the symbol is transmitted. Next, at the receiving end, the receiver checks the transmitted symbol, estimates the antenna number, and de-maps the corresponding message bits. A block diagram of the SSK model shown in Fig. 2.4, consists of  $N_t$  number of

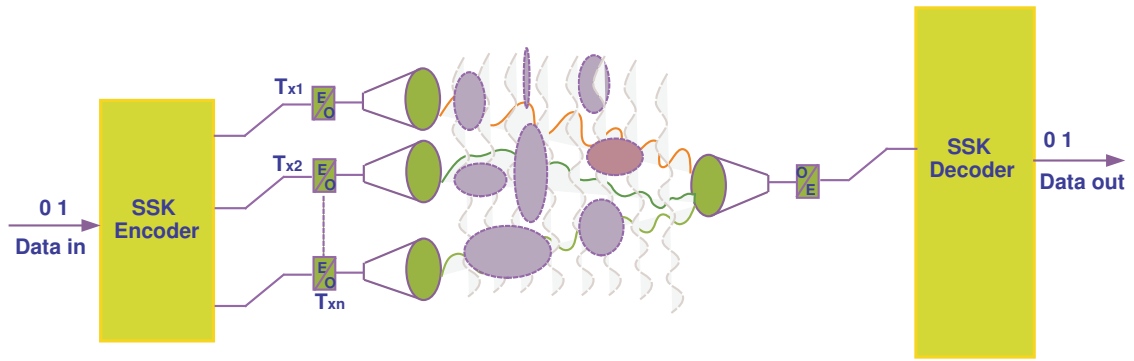


FIGURE 2.4: A typical SSK system with  $N_t$  transmitters and a single receiver.

transmitter antennas and one receiver antenna. Let us consider a random sequence of input bits  $b = [b_1, b_2, b_3, \dots, b_m]$  enter into the SSK encoder and the corresponding output of the encoder is  $s = [s_1, s_2, s_3, \dots, s_n]$ , where  $m$  and  $n$  are the total numbers of input and output bits of the SSK encoder. Resultant encoded output comes into the SSK mapper to compose a group of  $t = \log_2 N_t$  bits producing a constellation vector  $x = [x_1, x_2, x_3, \dots, x_{N_t}]^T$ , with unit power. In the SSK transmission rule, during symbol transfer, only one antenna remains ON while all others remain in OFF mode. The mapped modulated signal is next transmitted over the channel and experiences the additive white Gaussian noise (AWGN). At the receiver end, the received signal is expressed by  $y = \sqrt{\bar{\gamma}}HX + N$ , where  $\bar{\gamma}$  indicates the average SNR at every received antenna, where,  $H$  and  $N$  are respectively the channel gain matrix and the additive noise. The channel gain matrix is represented as  $H = [h_1, h_2, \dots, h_{N_t}]$

In the transmission process of the SSK scheme, the estimated modulated signal is grouped into  $t = \log_2 N_t$  bits and mapped by a symbol of  $x_j$ . After being mapped together, they are transmitted from the  $x_j$  antenna at the transmitting terminal. During the transmission period of the symbol, only  $x_j$  antenna remains ON, and the rest of the antennas are in OFF mode, which means  $x_j = 1$  for all value of  $j$ . Thus, vector position ' $j$ ' indicates the active antenna at the data transmitting period.

$$x_j \triangleq [0, 0, \dots, 1(j^{th}), 0 \dots 0]^T \quad (2.52)$$

where  $[\cdot]^T$  represents the transpose of the matrix element. The received signal for each transmitter antenna can be derived by mathematical expression as

$$Y = \sqrt{\gamma} x_j h_j + N \quad (2.53)$$

At the receiver end, first, the decoder estimates the source index and then demaps the symbol. According to the detection principle of the SSK modulation technique, the optimal detector follows the maximum likelihood approach. The estimated antenna index is given by [102]

$$\hat{j} = \underset{j}{\operatorname{argmax}} P_y(Y|x_j, H) = \underset{j}{\operatorname{argmin}} |Y - \sqrt{\gamma} h_j|^2 \quad (2.54)$$

with ,  $1 \leq j \leq N_t$  .

## 2.6.2 Receive diversity

The receiver diversity is a technique to reduce the fading effect at the receiving end of the system. In this scheme, the receiver aperture collects the multi-branch signal from multiple directions and combines them to produce the estimated output. Thus, receiver diversity techniques essentially result in SIMO FSO configuration [103, 104]. At the receiver end, various combining techniques such as SC, equal gain

combining (EGC), maximal ratio combining (MRC), and many more [105, 106, 107] are adopted to derive the desired output from the multiple signals received. Out of these techniques, SC is the simplest and requires only one active receiver chain. In addition to SC, a different diversity method known as switch-and-examine (SEC) combining will also be investigated in this thesis. Compared to SC, SEC reduces switching between branches and is an excellent choice to implement diversity in an FSO link in order to mitigate the fading effect.

### 2.6.2.1 Switch-and-examine combining

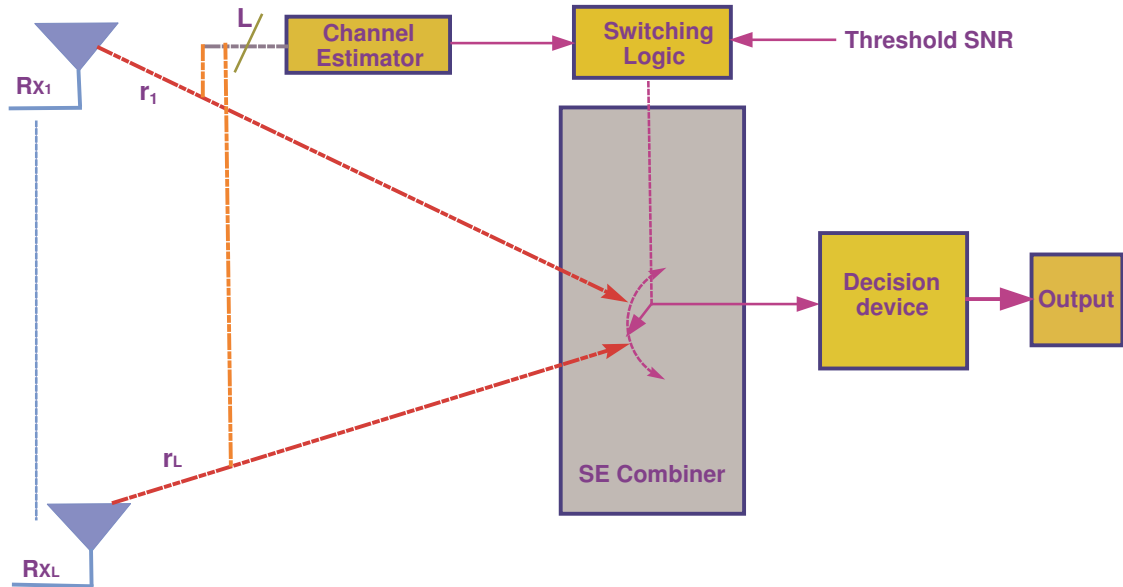


FIGURE 2.5: The classical multi-branch switch-and-examine combining.

Fig. 2.5 presents the classical  $L$ -branch SEC scheme. It is one type of the switch-and-stay combining (SSC) technique. Generally, the SSC scheme fits two branch diversity orders and is not suitable for additional branches when the branches are equicorrelated and identically distributed [108]. On the other hand, an SEC combining technique can efficiently handle signals in multiple (more than two) branches. In this scheme, if the signal quality of the current branch is not satisfactory, the combiner switches to the next available branch and checks the [intensity](#) of the signal

in that branch. This process is repeated until either the acceptable path is found or all diversity branches are examined. Finally, the combiner chooses the best of all the explored paths [109] of the receiver terminal. The CDF, PDF, and MGF of the classical multi-branch SEC scheme are given below:

**CDF:** The diversity branches are assumed to be i.i.d or equicorrelated. In that case, the CDF of the system in terms of end-to-end SNR ( $\gamma$ ) with classical multi-branch SEC is described as [110, eq. (9.340)]

$$F_{\gamma_{SEC}}(\gamma) = \begin{cases} [F_{\gamma}(\gamma_{th})]^{N_r-1} F_{\gamma}(\gamma) & ; \gamma < \gamma_{th} \\ \sum_{j=0}^{N_r-1} [F_{\gamma}(\gamma) - F_{\gamma}(\gamma_{th})] [F_{\gamma}(\gamma_{th})]^j + [F_{\gamma}(\gamma_{th})]^{N_r} & ; \gamma \geq \gamma_{th} \end{cases} \quad (2.55)$$

where  $F_{\gamma}(\gamma_{th})$  represents the common CDF of the SNR for the individual diversity branch,  $\gamma_{th}$  is the standard predetermined switching threshold of the system, and  $N_r$  indicates the number of diversity path.

**PDF:** The PDF can be obtained by differentiating the equation (2.55) with respect to  $\gamma$ , and the resultant expression is as follows [108, eq. (35)]

$$f_{\gamma_{SEC}}(\gamma) = \begin{cases} f_{\gamma}(\gamma) [F_{\gamma}(\gamma_{th})]^{N_r-1} & ; \gamma < \gamma_{th} \\ f_{\gamma}(\gamma) \sum_{j=0}^{N_r-1} [F_{\gamma}(\gamma_{th})]^j & ; \gamma \geq \gamma_{th} \end{cases} \quad (2.56)$$

where  $f_{\gamma}(\gamma)$  indicates the common PDF of each diversity path of the system.

**MGF:** The MGF of classical multi-path SEC scheme may be defined with "partial" MGF as given by [110, eq. (9.342)]

$$\mathcal{M}_{\gamma_{SEC}}(s) = [F_{\gamma}(\gamma_{th})]^{N_r-1} \mathcal{M}_{\gamma}(s) + \sum_{j=0}^{N_r-2} [F_{\gamma}(\gamma_{th})]^j \Psi(s) \quad (2.57)$$

where  $\mathcal{M}_{\gamma}(s)$  is the common MGF of the individual diversity branch, and  $\Psi(s) = \int_{\gamma_{th}}^{\infty} \exp(s\gamma) f_{\gamma}(\gamma) d\gamma$ , where,  $f_{\gamma}(\gamma)$  is the PDF of the individual diversity branch.

The equation (2.57) is called the "partial" MGF of the system, and that could be expressed in closed-form for distinct fading environment.

### 2.6.2.2 Selection combining

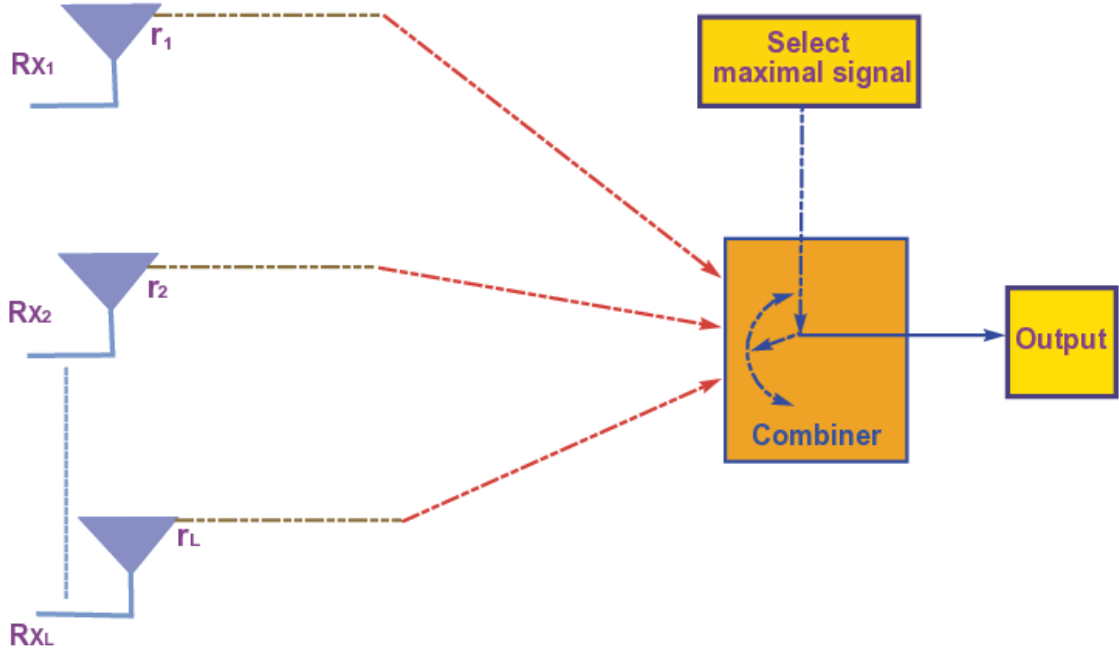


FIGURE 2.6: The classical selection combining technique.

Selection combining (SC) is a linear type receiver diversity scheme extensively applied in the receiver terminal of the communication system for digital signals transmitted over multi-path fading channels [111, 110]. This scheme has a simple architectural setup since it naturally works with only one diversity branch out of many branches in the system. Fig. 2.7a indicates the classical SC technique with L diversity branches. Generally, the combiner selects the diversity branch with the highest SNR among all other available branches [112]. The combiner selects the branch which has the maximal SNR of all diversity branches, and it may be written as  $\gamma_{out} = \arg \max(\gamma_L)$ . In Chapter 6, we have incorporated this diversity scheme to develop the SSK-SC- based MIMO FSO system.

## 2.7 Performance metrics

The performance of the FSO communication system is analyzed by three standard performance metrics: outage probability, average bit error rate, and average capacity. Analytical closed-form expression of each of the above parameters will be derived in the present chapter. The definition, along with the mathematical expression of each metric, will be presented first. Next, these parameters will be evaluated for a SISO FSO system under different degrees of turbulence conditions and in the absence and presence of pointing error.

### 2.7.1 Outage probability

The outage probability (OP), as the name implies, is known as the probability of a fade or outage of the system. It defines the point at which the power level of the received signal falls below a target power level, the power level being expressed in terms of the SNR of the system. If the instantaneous end-to-end SNR of a system is  $\gamma$ , and the corresponding minimum threshold level is  $\gamma_{th}$ . The condition of the probability of the outage event is  $Pr(\gamma \leq \gamma_{th})$ . The OP is a critical parameter to provide the QoS of any communication system. Its useful mathematical definition can be given as

$$\begin{aligned} P_{out}(\gamma_{th}) &= Pr(\gamma \leq \gamma_{th}) = \int_0^{\gamma_{th}} f_{\gamma}(\gamma) d\gamma \\ &= F_{\gamma}(\gamma_{th}) \end{aligned} \tag{2.58}$$

where  $f_{\gamma}(\cdot)$  is the PDF of the turbulent link characterized by a statistical distribution that suits the severity of weather conditions.

### 2.7.2 Average bit error rate

The average bit error rate (ABER) is a key parameter used to calculate how many erroneous bit arrives at the user end during the data transmission period. It is a simple ratio between the number of error bits received at the remote end and the total number of bits transmitted from the transmitter terminal,  $\text{BER} = \frac{\text{number of error bits}}{\text{total number of bits transmitted}}$ . Estimation of BER becomes complex as a transmitted signal gets corrupted by noise in the communicating medium. Generally, for a noisy medium, the BER of the system is presented in terms of probability of error function  $P_e(\gamma)$ , and it is the function of the normalized SNR, where  $\text{SNR}(\gamma) = E_b/N_0$ , with  $E_b$  denoting energy per bit and  $N_0$  is the noise power spectral density. The probability of error function is different for different modulation schemes. The average BER of the system can be presented in the integral form under fading channel as

$$P_e = \int_0^{\infty} P_e(\gamma) f_{\gamma}(\gamma) d\gamma \quad (2.59)$$

where  $f_{\gamma}(\cdot)$  is the PDF of the turbulence-induced fading channel.

### 2.7.3 Average capacity

The maximum data transmission rate through the communication medium in a single signaling interval is called the channel capacity (C). It is one of the most vital parameters for any communication system, measuring the maximum average data transmission rate (bits/s/Hz) of the system. For turbulence-induced fading channels, a reduced power level of the transmitted signal causes channel capacity to fluctuate. In fading channel, the capacity is determined using the well-known Shannon's formula in terms of instantaneous SNR ( $\gamma$ ) as  $C(\gamma) = B \log_2(1 + \gamma)$ , where,  $B$  is the bandwidth of the transmitted signal. To find the average channel capacity under different fading channels, it needs to average the  $C(\gamma)$  over the PDF



of the system. Thus,  $C(\gamma)$  can be expressed as

$$C(\gamma) = B \int_0^{\infty} \log_2(1 + \gamma) f_{\gamma}(\gamma) d\gamma \quad (2.60)$$

## 2.8 Numerical results and discussion for SISO FSO link

In this chapter, we have provided the OP of the SISO FSO system based on the GG and general Málaga distribution model for various atmospheric turbulence conditions with the presence of pointing error and the absence of a pointing error regime.

The average BER of the system will be estimated here using on-off-keying (OOK) modulation, the simplest possible digital modulation scheme for a light carrier. Using the probability of error function of the OOK modulation scheme (2.59), the ABER may be expressed as

$$\begin{aligned} P_e &= \int_0^{\infty} Q(\sqrt{\gamma}) f_{\gamma}(\gamma) d\gamma \\ &= \frac{1}{2} \int_0^{\infty} \text{erfc}\left(\sqrt{\frac{\gamma}{2}}\right) f_{\gamma}(\gamma) d\gamma \end{aligned} \quad (2.61)$$

where,  $Q(\sqrt{\cdot})$  is called the Q-function, expressed as  $Q(x) = \frac{1}{2} \text{erfc}\left(\frac{x}{\sqrt{2}}\right)$ ,  $\text{erfc}(\cdot)$ , being the complimentary error function.

The average capacity for a single FSO link, considering the influences of pointing error and absence of pointing error, is also presented in this section.

To represent various atmospheric severity, we consider three sets of atmospheric turbulence parameters  $\{\alpha_t, \beta_t\} = \{(4.20, 2.72), (3.99, 1.65), (2.20, 0.65)\}$  under GG distribution and another three sets for general Málaga distribution as  $\{\alpha_t, \beta_t\} = \{(5.41, 32), (2.292), (2.29, 1)\}$ . All sets of atmospheric turbulence parameters were calculated based on Eq.(2.15) and Eq.(2.16). On the other hand, pointing errors are

Performance metric	Parameters		
Outage probability	Threshold SNR ( $\gamma_{th}$ )	2 dB and 5 dB	
	SNR ()	0 – 60 dB, with 3 dB interval	
	Number of Iteration	20	
	Iteration point	$10^5$	
Average bit error rate	Number of bits	$10^6$	
	SNR ()	0 – 60 dB, with 3 dB interval	
	Number of Iteration	20	
Average capacity	SNR ()	0 – 30 dB, with 3 dB interval	
	Number of Iteration	20	
	Iteration Point	$10^5$	
Pointing Error	0.5607, 0.6636, 0.8565		
Atmospheric Turbulence	Gamma-Gamma		
	$\alpha_t = 4.20$	$\alpha_t = 3.99$	$\alpha_t = 2.20$
	$\beta_t = 2.72$	$\beta_t = 1.65$	$\beta_t = 0.65$
	Málaga		
	$\alpha_t = 5.41$	$\alpha_t = 2.29$	$\alpha_t = 2.29$
	$\beta_t = 3$	$\beta_t = 2$	$\beta_t = 1$

calculated using the pointing error setting parameters as on Table 2.2. Parameters associated with the general Málaga statistical distribution are,  $\rho = 0.988$ ,  $b_0 = 0.6525$ ,  $\Omega = 0.4618$ , and  $\Phi_A - \Phi_B = \frac{\pi}{2}$ .

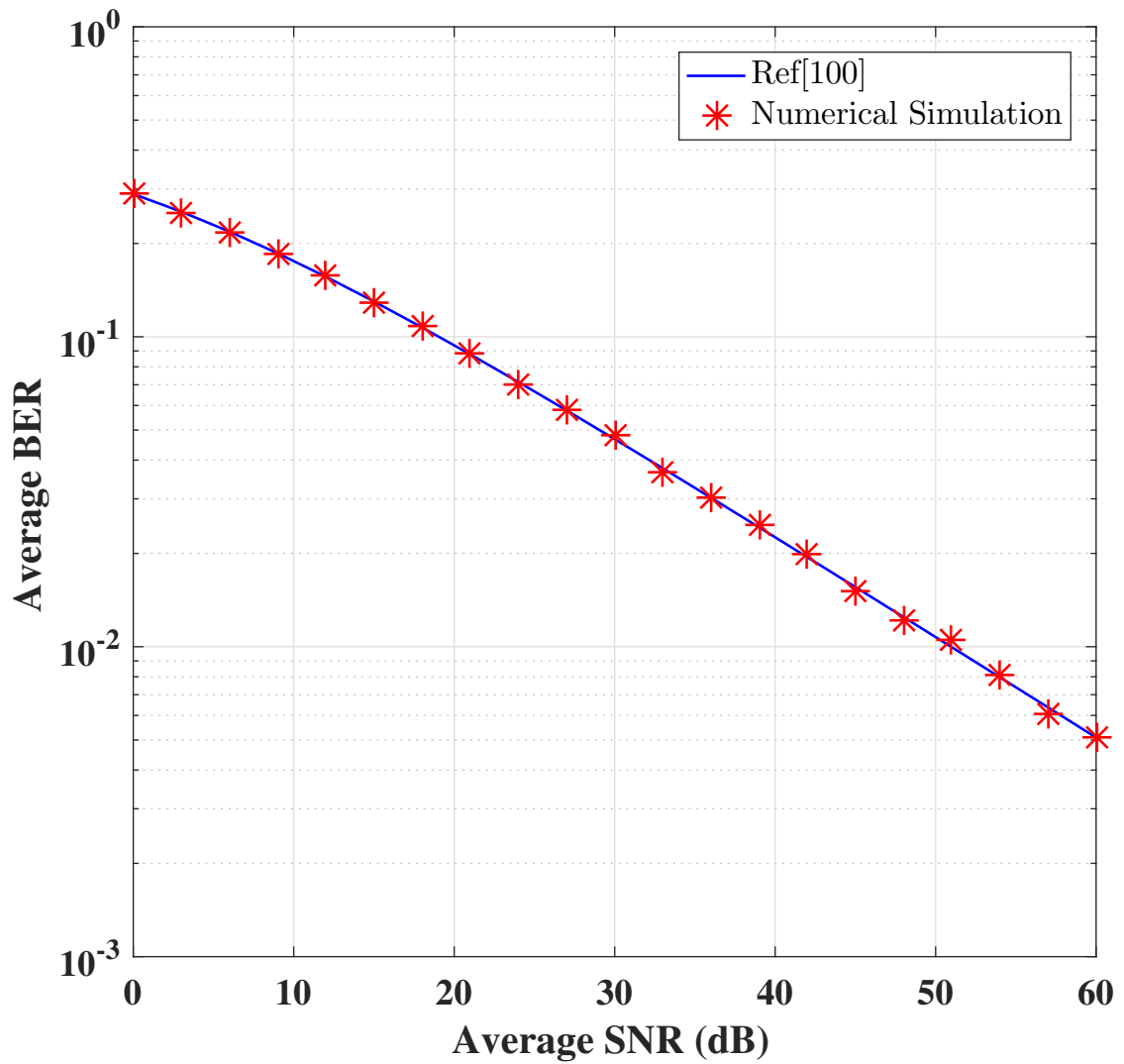


Figure 2.7 (a) Validation of the numerical simulation approach. [SISO-FSO, GG turbulence  $\alpha_t = 2.20$  and  $\alpha_t = 0.65$ , No pointing error].

With all the above parameters, OP, ABER, and average capacity are determined using their mathematical expressions and plotted against average SNR. All the analytical results are compared with the results from the Monte Carlo simulation. Details of the code for turbulent channel simulations are provided in Appendix(G). The OP of the SISO FSO link for various atmospheric turbulence conditions without and with the influence of misalignment fading Fig. 2.8(a) and Fig. 2.8(b) present analytical and simulation results using Gamma-Gamma distribution model for the turbulent channel, while Fig. 2.8(c) and Fig. 2.8(d) are those for Málaga distribution model. Analytical and simulation results are found to match closely. All the graphical plots reveal that the system performance strongly depends on the severity of the weather condition and the effect of misalignment fading. Similarly, the average BER of the SISO FSO link is presented in Fig. 2.9(a) to Fig. 2.9(d) and average capacity in Fig. 2.10(a) to Fig. 2.10(d).

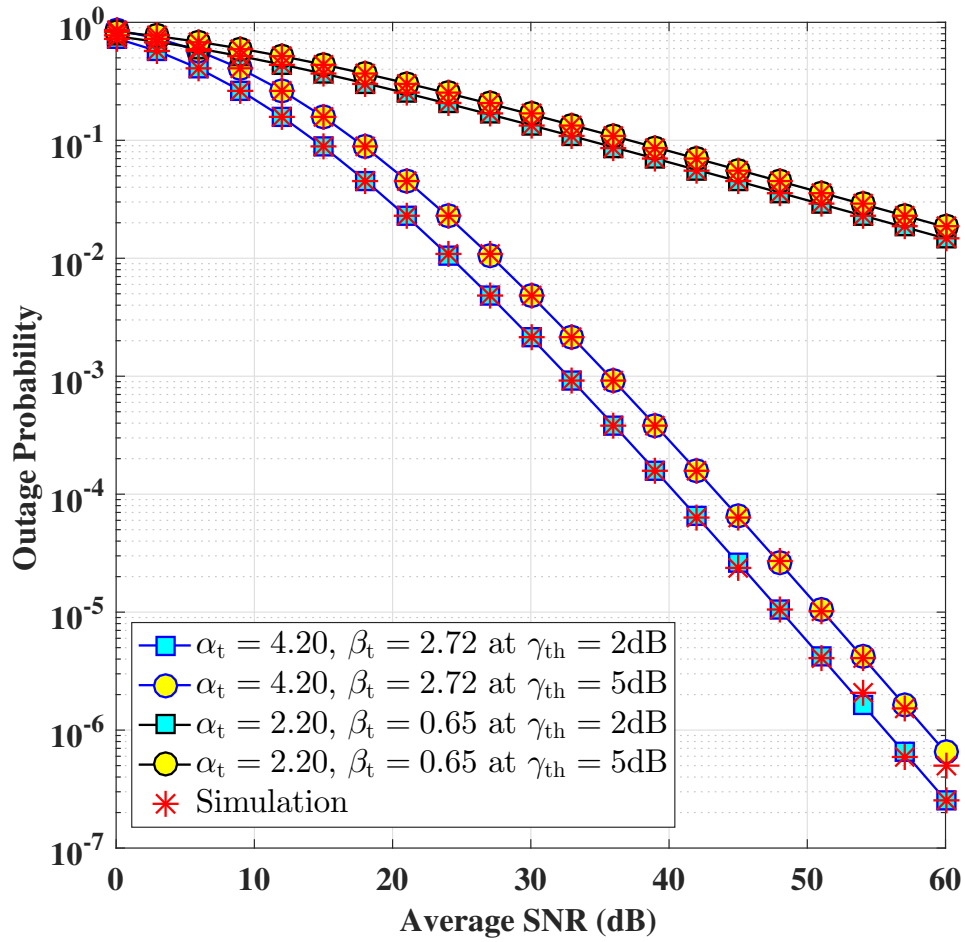


Figure 2.8 (a) Outage probability of single FSO link under Gamma-Gamma distribution in the absence of pointing error.

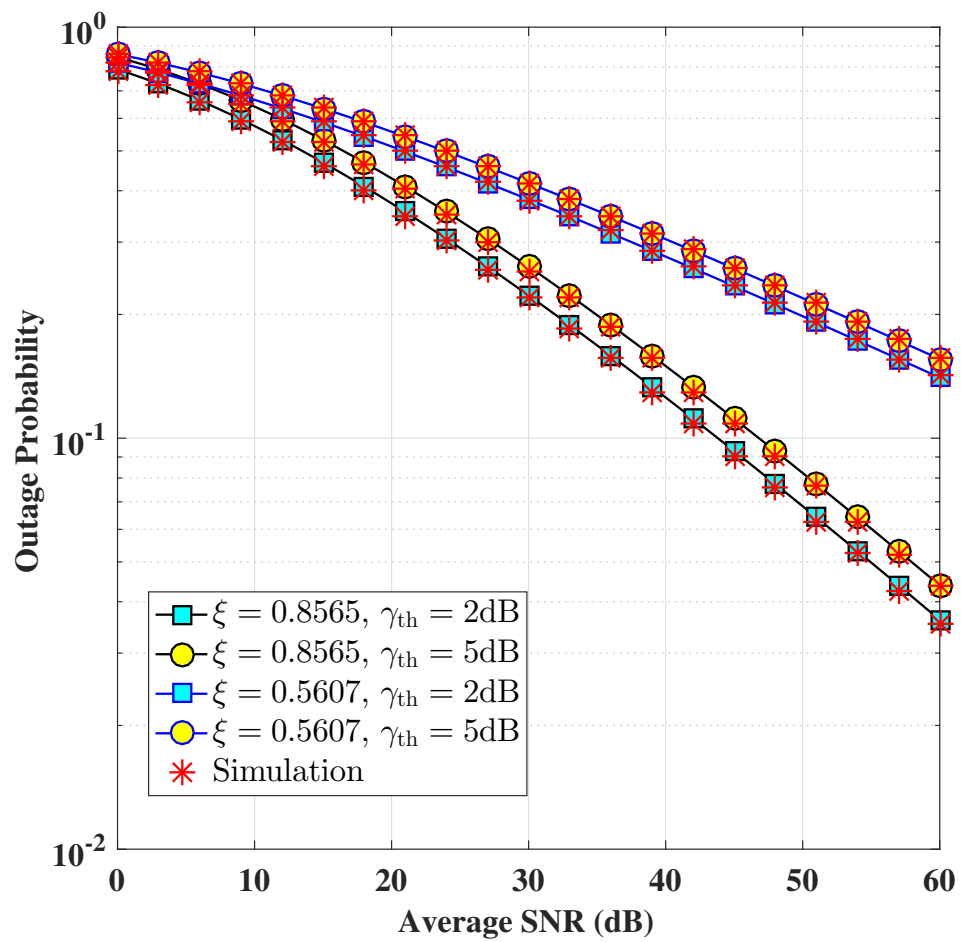


Figure 2.8 (b) Outage probability of single FSO link under Gamma-Gamma distribution in the presence of pointing error.

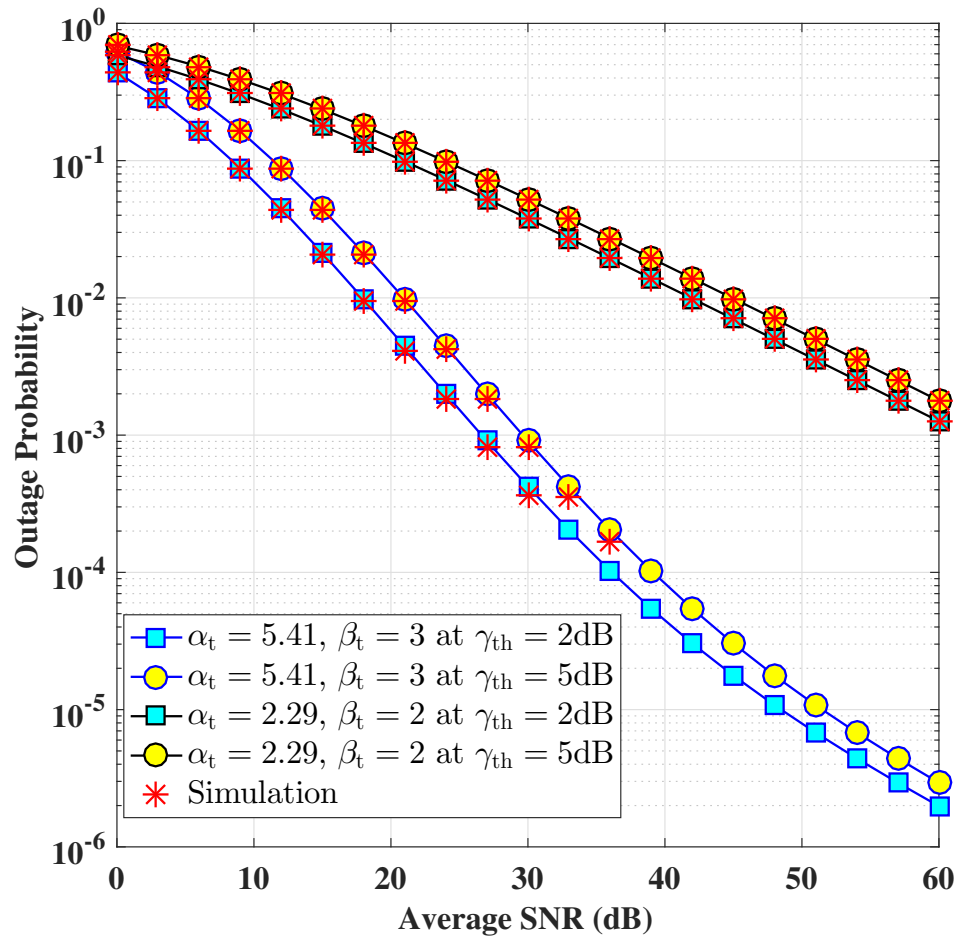


Figure 2.8 (c) Outage probability of single FSO link under Málaga distribution in the absence of pointing error.

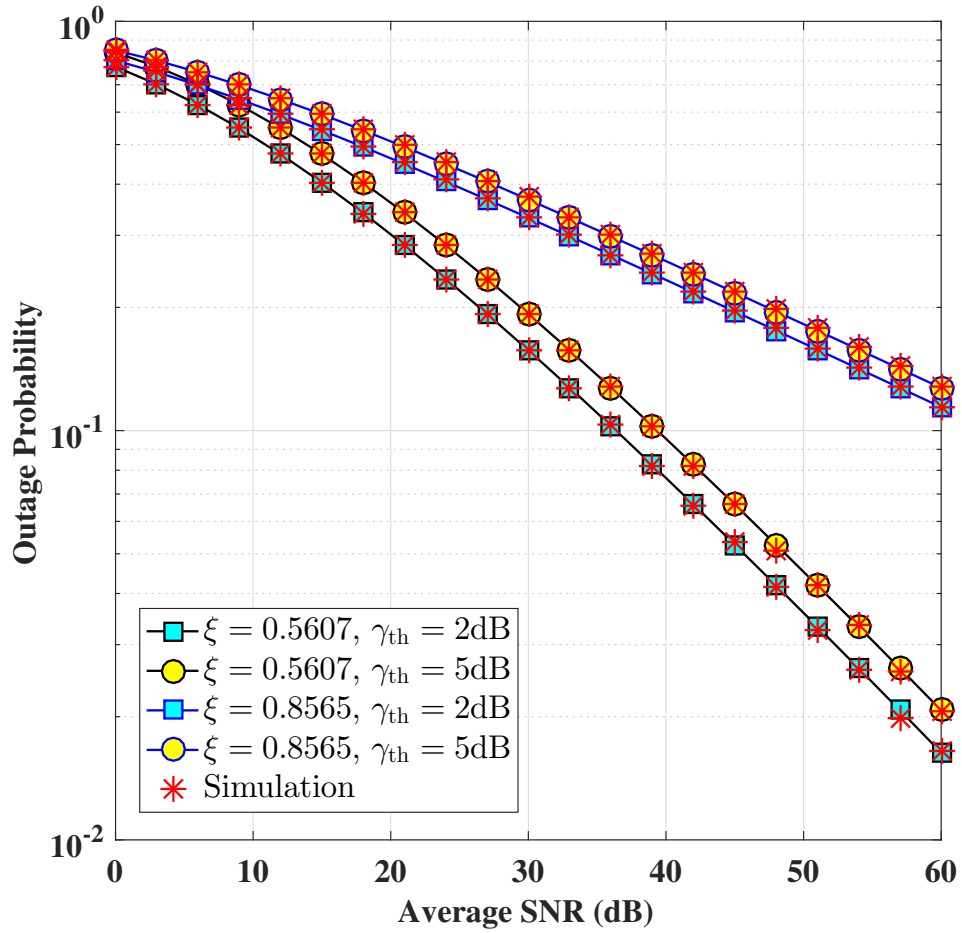


Figure 2.8 (d) Outage probability of single FSO link under Málaga distribution in the presence of pointing error.

FIGURE 2.8: Outage Probability of the single FSO link under different atmospheric turbulence condition in the absence and presence of pointing error regime.



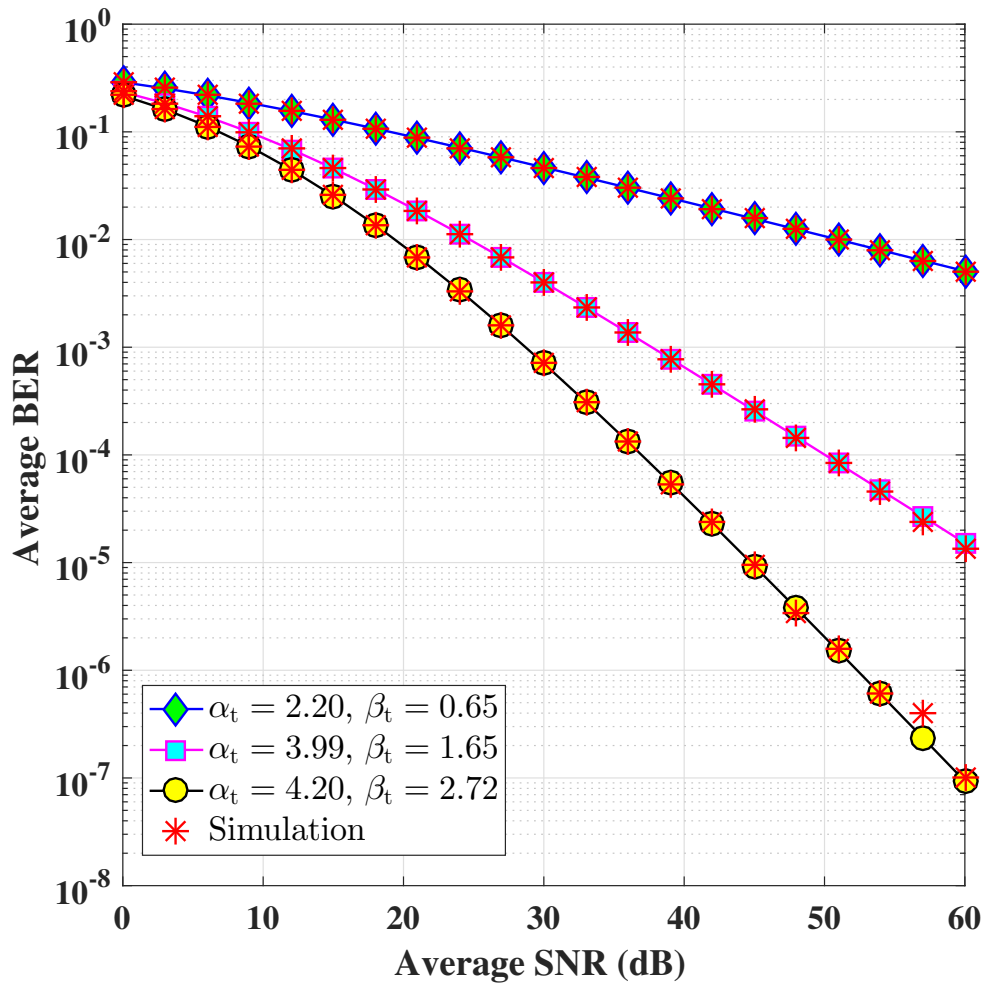
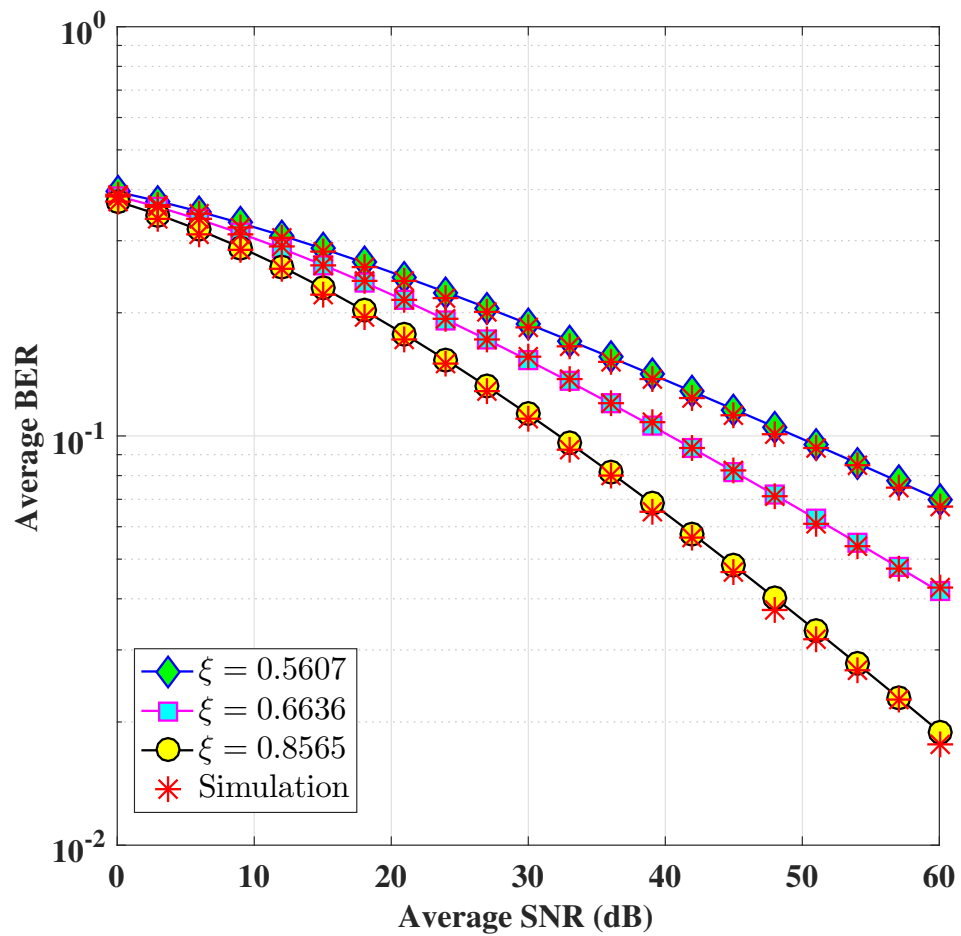


Figure 2.9 (a) Average bit error rate of single FSO link under Gamma-Gamma distribution in the absence of pointing error.



**Figure 2.9 (b)** Average bit error rate of single FSO link under Gamma-Gamma distribution in the presence of pointing error using  $\alpha_t = 2.20$  and  $\beta_t = 0.65$ .

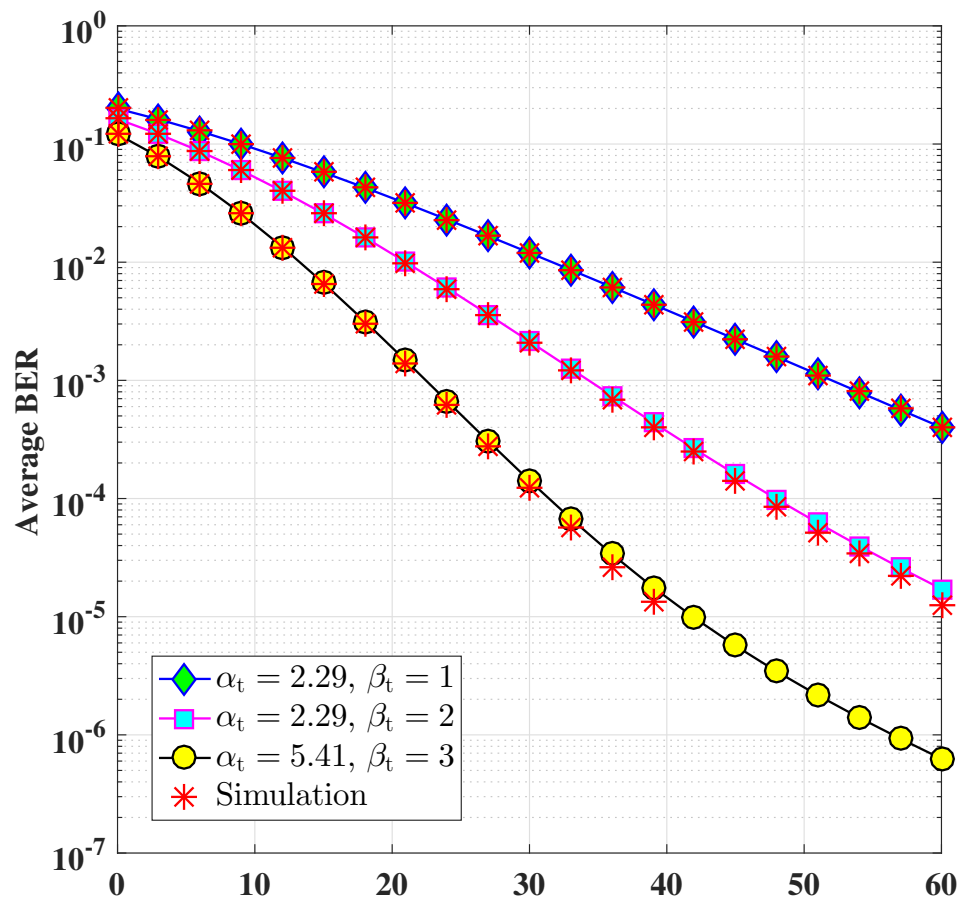
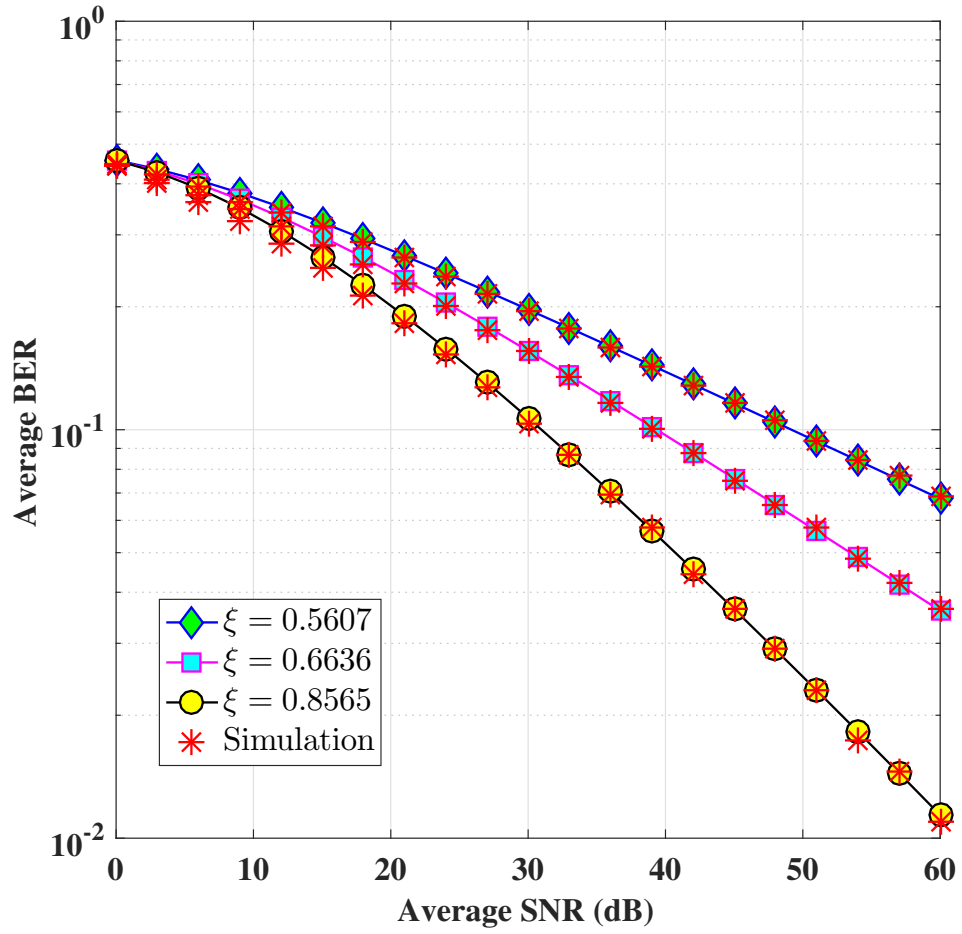


Figure 2.9 (c) Average bit error rate of single FSO link under Málaga distribution in the absence of pointing error.



**Figure 2.9 (d)** Average bit error rate of single FSO link under Málaga distribution in the presence of pointing error using  $\alpha_t = 2.29$  and  $\beta_t = 1$ .

FIGURE 2.9: Average bit error rate of the single FSO link under different atmospheric turbulence condition in the absence and presence of pointing error regime.

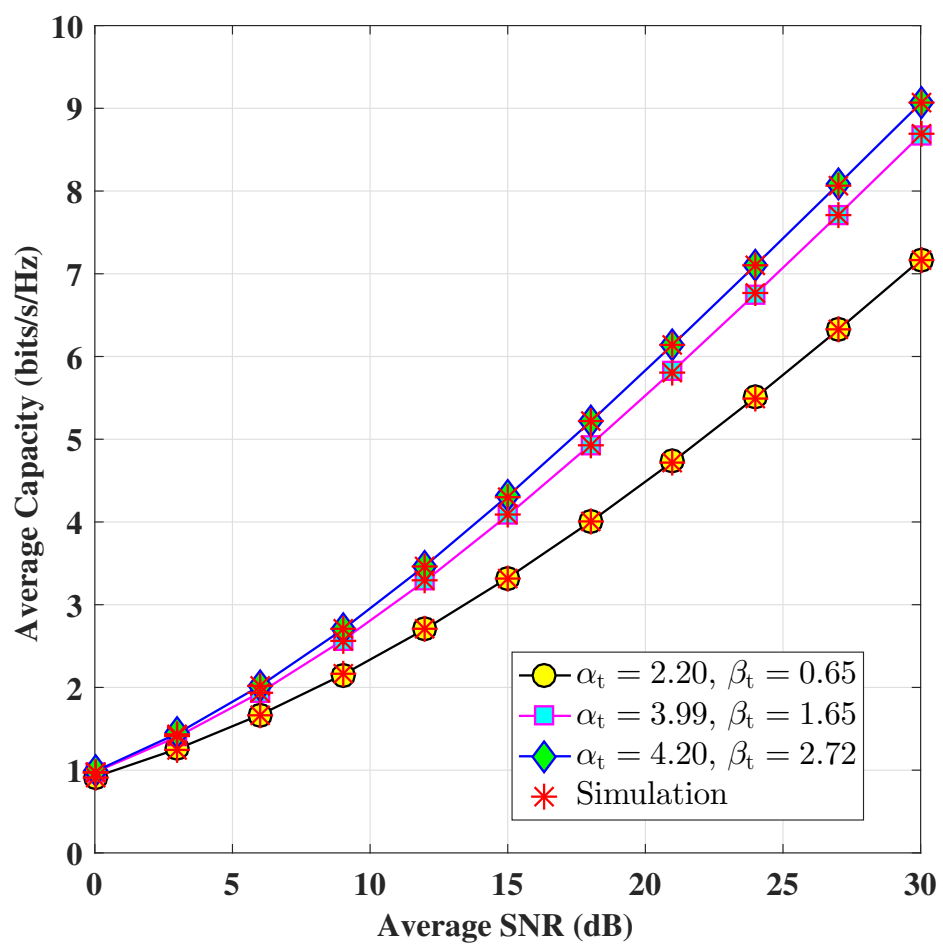


Figure 2.10 (a) Average capacity of single FSO link under Gamma-Gamma distribution in the absence of pointing error.

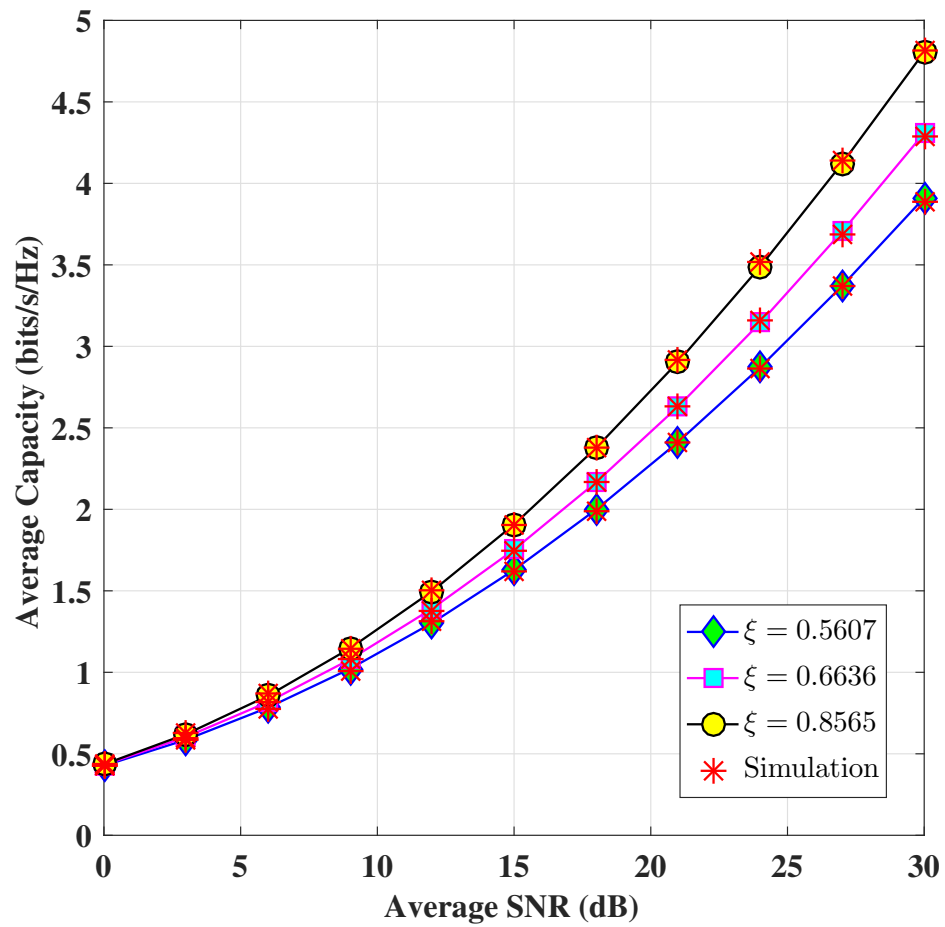


Figure 2.10 (b) Average capacity of single FSO link under Gamma-Gamma distribution in the presence of pointing error using  $\alpha_t = 2.20$  and  $\beta_t = 0.65$ .

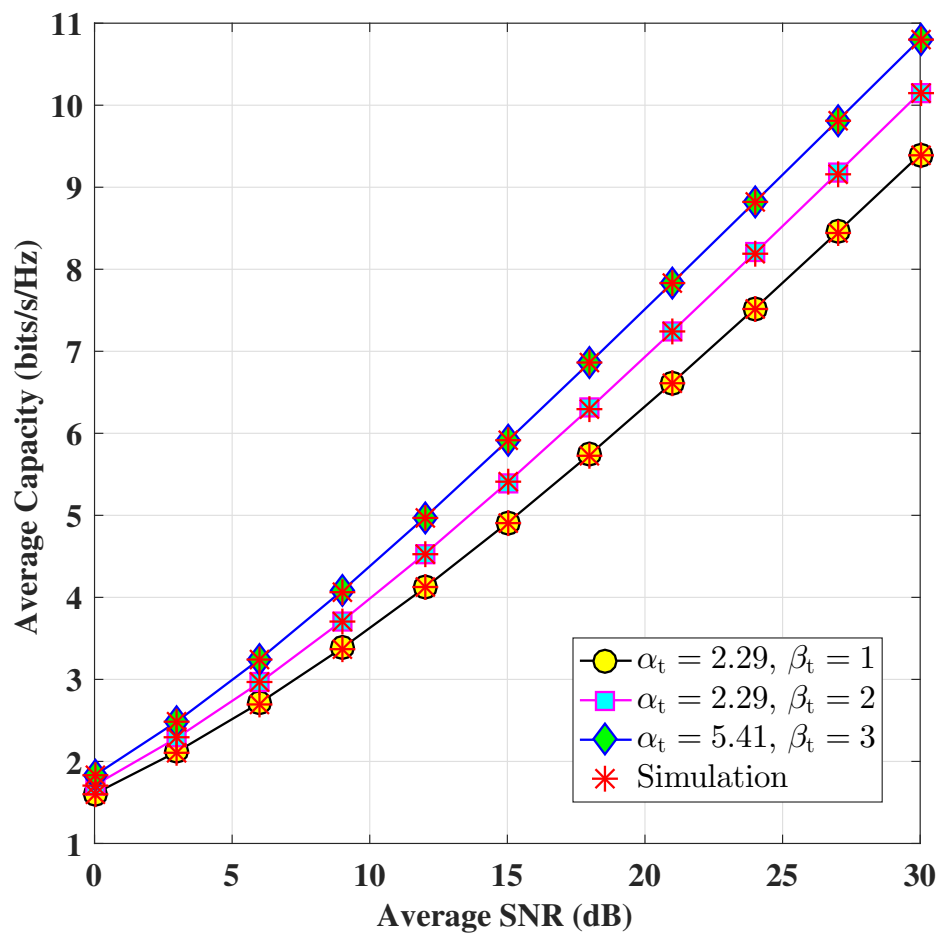
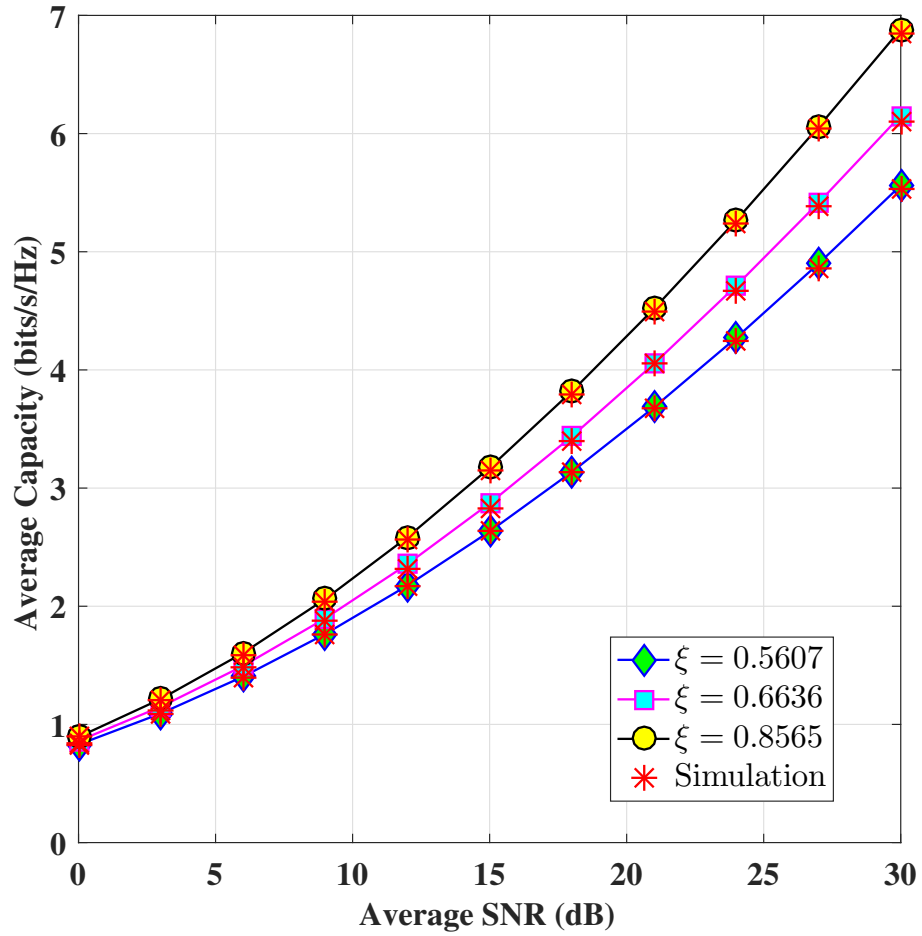


Figure 2.10 (c) Average capacity of single FSO link under Málaga distribution in the absence of pointing error.



**Figure 2.10 (d)** Average capacity of single FSO link under Málaga distribution in the presence of pointing error using  $\alpha_t = 2.29$  and  $\beta_t = 1$ .

FIGURE 2.10: Average capacity of the single FSO link under different atmospheric turbulence condition in the absence and presence of pointing error regime.



## 2.9 Chapter summary

In this chapter, we have discussed some important parameters related to the architectural setup of an FSO communication system and its link characterization. Statistical distribution appropriate for characterizing the fading channel. The Gamma-Gamma statistical distribution has been chosen to model the link under moderate-strong atmospheric turbulence conditions, while a more generalized distribution, the Málaga distribution, has been considered for a wide range of atmospheric turbulence environments. The statistical distribution has been described in the presence and absence of pointing errors. Besides a general discussion, employing diversity techniques to mitigate signal fading has also been presented. In the present dissertation, two transmit diversity, and two receiver diversity techniques are employed. The Alamouti STBC and SSK are considered under transmit diversity technique, and SC and SEC are used as the receiver diversity scheme. The useful performance metrics such as OP, ABER, and average capacity of the system have been determined also mathematical analysis and also by Monte Carlo simulation. The close match between two sets of results indicates the validity of our model that will be employed for further investigations presented in the subsequent chapter.

## Chapter 3

# Performance Analysis of FSO Communication Channel with Alamouti Transmit Diversity

**Chapter contributions:** Overall MGF of the MISO FSO system under the absence and presence of pointing error conditions for both statistical distributions associated with the characterization of the FSO channel has been carried out in this chapter. The performance metrics have been measured with the help of the system's overall MGF, and the outcomes have been compared with the fundamental FSO system.

---

The work of this chapter is published in:

*Optics Continuum*, 1(2), 366–387, Feb. 2022 [\[link\]](#)

---

## 3.1 Introduction

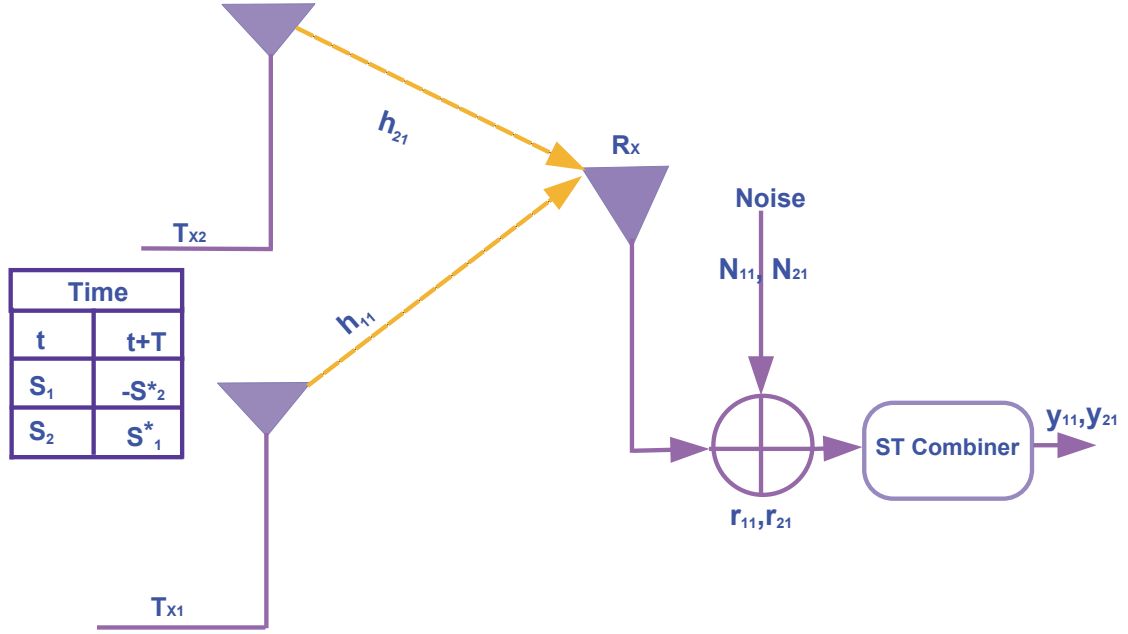
The MISO FSO link configuration is developed employing Alamouti transmit diversity, where the transmitter sends the same message signal by transmitting multiple beams to the receiver through free space. In this chapter, we will focus on the derivation of the performance metrics for the MISO FSO link under the Alamouti STBC transmit diversity technique. All investigations will be made under different channel conditions in the absence and presence of pointing errors.

## 3.2 Organization

In this chapter, analytical derivation has been done based on the overall MGF of the communication link. Overall MGF of the GG distribution in the absence of pointing error will be described in Section 3.3.1. Section 3.3.1.1 to Section 3.3.1.3 will provide the procedural steps for analytical computing of each performance metric. In Section 3.3.2 to Section 3.3.4 the overall MGF of Málaga distribution techniques will be determined with and without the influence of pointing error into the propagation path. Numerical results and discussion of the MISO FSO link will be covered in Section 3.4. Finally, the chapter ends with a chapter summary presented in Section 3.5.

## 3.3 Performance analysis with Alamouti STBC

In this section, the performance of a MISO FSO communication system under the Alamouti-STBC transmit diversity scheme will be studied; the FSO system consisting of two transmitter antennas and a single receiver aperture is shown in Fig. 3.1. Here, the random fluctuation of the channel coefficient of the free-space medium ( $h_{x1}$ ) is characterized by either GG or Málaga statistical distribution.

FIGURE 3.1: Alamouti STBC-based  $2 \times 1$  MISO FSO communication system.

### 3.3.1 Gamma-Gamma turbulence in absence of pointing error

In this chapter, we develop the MISO FSO system in which the turbulent channel is modeled by GG statistical distribution. We also assume that the system works in the absence of pointing errors. Based on the Alamouti-STBC scheme [as in 2.5.1.1 Ch.(2)] and using the MGF of the GG statistical distribution [as in 2.4.1.3 Ch.(2)] the overall MGF of the MISO FSO system in terms of end-to-end SNR may be presented as [113] [details in Appendix(A)]

$$\begin{aligned}
 \mathcal{M}_{\gamma Ala}(s) &= \mathcal{M}_{\gamma}(s) \times \mathcal{M}_{\gamma}(s) \\
 &= \left[ \frac{(\alpha_t \beta_t)^{\frac{(\alpha_t + \beta_t)}{2}}}{4\pi \Gamma(\alpha_t) \Gamma(\beta_t) (\bar{\gamma})^{\frac{(\alpha_t + \beta_t)}{4}}} (s)^{-\frac{\alpha_t + \beta_t}{4}} G_{1 \ 4}^4 \left[ \frac{\alpha_t^2 \beta_t^2}{16 \bar{\gamma} s} \middle| \frac{1 - \frac{\alpha_t + \beta_t}{4}}{\frac{\alpha_t - \beta_t}{4}, \frac{\alpha_t - \beta_t + 2}{4}, \frac{\beta_t - \alpha_t}{4}, \frac{\beta_t - \alpha_t + 2}{4}} \right] \right]^2 \quad (3.1)
 \end{aligned}$$

### 3.3.1.1 Outage probability

The OP of the MISO FSO communication system is derived using the overall MGF of the system. The OP is expressed as [113]

$$\begin{aligned}
 P_{out} &= Pr(Y \leq y) \\
 &= \frac{2^{-M} \exp(\frac{B}{2})}{y} \sum_{m=0}^M \binom{M}{m} \sum_{p=0}^{P+m} \frac{(-1)^p}{\alpha_p} \mathcal{M}_y\left(-\frac{B+2\pi jn}{2y}\right) + E(B, MP)
 \end{aligned} \tag{3.2}$$

where  $E(B, M, P)$  is the overall error term, bounded by

$$E(B, M, P) \simeq \frac{\exp(-B)}{1-\exp(-B)} + \left| \frac{2^{-P} \exp(\frac{B}{2})}{y} \sum_{p=0}^P (-1)^{1+p+M} \binom{P}{p} \mathcal{M}_y\left(-\frac{B+2\pi j(M+1+p)}{2y}\right) \right| \tag{3.3}$$

For numeral calculation, we take  $B = 12$ ,  $M = 15$ , and  $p = 5$  to ensure the maximum accuracy. Next, in (3.1), 's' is replaced by  $\left(-\frac{B+2\pi jn}{2y}\right)$ , and 'y' by  $\gamma_{th}$ , in order to get the corresponding MGF of the system. Finally, with the help of (3.2), the OP of the system is estimated.

### 3.3.1.2 Average bit error rate

In this subsection, the expression for the average BER of the MISO FSO system under the Alamouti STBC transmits diversity scheme is derived using the MGF of the system. Instead of using the direct Gaussian Q-function of the error function of the modulation scheme, the integral form of the Gaussian Q-function is used. The average BER of the system using OOK modulation can be expressed as [details in Appendix (B)]

$$P_e = \frac{1}{\pi} \int_0^{\frac{\pi}{2}} \mathcal{M}_{\gamma Ala} \left( -\frac{1}{2 \sin^2 \theta} \right) d\theta \tag{3.4}$$

### 3.3.1.3 Average capacity

To calculate the average capacity of the MISO FSO system under Alamouti STBC transmit diversity scheme, the average capacity defined in (2.60) is written as

$$C(\gamma) = \frac{1}{\ln(2)} \int_0^\infty E_i(-\gamma) \mathcal{M}_\gamma^{(1)}(\gamma) d\gamma \quad (3.5)$$

where,  $E_i(-\cdot)$  is the negative exponential integral function, and  $\mathcal{M}_\gamma^{(1)}(\cdot)$  denotes the 1<sup>st</sup> derivative of the MGF. The above equation can be computed, following [97], as

$$C(\gamma) = \frac{\pi}{Q \ln(2)} \sum_{q=1}^Q \left[ \frac{H\left(\frac{\tan(\theta_Q)}{\sqrt{2}}\right)}{\sin(2\theta_Q)} \right] + R_Q \quad (3.6)$$

where,  $\theta_Q$  is defined as  $\frac{(2q-1)\pi}{4Q}$ ,  $R_Q$  is known as error component that depends on the number of points  $Q$ . However as the numeral values of  $Q$  is very small, it can be ignored during calculation of the average capacity,  $H(\cdot)$  is the function of negative exponential integral and 1<sup>st</sup> derivative of the MGF, can be expressed as  $H(s) = sE_i(-s)\mathcal{M}_\gamma^{(1)}(s)$ .

With the help of [94, Eq.(8.2.2.14, 8.2.2.30)], the 1<sup>st</sup> derivative of  $\mathcal{M}_{\gamma Ala}(s)$  can be derived as

$$\begin{aligned} \mathcal{M}_{\gamma Ala}^{(1)}(s) &= -2 \left[ \frac{(\alpha_t \beta_t)^{\frac{(\alpha_t + \beta_t)}{2}}}{4\pi \Gamma(\alpha_t) \Gamma(\beta_t) (\bar{\gamma})^{\frac{(\alpha_t + \beta_t)}{4}}} \right]^2 (s)^{-\frac{\alpha_t + \beta_t}{4}} \\ &\times G_{1 \ 4}^4 \left[ \frac{\alpha_t^2 \beta_t^2}{16 \bar{\gamma} s} \middle| \begin{matrix} 1 - \frac{\alpha_t + \beta_t}{4} \\ \frac{\alpha_t - \beta_t}{4}, \frac{\alpha_t - \beta_t + 2}{4}, \frac{\beta_t - \alpha_t}{4}, \frac{\beta_t - \alpha_t + 2}{4} \end{matrix} \right] (s)^{-\frac{\alpha_t + \beta_t}{4} - 1} \\ &\times G_{5 \ 2}^2 \left[ \frac{16 \bar{\gamma} s}{\alpha_t^2 \beta_t^2} \middle| \begin{matrix} 1 - \frac{\alpha_t - \beta_t}{4}, 1 - \frac{\alpha_t - \beta_t + 2}{4}, 1 - \frac{\beta_t - \alpha_t}{4}, 1 - \frac{\beta_t - \alpha_t + 2}{4} \\ 1 + \frac{\alpha_t + \beta_t}{4}, \frac{\alpha_t + \beta_t}{4} \end{matrix} \right] \end{aligned} \quad (3.7)$$

Next, during computation of (3.6) in calculation of the average capacity of the system, the parameter  $s$  in  $H(s)$  is replaced by  $\frac{\tan(\theta_Q)}{\sqrt{2}}$  [97].

Following the same steps, the closed-form expressions for the performance metrics of the MISO FSO system are derived using the Alamouti STBC under different turbulence conditions and considering the pointing error effect.

### 3.3.2 Gamma-Gamma turbulence in presence of pointing error

Using the principle of Alamouti-STBC scheme [2.5.1.1 Ch.(2)] and the MGF of the GG statistical distribution in the presence of pointing error (2.41), the resultant MGF of a MISO FSO communication system is written as

$$\begin{aligned} \mathcal{M}_{\gamma Ala}^p(s) &= \mathcal{M}_\gamma(s) \times \mathcal{M}_\gamma(s) \\ &= \left[ \frac{\xi^2(2)^{(\alpha_t+\beta_t)}}{8\pi\Gamma(\alpha_t)\Gamma(\beta_t)} G_{3\ 6}^{6\ 1} \left[ \frac{\alpha_t^2\beta_t^2\mathcal{K}^2}{16\bar{\gamma}s} \middle| \begin{matrix} 1, \frac{\xi^2+1}{2}, \frac{\xi^2+2}{2} \\ \frac{\xi^2}{2}, \frac{\xi^2+1}{2}, \frac{\alpha_t}{2}, \frac{\alpha_t+1}{2}, \frac{\beta_t}{2}, \frac{\beta_t+1}{2} \end{matrix} \right] \right]^2 \end{aligned} \quad (3.8)$$

The 1<sup>st</sup> derivative of  $\mathcal{M}_{\gamma Ala}^p(s)$  is derived with the help of [94, Eq.(8.2.2.34)] and is expressed as

$$\begin{aligned} \mathcal{M}_{\gamma Ala}^{p(1)}(s) &= -2(s)^{-1} \left[ \frac{\xi^2(2)^{(\alpha_t+\beta_t)}}{8\pi\Gamma(\alpha_t)\Gamma(\beta_t)} \right]^2 G_{3\ 6}^{6\ 1} \left[ \frac{\alpha_t^2\beta_t^2\mathcal{K}^2}{16\bar{\gamma}s} \middle| \begin{matrix} 1, \frac{\xi^2+1}{2}, \frac{\xi^2+2}{2} \\ \frac{\xi^2}{2}, \frac{\xi^2+1}{2}, \frac{\alpha_t}{2}, \frac{\alpha_t+1}{2}, \frac{\beta_t}{2}, \frac{\beta_t+1}{2} \end{matrix} \right] \\ &\quad \times G_{3\ 6}^{6\ 1} \left[ \frac{\alpha_t^2\beta_t^2\mathcal{K}^2}{16\bar{\gamma}s} \middle| \begin{matrix} 0, \frac{\xi^2+1}{2}, \frac{\xi^2+2}{2} \\ \frac{\xi^2}{2}, \frac{\xi^2+1}{2}, \frac{\alpha_t}{2}, \frac{\alpha_t+1}{2}, \frac{\beta_t}{2}, \frac{\beta_t+1}{2} \end{matrix} \right] \end{aligned} \quad (3.9)$$

### 3.3.3 Málaga turbulence in absence of pointing error

The overall MGF of the MISO FSO configuration under Málaga statistical distribution, in the absence of the misalignment fading effect, can be written with the

help of (2.31) as [114]

$$\mathcal{M}_{\gamma Ala}(s) = \left[ \frac{\mathcal{A}}{8\pi} \sum_{k_t=1}^{\beta_t} \frac{a_k}{(\tilde{\gamma})^{\frac{\alpha_t+k_t}{4}}} (s)^{-\frac{\alpha_t+k_t}{4}} G_{1 \ 4}^{4 \ 1} \left[ \frac{\mathcal{B}^4 \alpha_t^2 \beta_t^2}{256 \tilde{\gamma} s} \middle| \begin{matrix} 1 - \frac{\alpha_t+k_t}{4} \\ \frac{\alpha_t-k_t}{4}, \frac{\alpha_t-k_t+2}{4}, \frac{k_t-\alpha_t}{4}, \frac{k_t-\alpha_t+2}{4} \end{matrix} \right] \right]^2 \quad (3.10)$$

The 1<sup>st</sup> derivative of  $\mathcal{M}_{\gamma Ala}(s)$  is derived similarly, with the help of [94, Eq.(8.2.2.34)], as

$$\begin{aligned} \mathcal{M}_{\gamma Ala}^{(1)}(s) = & -2 \left[ \frac{\mathcal{A}}{8\pi} \sum_{k_t=1}^{\beta_t} \frac{a_k}{(\tilde{\gamma})^{\frac{\alpha_t+k_t}{4}}} \right]^2 (s)^{-\frac{\alpha_t+k_t}{4}} G_{1 \ 4}^{4 \ 1} \left[ \frac{\mathcal{B}^4 \alpha_t^2 \beta_t^2}{256 \tilde{\gamma} s} \middle| \begin{matrix} 1 - \frac{\alpha_t+k_t}{4} \\ \frac{\alpha_t-k_t}{4}, \frac{\alpha_t-k_t+2}{4}, \frac{k_t-\alpha_t}{4}, \frac{k_t-\alpha_t+2}{4} \end{matrix} \right] \\ & \times (s)^{-\frac{\alpha_t+k_t}{4}-1} G_{1 \ 4}^{4 \ 1} \left[ \frac{\mathcal{B}^4 \alpha_t^2 \beta_t^2}{256 \tilde{\gamma} s} \middle| \begin{matrix} -\frac{\alpha_t+k_t}{4} \\ \frac{\alpha_t-k_t}{4}, \frac{\alpha_t-k_t+2}{4}, \frac{k_t-\alpha_t}{4}, \frac{k_t-\alpha_t+2}{4} \end{matrix} \right] \end{aligned} \quad (3.11)$$

### 3.3.4 Málaga turbulence in presence of pointing error

The MGF of the MISO FSO network in the presence of a pointing error is expressed with the help of (2.48) as

$$\mathcal{M}_{\gamma Ala}^p(s) = \left[ \frac{\xi^2 \mathcal{A}}{8\pi} \sum_{k_t=1}^{\beta_t} b_k(2)^{\alpha_t+\beta_t-1} G_{3 \ 6}^{6 \ 1} \left[ \frac{\mathcal{B}^2}{16s\tilde{\gamma}} \middle| \begin{matrix} 1, \frac{\xi^2+1}{2}, \frac{\xi^2+2}{2} \\ \frac{\xi^2}{2}, \frac{\xi^2+1}{2}, \frac{\alpha_t}{2}, \frac{\alpha_t+1}{2}, \frac{k_t}{2}, \frac{k_t+1}{2} \end{matrix} \right] \right]^2 \quad (3.12)$$

Here using [94, Eq.(8.2.2.34)] the 1<sup>st</sup> derivative of  $\mathcal{M}_{\gamma Ala}^p(s)$  is derived as

$$\begin{aligned} \mathcal{M}_{\gamma Ala}^{p(1)}(s) = & -2(s)^{-1} \left[ \frac{\xi^2 \mathcal{A}}{8\pi} \sum_{k_t=1}^{\beta_t} b_k(2)^{\alpha_t+\beta_t-1} \right]^2 G_{3 \ 6}^{6 \ 1} \left[ \frac{\mathcal{B}^2}{16s\tilde{\gamma}} \middle| \begin{matrix} 1, \frac{\xi^2+1}{2}, \frac{\xi^2+2}{2} \\ \frac{\xi^2}{2}, \frac{\xi^2+1}{2}, \frac{\alpha_t}{2}, \frac{\alpha_t+1}{2}, \frac{k_t}{2}, \frac{k_t+1}{2} \end{matrix} \right] \\ & \times G_{3 \ 6}^{6 \ 1} \left[ \frac{\mathcal{B}^2}{16s\tilde{\gamma}} \middle| \begin{matrix} 0, \frac{\xi^2+1}{2}, \frac{\xi^2+2}{2} \\ \frac{\xi^2}{2}, \frac{\xi^2+1}{2}, \frac{\alpha_t}{2}, \frac{\alpha_t+1}{2}, \frac{k_t}{2}, \frac{k_t+1}{2} \end{matrix} \right] \end{aligned} \quad (3.13)$$



TABLE 3.1: Fading distribution parameters for numerical analysis and simulation

FD	Gamma-Gamma			Málaga		
AT	Weak	Medium	Strong	Weak	Medium	Strong
PV	$\alpha_t = 4.20$ $\beta_t = 2.72$	$\alpha_t = 3.99$ $\beta_t = 1.65$	$\alpha_t = 2.20$ $\beta_t = 0.65$	$\alpha_t = 5.41$ $\beta_t = 3$	$\alpha_t = 2.29$ $\beta_t = 2$	$\alpha_t = 2.29$ $\beta_t = 1$
FD: Fading Distribution , AT: Atmospheric Turbulence , PV: Parameter Value.						

### 3.4 Numerical results and discussion for MISO FSO link

We compute the numerical results based on our analytical derivation and validate them with those obtained from Monte Carlo simulation using MATLAB, the fading distribution parameters for numerical analysis and simulation are provided in TABLE 3.1 and TABLE 3.2 summarized the equations used for Fig. 3.2 to Fig. 3.4. Fig. 3.2(a) indicates the OP of the MISO FSO link for GG statistical distribution in the absence of a pointing error. The figure shows that the system's outage significantly depends on the threshold SNR ( $\gamma_{th}$ ) and weather conditions. Comparison of OP for the SISO FSO link (Fig. 2.7a(a)) and MISO FSO link (Fig. 3.2(a)), both under strong atmospheric turbulence conditions ( $\alpha_t = 2.20$  and  $\beta_t = 0.65$ ) shows at 60 dB of average SNR an MISO FSO link provides  $10^{-2}$  order less OP than an SISO FSO link under threshold SNR of 2 dB. From Fig. 3.2(b) and Fig. 2.7a (b) the OP is found to improved in relative percentage is  $\approx 92\%$  in pointing error ( $\xi = 0.5607$ ) regime under same weather conditions. It is also observed that the amount of outage improves from SISO to MISO FSO link with and without the pointing error effect under general Málaga distribution. The average BER performance of the MISO FSO link has been presented in Fig. 3.3 for all weather conditions in the absence and presence of pointing error conditions. In the general Málaga statistical distribution scenario under strong AT condition ( $\alpha_t = 2.29$  and  $\beta_t = 1$ ) in the absence of pointing error and at 45 dB average SNR, the ABER is  $1.2 \times 10^{-5}$  for the MISO FSO link Fig. 3.3 (c) and  $2.2 \times 10^{-3}$  for the SISO FSO link Fig. 2.8 (c). Similar

TABLE 3.2: Summary of the equations used for figures, Fig. 3.2 to Fig. 3.4.

Figure	Scenario	Equation
Fig. 3.2a	GG	Eq. 3.1 and Eq. 3.2
Fig. 3.2b	GG + pointing	Eq. 3.8 and Eq. 3.2
Fig. 3.2c	Málaga	Eq. 3.10 and Eq. 3.2
Fig. 3.2d	Málaga + pointing	Eq. 3.12 and Eq. 3.2
Fig. 3.3a	GG	Eq. 3.1 and Eq. 3.4
Fig. 3.3b	GG + pointing	Eq. 3.8 and Eq. 3.4
Fig. 3.3c	Málaga	Eq. 3.10 and Eq. 3.4
Fig. 3.3d	Málaga + pointing	Eq. 3.12 and Eq. 3.4
Fig. 3.4a	GG	Eq. 3.7 and Eq. 3.6
Fig. 3.4b	GG+pointing	Eq. 3.9 and Eq. 3.6
Fig. 3.4c	Málaga	Eq. 3.11 and Eq. 3.6
Fig. 3.4d	Málaga + pointing	Eq. 3.13 and Eq. 3.6

results in presence of pointing error ( $\xi = 0.5607$ ) are  $2.0 \times 10^{-2}$  Fig. 3.2 (d) and  $1.1 \times 10^{-1}$  Fig. 2.8 (d) respectively for MISO FSO and SISO FSO links. Results indicate that the MISO FSO link offers a noticeable improvement in ABER. A canvas of the graphical presentation has been provided in Fig. 3.4 (a) - (d) to describe the average capacity of the MISO FSO communication system. The average capacity deteriorates as the effect of pointing error strengthens. Besides, comparison of Fig. 3.4 and Fig. 2.9, proves that a MISO FSO configuration produces a remarkable improvement in its performance in terms of average capacity with respect to that of a SISO FSO link under any weather condition. Overall, it may be concluded that a MISO FSO communication system is quite efficient than a SISO FSO link.

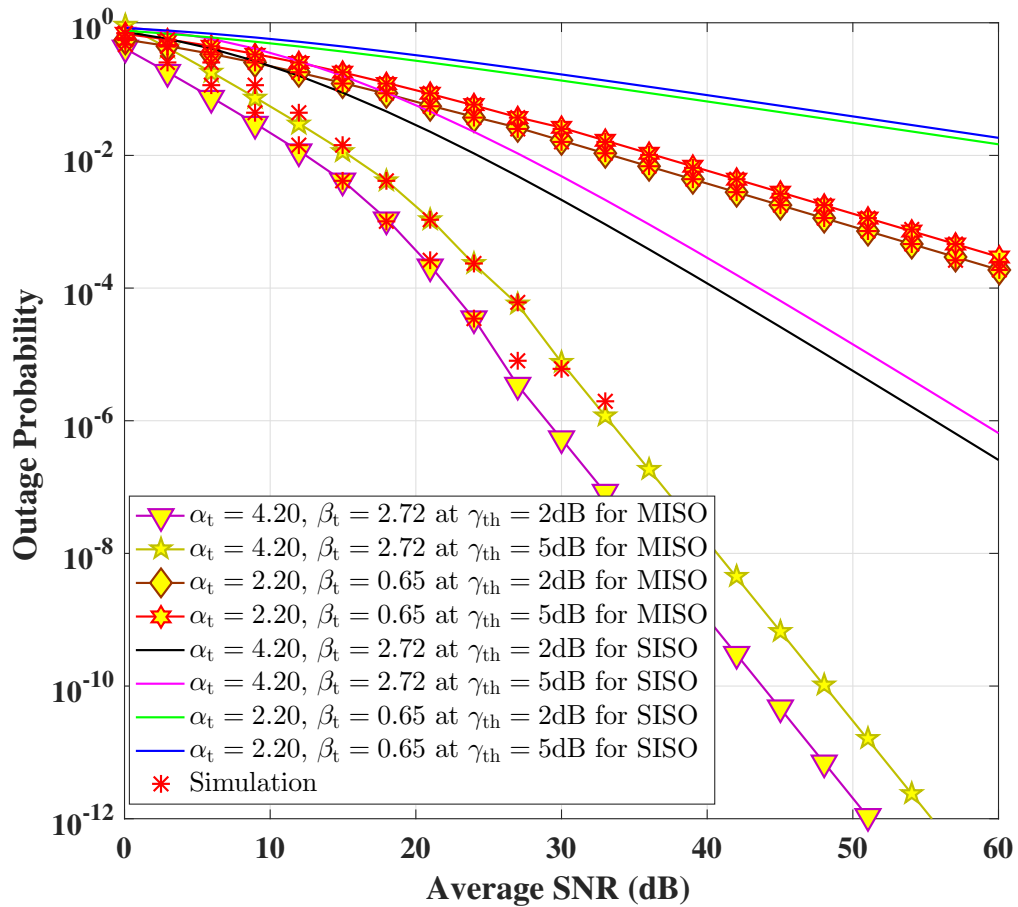
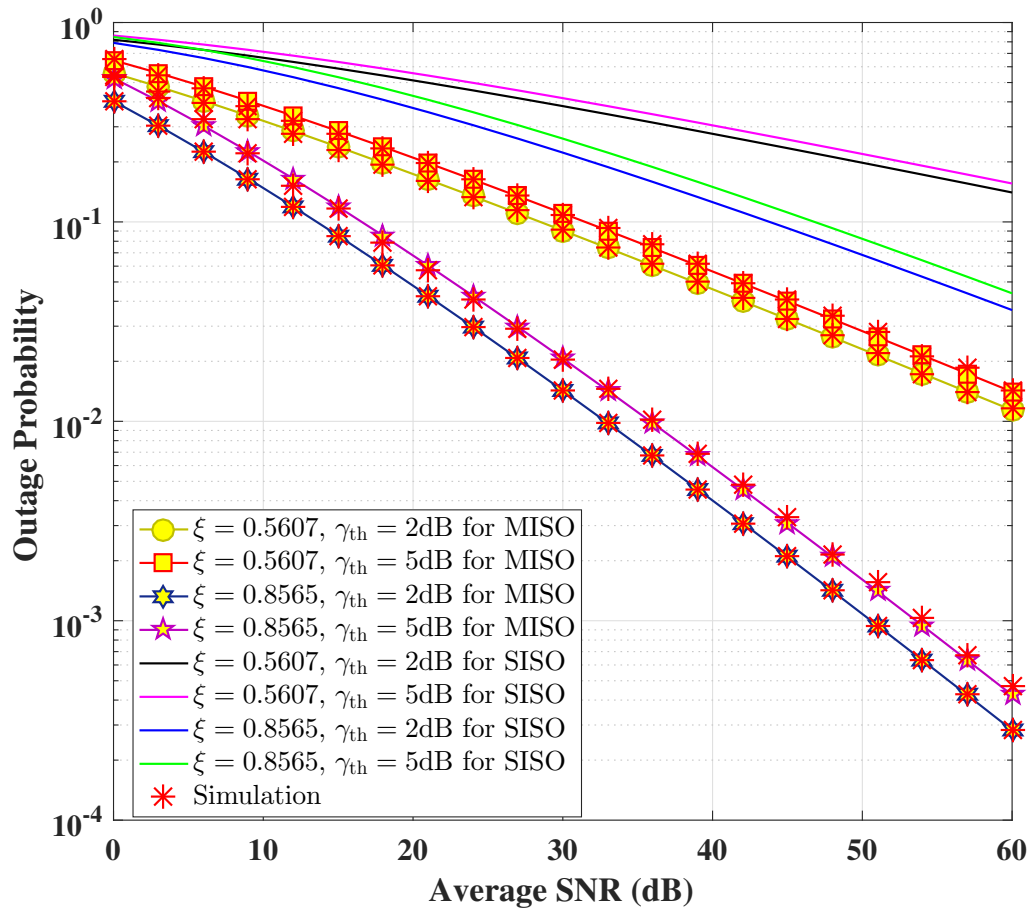


Figure 3.2 (a) Outage probability of MISO FSO link under Gamma-Gamma distribution and Alamouti transmit diversity scheme in the absence of pointing error.



**Figure 3.2 (b)** Outage probability of MISO FSO link under Gamma-Gamma distribution and Alamouti transmit diversity scheme in the presence of pointing error ( $\xi = 0.5607$  and  $0.8565$ ) using  $\alpha_t = 2.20$  and  $\beta_t = 0.65$ .

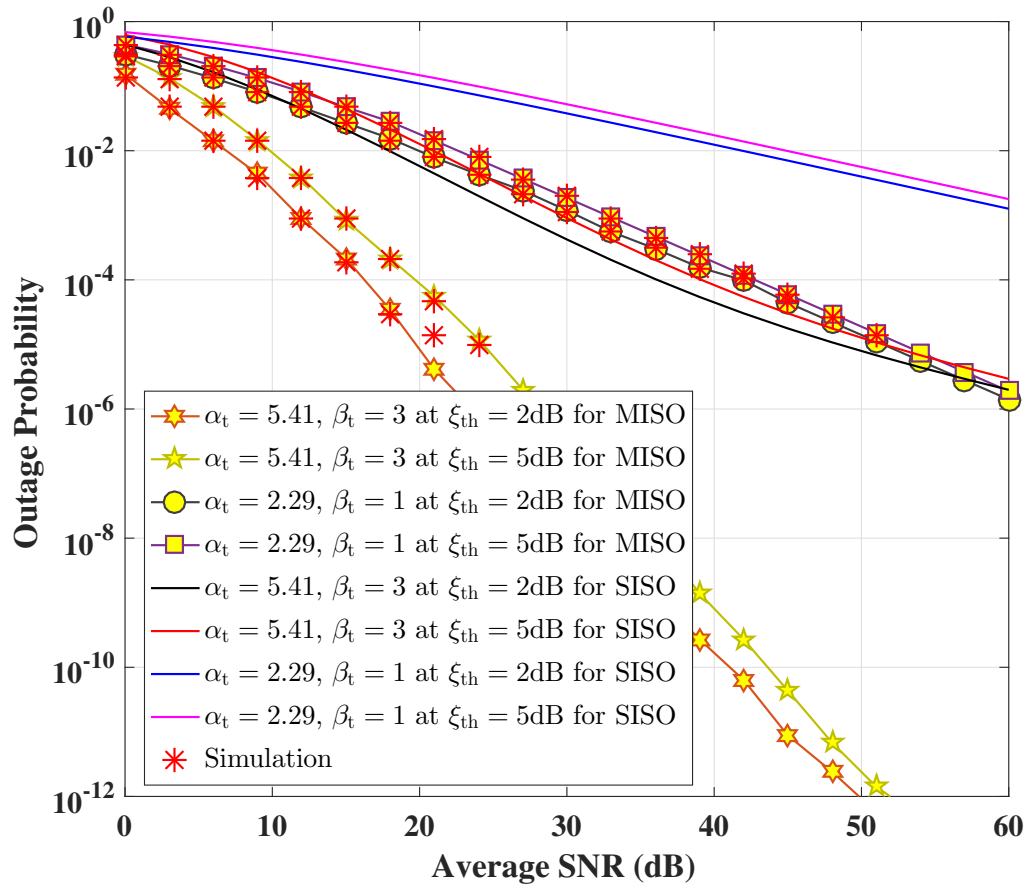
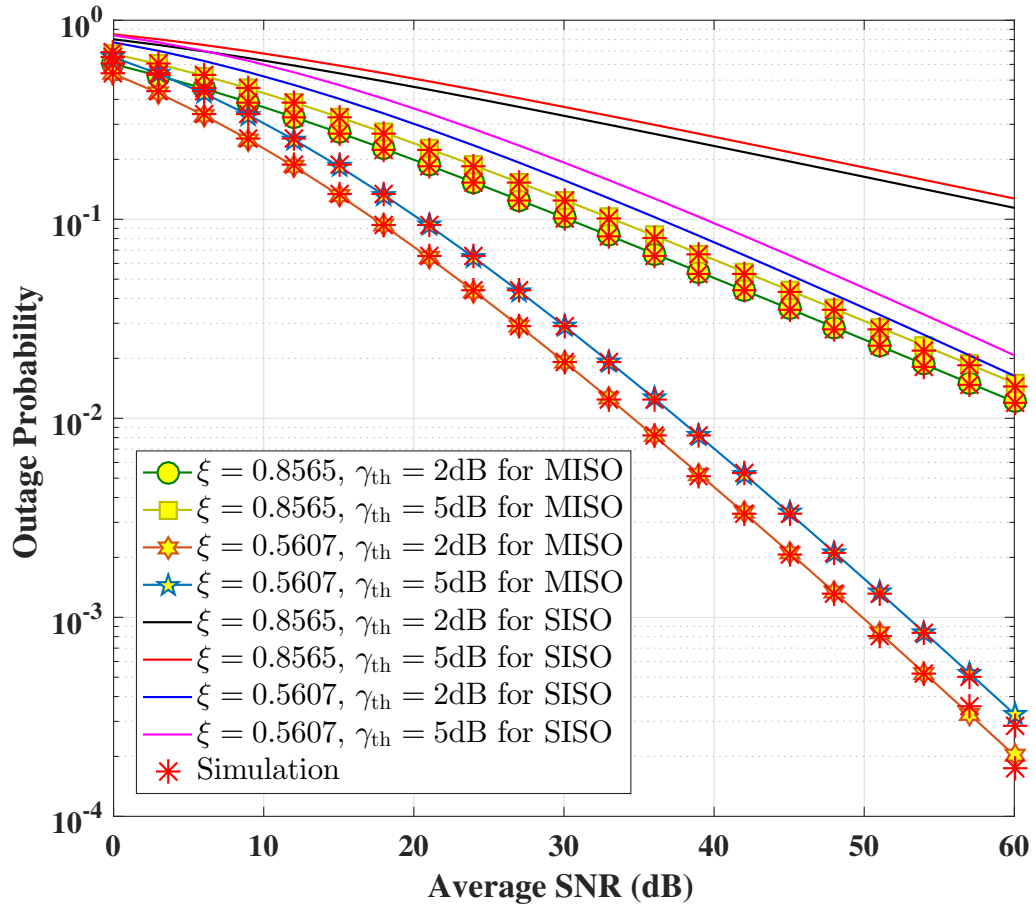
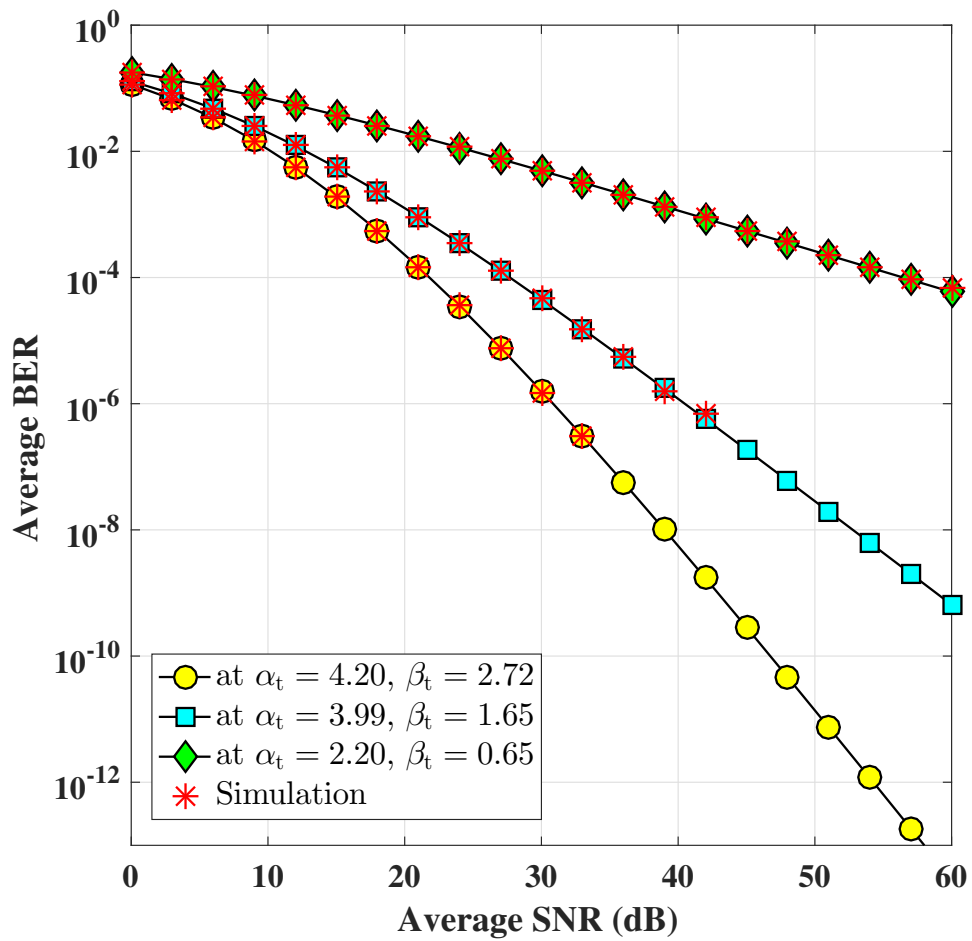


Figure 3.2 (c) Outage probability of MISO FSO link under Málaga distribution and Alamouti transmit diversity scheme in the absence of pointing error.



**Figure 3.2 (d)** Outage probability of MISO FSO link under Málaga distribution and Alamouti transmit diversity scheme in the presence of pointing error ( $\xi = 0.5607$  and  $0.8565$ ) using  $\alpha_t = 2.29$  and  $\beta_t = 1$ .

FIGURE 3.2: Outage Probability of the MISO FSO link employing Alamouti STBC scheme at the transmitter end with different atmospheric turbulence conditions in the absence and presence of pointing error.



**Figure 3.3 (a)** Average bit error rate of MISO FSO link under Gamma-Gamma distribution and Alamouti transmit diversity scheme in the absence of pointing error.

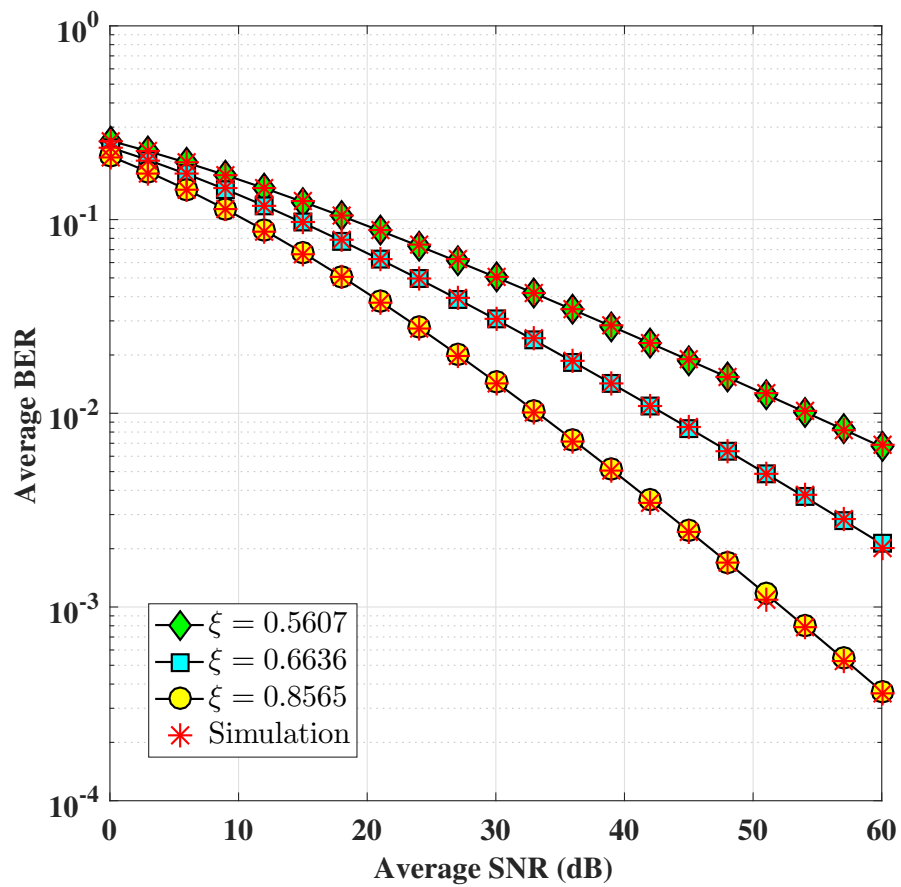


**Figure 3.3 (b)** Average bit error rate of MISO FSO link under Gamma-Gamma distribution and Alamouti transmit diversity scheme in the presence of pointing error ( $\xi = 0.5607, 0.6636$  and  $0.8565$ ) using  $\alpha_t = 2.20$  and  $\beta_t = 0.65$ .



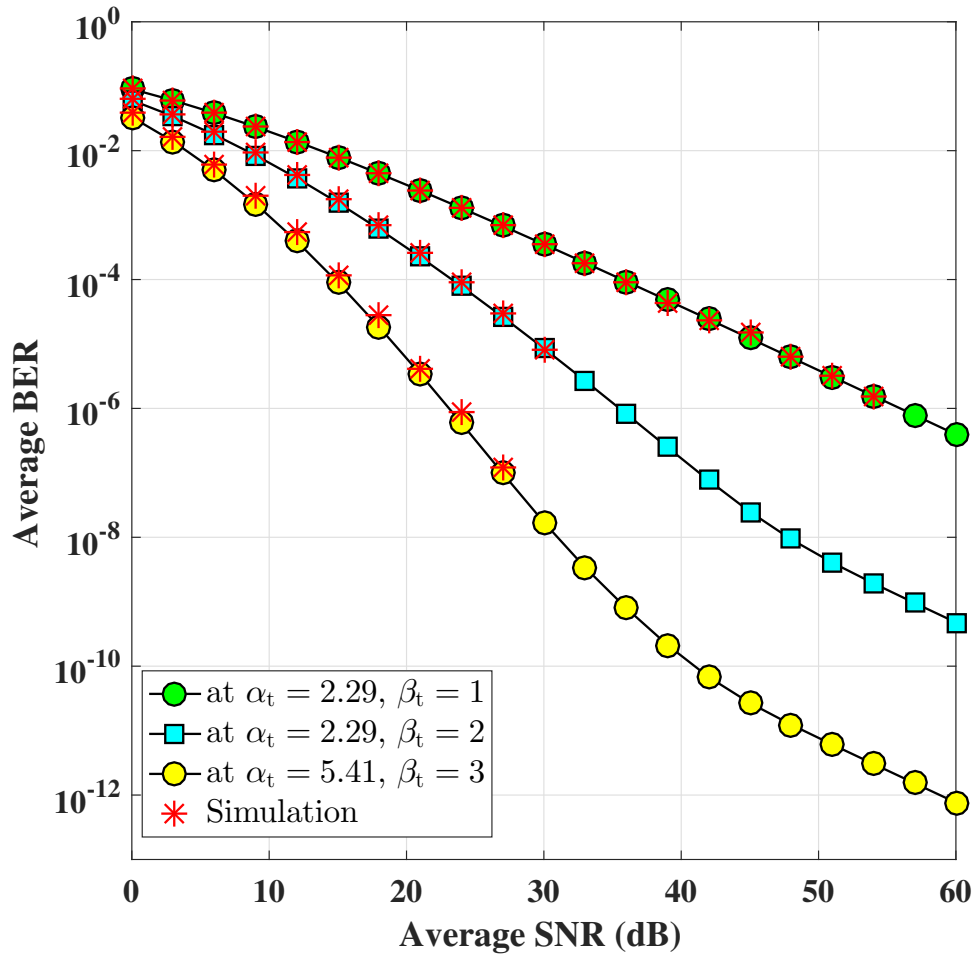


**Figure 3.3 (c)** Average bit error rate of MISO FSO link under Málaga distribution and Alamouti transmit diversity scheme in the absence of pointing error.

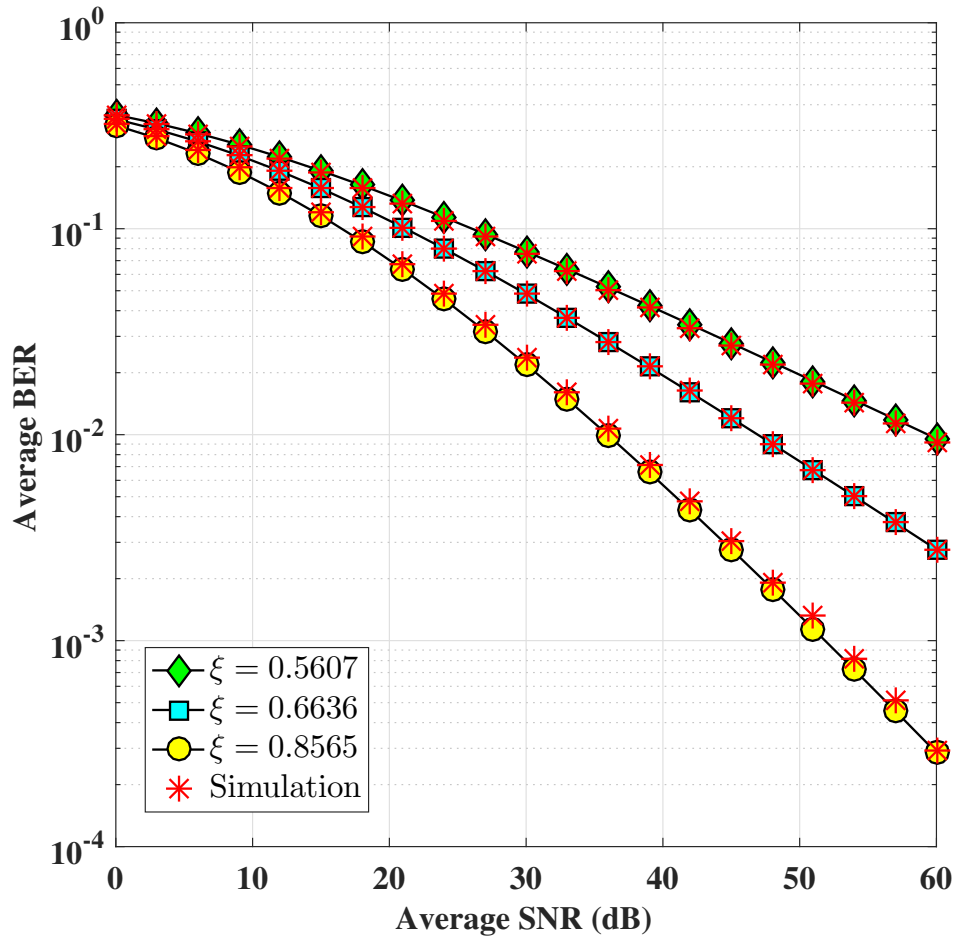


**Figure 3.3 (d)** Average bit error rate of MISO FSO link under Málaga distribution and Alamouti transmit diversity scheme in the presence of pointing error ( $\xi = 0.5607, 0.6636$  and  $0.8565$ ) using  $\alpha_t = 2.29$  and  $\beta_t = 1$ .

FIGURE 3.3: Average bit error rate of the MISO FSO link employing Alamouti STBC scheme at the transmitter end with different atmospheric turbulence condition in the absence and presence of pointing error.

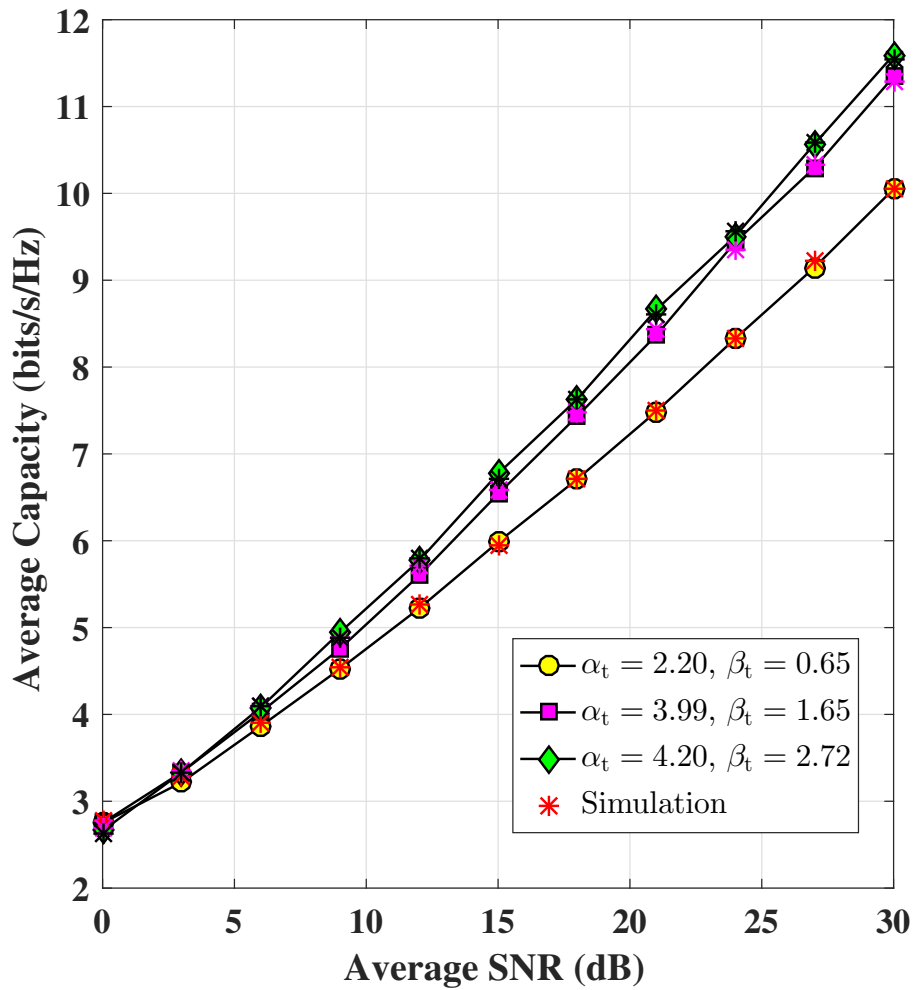


**Figure 3.4 (a)** Average capacity of MISO FSO link under Gamma-Gamma distribution and Alamouti transmit diversity scheme in the absence of pointing error.

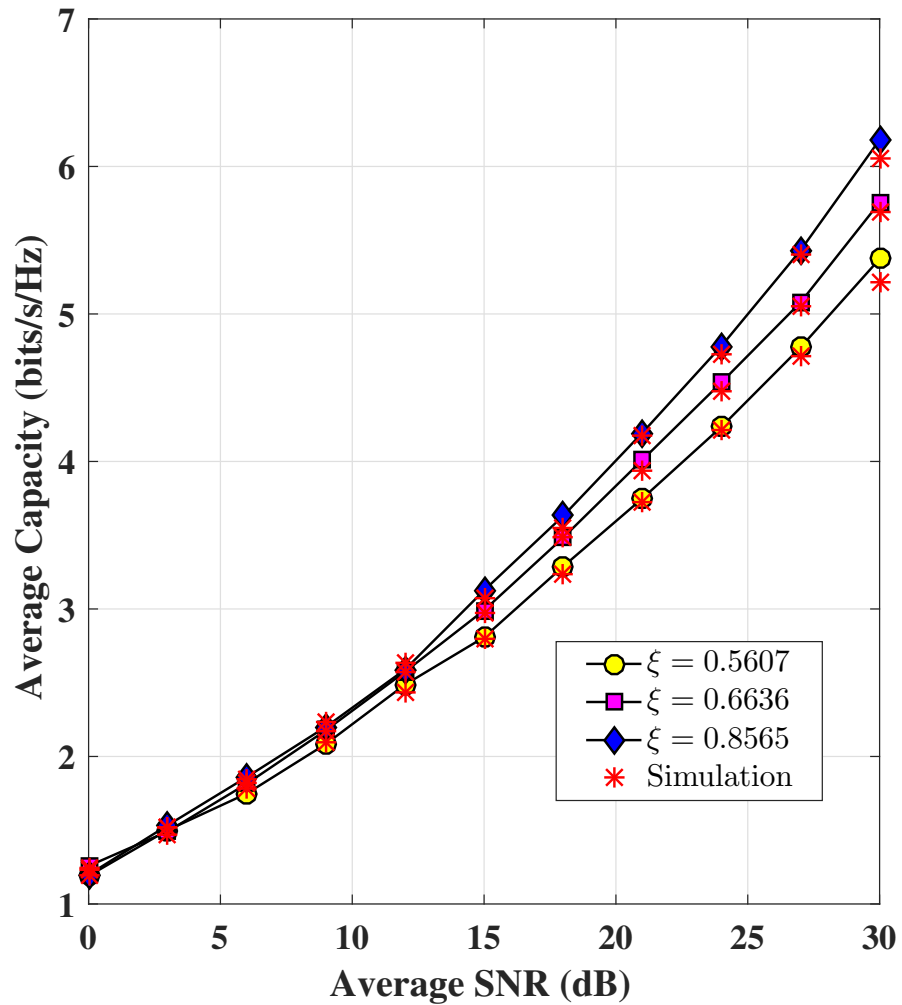


**Figure 3.4 (b)** Average capacity of MISO FSO link under Gamma-Gamma distribution and Alamouti transmit diversity scheme in the presence of pointing error ( $\xi = 0.5607, 0.6636$  and  $0.8565$ ) using  $\alpha_t = 2.20$  and  $\beta_t = 0.65$ .

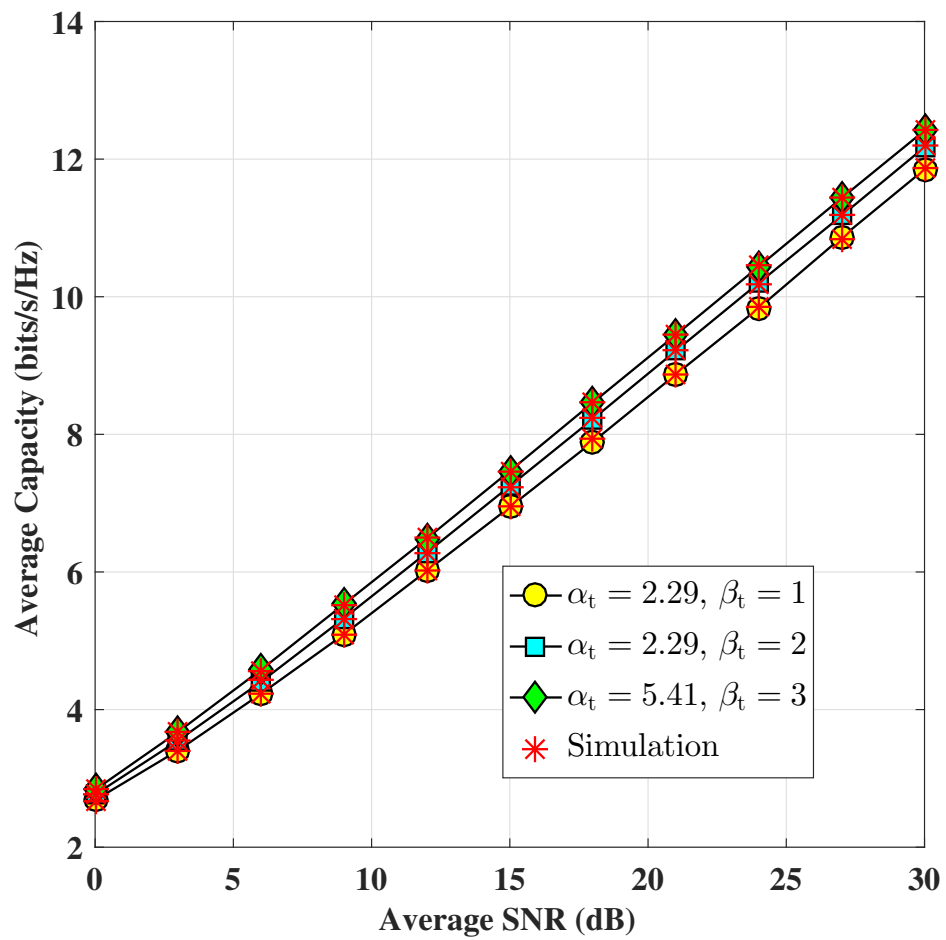
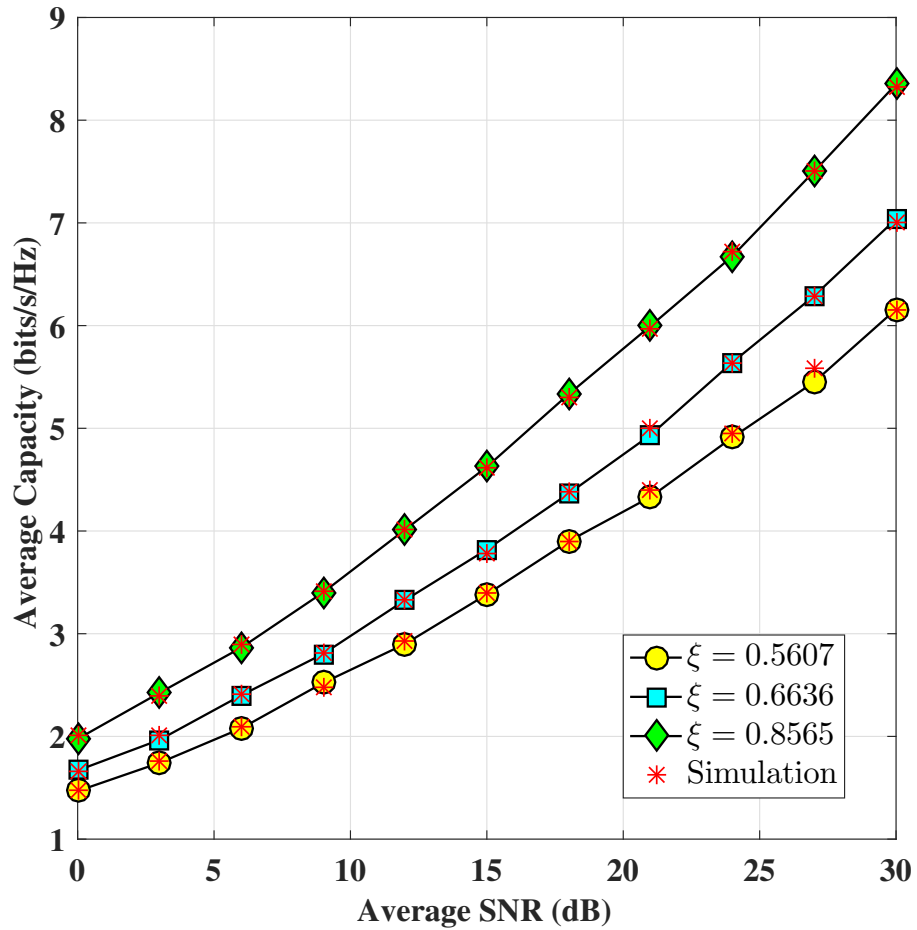


Figure 3.4 (c) Average capacity of MISO FSO link under Málaga distribution and Alamouti transmit diversity scheme in the absence of pointing error.



**Figure 3.4 (d)** Average capacity of MISO FSO link under Málaga distribution and Alamouti transmit diversity scheme in the presence of pointing error ( $\xi = 0.5607, 0.6636$  and  $0.8565$ ) using  $\alpha_t = 2.29$  and  $\beta_t = 1$ .

FIGURE 3.4: Average capacity of the MISO FSO link employing Alamouti STBC scheme at the transmitter end with different atmospheric turbulence condition in the absence and presence of pointing error.

### 3.5 Chapter summary

A MISO FSO architecture has been investigated in this chapter by introducing the Alamouti STBC transmit diversity scheme in the primary FSO communication system. First, the analytical derivations of different performance metrics of the system under various atmospheric turbulence conditions, and with and without pointing error, have been presented. Next, the analytical results have been compared with Monte Carlo simulation results. The results established that an Alamouti STBC-based MISO FSO link performs better in all respects than a fundamental FSO (SISO FSO) link under any weather condition. So, it can be undoubtedly said that the performance of the primary FSO link can be improved under any AT condition by employing the transmit diversity scheme in the system.

## Chapter 4

# Performance Analysis of FSO Communication Channel with SEC Receive Diversity

**Chapter contributions:** In this chapter, the performance of the SIMO FSO system has been obtained by introducing the switch and examine combining (SEC), a receiver diversity technique. During the performance measurement, we considered fixed and optimal switching conditions under the absence and presence of a pointing error regime. Also, we compared the outcomes with the two architectures of the FSO system that were previously mentioned.

---

The work of this chapter is published in:

*Optics Communications*, 456, 124591, Feb. 2020 [\[link\]](#)

---



## 4.1 Introduction

The switch-and-examine combining (SEC) is a classical receive diversity technique consisting of a single transmit antenna and  $N_r$  number of receiver apertures. The primary objective of using this diversity scheme is to improve the quality of service (QoS) of the entire system with respect to the SISO FSO system. The combiner scheme will be employed at the receiver terminal to configure a SIMO FSO network, and different performance metrics of the network will be studied in the present chapter. All performance metrics will be examined with fixed and optimal switching thresholds for a series of SNR values.

## 4.2 Organization

After the introduction, this chapter is organized in the following sequence. Analytical derivation of the measuring metrics under moderate-to-strong turbulence, i.e. GG distribution, is provided in Section 4.3. In Section 4.4, the above investigations are repeated in the presence of a pointing error. Detailed calculation of performance metrics under the general Málaga distribution is carried out in Section 4.5. The numerical results for SISO FSO and SIMO FSO links are compared in Section 4.7. The chapter ends with the summary presented in Section 4.8.

## 4.3 Gamma-Gamma turbulence in absence of pointing error

This section presents the mathematical framework for determining the performance metrics of SIMO FSO configuration, as shown in Fig. 4.1. The communicating link is characterized by a GG distribution model with different degrees of pointing error.

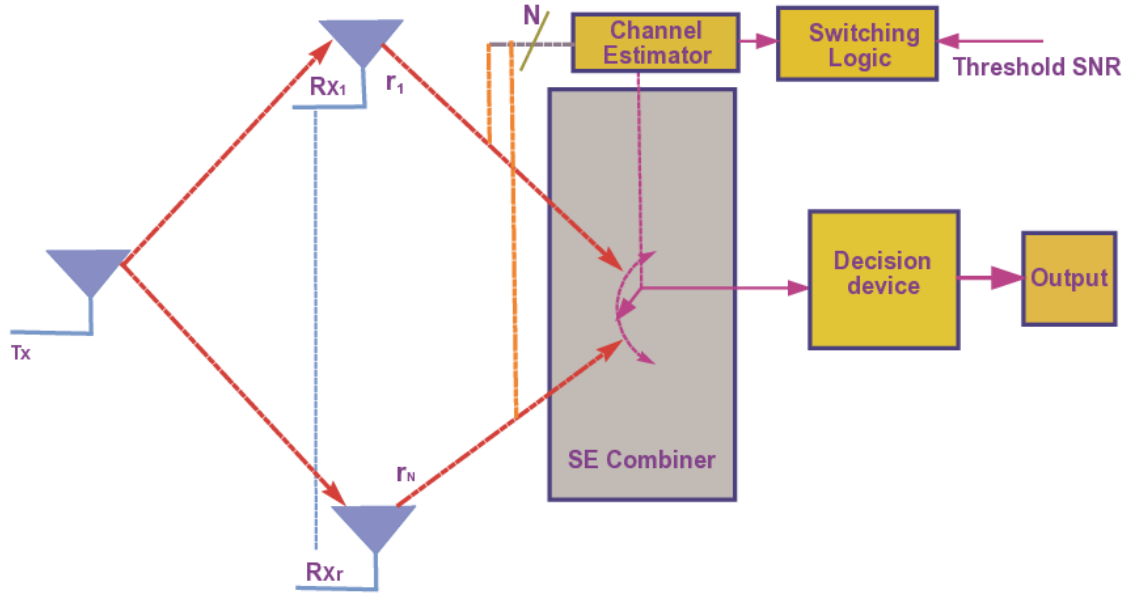


FIGURE 4.1: The SEC-based SIMO FSO communication system using one transmit antenna and  $N_r$  receiver antennas.

The detailed derivations of the analytical closed-form expressions for the OP, ABER, and average capacity of the considered system, in the absence of pointing error, are as follows:

### 4.3.1 Outage probability

The mathematical expression for the OP at the combiner output can be derived as follows

$$P_{out} = Pr(\gamma < \gamma_0) = \int_0^{\gamma_0} f_{\gamma_{SEC}}(\gamma) d\gamma \quad (4.1)$$

where,  $f_{\gamma_{SEC}}(\gamma)$  is the PDF of the SEC combiner. The above equation can be rewritten using (2.55) as

$$P_{out} = [F_{\gamma}(\gamma_{th})]^{N_r-1} \int_0^{\gamma_{th}} f_{\gamma}(\gamma) d\gamma + \sum_{j=0}^{N_r-1} [F_{\gamma}(\gamma_{th})]^j \int_{\gamma_{th}}^{\gamma_0} f_{\gamma}(\gamma) d\gamma \quad (4.2)$$

where,  $f_{\gamma}(\gamma)$  is the PDF of the SISO FSO link, and  $N_r$  defines the number of receiver path. Assuming  $I_1 = \int_0^{\gamma_{th}} f_{\gamma}(\gamma) d\gamma$ ,  $I_2 = \int_{\gamma_{th}}^{\gamma_0} f_{\gamma}(\gamma) d\gamma$ , and using (2.17) the integral component of the above equation can be written as

$$I_1 = \frac{(\alpha_t \beta_t)^{\frac{(\alpha_t + \beta_t)}{2}}}{\Gamma(\alpha_t) \Gamma(\beta_t) (\bar{\gamma})^{\frac{(\alpha_t + \beta_t)}{4}}} \int_0^{\gamma_{th}} (\gamma)^{\frac{(\alpha_t + \beta_t)}{4} - 1} K_{\alpha_t - \beta_t} \left( 2 \sqrt{\alpha_t \beta_t} \sqrt{\frac{\gamma}{\bar{\gamma}}} \right) d\gamma \quad (4.3a)$$

$$I_2 = \frac{(\alpha_t \beta_t)^{\frac{(\alpha_t + \beta_t)}{2}}}{\Gamma(\alpha_t) \Gamma(\beta_t) (\bar{\gamma})^{\frac{(\alpha_t + \beta_t)}{4}}} \int_{\gamma_{th}}^{\gamma_0} (\gamma)^{\frac{(\alpha_t + \beta_t)}{4} - 1} K_{\alpha_t - \beta_t} \left( 2 \sqrt{\alpha_t \beta_t} \sqrt{\frac{\gamma}{\bar{\gamma}}} \right) d\gamma \quad (4.3b)$$

With the help of [94, Eq.(8.4.23.1)] and [96, Eq.(26)], the closed-form expression for  $I_1$  is given by

$$I_1 = \frac{(\alpha_t \beta_t)^{\frac{(\alpha_t + \beta_t)}{2}}}{\Gamma(\alpha_t) \Gamma(\beta_t) (\bar{\gamma})^{\frac{(\alpha_t + \beta_t)}{4}}} (\gamma_{th})^{\frac{(\alpha_t + \beta_t)}{4}} G_{1 \ 3}^2 \left[ \alpha_t \beta_t \sqrt{\frac{\gamma_{th}}{\bar{\gamma}}} \middle| \begin{matrix} 1 - \frac{\alpha_t + \beta_t}{2} \\ \frac{\alpha_t - \beta_t}{2}, \frac{\beta_t - \alpha_t}{2}, -\frac{\alpha_t + \beta_t}{2} \end{matrix} \right] \quad (4.4)$$

For  $I_2$ , the following indefinite integral [115, Eq.(03.04.21.0016.01)] is considered.

$$\int \mathcal{Z}^{\alpha-1} K_v(a \mathcal{Z}^r) d\mathcal{Z} = (A/r)(B - C) \quad (4.5)$$

where,  $A = 2^{-v-2} \pi \mathcal{Z}^{\alpha} (a \mathcal{Z}^r)^{-v} \csc(\pi v)$ ,  $B = 4^v \Gamma(w) {}_1\tilde{F}_2(w; x, y; z)$ ,  $C = (a \mathcal{Z}^r)^{2v} \Gamma(m) {}_1\tilde{F}_2(m; n, p; q)$ ,  $w = \frac{\alpha - rv}{2r}$ ,  $x = 1 - v$ ,  $y = \frac{1}{2} \left( \frac{\alpha}{r} - v + 2 \right)$ ,  $z = \frac{1}{4} a^2 \mathcal{Z}^{2r}$ ,  $m = \frac{\alpha + rv}{2r}$ ,  $n = 1 + v$ ,  $p = \frac{\alpha + r(v+2)}{2r}$ , and  $q = \frac{1}{4} a^2 \mathcal{Z}^{2r}$ .

### 4.3.2 Average bit error rate

The average BER of the  $1 \times N_r$  FSO communication system with the OOK modulation scheme is defined as follows [details in Appendix (B)]

$$P_e = \frac{1}{\pi} \int_0^{\frac{\pi}{2}} \mathcal{M}_{\gamma SEC} \left( -\frac{1}{2 \sin^2 \theta} \right) d\theta \quad (4.6)$$

where,  $\mathcal{M}_{\gamma SEC}(\cdot)$  is the MGF of the SEC. Now using (2.56), the MGF is written as

$$\mathcal{M}_{\gamma SEC}(s) = [F_\gamma(\gamma_{th})]^{N_r-1} \mathcal{M}_\gamma(s) + \sum_{j=0}^{N_r-2} [F_\gamma(\gamma_{th})]^j \Psi(s) \quad (4.7)$$

where  $\mathcal{M}_\gamma(s)$  is the common MGF of the individual diversity branch, and  $\Psi(s) = \int_{\gamma_{th}}^{\infty} \exp(s\gamma) f_\gamma(\gamma) d\gamma$ , where,  $f_\gamma(\gamma)$  is the PDF of the individual diversity branch. For GG fading without pointing error environment, the  $\mathcal{M}_\gamma(s)$  is already defined in (2.23). To derive the analytical closed-form of the other factor ( $\Psi(s)$ ), we may write the following equation for  $\Psi(s)$  using (2.18), as

$$\Psi(s) = \frac{(\alpha_t \beta_t)^{\frac{(\alpha_t + \beta_t)}{2}}}{2\Gamma(\alpha_t)\Gamma(\beta_t)(\bar{\gamma})^{\frac{(\alpha_t + \beta_t)}{4}}} \int_{\gamma_{th}}^{\infty} \exp(s\gamma) (\gamma)^{\frac{(\alpha_t + \beta_t)}{4}-1} G_{0\ 2}^{2\ 0} \left[ \alpha_t \beta_t \sqrt{\frac{\gamma}{\bar{\gamma}}} \middle| \begin{matrix} - \\ \frac{\alpha_t - \beta_t}{2}, \frac{\beta_t - \alpha_t}{2} \end{matrix} \right] d\gamma \quad (4.8)$$

Next, using [95, Eq.(1.211.1)], the above equation can be presented as

$$\Psi(s) = \frac{(\alpha_t \beta_t)^{\frac{(\alpha_t + \beta_t)}{2}}}{2\Gamma(\alpha_t)\Gamma(\beta_t)(\bar{\gamma})^{\frac{(\alpha_t + \beta_t)}{4}}} \sum_{k=0}^{\infty} \frac{s^k}{k!} \int_{\gamma_{th}}^{\infty} (\gamma)^{k + \frac{(\alpha_t + \beta_t)}{4} - 1} G_{0\ 2}^{2\ 0} \left[ \alpha_t \beta_t \sqrt{\frac{\gamma}{\bar{\gamma}}} \middle| \begin{matrix} - \\ \frac{\alpha_t - \beta_t}{2}, \frac{\beta_t - \alpha_t}{2} \end{matrix} \right] d\gamma \quad (4.9)$$

Using [115, eq. (07.34.21.0085.01)], (4.9) can further be written as

$$\Psi(s) = \frac{(\alpha_t \beta_t)^{\frac{(\alpha_t + \beta_t)}{2}}}{4\pi\Gamma(\alpha_t)\Gamma(\beta_t)(\bar{\gamma})^{\frac{(\alpha_t + \beta_t)}{4}}} \sum_{k=0}^{\infty} \frac{s^k}{k!} \frac{1}{(\gamma_{th})^{1-k-\frac{(\alpha_t + \beta_t)}{4}}} \times G_{1\ 5}^{5\ 0} \left[ \frac{(\alpha_t \beta_t)^2 \gamma_{th}}{16\bar{\gamma}} \middle| \begin{matrix} 1-k-\frac{(\alpha_t + \beta_t)}{4} \\ 1-k-\frac{(\alpha_t + \beta_t)}{4}, P \end{matrix} \right] \quad (4.10)$$

where,  $P \in \left\{ \frac{(\alpha_t - \beta_t)}{4}, \frac{(\alpha_t - \beta_t + 2)}{4}, \frac{(\beta_t - \alpha_t)}{4}, \frac{(\beta_t - \alpha_t + 2)}{4} \right\}$

### 4.3.3 Average capacity

Using (2.60) and (2.55), and after some mathematical manipulation, the average capacity of the SIMO FSO system can be written as [113]

$$C = B \log_2 \left[ \exp \left\{ \left[ [F_\gamma(\gamma_{th})]^{N_r-1} - \sum_{j=0}^{N_r-1} [F_\gamma(\gamma_{th})]^j \right] \int_0^{\gamma_{th}} \Phi(\gamma) d\gamma \right\} \right] \\ + B \log_2 \left[ \exp \left\{ \left[ \sum_{j=0}^{N_r-1} [F_\gamma(\gamma_{th})]^j \right] \int_0^\infty \Phi(\gamma) d\gamma \right\} \right] \quad (4.11)$$

where,  $\Phi(\gamma) = \ln(1 + \gamma) f_\gamma(\gamma)$ . Considering  $\mathcal{J}_1 = \int_0^{\gamma_{th}} \Phi(\gamma) d\gamma$  and  $\mathcal{J}_2 = \int_0^\infty \Phi(\gamma) d\gamma$ , to obtain the closed-form expression for  $\mathcal{J}_1$  and  $\mathcal{J}_2$ , we can derive the following two equations with the help of (2.18) as

$$\mathcal{J}_1 = \frac{(\alpha_t \beta_t)^{\frac{(\alpha_t + \beta_t)}{2}}}{2\Gamma(\alpha_t)\Gamma(\beta_t)(\bar{\gamma})^{\frac{(\alpha_t + \beta_t)}{4}}} \int_0^{\gamma_{th}} (\gamma)^{\frac{(\alpha_t + \beta_t)}{4}-1} \ln(1 + \gamma) G_{0\ 2}^{2\ 0} \left[ \alpha_t \beta_t \sqrt{\frac{\gamma}{\bar{\gamma}}} \middle| \begin{matrix} - \\ \alpha_t - \beta_t, \beta_t - \alpha_t \end{matrix} \right] d\gamma \quad (4.12a)$$

$$\mathcal{J}_2 = \frac{(\alpha_t \beta_t)^{\frac{(\alpha_t + \beta_t)}{2}}}{2\Gamma(\alpha_t)\Gamma(\beta_t)(\bar{\gamma})^{\frac{(\alpha_t + \beta_t)}{4}}} \int_0^\infty (\gamma)^{\frac{(\alpha_t + \beta_t)}{4}-1} \ln(1 + \gamma) G_{0\ 2}^{2\ 0} \left[ \alpha_t \beta_t \sqrt{\frac{\gamma}{\bar{\gamma}}} \middle| \begin{matrix} - \\ \alpha_t - \beta_t, \beta_t - \alpha_t \end{matrix} \right] d\gamma \quad (4.12b)$$

After some mathematical manipulation the closed-forms of above two equations can finally be written as [details in Appendix E]

$$\mathcal{J}_1 = \frac{(\alpha_t \beta_t)^{\frac{(\alpha_t + \beta_t)}{2}}}{\Gamma(\alpha_t)\Gamma(\beta_t)(\bar{\gamma})^{\frac{(\alpha_t + \beta_t)}{4}}} \sum_{p=1}^{\infty} \frac{(-1)^{p+1}}{p} (\sqrt{\gamma_{th}})^{2p + \frac{(\alpha_t + \beta_t)}{2}} \\ \times G_{1\ 3}^{2\ 1} \left[ \alpha_t \beta_t \sqrt{\frac{\gamma_{th}}{\bar{\gamma}}} \middle| \begin{matrix} 1 - 2p - \frac{(\alpha_t + \beta_t)}{2} \\ \alpha_t - \beta_t, \beta_t - \alpha_t, -2p - \frac{(\alpha_t + \beta_t)}{2} \end{matrix} \right] \quad (4.13)$$

and

$$\mathcal{J}_2 = \frac{(\alpha_t \beta_t)^{\frac{(\alpha_t + \beta_t)}{2}}}{4\pi\Gamma(\alpha_t)\Gamma(\beta_t)(\bar{\gamma})^{\frac{(\alpha_t + \beta_t)}{4}}} G_{2\ 6}^{6\ 1} \left[ \frac{(\alpha_t \beta_t)^2}{16\bar{\gamma}} \middle| \begin{matrix} -\frac{(\alpha_t + \beta_t)}{4}, 1 - \frac{(\alpha_t + \beta_t)}{4} \\ P, -\frac{(\alpha_t + \beta_t)}{4}, -\frac{(\alpha_t + \beta_t)}{4} \end{matrix} \right] \quad (4.14)$$

## 4.4 Gamma-Gamma turbulence in presence of pointing error

In this subsection, the analytical expressions of the performance metrics of a SIMO FSO network, in the presence of a pointing error are derived.

### 4.4.1 Outage probability

To calculate the OP in this environment, we follow the same procedure as in (4.2.1.1). Using (4.2), the OP is expressed, in terms of  $I_{1P}$  and  $I_{2P}$ , as

$$P_{out} = [F_{\gamma}(\gamma_{th})]^{N_r-1} I_{1p} + \sum_{j=0}^{N_r-1} [F_{\gamma}(\gamma_{th})]^j I_{2p} \quad (4.15)$$

Assuming  $I_{1p} = \int_0^{\gamma_{th}} f_{\gamma}(\gamma) d\gamma$ , and  $I_{2p} = \int_{\gamma_{th}}^{\gamma_0} f_{\gamma}(\gamma) d\gamma$  and also using (2.37), the integral component of the above equations can be written as

$$I_{1p} = \frac{\xi^2}{2\Gamma(\alpha_t)\Gamma(\beta_t)} \int_0^{\gamma_{th}} (\gamma)^{-1} G_{1\ 3}^{3\ 0} \left[ \alpha_t \beta_t \mathcal{K} \sqrt{\frac{\gamma}{\bar{\gamma}}} \Big|_{\xi^2, \alpha_t, \beta_t}^{\xi^2+1} \right] d\gamma \quad (4.16a)$$

$$I_{2p} = \frac{\xi^2}{2\Gamma(\alpha_t)\Gamma(\beta_t)} \int_{\gamma_{th}}^{\gamma_0} (\gamma)^{-1} G_{1\ 3}^{3\ 0} \left[ \alpha_t \beta_t \mathcal{K} \sqrt{\frac{\gamma}{\bar{\gamma}}} \Big|_{\xi^2, \alpha_t, \beta_t}^{\xi^2+1} \right] d\gamma \quad (4.16b)$$

Now, with the help of [96, Eq.(26)], the closed-form of  $I_{1p}$  becomes

$$I_{1p} = \frac{\xi^2}{\Gamma(\alpha_t)\Gamma(\beta_t)} G_{2\ 4}^{3\ 1} \left[ \alpha_t \beta_t \mathcal{K} \sqrt{\frac{\gamma_{th}}{\bar{\gamma}}} \Big|_{\xi^2, \alpha_t, \beta_t, 0}^{1, \xi^2+1} \right] \quad (4.17)$$

The closed-form equation of  $I_{2p}$  can be expressed, using (4.16b) and taking help of [115, eq. (07.34.21.0001.01)] and [94, eq.(8.2.2.15)], as

$$I_{2p} = \frac{\xi^2}{\Gamma(\alpha_t)\Gamma(\beta_t)} G_{2 \ 4}^{3 \ 1} \left[ \alpha_t \beta_t \mathcal{K} \sqrt{\frac{\gamma_0}{\bar{\gamma}}} \middle|_{\xi^2, \alpha_t, \beta_t, 0}^{1, \xi^2+1} \right] - \frac{\xi^2}{\Gamma(\alpha_t)\Gamma(\beta_t)} G_{2 \ 4}^{3 \ 1} \left[ \alpha_t \beta_t \mathcal{K} \sqrt{\frac{\gamma_{th}}{\bar{\gamma}}} \middle|_{\xi^2, \alpha_t, \beta_t, 0}^{1, \xi^2+1} \right] \quad (4.18)$$

#### 4.4.2 Average bit error rate

For calculating the average BER of the system, following the same procedure as in section 4.2.1.2, (4.7), the MGF of the SEC can be written as

$$\mathcal{M}_{\gamma_{SEC}}^p(s) = [F_\gamma(\gamma_{th})]^{N_r-1} \mathcal{M}_\gamma^p(s) + \sum_{j=0}^{N_r-2} [F_\gamma(\gamma_{th})]^j \Psi^p(s) \quad (4.19)$$

where  $\mathcal{M}_\gamma^p(s)$  is the common MGF of the individual diversity branch in presence of pointing error, and  $\Psi^p(s) = \int_{\gamma_{th}}^{\infty} \exp(s\gamma) f_\gamma(\gamma) d\gamma$ , where,  $f_\gamma(\gamma)$  is the PDF of the individual diversity branch in presence of pointing error. For GG turbulence with pointing error, the  $\mathcal{M}_\gamma(s)$  has already been defined in (2.41). Now, the mathematical framework for deriving ( $\Psi^p(s)$ ), we may write (2.37)

$$\Psi^p(s) = \frac{\xi^2}{2\Gamma(\alpha_t)\Gamma(\beta_t)} \int_{\gamma_{th}}^{\infty} (\gamma)^{-1} \exp(s\gamma) G_{1 \ 3}^{3 \ 0} \left[ \alpha_t \beta_t \mathcal{K} \sqrt{\frac{\gamma}{\bar{\gamma}}} \middle|_{\xi^2, \alpha_t, \beta_t}^{\xi^2+1} \right] d\gamma \quad (4.20)$$

Next, with the help of [95, Eq.(1.211.1)], the above equation can be modified as

$$\Psi^p(s) = \frac{\xi^2}{2\Gamma(\alpha_t)\Gamma(\beta_t)} \sum_{k=0}^{\infty} \frac{s^k}{k!} \int_{\gamma_{th}}^{\infty} (\gamma)^{k-1} G_{1 \ 3}^{3 \ 0} \left[ \alpha_t \beta_t \mathcal{K} \sqrt{\frac{\gamma}{\bar{\gamma}}} \middle|_{\xi^2, \alpha_t, \beta_t}^{\xi^2+1} \right] d\gamma \quad (4.21)$$

and further, utilizing [115, eq. (07.34.21.0085.01)], (4.21) can be written as

$$\Psi^p(s) = \frac{\xi^2}{2\Gamma(\alpha_t)\Gamma(\beta_t)} \sum_{k=0}^{\infty} \frac{s^k}{k!} (\gamma_{th})^k G_{3 \ 7}^{7 \ 0} \left[ \frac{(\alpha_t \beta_t \mathcal{K})^2 \gamma_{th}}{16\bar{\gamma}} \middle|_{-k, \frac{\xi^2}{2}, \frac{\xi^2+1}{2}, \frac{\alpha_t}{2}, \frac{\alpha_t+1}{2}, \frac{\beta_t}{2}, \frac{\beta_t+1}{2}}^{\frac{\xi^2+1}{2}, \frac{\xi^2+2}{2}, 1-k} \right] \quad (4.22)$$

### 4.4.3 Average capacity

Based on (2.60) and (2.55), the average capacity of the SIMO FSO system can be written as [113]

$$C = B \log_2 \left[ \exp \left\{ \left[ [F_\gamma(\gamma_{th})]^{N_r-1} - \sum_{j=0}^{N_r-1} [F_\gamma(\gamma_{th})]^j \right] \int_0^{\gamma_{th}} \Phi^p(\gamma) d\gamma \right\} \right] \\ + B \log_2 \left[ \exp \left\{ \left[ \sum_{j=0}^{N_r-1} [F_\gamma(\gamma_{th})]^j \right] \int_0^\infty \Phi^p(\gamma) d\gamma \right\} \right] \quad (4.23)$$

where,  $\Phi^p(\gamma) = \ln(1+\gamma)f_\gamma(\gamma)$ . Assuming  $\mathcal{J}_1^p = \int_0^{\gamma_{th}} \Phi^p(\gamma) d\gamma$  and  $\mathcal{J}_2^p = \int_0^\infty \Phi^p(\gamma) d\gamma$ , their closed-form expressions can be derived, with the help of (2.18), as

$$\mathcal{J}_1^p = \frac{\xi^2}{2\Gamma(\alpha_t)\Gamma(\beta_t)} \int_0^{\gamma_{th}} (\gamma)^{-1} \ln(1+\gamma) G_{1\ 3}^{3\ 0} \left[ \alpha_t \beta_t \mathcal{K} \sqrt{\frac{\gamma}{\bar{\gamma}}} \middle|_{\xi^2, \alpha_t, \beta_t}^{\xi^2+1} \right] d\gamma \quad (4.24a)$$

$$\mathcal{J}_2^p = \frac{\xi^2}{2\Gamma(\alpha_t)\Gamma(\beta_t)} \int_0^\infty (\gamma)^{-1} \ln(1+\gamma) G_{1\ 3}^{3\ 0} \left[ \alpha_t \beta_t \mathcal{K} \sqrt{\frac{\gamma}{\bar{\gamma}}} \middle|_{\xi^2, \alpha_t, \beta_t}^{\xi^2+1} \right] d\gamma \quad (4.24b)$$

after some mathematical manipulation, the closed-form of the above two equation can finally be written as [details in Appendix E]

$$\mathcal{J}_1^p = \frac{\xi^2}{\Gamma(\alpha_t)\Gamma(\beta_t)} \sum_{p=1}^{\infty} \frac{(-1)^{p+1}}{p} (\sqrt{\gamma_{th}})^{2p} G_{2\ 3}^{3\ 1} \left[ \alpha_t \beta_t \mathcal{K} \sqrt{\frac{\gamma_{th}}{\bar{\gamma}}} \middle|_{\xi^2, \alpha_t, \beta_t, -2p}^{1-2p, \xi^2+1} \right] \quad (4.25)$$

and

$$\mathcal{J}_2^p = \frac{\xi^2 (2)^{\alpha_t + \beta_t - 1}}{4\pi \Gamma(\alpha_t)\Gamma(\beta_t)} G_{4\ 8}^{8\ 1} \left[ \frac{(\alpha_t \beta_t \mathcal{K})^2}{16\bar{\gamma}} \middle|_{\frac{\xi^2}{2}, \frac{\xi^2+1}{2}, \frac{\alpha_t}{2}, \frac{\alpha_t+1}{2}, \frac{\beta_t}{2}, \frac{\beta_t+1}{2}, 0, 0}^{0, 1, \frac{\xi^2+1}{2}, \frac{\xi^2+2}{2}} \right] \quad (4.26)$$



## 4.5 Málaga turbulence in absence of pointing error

In this section, the performance metrics of a SIMO FSO system will be determined under the Málaga statistical distribution without and with the effect of pointing error in the system.

Consider our system working in the absence of a pointing error. The analytical framework for different performance metrics of the system is given below:

### 4.5.1 Outage probability

Derivation of OP is similar to that presented in section 4.2.1.1., with only the difference in the closed-form of two integral components  $I_1$  and  $I_2$ . We, therefore, present here the closed-form of two integral components only. Using (2.25) and their mathematical definitions,  $I_1$  and  $I_2$  are expressed as

$$I_1 = \frac{\mathcal{A}}{2} \sum_{k_t=1}^{\beta_t} \frac{a_k}{(\bar{\gamma})^{\frac{\alpha_t+k_t}{4}}} \int_0^{\gamma_{th}} (\gamma)^{\left(\frac{\alpha_t+k_t}{4}\right)-1} K_{\alpha_t-k_t} \left( \mathcal{B} \sqrt{\alpha_t \beta_t} \sqrt{\frac{\gamma}{\bar{\gamma}}} \right) d\gamma \quad (4.27a)$$

$$I_2 = \frac{\mathcal{A}}{2} \sum_{k_t=1}^{\beta_t} \frac{a_k}{(\bar{\gamma})^{\frac{\alpha_t+k_t}{4}}} \int_{\gamma_{th}}^{\gamma_0} (\gamma)^{\left(\frac{\alpha_t+k_t}{4}\right)-1} k_{\alpha_t-k_t} \left( \mathcal{B} \sqrt{\alpha_t \beta_t} \sqrt{\frac{\gamma}{\bar{\gamma}}} \right) d\gamma \quad (4.27b)$$

With the help of [94, Eq.(8.4.23.1)] and [96, Eq.(26)], the closed-form equation of the  $I_1$  is written as

$$I_1 = \frac{\mathcal{A}}{2} \sum_{k_t=1}^{\beta_t} \frac{a_k}{(\bar{\gamma})^{\frac{\alpha_t+k_t}{4}}} (\gamma_{th})^{\frac{\alpha_t+k_t}{4}} G_{1 \ 3}^{2 \ 1} \left[ \frac{\mathcal{B}^2 \alpha_t \beta_t}{4} \sqrt{\frac{\gamma_{th}}{\bar{\gamma}}} \middle| \begin{matrix} 1 - \frac{\alpha_t+k_t}{2} \\ \frac{\alpha_t-k_t}{2}, \frac{k_t-\alpha_t}{2}, -\frac{\alpha_t+k_t}{2} \end{matrix} \right] \quad (4.28)$$

and, for  $I_2$  we have followed (4.5).

### 4.5.2 Average bit error rate

To define an analytical framework for the average BER performance of the system, the following equation is derived using (2.59) for the OOK modulation scheme, as

$$P_e = \frac{1}{2} \int_0^\infty \operatorname{erfc} \left( \sqrt{\frac{\gamma}{2}} \right) f_{\gamma_{SEC}}(\gamma) d\gamma \quad (4.29)$$

where,  $f_{\gamma_{SEC}}(\gamma)$  is the PDF of considered receiver diversity scheme in this system, and it is the function of the PDF ( $f_\gamma(\gamma)$ ) of individual diversity path. With the help of (2.55) and after some mathematical manipulation, the BER can be presented as

$$\begin{aligned} P_e = \frac{1}{2} & \left[ [f_\gamma(\gamma_{th})]^{N_r-1} - \sum_{j=0}^{N_r-1} [f_\gamma(\gamma_{th})]^j \right] \int_0^{\gamma_{th}} \operatorname{erfc} \left( \sqrt{\frac{\gamma}{2}} \right) f_\gamma(\gamma) d\gamma \\ & + \frac{1}{2} \sum_{j=0}^{N_r-1} [f_\gamma(\gamma_{th})]^j \int_0^\infty \operatorname{erfc} \left( \sqrt{\frac{\gamma}{2}} \right) f_\gamma(\gamma) d\gamma \end{aligned} \quad (4.30)$$

Now, assuming  $\mathcal{P}_1 = \frac{1}{2} \int_0^{\gamma_{th}} \operatorname{erfc} \left( \sqrt{\frac{\gamma}{2}} \right) f_\gamma(\gamma) d\gamma$ , and  $\mathcal{P}_2 = \frac{1}{2} \int_0^\infty \operatorname{erfc} \left( \sqrt{\frac{\gamma}{2}} \right) f_\gamma(\gamma) d\gamma$ ,  $\mathcal{P}_1$  and  $\mathcal{P}_2$  can be expressed, using (2.26), as

$$\mathcal{P}_1 = \frac{\mathcal{A}}{8} \sum_{k_t=1}^{\beta_t} \frac{a_k}{(\bar{\gamma})^{\frac{\alpha_t+k_t}{4}}} \int_0^{\gamma_{th}} (\gamma)^{\frac{\alpha_t+k_t}{4}-1} \operatorname{erfc} \left( \sqrt{\frac{\gamma}{2}} \right) G_{0 \ 2}^{2 \ 0} \left[ \frac{\mathcal{B}^2 \alpha_t \beta_t}{4} \sqrt{\frac{\gamma}{\bar{\gamma}}} \middle| \begin{matrix} - \\ \frac{\alpha_t-k_t}{2}, \frac{k_t-\alpha_t}{2} \end{matrix} \right] d\gamma \quad (4.31)$$

and

$$\mathcal{P}_2 = \frac{\mathcal{A}}{8} \sum_{k_t=1}^{\beta_t} \frac{a_k}{(\bar{\gamma})^{\frac{\alpha_t+k_t}{4}}} \int_0^\infty (\gamma)^{\frac{\alpha_t+k_t}{4}-1} \operatorname{erfc} \left( \sqrt{\frac{\gamma}{2}} \right) G_{0 \ 2}^{2 \ 0} \left[ \frac{\mathcal{B}^2 \alpha_t \beta_t}{4} \sqrt{\frac{\gamma}{\bar{\gamma}}} \middle| \begin{matrix} - \\ \frac{\alpha_t-k_t}{2}, \frac{k_t-\alpha_t}{2} \end{matrix} \right] d\gamma \quad (4.32)$$

Next, the closed-form equations for  $\mathcal{P}_1$  and  $\mathcal{P}_2$  are written as [details in Appendix F]

$$\begin{aligned}
\mathcal{P}_1 &= \frac{\mathcal{A}}{24} \sum_{k_t=1}^{\beta_t} \frac{a_k}{(\bar{\gamma})^{\frac{\alpha_t+k_t}{4}}} \sum_{m=0}^{\infty} \frac{(-1)^m}{(2)^m (m!)} (\sqrt{\gamma_{th}})^{\frac{\alpha_t+k_t}{4}+2m} \\
&\quad \times G_{1\ 3}^{2\ 1} \left[ \frac{\mathcal{B}^2 \alpha_t \beta_t}{4} \sqrt{\frac{\gamma_{th}}{\bar{\gamma}}} \left| \begin{matrix} 1-2m-\frac{\alpha_t+k_t}{2} \\ \frac{\alpha_t-k_t}{2}, \frac{k_t-\alpha_t}{2}, -2m-\frac{\alpha_t+k_t}{2} \end{matrix} \right. \right] \\
&+ \frac{\mathcal{A}}{8} \sum_{k_t=1}^{\beta_t} \frac{a_k}{(\bar{\gamma})^{\frac{\alpha_t+k_t}{4}}} \sum_{m=0}^{\infty} \frac{(-1)^m (2)^m}{(3)^m (m!)} (\sqrt{\gamma_{th}})^{\frac{\alpha_t+k_t}{4}+2m} \\
&\quad \times G_{1\ 3}^{2\ 1} \left[ \frac{\mathcal{B}^2 \alpha_t \beta_t}{4} \sqrt{\frac{\gamma_{th}}{\bar{\gamma}}} \left| \begin{matrix} 1-2m-\frac{\alpha_t+k_t}{2} \\ \frac{\alpha_t-k_t}{2}, \frac{k_t-\alpha_t}{2}, -2m-\frac{\alpha_t+k_t}{2} \end{matrix} \right. \right]
\end{aligned} \tag{4.33}$$

and

$$\begin{aligned}
\mathcal{P}_2 &= \frac{\mathcal{A}}{16\pi\sqrt{\pi}} \sum_{k_t=1}^{\beta_t} \frac{a_k}{(\bar{\gamma})^{\frac{\alpha_t+k_t}{4}}} \left( \frac{1}{2} \right)^{-\frac{\alpha_t+k_t}{4}} \\
&\times G_{2\ 5}^{4\ 2} \left[ \frac{\mathcal{B}^4 \alpha_t^2 \beta_t^2}{128\bar{\gamma}} \left| \begin{matrix} 1-\frac{\alpha_t+k_t}{4}, \frac{1}{2}-\frac{\alpha_t+k_t}{4} \\ \frac{\alpha_t-k_t}{4}, \frac{\alpha_t-k_t+2}{4}, \frac{k_t-\alpha_t}{4}, \frac{k_t-\alpha_t+2}{4}, -\frac{\alpha_t+k_t}{4} \end{matrix} \right. \right]
\end{aligned} \tag{4.34}$$

### 4.5.3 Average capacity

Here, we have developed a mathematical framework for the average capacity of the system. The average capacity, is given, based on (2.60) and (2.55), as

$$\begin{aligned}
C &= B \left[ [f_\gamma(\gamma_{th})]^{N_r-1} - \sum_{j=0}^{N_r-1} [f_\gamma(\gamma_{th})]^j \right] \int_0^{\gamma_{th}} \log_2(1+\gamma) f_\gamma(\gamma) d\gamma \\
&\quad + B \left[ \sum_{j=0}^{N_r-1} [f_\gamma(\gamma_{th})]^j \right] \int_0^{\infty} \log_2(1+\gamma) f_\gamma(\gamma) d\gamma
\end{aligned} \tag{4.35}$$

where,  $f_\gamma(\gamma)$  is the PDF of individual diversity branch. Assuming  $\mathcal{I}_1 = \int_0^{\gamma_{th}} \log_2(1+\gamma) f_\gamma(\gamma) d\gamma$  and  $\mathcal{I}_2 = \int_0^{\infty} \log_2(1+\gamma) f_\gamma(\gamma) d\gamma$ , and using (2.26), we derive two equations

for  $\mathcal{I}_1$  and  $\mathcal{I}_2$  as

$$\mathcal{I}_1 = \frac{\mathcal{A}}{4 \ln(2)} \sum_{k_t=1}^{\beta_t} \frac{a_k}{(\bar{\gamma})^{\frac{\alpha_t+k_t}{4}}} \int_0^{\gamma_{th}} (\gamma)^{\left(\frac{\alpha_t+k_t}{4}\right)-1} \ln(1+\gamma) G_{0 \ 2}^{2 \ 0} \left[ \frac{\mathcal{B}^2 \alpha_t \beta_t}{4} \sqrt{\frac{\gamma}{\bar{\gamma}}} \middle| \begin{matrix} - \\ \frac{\alpha_t-k_t}{2}, \frac{k_t-\alpha_t}{2} \end{matrix} \right] d\gamma \quad (4.36a)$$

$$\mathcal{I}_2 = \frac{\mathcal{A}}{4 \ln(2)} \sum_{k_t=1}^{\beta_t} \frac{a_k}{(\bar{\gamma})^{\frac{\alpha_t+k_t}{4}}} \int_0^{\infty} (\gamma)^{\left(\frac{\alpha_t+k_t}{4}\right)-1} \ln(1+\gamma) G_{0 \ 2}^{2 \ 0} \left[ \frac{\mathcal{B}^2 \alpha_t \beta_t}{4} \sqrt{\frac{\gamma}{\bar{\gamma}}} \middle| \begin{matrix} - \\ \frac{\alpha_t-k_t}{2}, \frac{k_t-\alpha_t}{2} \end{matrix} \right] d\gamma \quad (4.36b)$$

The closed-form equation of  $\mathcal{I}_1$  and  $\mathcal{I}_2$  can finally be expressed using appendix (E) as

$$\begin{aligned} \mathcal{I}_1 = & \frac{\mathcal{A}}{2 \ln(2)} \sum_{k_t=1}^{\beta_t} \frac{a_k}{(\bar{\gamma})^{\frac{\alpha_t+k_t}{4}}} \sum_{P=1}^{\infty} \frac{(-1)^{P+1}}{P} (\sqrt{\gamma_{th}})^{2P+\left(\frac{\alpha_t+k_t}{2}\right)} \\ & \times G_{1 \ 3}^{2 \ 1} \left[ \frac{\mathcal{B}^2 \alpha_t \beta_t}{4} \sqrt{\frac{\gamma_{th}}{\bar{\gamma}}} \middle| \begin{matrix} 1-2P-\left(\frac{\alpha_t+k_t}{2}\right) \\ \frac{\alpha_t-k_t}{2}, \frac{k_t-\alpha_t}{2}, -2P-\left(\frac{\alpha_t+k_t}{2}\right) \end{matrix} \right] \end{aligned} \quad (4.37)$$

and,

$$\mathcal{I}_2 = \frac{\mathcal{A}}{8\pi \ln(2)} \sum_{k_t=1}^{\beta_t} \frac{a_k}{(\bar{\gamma})^{\frac{\alpha_t+k_t}{4}}} G_{2 \ 6}^{6 \ 1} \left[ \frac{\mathcal{B}^4 \alpha_t^2 \beta_t^2}{256 \bar{\gamma}} \middle| \begin{matrix} -\frac{\alpha_t+k_t}{4}, 1-\frac{\alpha_t+k_t}{4} \\ \frac{\alpha_t-k_t}{4}, \frac{\alpha_t-k_t+2}{4}, \frac{k_t-\alpha_t}{4}, \frac{k_t-\alpha_t+2}{4}, -\frac{\alpha_t+k_t}{4}, -\frac{\alpha_t+k_t}{4} \end{matrix} \right] \quad (4.38)$$

## 4.6 Málaga turbulence in presence of pointing error

In this subsection, we have derived the analytical calculation for different performance metrics of SIMO FSO system experiencing misalignment fading.

### 4.6.1 Outage probability

The OP is derived as (4.15)

$$P_{out} = [f_{\gamma}(\gamma_{th})]^{N_r-1} \mathcal{I}_{1P} + \sum_{j=0}^{N_r-1} [f_{\gamma}(\gamma_{th})]^j \mathcal{I}_{2P} \quad (4.39)$$

where,  $\mathcal{I}_{1P} = \int_0^{\gamma_{th}} f_{\gamma}(\gamma) d\gamma$  and  $\mathcal{I}_{2P} = \int_{\gamma_{th}}^{\gamma_0} f_{\gamma}(\gamma) d\gamma$

Now, using (2.44), the integral component of the above equation can be written as

$$\mathcal{I}_{1P} = \frac{\xi^2 \mathcal{A}}{4} \sum_{k_t=1}^{\beta_t} B_k \int_0^{\gamma_{th}} (\gamma)^{-1} G_{1 \ 3}^{3 \ 0} \left[ \mathcal{B} \sqrt{\frac{\gamma}{\bar{\gamma}}} \middle|_{\xi^2, \alpha_t, k_t}^{\xi^2+1} \right] d\gamma \quad (4.40a)$$

$$\mathcal{I}_{2P} = \frac{\xi^2 \mathcal{A}}{4} \sum_{k_t=1}^{\beta_t} B_k \int_{\gamma_{th}}^{\gamma_0} (\gamma)^{-1} G_{1 \ 3}^{3 \ 0} \left[ \mathcal{B} \sqrt{\frac{\gamma}{\bar{\gamma}}} \middle|_{\xi^2, \alpha_t, k_t}^{\xi^2+1} \right] d\gamma \quad (4.40b)$$

With the help of [96, Eq.(26)], the closed-form of  $\mathcal{I}_{1P}$  is given by

$$\mathcal{I}_{1P} = \frac{\xi^2 \mathcal{A}}{2} \sum_{k_t=1}^{\beta_t} B_k G_{2 \ 4}^{3 \ 1} \left[ \mathcal{B} \sqrt{\frac{\gamma_{th}}{\bar{\gamma}}} \middle|_{\xi^2, \alpha_t, k_t, 0}^{1, \xi^2+1} \right] \quad (4.41)$$

and, the closed-form equation of  $\mathcal{I}_{2P}$  can be expressed, using (4.40b) and taking help of [115, eq. (07.34.21.0001.01)] and [94, eq.(8.2.2.15)], as

$$\mathcal{I}_{2P} = \frac{\xi^2 \mathcal{A}}{2} \sum_{k_t=1}^{\beta_t} B_k G_{2 \ 4}^{3 \ 1} \left[ \mathcal{B} \sqrt{\frac{\gamma_0}{\bar{\gamma}}} \middle|_{\xi^2, \alpha_t, k_t, 0}^{1, \xi^2+1} \right] - \frac{\xi^2 \mathcal{A}}{2} \sum_{k_t=1}^{\beta_t} B_k G_{2 \ 4}^{3 \ 1} \left[ \mathcal{B} \sqrt{\frac{\gamma_{th}}{\bar{\gamma}}} \middle|_{\xi^2, \alpha_t, k_t, 0}^{1, \xi^2+1} \right] \quad (4.42)$$

### 4.6.2 Average bit error rate

The ABER of the system, in the presence of pointing error, is derived based on (4.29) and (4.30), as

$$P_e = \frac{1}{2} \left[ [f_\gamma(\gamma_{th})]^{N_r-1} - \sum_{j=0}^{N_r-1} [f_\gamma(\gamma_{th})]^j \right] \mathcal{P}_1^P + \frac{1}{2} \sum_{j=0}^{N_r-1} [f_\gamma(\gamma_{th})]^j \mathcal{P}_2^P \quad (4.43)$$

where,  $\mathcal{P}_1^P = \frac{1}{2} \int_0^{\gamma_{th}} \text{erfc}(\sqrt{\frac{\gamma}{2}}) f_\gamma(\gamma) d\gamma$  and  $\mathcal{P}_2^P = \frac{1}{2} \int_0^\infty \text{erfc}(\sqrt{\frac{\gamma}{2}}) f_\gamma(\gamma) d\gamma$ . These two equations can be further expressed with its closed-form expression as

$$\mathcal{P}_1^P = \frac{\xi^2 \mathcal{A}}{8} \sum_{k_t=1}^{\beta_t} B_k \int_0^{\gamma_{th}} (\gamma)^{-1} \text{erfc} \left( \sqrt{\frac{\gamma}{2}} \right) G_{1 \ 3}^{3 \ 0} \left[ \mathcal{B} \sqrt{\frac{\gamma}{\bar{\gamma}}} \middle|_{\xi^2, \alpha_t, k_t}^{\xi^2+1} \right] d\gamma \quad (4.44)$$

and

$$\mathcal{P}_2^P = \frac{\xi^2 \mathcal{A}}{8} \sum_{k_t=1}^{\beta_t} B_k \int_0^\infty (\gamma)^{-1} \text{erfc} \left( \sqrt{\frac{\gamma}{2}} \right) G_{1 \ 3}^{3 \ 0} \left[ \mathcal{B} \sqrt{\frac{\gamma}{\bar{\gamma}}} \middle|_{\xi^2, \alpha_t, k_t}^{\xi^2+1} \right] d\gamma \quad (4.45)$$

Next, the closed-form equations for  $\mathcal{P}_1^P$  and  $\mathcal{P}_2^P$  are obtained [detailed derivation in Appendix F] as

$$\begin{aligned} \mathcal{P}_1^P &= \frac{\xi^2 \mathcal{A}}{24} \sum_{k_t=1}^{\beta_t} B_k \sum_{m=0}^{\infty} \frac{(-1)^m}{(2)^m (m!)} (\sqrt{\gamma_{th}})^{2m} G_{2 \ 4}^{3 \ 1} \left[ \mathcal{B} \sqrt{\frac{\gamma_{th}}{\bar{\gamma}}} \middle|_{\xi^2, \alpha_t, k_t, -2m}^{1-2m, \xi^2+1} \right] \\ &+ \frac{\xi^2 \mathcal{A}}{8} \sum_{k_t=1}^{\beta_t} B_k \sum_{m=0}^{\infty} \frac{(-1)^m (2)^m}{(3)^m (m!)} (\sqrt{\gamma_{th}})^{2m} G_{2 \ 4}^{3 \ 1} \left[ \mathcal{B} \sqrt{\frac{\gamma_{th}}{\bar{\gamma}}} \middle|_{\xi^2, \alpha_t, k_t, -2m}^{1-2m, \xi^2+1} \right] \end{aligned} \quad (4.46)$$

and,

$$\mathcal{P}_2^P = \frac{\xi^2 \mathcal{A}}{16\pi\sqrt{\pi}} \sum_{k_t=1}^{\beta_t} B_k (2)^{\alpha_t+k_t-1} G_{4 \ 7}^{6 \ 2} \left[ \frac{\mathcal{B}^2}{8\bar{\gamma}} \middle|_{\xi^2, \frac{\xi^2+1}{2}, \frac{\alpha_t}{2}, \frac{\alpha_t+1}{2}, \frac{k_t}{2}, \frac{k_t+1}{2}, 0}^{1, \frac{1}{2}, \frac{\xi^2+1}{2}, \frac{\xi^2+2}{2}} \right] \quad (4.47)$$

### 4.6.3 Average capacity

According to (4.35), the average capacity is given as

$$C = B \left[ [f_\gamma(\gamma_{th})]^{N_r-1} - \sum_{j=0}^{N_r-1} [f_\gamma(\gamma_{th})]^j \right] \mathcal{I}_1^P + B \left[ \sum_{j=0}^{N_r-1} [f_\gamma(\gamma_{th})]^j \right] \mathcal{I}_2^P \quad (4.48)$$

where,  $\mathcal{I}_1^P = \int_0^{\gamma_{th}} \log_2(1+\gamma) f_\gamma(\gamma) d\gamma$  and  $\mathcal{I}_2^P = \int_0^\infty \log_2(1+\gamma) f_\gamma(\gamma) d\gamma$ . Using (2.44),  $\mathcal{I}_1^P$  and  $\mathcal{I}_2^P$  are given by

$$\mathcal{I}_1^P = \frac{\xi^2 \mathcal{A}}{4 \ln(2)} \sum_{k_t=1}^{\beta_t} B_k \int_0^{\gamma_{th}} (\gamma)^{-1} \ln(1+\gamma) G_{1 \ 3}^{3 \ 0} \left[ \mathcal{B} \sqrt{\frac{\gamma}{\bar{\gamma}}} \middle|_{\xi^2, \alpha_t, k_t}^{\xi^2+1} \right] d\gamma \quad (4.49)$$

$$\mathcal{I}_2^P = \frac{\xi^2 \mathcal{A}}{4 \ln(2)} \sum_{k_t=1}^{\beta_t} B_k \int_0^\infty (\gamma)^{-1} \ln(1+\gamma) G_{1 \ 3}^{3 \ 0} \left[ \mathcal{B} \sqrt{\frac{\gamma}{\bar{\gamma}}} \middle|_{\xi^2, \alpha_t, k_t}^{\xi^2+1} \right] d\gamma \quad (4.50)$$

The closed-form expressions of  $\mathcal{I}_1^P$  and  $\mathcal{I}_2^P$  finally become [detailed derivation in appendix (E)]

$$\mathcal{I}_1^P = \frac{\xi^2 \mathcal{A}}{2 \ln(2)} \sum_{k_t=1}^{\beta_t} B_k \sum_{P=1}^{\infty} \frac{(-1)^{P+1}}{P} (\sqrt{\gamma_{th}})^{2P} G_{2 \ 4}^{3 \ 1} \left[ \mathcal{B} \sqrt{\frac{\gamma_{th}}{\bar{\gamma}}} \middle|_{\xi^2, \alpha_t, k_t, -2P}^{1-2P, \xi^2+1} \right] \quad (4.51)$$

and

$$\mathcal{I}_2^P = \frac{\xi^2 \mathcal{A}}{8\pi \ln(2)} \sum_{k_t=1}^{\beta_t} B_k (2)^{\alpha_t+k_t-1} G_{4 \ 8}^{8 \ 1} \left[ \frac{\mathcal{B}^2}{16\bar{\gamma}} \middle|_{\xi^2, \frac{\xi^2+1}{2}, \frac{\alpha_t}{2}, \frac{\alpha_t+1}{2}, \frac{k_t}{2}, \frac{k_t+1}{2}, 0, 0}^{0, 1, \frac{\xi^2+1}{2}, \frac{\xi^2+2}{2}} \right] \quad (4.52)$$

## 4.7 Numerical results and discussion for SIMO FSO link

This section presents the numerical results for various performance metrics of a SIMO FSO communication system under various AT conditions without and with the consideration of pointing errors. For such numerical analysis and Monte Carlo

TABLE 4.1: Summary of the equations used for figures, Fig. 4.2 to Fig. 4.5.

Figure	Scenario	Equation
Fig. 4.2a	GG	Eq. 4.2 with Eq. 4.4 and Eq. 4.5
Fig. 4.2b	GG	Eq. 4.2 with Eq. 4.4 and Eq. 4.5
Fig. 4.2c	GG	Eq. 4.2 with Eq. 4.4 and Eq. 4.5
Fig. 4.2d	GG	Eq. 4.2 with Eq. 4.4 and Eq. 4.5
Fig. 4.3a	GG + pointing	Eq. 4.15 with Eq. 4.17 and Eq. 4.18
Fig. 4.3b	GG + pointing	Eq. 4.15 with Eq. 4.17 and Eq. 4.18
Fig. 4.3c	GG + pointing	Eq. 4.15 with Eq. 4.17 and Eq. 4.18
Fig. 4.3d	GG + pointing	Eq. 4.15 with Eq. 4.17 and Eq. 4.18
Fig. 4.4a	Málaga	Eq. 4.2 with Eq. 4.28 and Eq. 4.5
Fig. 4.4b	Málaga	Eq. 4.2 with Eq. 4.28 and Eq. 4.5
Fig. 4.4c	Málaga	Eq. 4.2 with Eq. 4.28 and Eq. 4.5
Fig. 4.4d	Málaga	Eq. 4.2 with Eq. 4.28 and Eq. 4.5
Fig. 4.5a	Málaga + pointing	Eq. 4.39 with Eq. 4.41 and Eq. 4.42
Fig. 4.5b	Málaga + pointing	Eq. 4.39 with Eq. 4.41 and Eq. 4.42
Fig. 4.5c	Málaga + pointing	Eq. 4.39 with Eq. 4.41 and Eq. 4.42
Fig. 4.5d	Málaga + pointing	Eq. 4.39 with Eq. 4.41 and Eq. 4.42

simulation, values of atmospheric turbulence parameters and amount of misalignment are taken from Section 2.9. Variations of all the performance metrics with average SNR are presented in Fig. 4.2 to Fig. 4.13 and Table 4.1, Table 4.2 and Table 4.12 summarized the equation used for those figures.

Fig. 4.2 exhibits the OP of the SIMO FSO communication link without pointing error. Fig. 4.2 (a) depicts the OP of the system under different weather conditions with a fixed switching threshold of 2 dB and an optimal switching threshold of 3 dB. On the other hand, Fig. 4.2 (b) indicates the same performance metric with identical scenarios as in Fig. 4.2 (a). The system enjoys the same threshold value here for fixed and optimal switching. Fig. 4.2 (a) and Fig. 4.2 (b) indicate that the system gives better outcomes when the system follows the same threshold value for fixed and optimal switching.



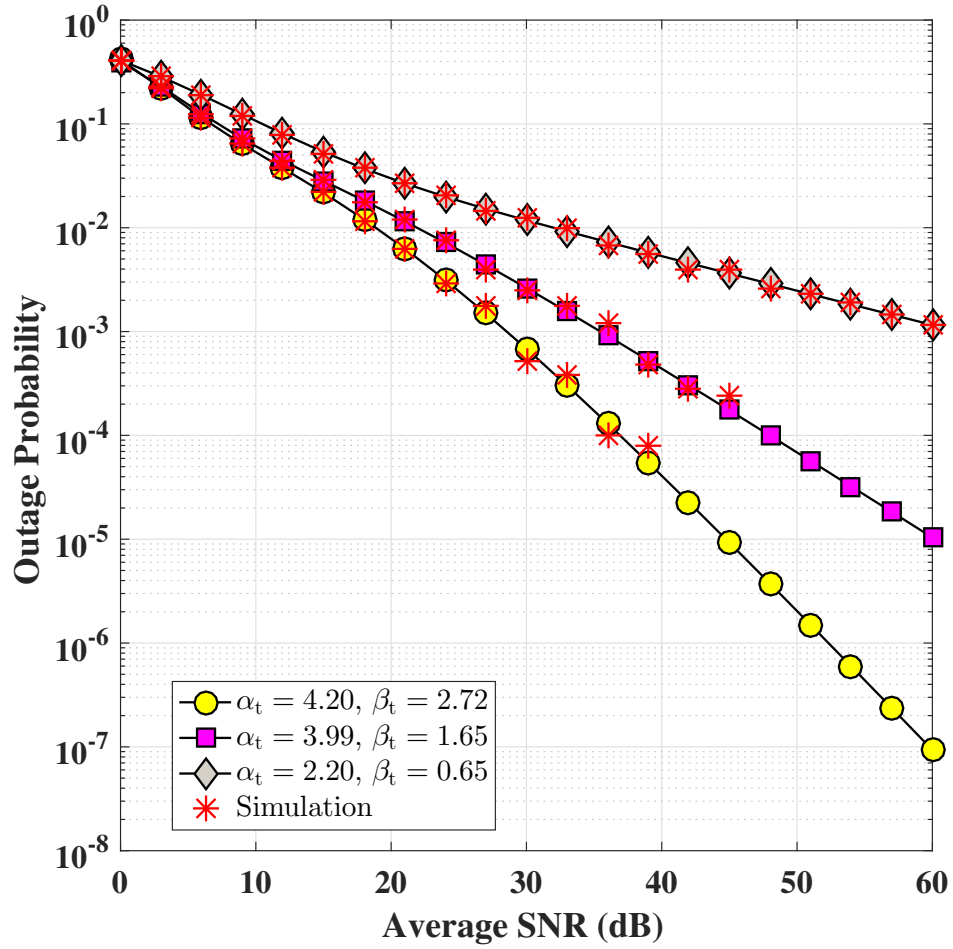
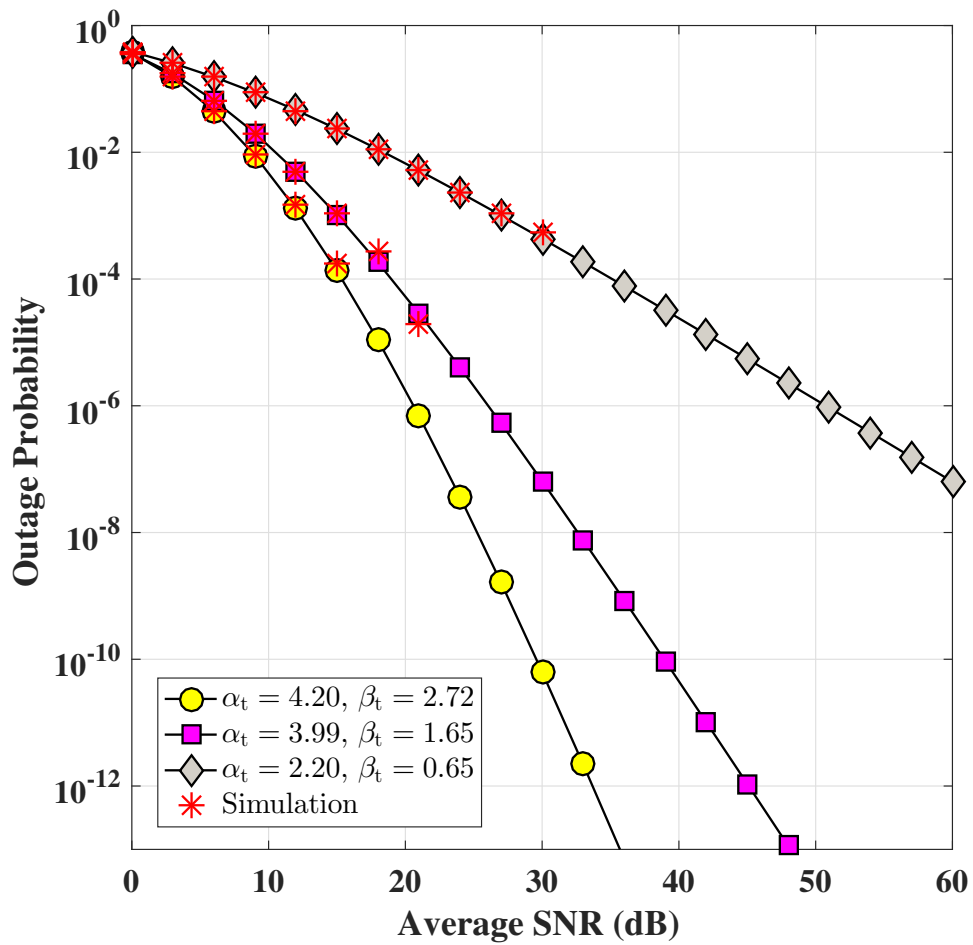
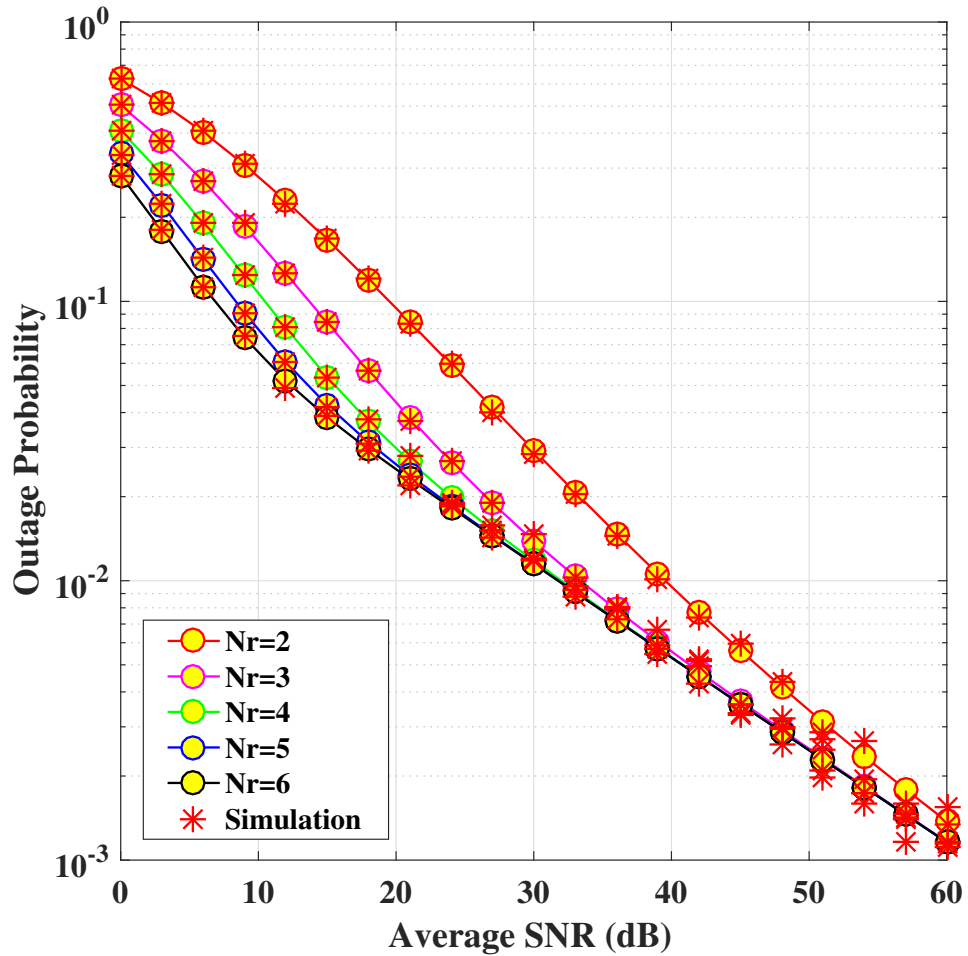


Figure 4.2 (a) Outage probability of SIMO FSO link under Gamma-Gamma distribution in the absence of pointing error for different atmospheric turbulence with  $\gamma_{th} = 2$  dB and  $\gamma_0 = 3$  dB.



**Figure 4.2 (b)** Outage probability of SIMO FSO link under Gamma-Gamma distribution in the absence of pointing error for different atmospheric turbulence with  $\gamma_{th} = 3$  dB and  $\gamma_0 = 3$  dB.



**Figure 4.2 (c)** Outage probability of SIMO FSO link under Gamma-Gamma distribution in the absence of pointing error for different receiver diversity order with  $\alpha_t = 2.20$  and  $\beta_t = 0.65$ ,  $\gamma_{th} = 2$  dB and  $\gamma_0 = 3$  dB.

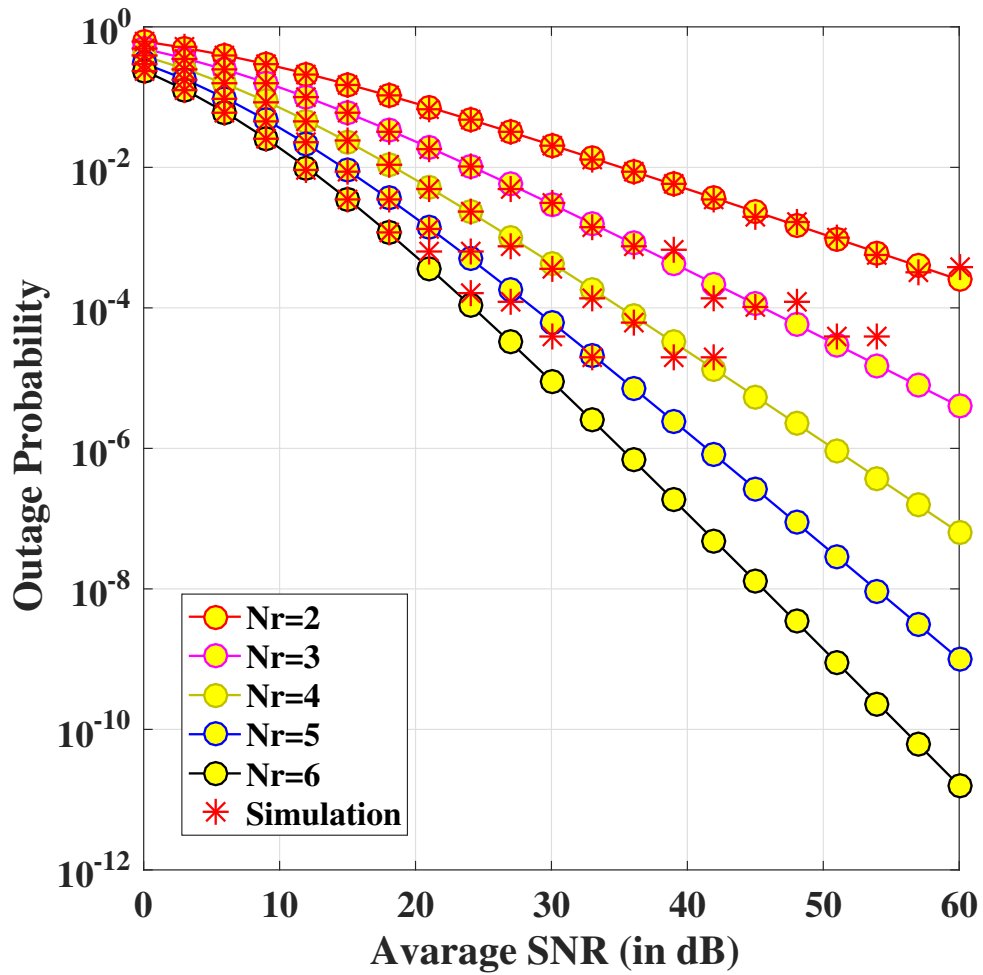


**Figure 4.2 (d)** Outage probability of SIMO FSO link under Gamma-Gamma distribution in the absence of pointing error for different receiver diversity order with  $\alpha_t = 2.20$  and  $\beta_t = 0.65$ ,  $\gamma_{th} = 3$  dB and  $\gamma_0 = 3$  dB.

FIGURE 4.2: Outage Probability of the SIMO FSO link employing switch and examine combining scheme at the receiver end with Gamma-Gamma distribution using different atmospheric turbulence conditions in the absence of pointing error.

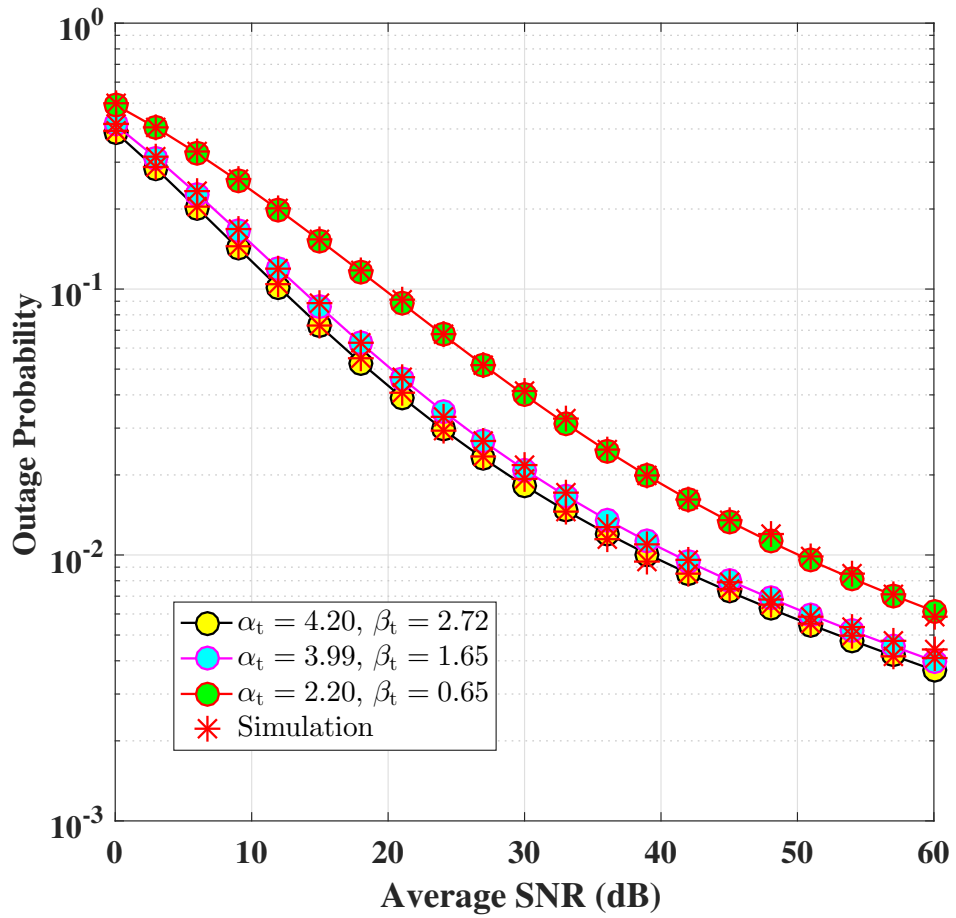


**Figure 4.3 (a)** Outage probability of SIMO FSO link under Gamma-Gamma distribution in the presence of pointing error ( $\xi = 0.5607$ ) for different atmospheric turbulence with  $\gamma_{th} = 2$  dB and  $\gamma_0 = 3$  dB.

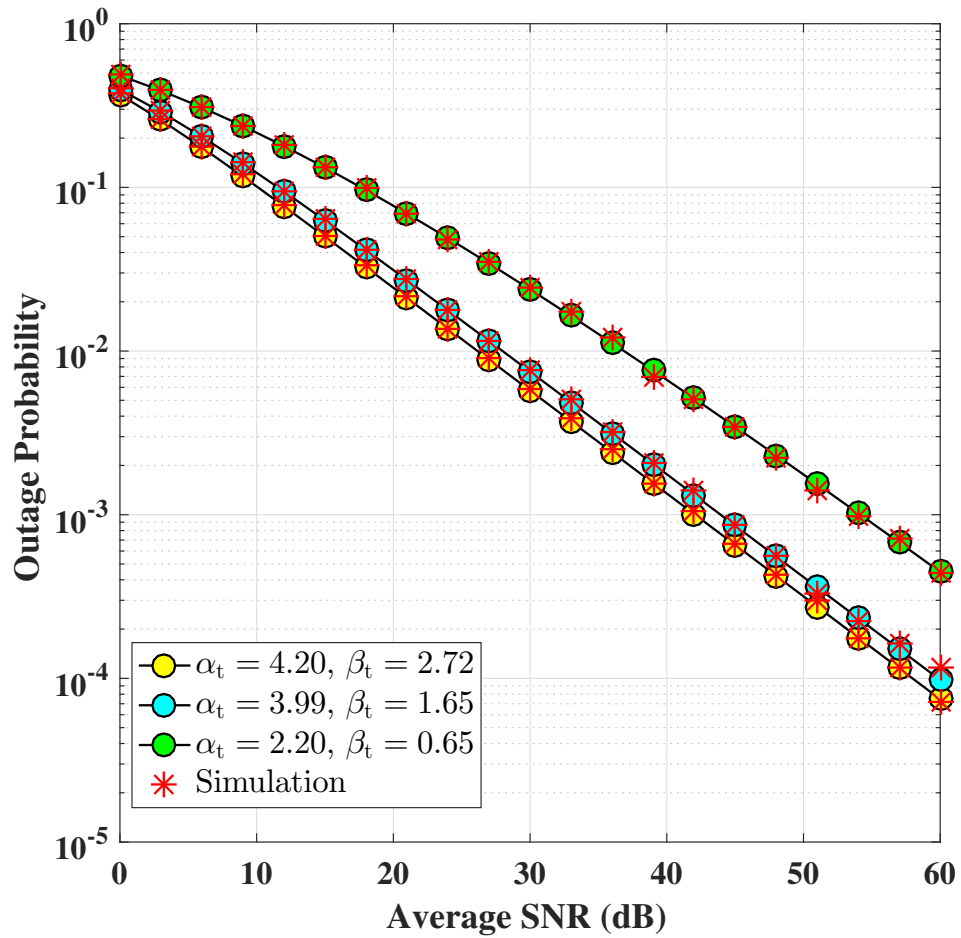


**Figure 4.3 (b)** Outage probability of SIMO FSO link under Gamma-Gamma distribution in the presence of pointing error ( $\xi = 0.5607$ ) for different atmospheric turbulence with  $\gamma_{th} = 3$  dB and  $\gamma_0 = 3$  dB.

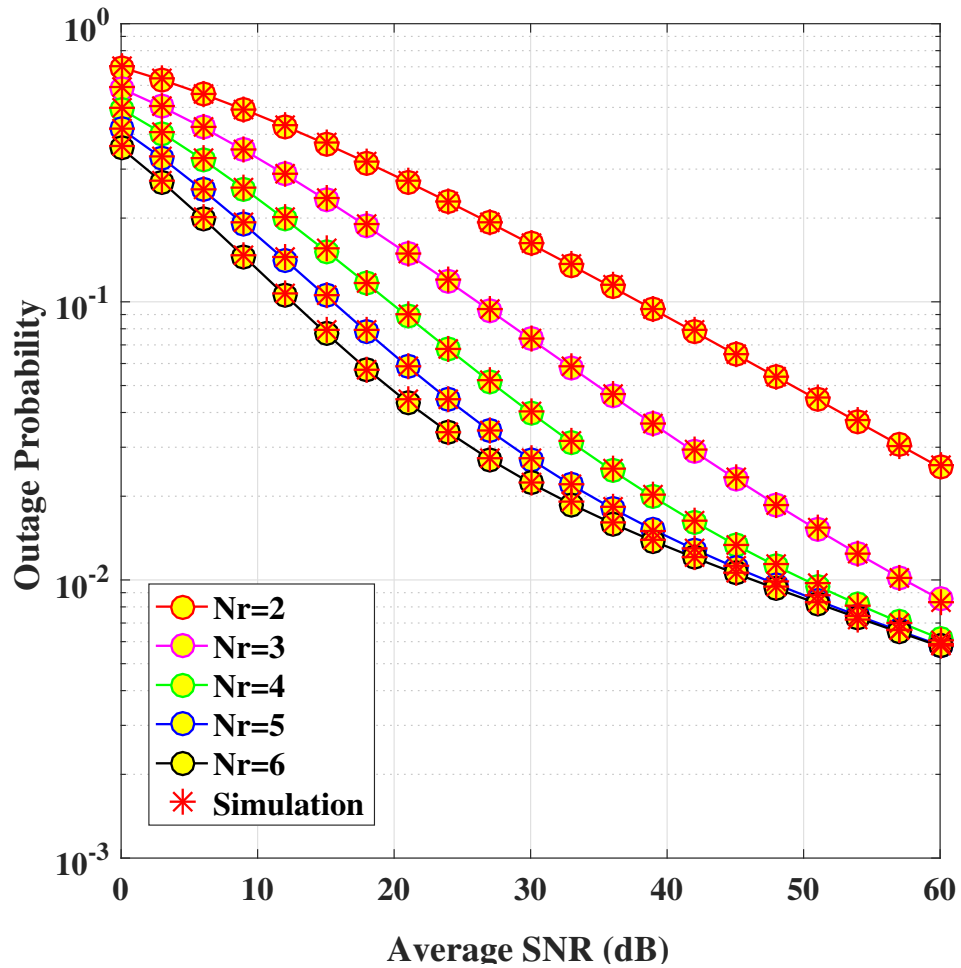


**Figure 4.3 (c)** Outage probability of SIMO FSO link under Gamma-Gamma distribution in the presence of pointing error ( $\xi = 0.5607$ ) for different receiver diversity order with  $\alpha_t = 2.20$  and  $\beta_t = 0.65$ ,  $\gamma_{th} = 2$  dB and  $\gamma_0 = 3$  dB.

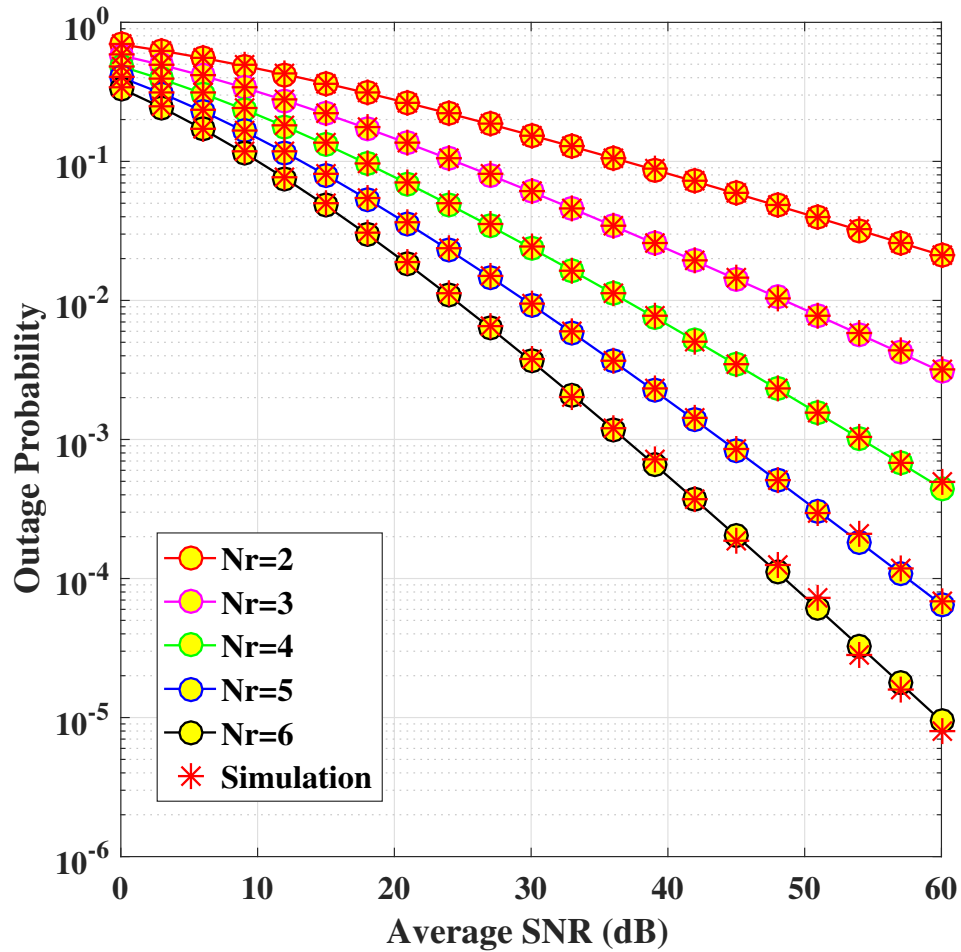
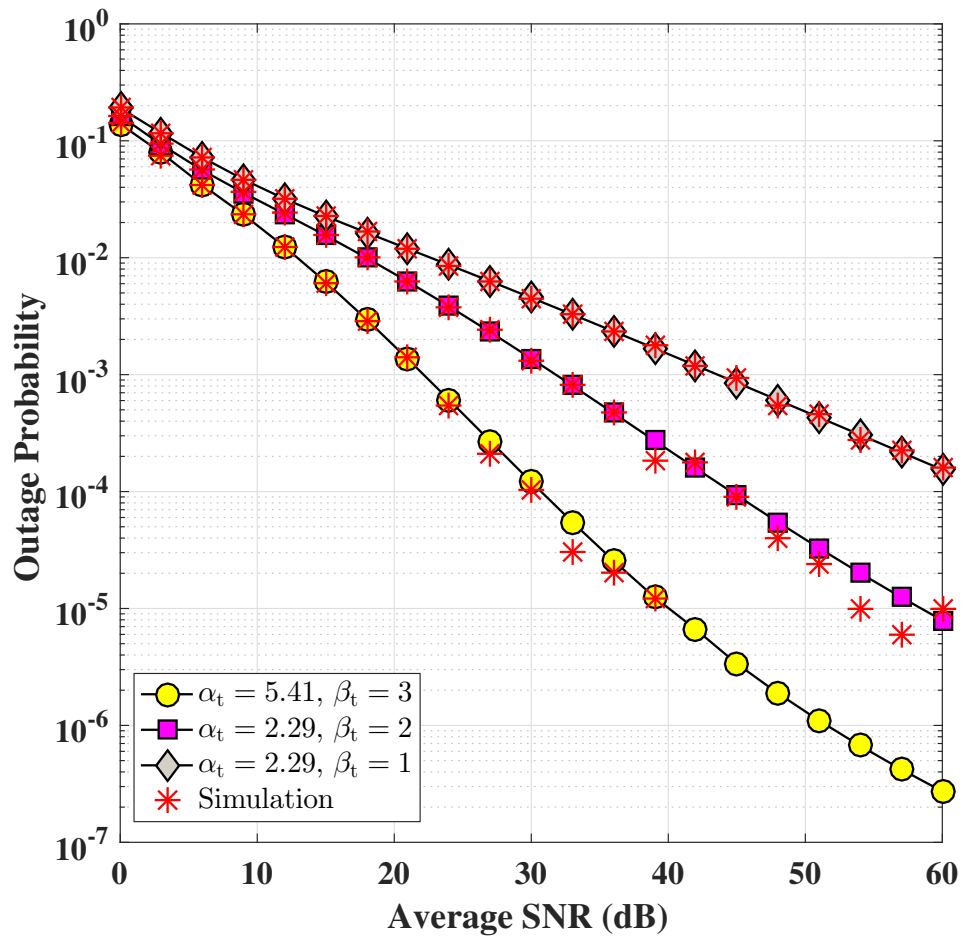


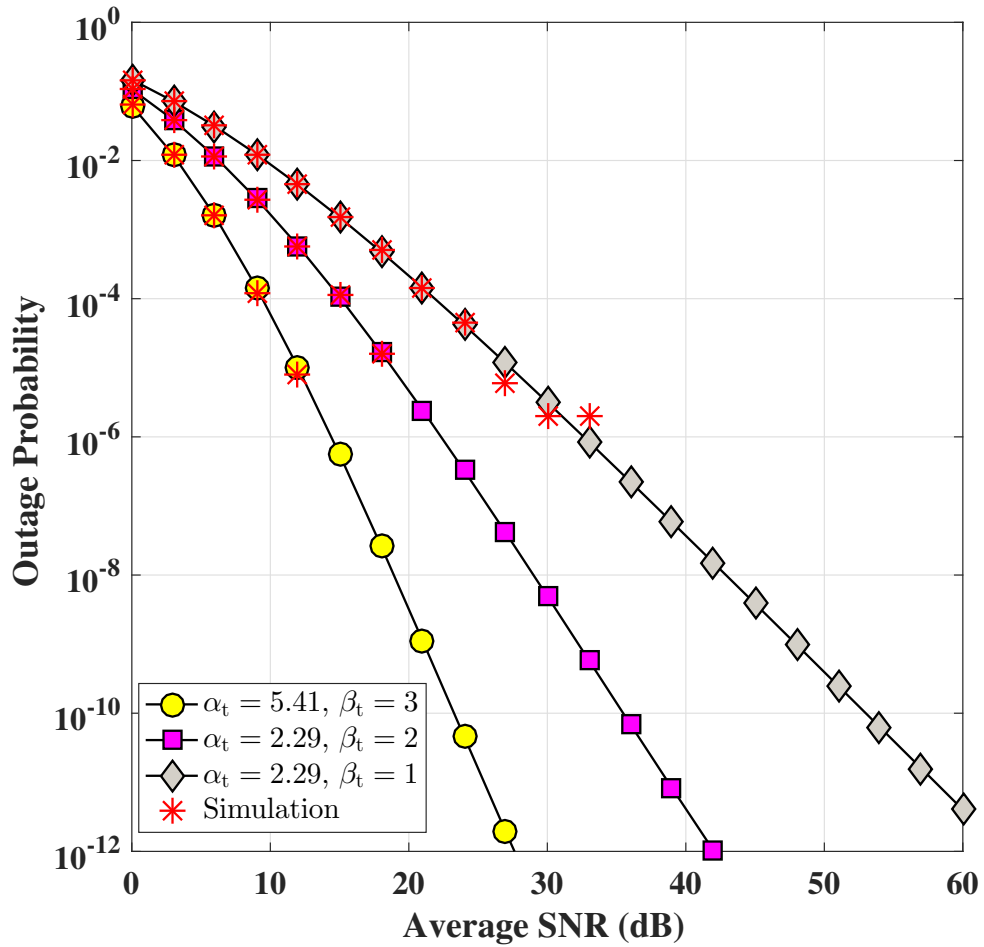
Figure 4.3 (d) Outage probability of SIMO FSO link under Gamma-Gamma distribution in the presence of pointing error ( $\xi = 0.5607$ ) for different receiver diversity order with  $\alpha_t = 2.20$  and  $\beta_t = 0.65$ ,  $\gamma_{th} = 3$  dB and  $\gamma_0 = 3$  dB.

FIGURE 4.3: Outage Probability of the SIMO FSO link employing switch and examine combining scheme in the receiver end with Gamma-Gamma distribution using different atmospheric turbulence conditions in the presence of pointing error.





**Figure 4.4 (a)** Outage probability of SIMO FSO link under Málaga distribution in the absence of pointing error for different atmospheric turbulence with  $\gamma_{th} = 2$  dB and  $\gamma_0 = 3$  dB.



**Figure 4.4 (b)** Outage probability of SIMO FSO link system under Málaga distribution in the absence of pointing error for different atmospheric turbulence with  $\gamma_{th} = 3$  dB and  $\gamma_0 = 3$  dB.

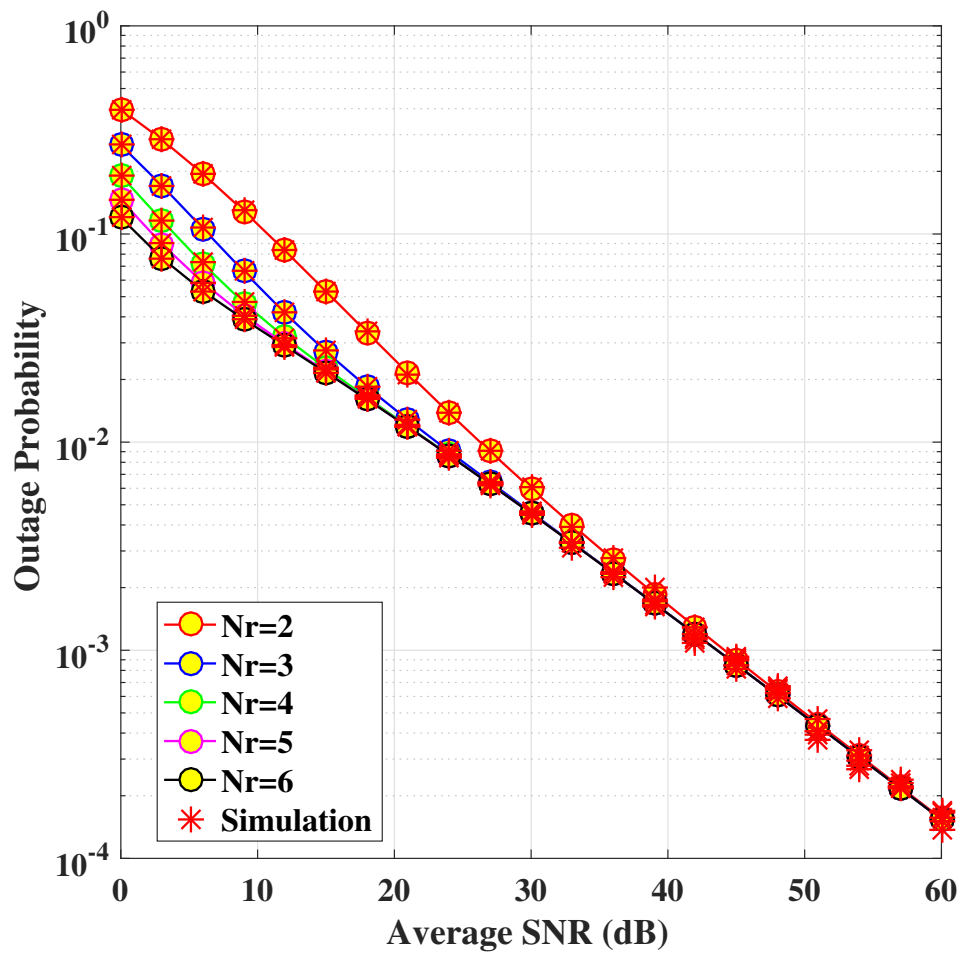
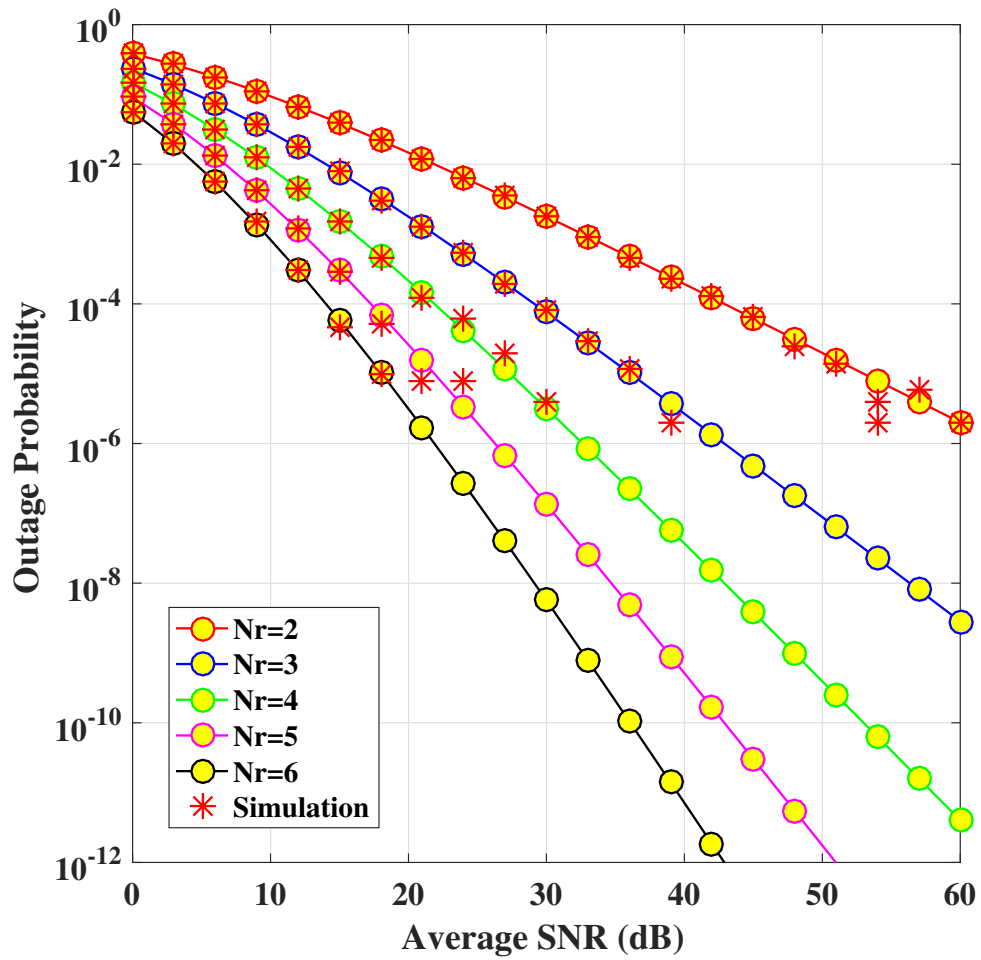
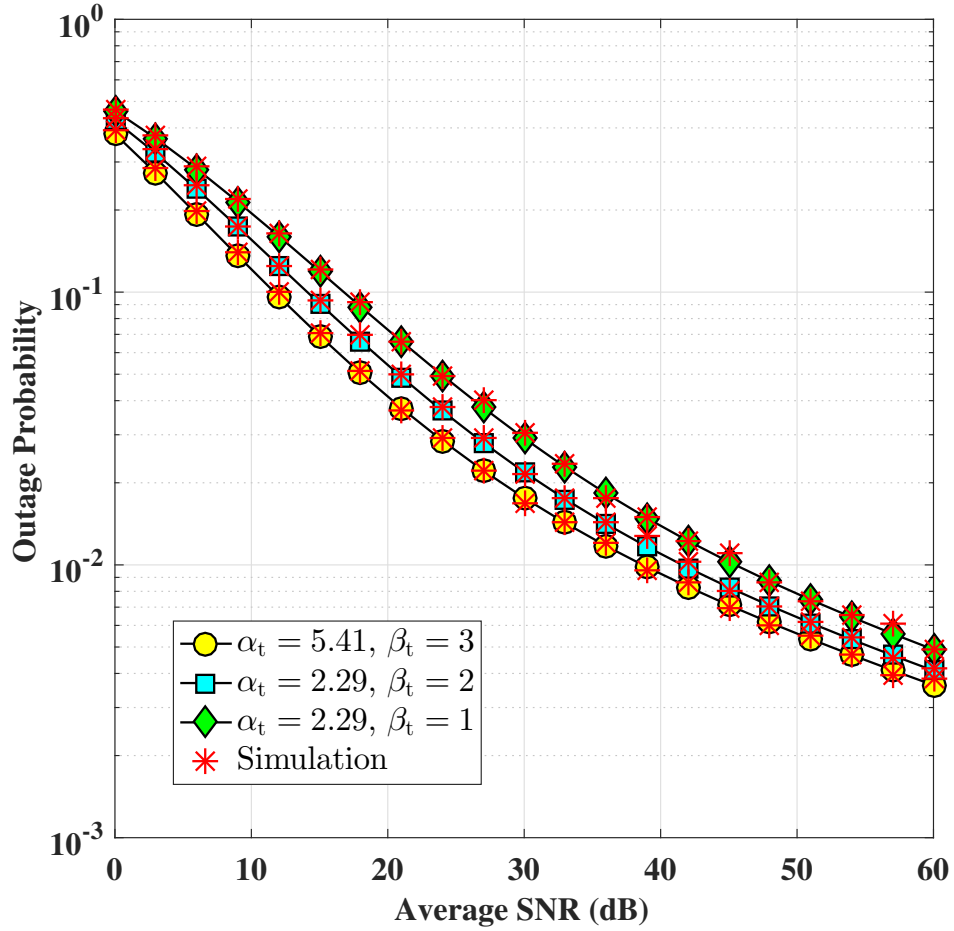


Figure 4.4 (c) Outage probability under Málaga distribution in the absence of pointing error for different receiver diversity order with  $\alpha_t = 2.29$  and  $\beta_t = 1$ ,  $\gamma_{th} = 2$  dB and  $\gamma_0 = 3$  dB.



**Figure 4.4 (d)** Outage probability under Málaga distribution in the absence of pointing error for different receiver diversity order with  $\alpha_t = 2.29$  and  $\beta_t = 1$ ,  $\gamma_{th} = 3$  dB and  $\gamma_0 = 3$  dB.

FIGURE 4.4: Outage Probability of the SIMO FSO link employing switch and examine combining scheme in the receiver end with Málaga distribution using different atmospheric turbulence condition in the absence of pointing error.



**Figure 4.5 (a)** Outage probability of SIMO FSO link under Málaga distribution in the presence of pointing error ( $\xi = 0.5607$ ) for different atmospheric turbulence with  $\gamma_{th} = 2$  dB and  $\gamma_0 = 3$  dB.

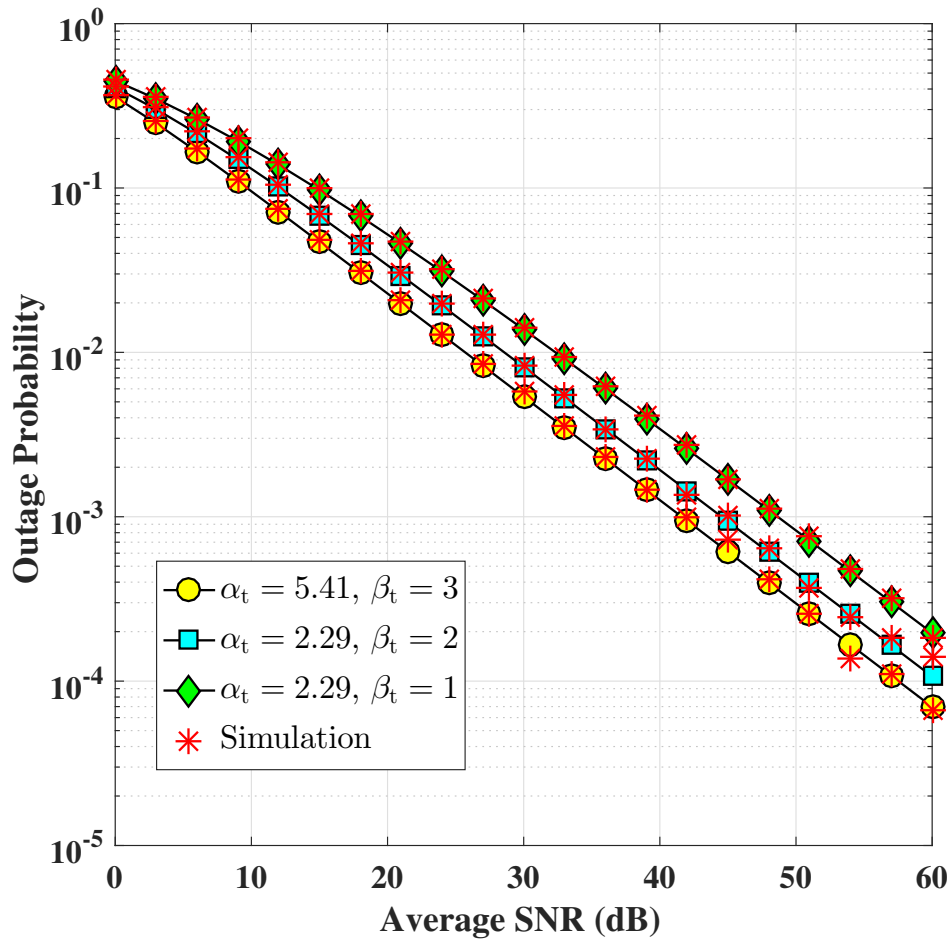
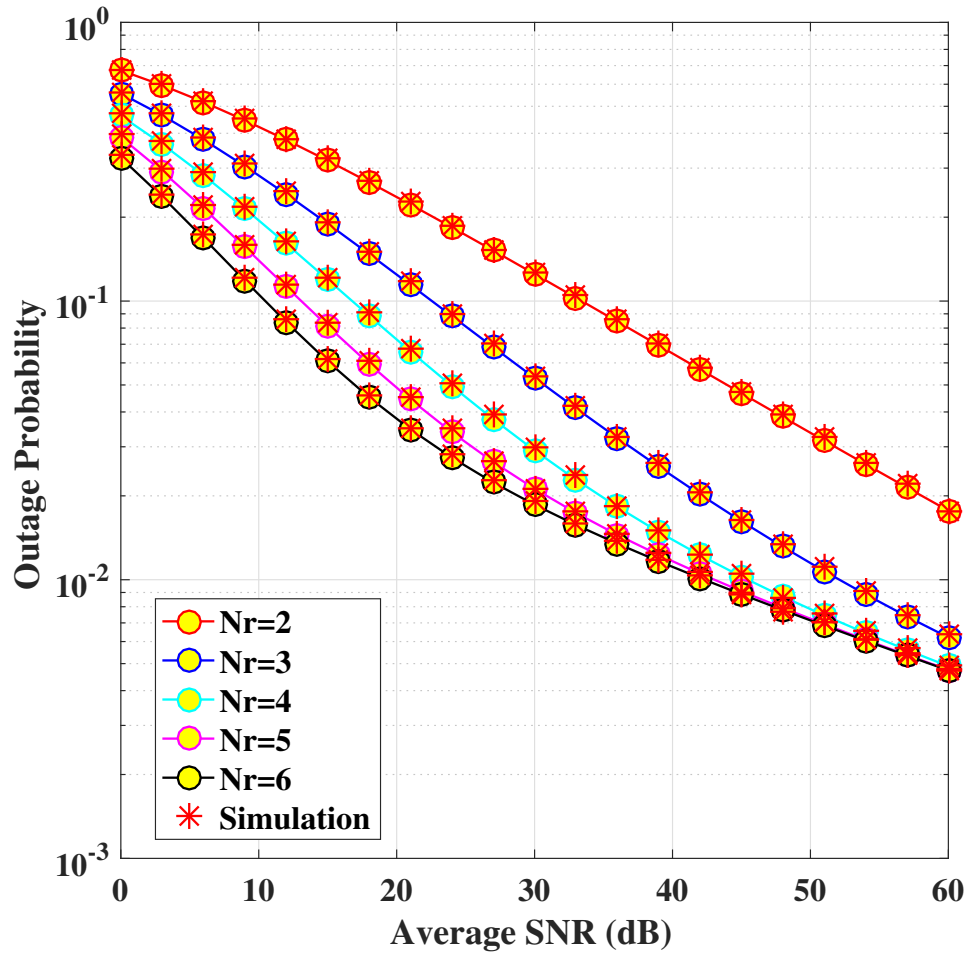
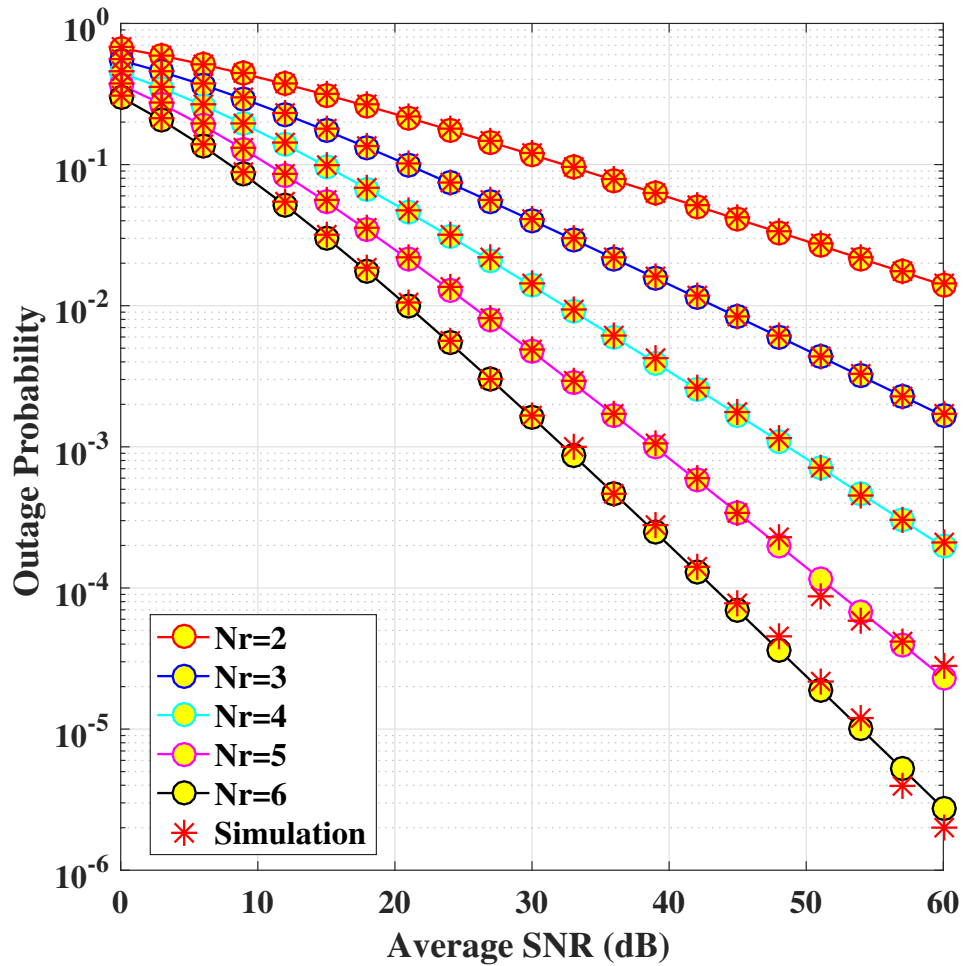


Figure 4.5 (b) Outage probability of SIMO FSO link under Málaga distribution in the presence of pointing error ( $\xi = 0.5607$ ) for different atmospheric turbulence with  $\gamma_{th} = 3$  dB and  $\gamma_0 = 3$  dB.



**Figure 4.5 (c)** Outage probability under Málaga distribution in the presence of pointing error ( $\xi = 0.5607$ ) for different receiver diversity order with  $\alpha_t = 2.29$  and  $\beta_t = 1$ ,  $\gamma_{th} = 2$  dB and  $\gamma_0 = 3$  dB.



**Figure 4.5 (d)** Outage probability under Málaga distribution in the presence of pointing error ( $\xi = 0.5607$ ) for different receiver diversity order with  $\alpha_t = 2.29$  and  $\beta_t = 1$ ,  $\gamma_{th} = 3$  dB and  $\gamma_0 = 3$  dB.

FIGURE 4.5: Outage Probability of the SIMO FSO link employing switch and examine combining scheme at the receiver end with Málaga distribution using different atmospheric turbulence conditions in the presence of pointing error.



TABLE 4.2: Summary of the equations used for figures, Fig. 4.6 to Fig. 4.9.

Figure	Scenario	Equation
Fig. 4.6a	GG	Eq. 4.6 with Eq. 4.7 and Eq. 4.10
Fig. 4.6b	GG	Eq. 4.6 with Eq. 4.7 and Eq. 4.10
Fig. 4.6c	GG	Eq. 4.6 with Eq. 4.7 and Eq. 4.10
Fig. 4.6d	GG	Eq. 4.6 with Eq. 4.7 and Eq. 4.10
Fig. 4.7a	GG + pointing	Eq. 4.6 with Eq. 4.19 and Eq. 4.22
Fig. 4.7b	GG + pointing	Eq. 4.6 with Eq. 4.19 and Eq. 4.22
Fig. 4.7c	GG + pointing	Eq. 4.6 with Eq. 4.19 and Eq. 4.22
Fig. 4.7d	GG + pointing	Eq. 4.6 with Eq. 4.19 and Eq. 4.22
Fig. 4.8a	Málaga	Eq. 4.30 with Eq. 4.33 and Eq. 4.34
Fig. 4.8b	Málaga	Eq. 4.30 with Eq. 4.33 and Eq. 4.34
Fig. 4.8c	Málaga	Eq. 4.30 with Eq. 4.33 and Eq. 4.34
Fig. 4.8d	Málaga	Eq. 4.30 with Eq. 4.33 and Eq. 4.34
Fig. 4.9a	Málaga + pointing	Eq. 4.43 with Eq. 4.46 and Eq. 4.47
Fig. 4.9b	Málaga + pointing	Eq. 4.43 with Eq. 4.46 and Eq. 4.47
Fig. 4.9c	Málaga + pointing	Eq. 4.43 with Eq. 4.46 and Eq. 4.47
Fig. 4.9d	Málaga + pointing	Eq. 4.43 with Eq. 4.46 and Eq. 4.47

Fig. 4.2 (c) plots the OP of the system against average SNR for receive diversity of order  $N_r$ . From this graphical presentation, it is evident that all the decay lines of the branches for  $N_r = 3, 4, 5$ , and 6 merges beyond the average SNR of 40 dB, indicating no improvement for higher diversity order. Fig. 4.2 (d) presents similar results with the same threshold for optimal switching, which eliminates the problem of OP being insensitive to  $N_r$  for average SNR  $\geq 40$  dB.

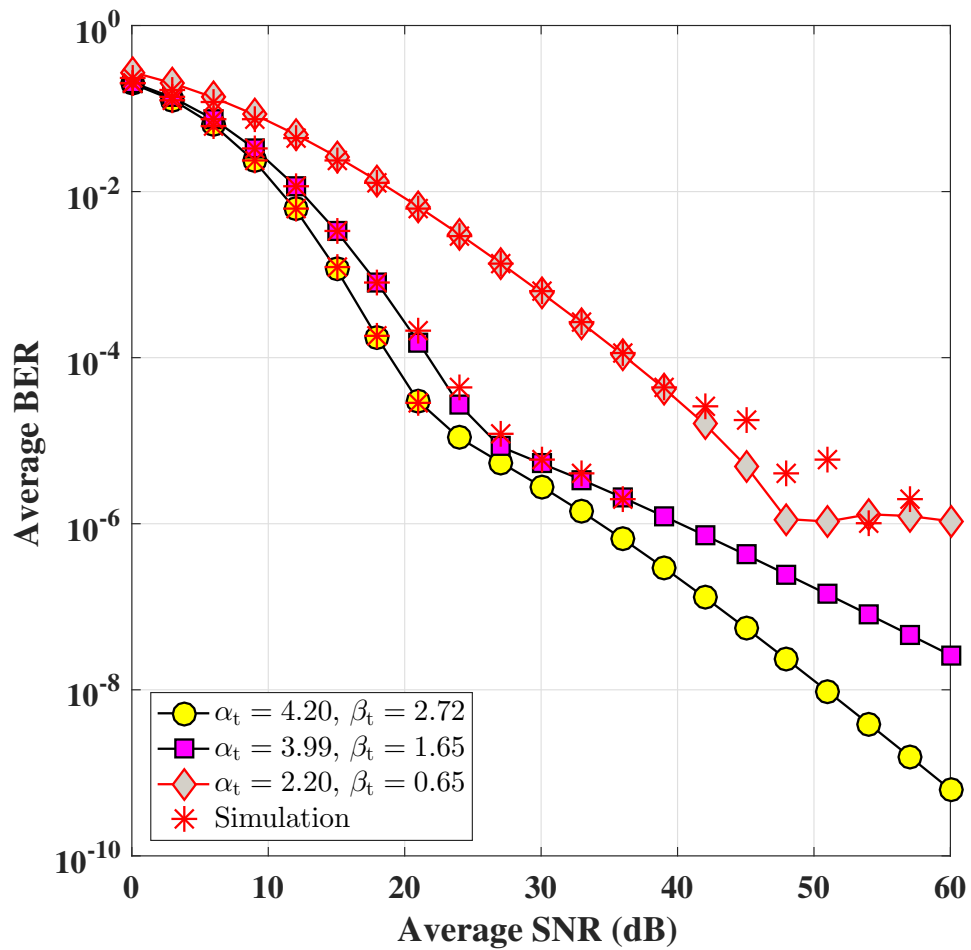
Under the same turbulence condition,  $\alpha_t = 4.20$  and  $\beta_t = 2.72$  with the threshold SNR of 2 dB, the outage at average SNR of 30 dB is obtained as  $2.1 \times 10^{-3}$  for SISO FSO link (Fig. 2.7a (a)), while it is  $6.8 \times 10^{-4}$  (Fig. 4.2 (a)), and  $6.29 \times 10^{-11}$  (Fig. 4.2 (b)), for the SIMO FSO link. Thus, a SIMO FSO link is more efficient than a SISO FSO link at the cost of system complexity. In the presence of a pointing error, the same results are repeated for all statistical distributions considered in this chapter, and the results are similar.

TABLE 4.3: Optimum switching threshold of  $1 \times N_r$  SIMO FSO system in the absence of pointing error with  $N_r = 2, 3, 4, 5$  and  $6$  for different average SNR with turbulence parameter  $\alpha_t = 2.20$  and  $\beta_t = 0.65$  .

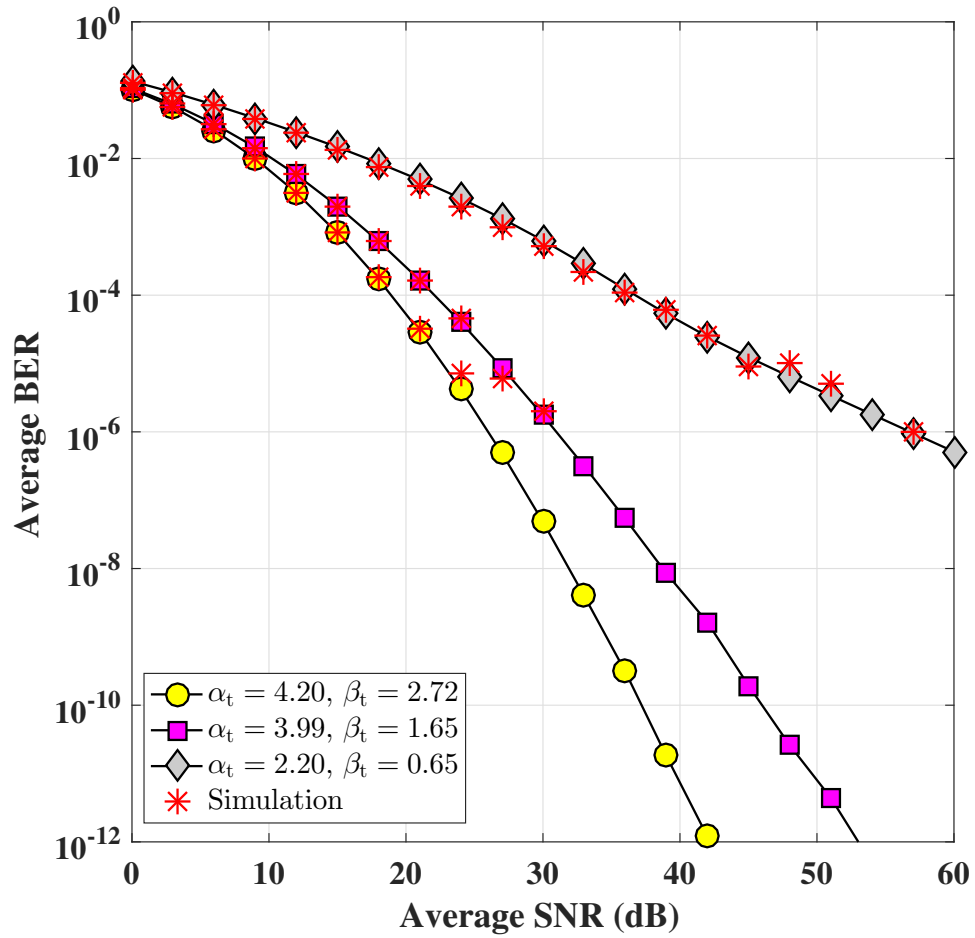
Avg. SNR (dB)	Optimum switching threshold ( $\gamma_0$ )				
	$N_r = 2$	$N_r = 3$	$N_r = 4$	$N_r = 5$	$N_r = 6$
0	0.31	0.49	0.68	0.85	1.02
3	0.44	0.70	0.96	1.22	1.46
6	0.60	0.96	1.32	1.67	2.00
9	0.80	1.28	1.75	2.21	2.67
12	1.02	1.64	2.26	2.86	3.45
15	1.27	2.05	2.83	3.60	4.35
18	1.55	2.51	3.48	4.44	5.38
21	1.84	3.01	4.19	5.36	6.52
24	2.15	3.55	4.97	6.38	7.78
27	2.48	4.12	5.80	7.48	9.14
30	2.82	4.73	6.69	8.65	10.59
33	3.17	5.36	7.62	9.89	12.14
36	3.53	6.02	8.60	11.19	13.76
39	3.90	6.71	9.62	12.54	15.44
42	4.28	7.41	10.66	13.94	17.19
45	4.66	8.13	11.74	15.37	18.99
48	5.04	8.87	12.85	16.85	20.83
51	5.43	9.62	13.97	18.35	22.71
54	5.82	10.38	15.11	19.87	24.61
57	6.22	11.15	16.27	21.42	30.02
60	6.61	11.93	17.44	22.99	30.02

TABLE 4.4: Optimum switching threshold of  $1 \times 4$  SIMO FSO system in the absence of pointing error with different average SNR for different turbulence parameter.

Avg. SNR (dB)	Optimum switching threshold ( $\gamma_0$ )		
	$\alpha_t = 4.20, \beta_t = 2.72$	$\alpha_t = 3.99, \beta_t = 1.65$	$\alpha_t = 2.20, \beta_t = 0.65$
0	1.03	0.95	0.68
3	1.64	1.46	0.96
6	2.49	2.15	1.32
9	3.61	3.03	1.75
12	5.04	4.11	2.26
15	6.79	5.41	2.83
18	8.89	6.92	3.48
21	11.32	8.64	4.19
24	14.09	10.56	4.97
27	17.17	12.66	5.80
30	20.55	14.94	6.69
33	24.21	17.36	7.62
36	30.02	19.91	8.60
39	32.21	22.57	9.62
42	39.95	30.02	10.66
45	39.95	30.02	11.74
48	45.53	30.02	12.85
51	50.27	39.95	13.97
54	55.08	39.95	15.11
57	59.99	39.95	16.27
60	64.97	39.95	17.44



**Figure 4.6 (a)** Average bit error rate of SIMO FSO link under Gamma-Gamma distribution in the absence of pointing error for different atmospheric turbulence condition with fixed switching threshold of 10 dB.



**Figure 4.6 (b)** Average bit error rate of SIMO FSO link under Gamma-Gamma distribution in the absence of pointing error for different atmospheric turbulence condition with optimal switching threshold.

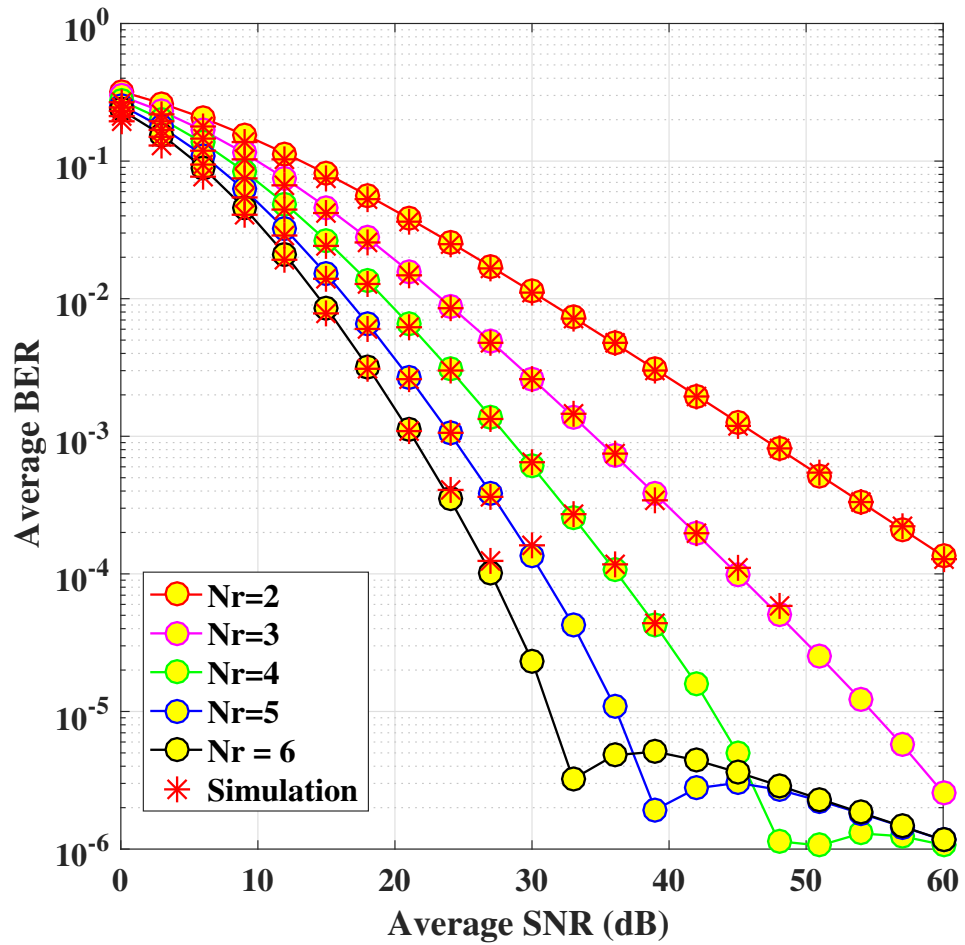
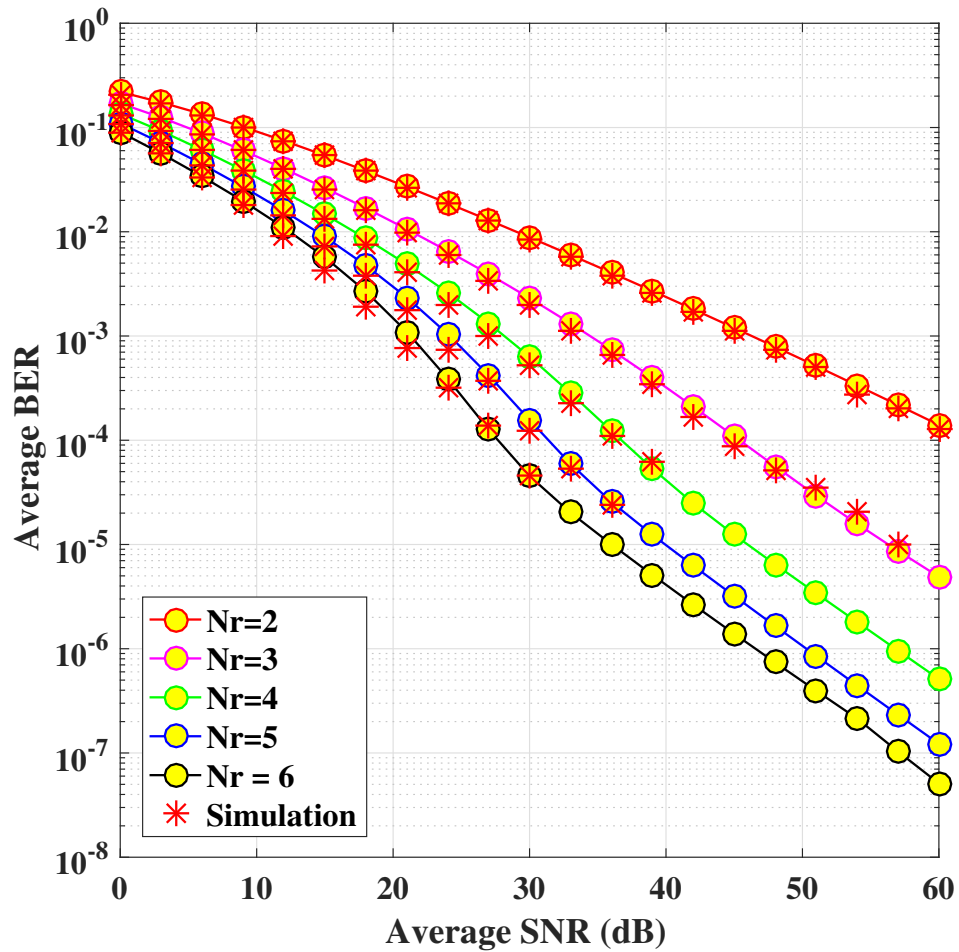


Figure 4.6 (c) Average bit error rate of SIMO FSO link under Gamma-Gamma distribution in the absence of pointing error for  $\alpha_t = 2.20$  and  $\beta_t = 0.65$  with fixed switching threshold of 10 dB.



**Figure 4.6 (d)** Average bit error rate of SIMO FSO link under Gamma-Gamma distribution in the absence of pointing error for  $\alpha_t = 2.20$  and  $\beta_t = 0.65$  with optimal switching threshold.

FIGURE 4.6: Average bit error rate of the SIMO FSO link employing switch and examine combining scheme in the receiver end with Gamma-Gamma distribution using different atmospheric turbulence conditions in the absence of pointing error.

TABLE 4.5: Optimum switching threshold of  $1 \times N_r$  SIMO FSO system in the presence of pointing error ( $\xi = 0.5607$ ) with  $N_r = 2, 3, 4, 5$  and  $6$  for different average SNR with turbulence parameter  $\alpha_t = 2.20$  and  $\beta_t = 0.65$ .

Avg. SNR (dB)	Optimum switching threshold ( $\gamma_0$ )				
	$N_r = 2$	$N_r = 3$	$N_r = 4$	$N_r = 5$	$N_r = 6$
0	21.83	21.83	21.83	21.83	21.83
5	22.33	22.33	22.33	22.33	22.33
10	22.88	22.88	22.88	22.88	22.88
15	23.46	23.46	23.46	23.46	23.46
20	24.07	24.07	24.07	24.07	24.07
25	24.69	24.69	24.69	24.69	24.69
30	25.33	25.33	25.33	25.33	25.33
35	25.97	25.97	25.97	25.97	25.97
40	26.61	26.61	26.61	26.61	26.61
45	27.25	27.25	27.25	27.25	27.25
50	27.87	27.87	27.87	27.87	27.87
55	28.48	28.48	28.48	28.48	28.48
60	29.07	29.07	29.07	29.07	29.07
65	29.65	29.65	29.65	29.65	29.65
70	30.19	30.19	30.19	30.19	30.19
75	30.71	30.71	30.71	30.71	30.71
80	31.20	31.20	31.20	31.20	31.20
85	31.65	31.65	31.65	31.65	31.65
90	32.06	32.06	32.06	32.06	32.06
95	32.45	32.45	32.45	32.45	32.45
100	32.79	32.79	32.79	32.79	32.79

Next, another important performance metric, ABER, will be studied under the misalignment effect in the system with different statistical distributions. Although we have displayed all 2D graphical representations of this metric without pointing error, a canvas of visual plot from Fig. 4.7 (a) - Fig. 4.7 (d) demonstrates the resultant ABER of SIMO FSO system under GG statistical distribution with the influence of pointing error in the system. The characteristics of ABER under various turbulence with pointing error ( $\xi = 0.5607$ ) are displayed in Fig. 4.7 (a), where the



TABLE 4.6: Optimum switching threshold of  $1 \times 4$  SIMO FSO system in the presence of pointing error ( $\xi = 0.5607$ ) with different average SNR for different turbulence parameter.

Avg. SNR (dB)	Optimum switching threshold ( $\gamma_0$ )		
	$\alpha_t = 4.20, \beta_t = 2.72$	$\alpha_t = 3.99, \beta_t = 1.65$	$\alpha_t = 2.20, \beta_t = 0.65$
0	22.18	22.03	21.83
5	22.96	22.74	22.33
10	23.68	23.46	22.88
15	24.36	24.15	23.46
20	25.01	24.82	24.07
25	25.64	25.46	24.69
30	26.23	26.08	25.33
35	26.80	26.66	25.97
40	27.34	27.22	26.61
45	27.84	27.75	27.25
50	28.31	28.24	27.87
55	28.74	28.70	28.48
60	29.13	29.12	29.07
65	29.48	29.50	29.65
70	29.80	29.85	30.19
75	30.08	30.15	30.71
80	30.33	30.43	31.20
85	30.55	30.67	31.65
90	30.74	30.87	32.06
95	30.90	31.06	32.45
100	31.04	31.21	32.79

system works with a fixed switching threshold of 10 dB against each average SNR. This figure shows that for moderate and weak turbulence conditions, the fall in of ABER graph slowed down with average SNR higher than 80 dB. However, this issue is resolved by choosing the optimum switching thresholds for each average SNR, presented in Table 4.6. The corresponding ABERs are shown in Fig. 4.7 (b). Since the ABER of the MISO FSO link is the function of threshold SNR ( $\gamma_{th}$ ), so we can find the optimal value of  $\gamma_{th}$  for which the ABER gets minimal. This optimal

switching threshold can be computed by using the first order differentiation of the ABER equation with setting the result equal to zero as  $\frac{dP_e}{d\gamma_{th}} = 0$ .

All graphical plots in Fig. 4.8 and Fig. 4.9 present the ABER of SIMO FSO communication system for Málaga statistical distribution under the effect of different degrees of AT and the receiver diversity order in the absence and a presence of a pointing error condition. The average capacity of the SIMO FSO link in the absence of pointing error is shown in Fig. 4.10 and in Fig. 4.11. Required numerical results of Fig. 4.10, and Fig. 4.11 are calculated under Gamma-Gamma statistical distribution; moreover, the effect of different AT and receiver diversity orders on the system is considered here. Depending on the degrees of severity by the AT and pointing error, the average capacity of the SIMO FSO system is plotted in Fig. 4.12 and Fig. 4.13 under Málaga statistical distribution, plots signify how the average capacity of the current system swinging with the number of receiver diversity orders.

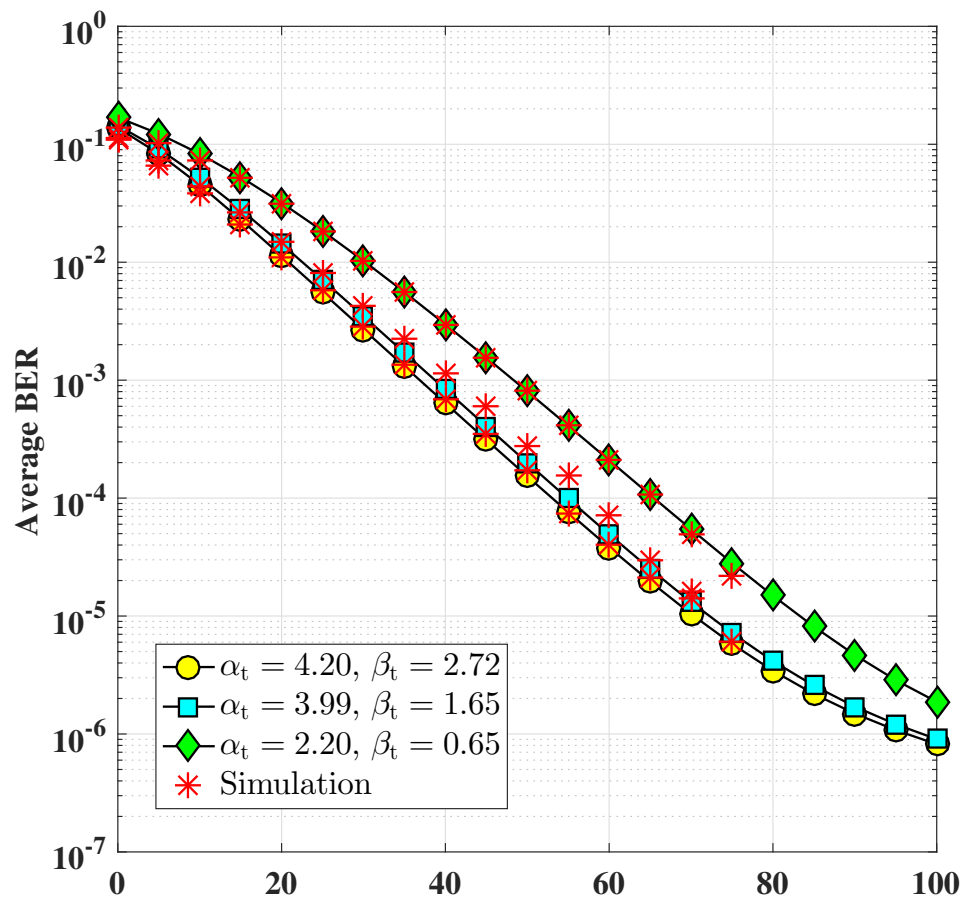


**Figure 4.7 (a)** Average bit error rate of SIMO FSO link under Gamma-Gamma distribution in the presence of pointing error ( $\xi = 0.5607$ ) for different atmospheric turbulence with fixed switching threshold of 10 dB.

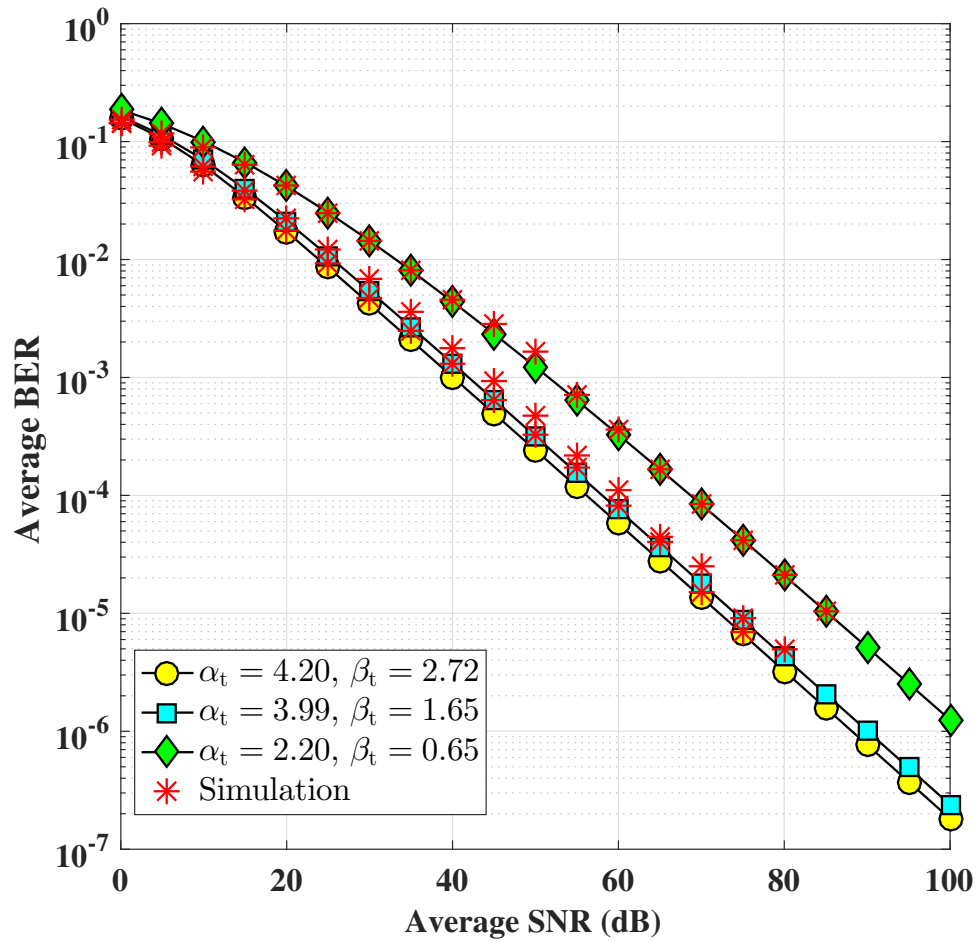


**Figure 4.7 (b)** Average bit error rate of SIMO FSO link under Gamma-Gamma distribution in the presence of pointing error ( $\xi = 0.5607$ ) for different atmospheric turbulence with optimal switching threshold.

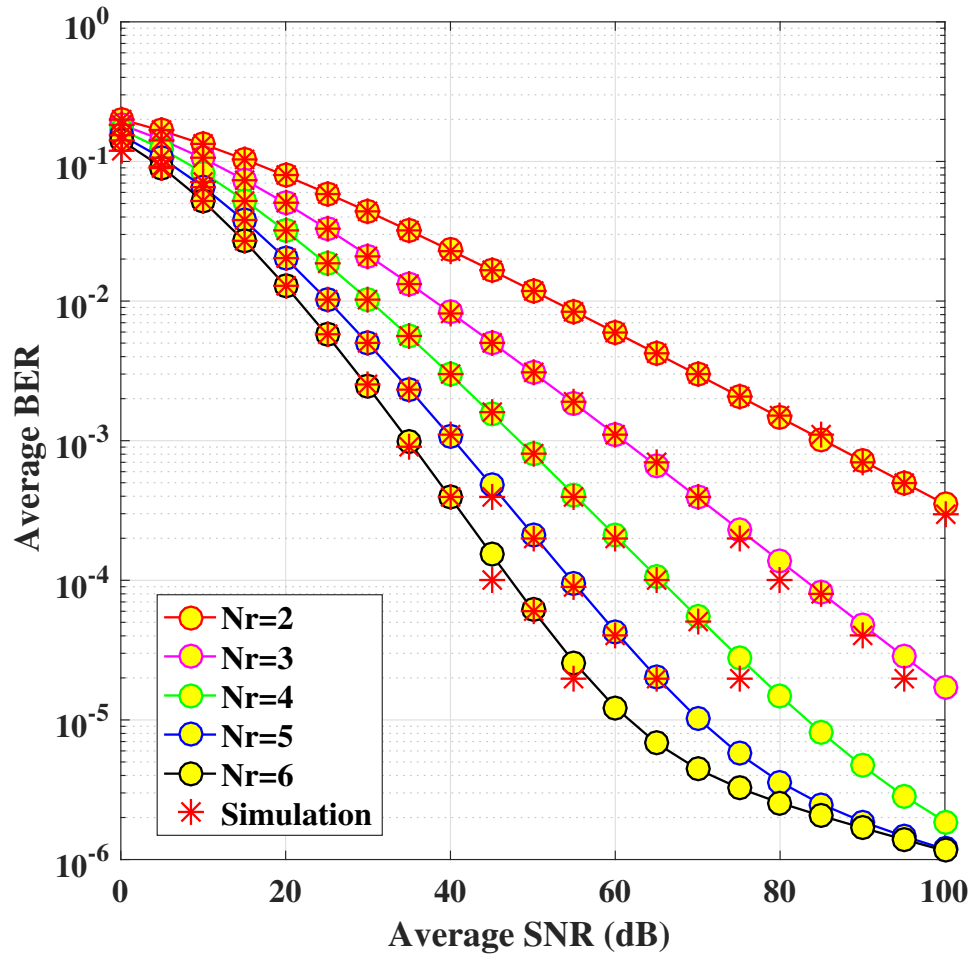


**Figure 4.7 (c)** Average bit error rate of SIMO FSO link under Gamma-Gamma distribution in the presence of pointing error ( $\xi = 0.5607$ ) for  $\alpha_t = 2.20$  and  $\beta_t = 0.65$  with fixed switching threshold of 10 dB.

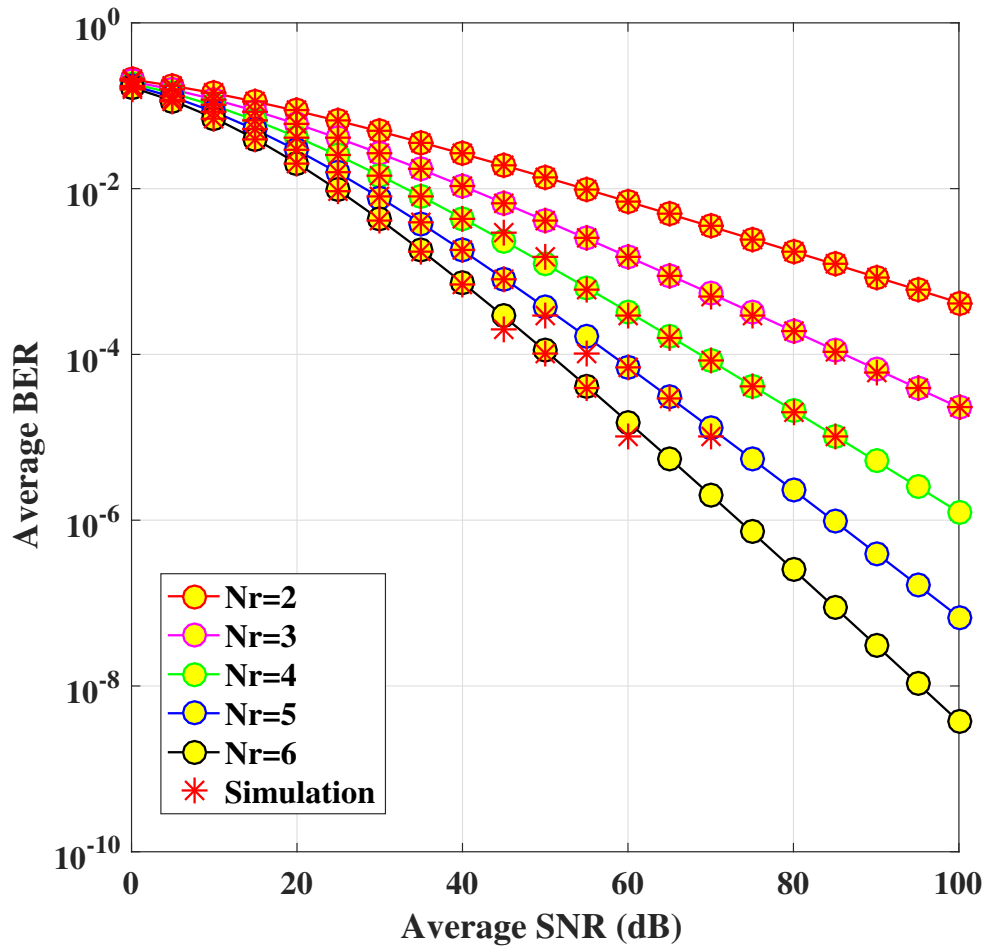


Figure 4.7 (d) Average bit error rate of SIMO FSO link under Gamma-Gamma distribution in the presence of pointing error ( $\xi = 0.5607$ ) for  $\alpha_t = 2.20$  and  $\beta_t = 0.65$  with optimal switching threshold.

FIGURE 4.7: Average bit error rate of the SIMO FSO link employing switch and examine combining scheme at the receiver end with Gamma-Gamma distribution using different atmospheric turbulence condition in the presence of pointing error.

TABLE 4.7: Optimum switching threshold of  $1 \times N_r$  SIMO FSO system in the absence of pointing error with  $N_r = 2, 3, 4, 5$  and  $6$  for different average SNR with turbulence parameter  $\alpha_t = 2.29$  and  $\beta_t = 1$ .

Avg. SNR (dB)	Optimum switching threshold ( $\gamma_0$ )				
	$N_r = 2$	$N_r = 3$	$N_r = 4$	$N_r = 5$	$N_r = 6$
0	12.74	12.74	12.74	12.74	12.74
3	9.75	9.73	9.73	9.73	9.73
6	21.47	11.42	11.42	11.42	11.42
9	13.26	13.24	13.24	13.24	13.24
12	25.36	14.36	14.36	14.36	14.36
15	27.06	15.05	15.05	15.05	15.05
18	28.73	21.34	21.34	21.34	21.34
21	31.25	23.23	23.23	23.23	23.23
24	32.38	19.80	19.80	19.80	19.80
27	23.69	23.61	23.61	23.61	23.61
30	21.08	21.06	21.06	21.06	21.06
33	24.54	24.54	24.54	24.54	24.54
36	40.12	24.37	24.37	24.37	24.37
39	31.91	31.91	31.91	31.91	31.91
42	43.61	28.59	28.59	28.59	28.59
45	45.44	29.68	29.68	29.68	29.68
48	34.39	34.39	34.39	34.39	34.39
51	39.87	39.87	39.87	39.87	39.87
54	34.62	34.62	34.62	34.62	34.62
57	53.99	36.72	36.72	36.72	36.72
60	55.77	45.81	45.81	45.81	45.81

TABLE 4.8: Optimum switching threshold of  $1 \times 4$  SIMO FSO system in the absence of pointing error with different average SNR for different turbulence parameters.

Avg. SNR (dB)	Optimum switching threshold ( $\gamma_0$ )		
	$\alpha_t = 5.41, \beta_t = 3$	$\alpha_t = 2.29, \beta_t = 2$	$\alpha_t = 2.29, \beta_t = 1$
0	13.91	9.91	12.74
3	12.63	9.57	9.73
6	10.95	10.92	11.42
9	13.02	10.66	13.24
12	13.73	12.25	14.36
15	13.39	11.12	15.05
18	11.50	11.89	21.34
21	10.47	11.59	23.23
24	10.59	12.37	19.80
27	11.33	11.78	23.61
30	12.45	12.33	21.06
33	11.05	13.23	24.54
36	11.61	12.48	24.37
39	11.02	13.14	31.91
42	12.33	13.85	28.59
45	12.18	13.73	29.68
48	13.57	13.73	34.39
51	16.23	14.70	39.87
54	16.06	15.01	34.62
57	18.76	14.63	36.72
60	18.25	14.48	45.81



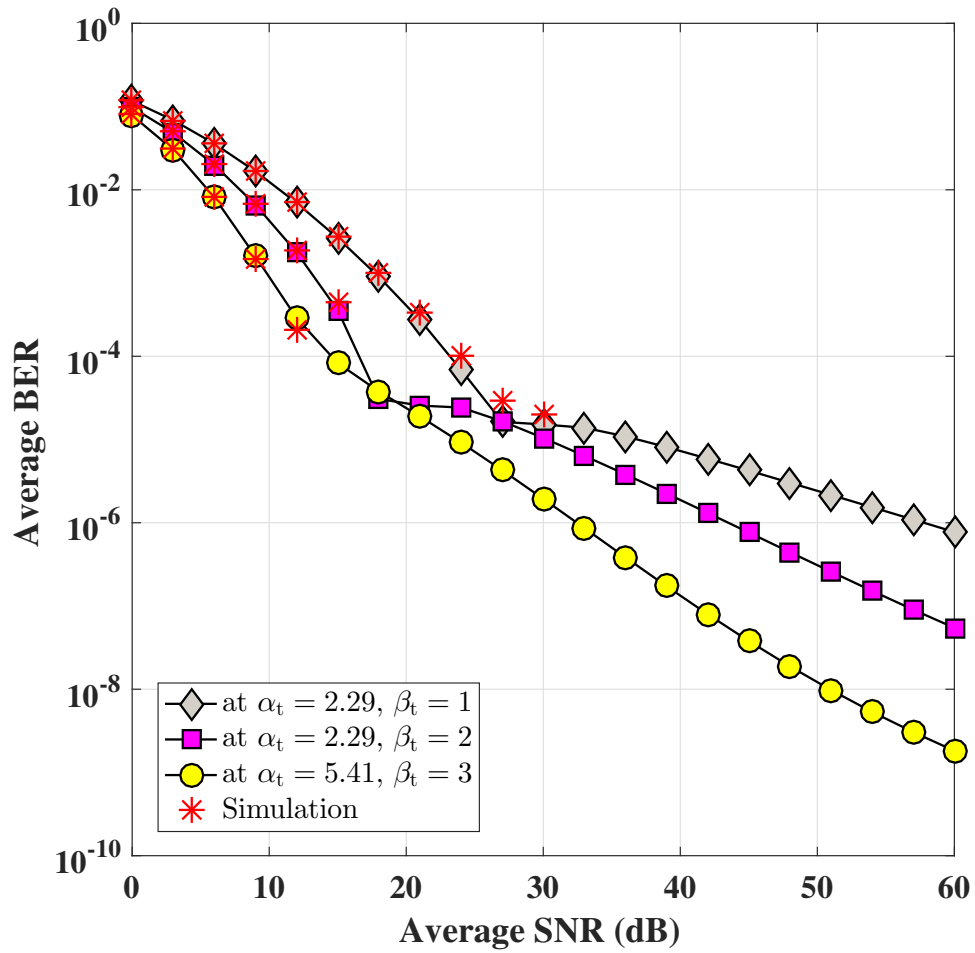


**Figure 4.8 (a)** Average bit error rate of SIMO FSO link under Málaga distribution in the absence of pointing error for different atmospheric turbulence condition with fixed switching threshold of 10 dB.

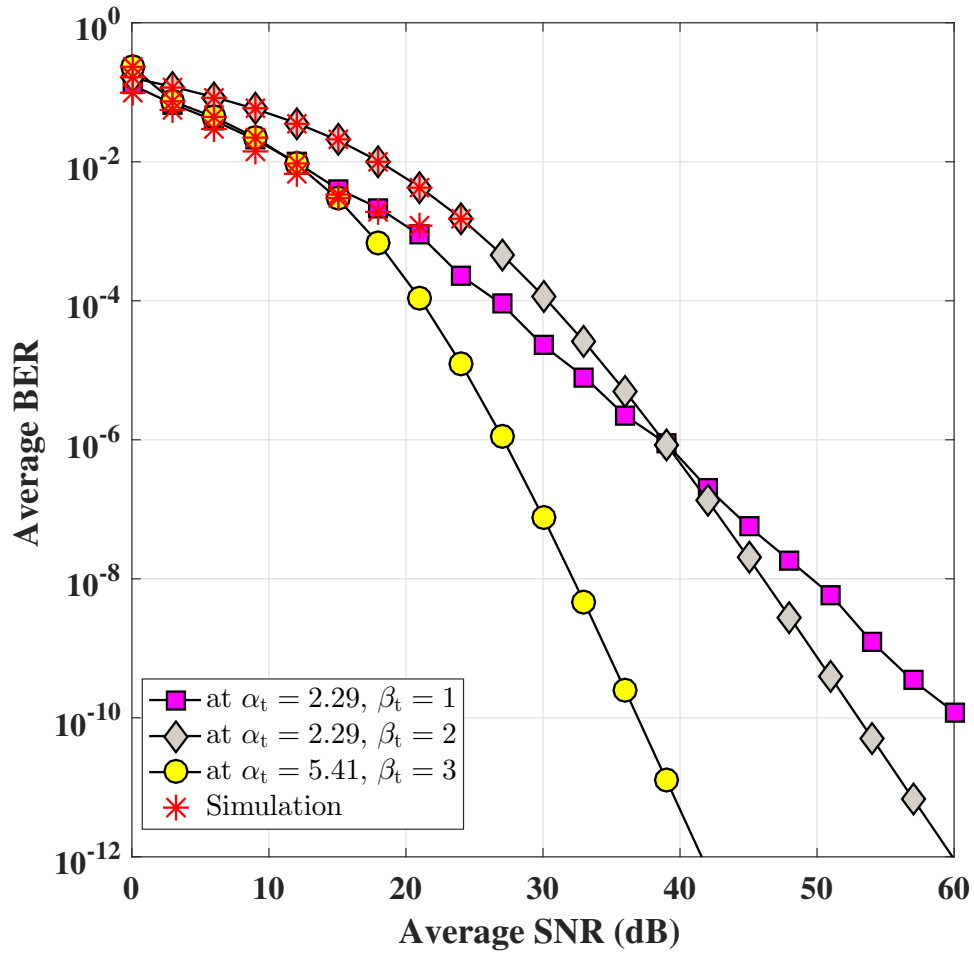


**Figure 4.8 (b)** Average bit error rate of SIMO FSO link under Málaga distribution in the absence of pointing error for different atmospheric turbulence condition with optimal switching threshold.

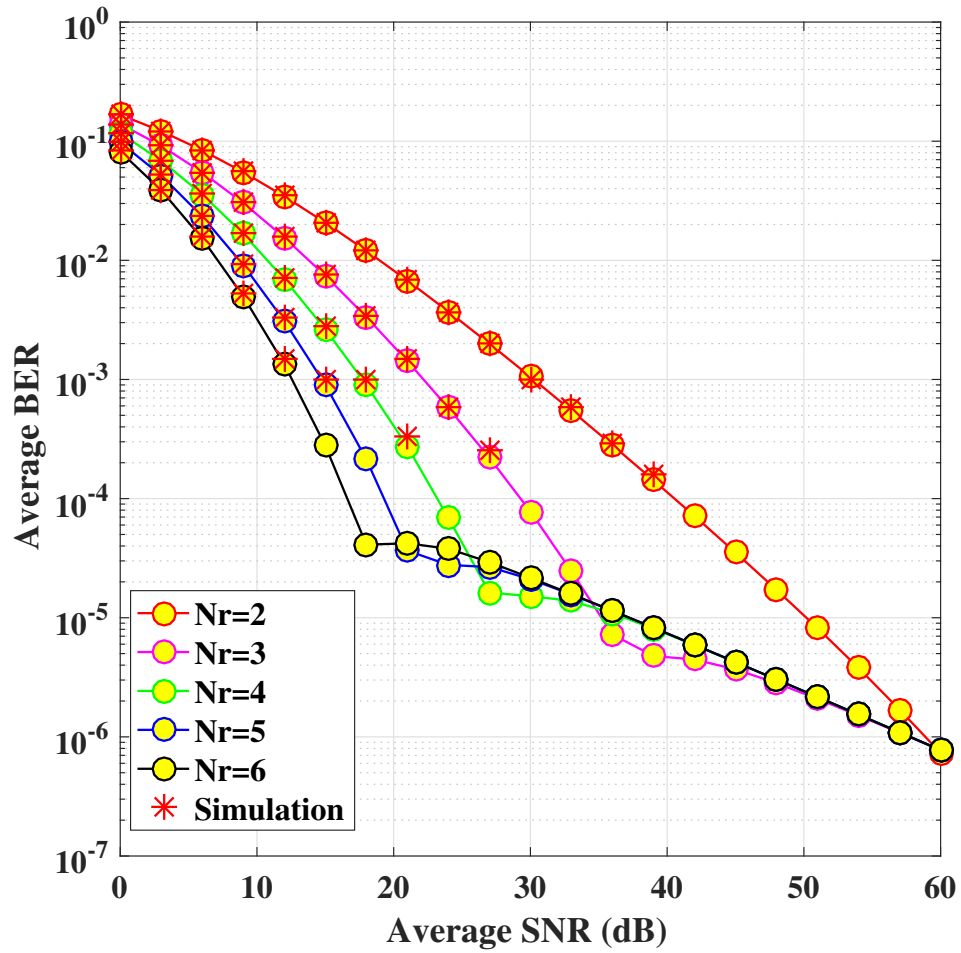
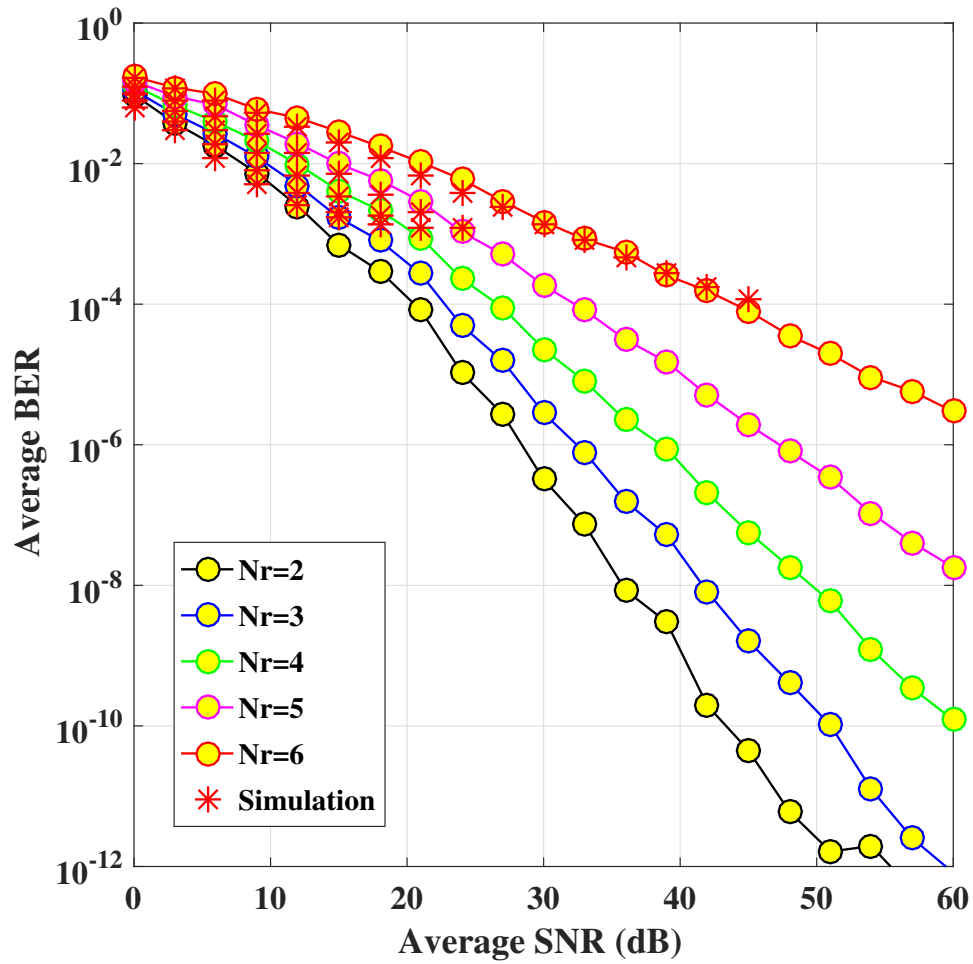


Figure 4.8 (c) Average bit error rate of SIMO FSO link under Málaga distribution in the absence of pointing error for  $\alpha_t = 2.29$  and  $\beta_t = 1$  with fixed switching threshold of 10 dB.



**Figure 4.8 (d)** Average bit error rate of SIMO FSO link under Málaga distribution in the absence of pointing error for  $\alpha_t = 2.29$  and  $\beta_t = 1$  with optimal switching threshold.

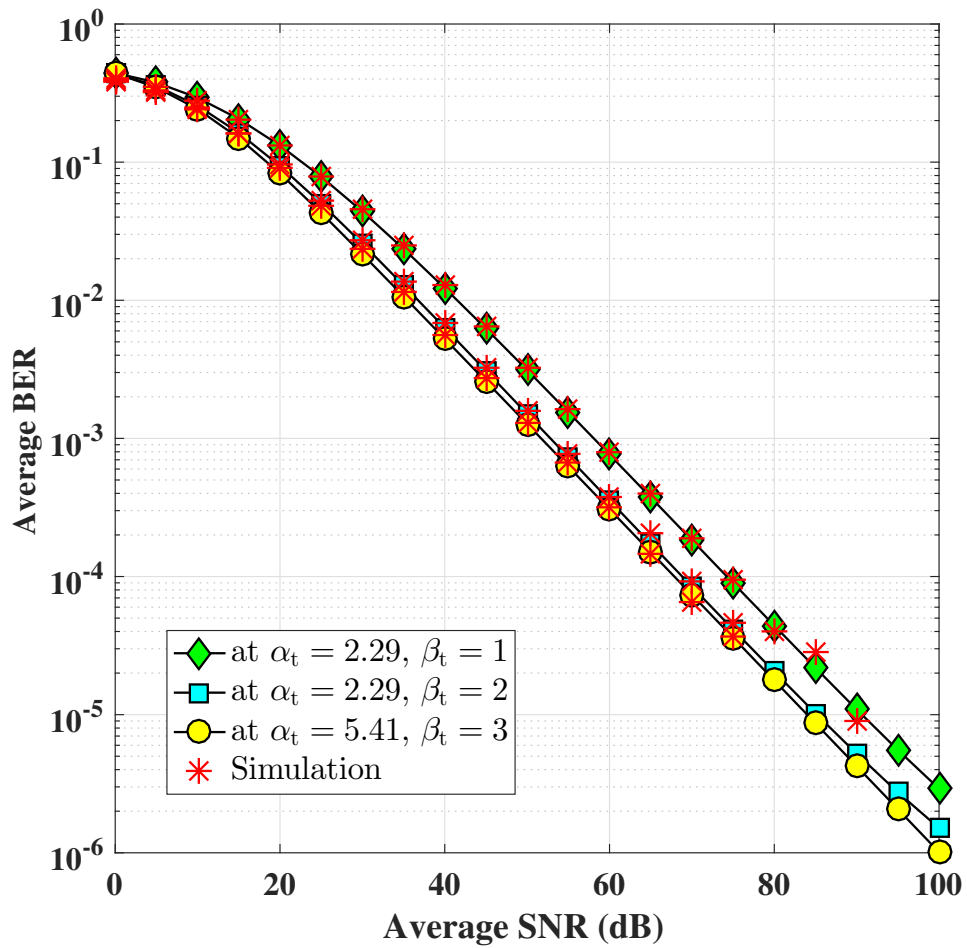
FIGURE 4.8: Average bit error rate of the SIMO FSO link employing switch and examine combining scheme at the receiver end with Málaga distribution using different atmospheric turbulence condition in the absence of pointing error.

TABLE 4.9: Optimum switching threshold of  $1 \times N_r$  SIMO FSO system in the presence of pointing error ( $\xi = 0.5607$ ) with  $N_r = 2, 3, 4, 5$  and 6 for different average SNR with turbulence parameter  $\alpha_t = 2.29$  and  $\beta_t = 1$ .

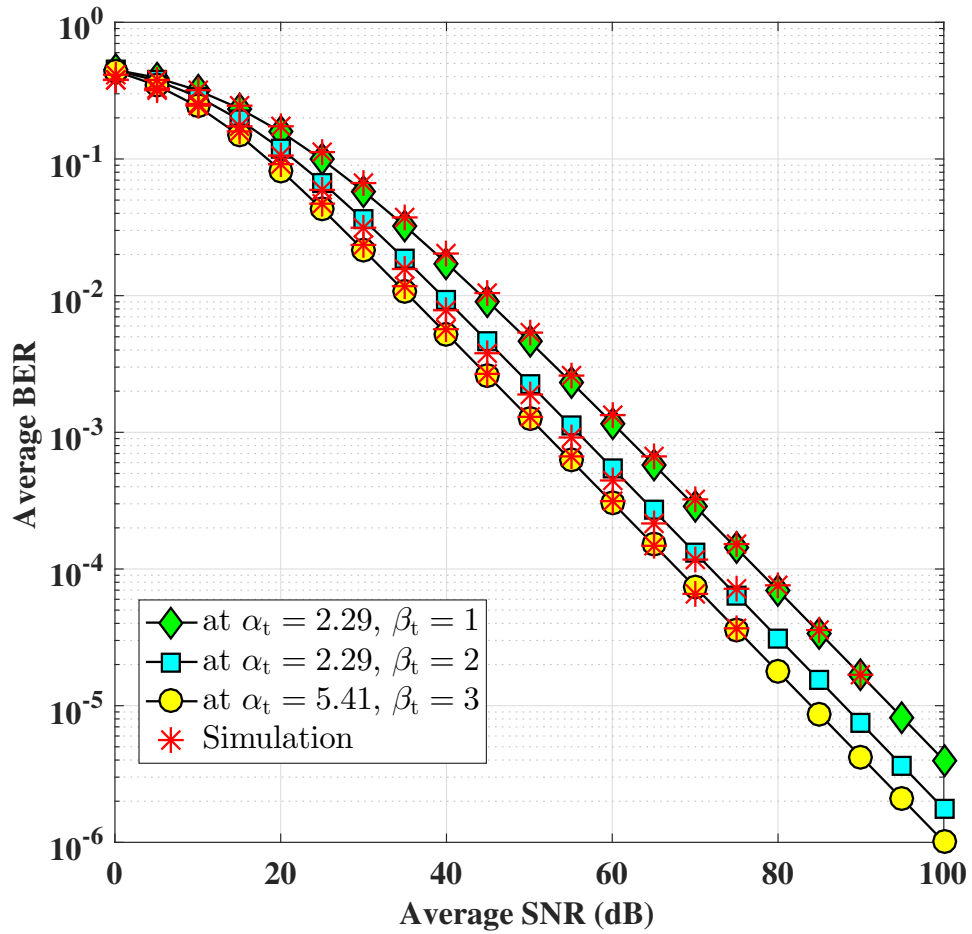
Avg. SNR (dB)	Optimum switching threshold ( $\gamma_0$ )				
	$N_r = 2$	$N_r = 3$	$N_r = 4$	$N_r = 5$	$N_r = 6$
0	18.01	18.01	18.01	18.01	18.01
5	18.39	18.39	18.39	18.39	18.39
10	18.89	18.89	18.89	18.89	18.89
15	19.48	19.48	19.48	19.48	19.48
20	20.13	20.13	20.13	20.13	20.13
25	20.80	20.80	20.80	20.80	20.80
30	21.50	21.50	21.50	21.50	21.50
35	22.19	22.19	22.19	22.19	22.19
40	22.89	22.89	22.89	22.89	22.89
45	23.58	23.58	23.58	23.58	23.58
50	24.26	24.26	24.26	24.26	24.26
55	24.93	24.93	24.93	24.93	24.93
60	25.58	25.58	25.58	25.58	25.58
65	26.20	26.20	26.20	26.20	26.20
70	26.80	26.80	26.80	26.80	26.80
75	27.38	27.38	27.38	27.38	27.38
80	27.92	27.92	27.92	27.92	27.92
85	28.43	28.43	28.43	28.43	28.43
90	28.91	28.91	28.91	28.91	28.91
95	29.35	29.35	29.35	29.35	29.35
100	29.75	29.75	29.75	29.75	29.75

TABLE 4.10: Optimum switching threshold of  $1 \times 4$  SIMO FSO system in the presence of pointing error ( $\xi = 0.5607$ ) with different average SNR for different turbulence parameter.

Avg. SNR (dB)	Optimum switching threshold ( $\gamma_0$ )		
	$\alpha_t = 5.41, \beta_t = 3$	$\alpha_t = 2.29, \beta_t = 2$	$\alpha_t = 2.29, \beta_t = 1$
0	18.22	17.92	18.01
5	19.03	18.42	18.39
10	19.92	19.06	18.89
15	20.76	19.76	19.48
20	21.54	20.48	20.13
25	22.31	21.18	20.80
30	23.06	21.86	21.50
35	23.81	22.52	22.19
40	24.55	23.15	22.89
45	25.28	23.76	23.58
50	26.00	24.34	24.26
55	26.71	24.89	24.93
60	27.41	25.40	25.58
65	28.09	25.88	26.20
70	28.75	26.32	26.80
75	29.39	26.73	27.38
80	30.01	27.10	27.92
85	30.60	27.43	28.43
90	31.16	27.73	28.91
95	31.69	27.99	29.35
100	32.18	28.22	29.75



**Figure 4.9 (a)** Average bit error rate of  $1 \times 4$  SIMO FSO link under Málaga distribution in the presence of pointing error ( $\xi = 0.5607$ ) for different atmospheric turbulence with fixed switching threshold 10 dB.



**Figure 4.9 (b)** Average bit error rate of  $1 \times 4$  SIMO FSO link under Málaga distribution in the presence of pointing error ( $\xi = 0.5607$ ) for different atmospheric turbulence with optimal switching threshold.



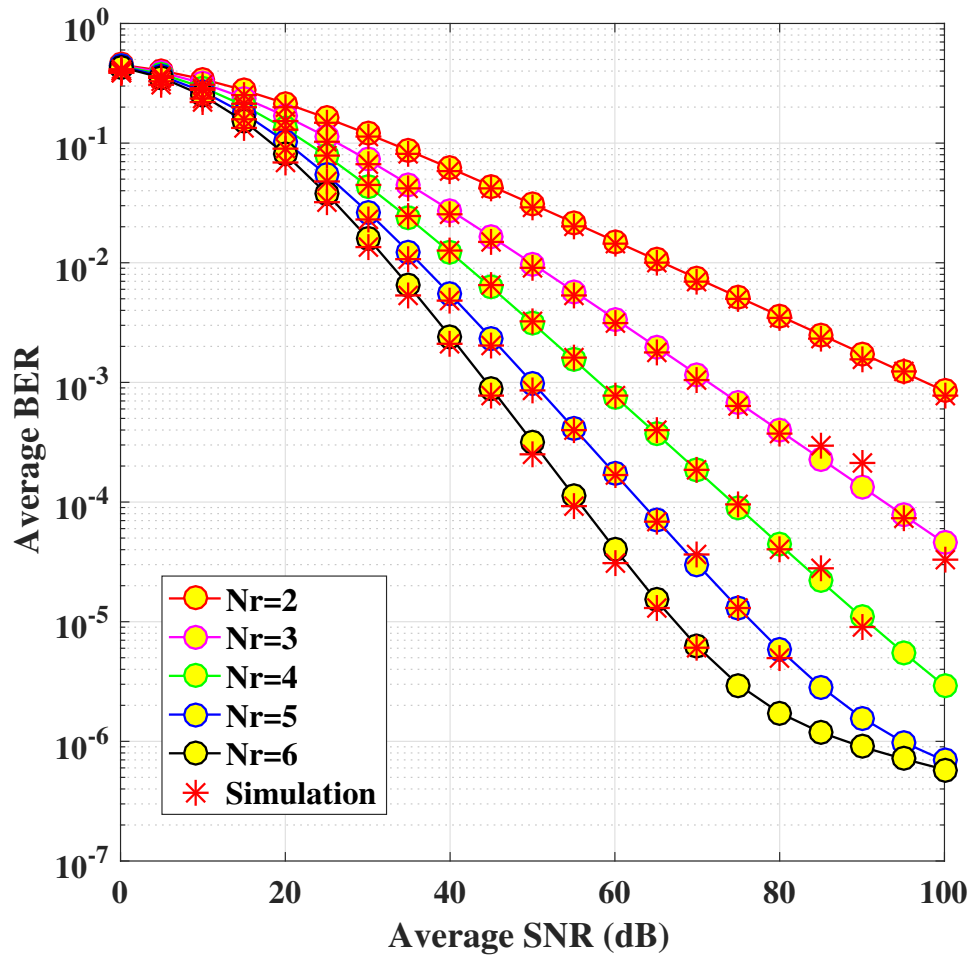


**Figure 4.9 (c)** Average bit error rate of SIMO FSO link under Málaga distribution in the presence of pointing error ( $\xi = 0.5607$ ) for  $\alpha_t = 2.29$  and  $\beta_t = 1$  with fixed switching threshold of 10 dB.

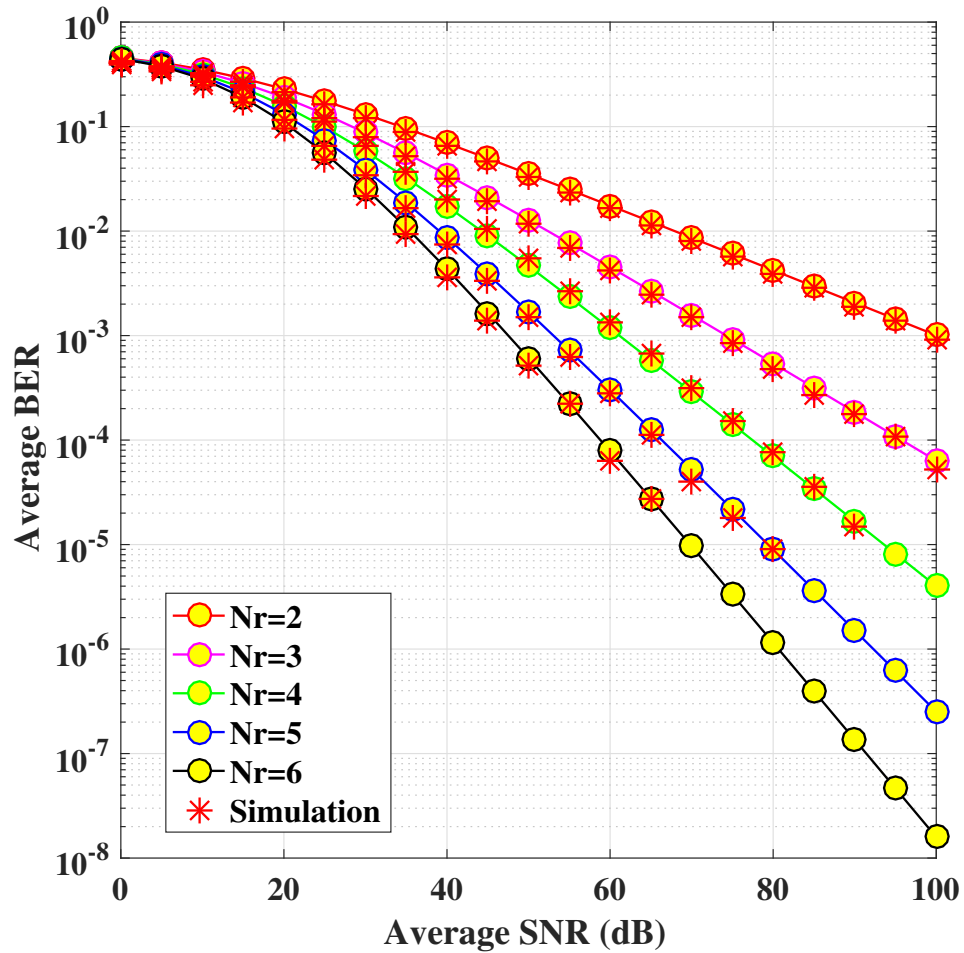


**Figure 4.9 (d)** Average bit error rate of SIMO FSO link under Málaga distribution in the presence of pointing error ( $\xi = 0.5607$ ) for  $\alpha_t = 2.29$  and  $\beta_t = 1$  with optimal switching threshold.

FIGURE 4.9: Average bit error rate of the SIMO FSO link employing switch and examine combining scheme at the receiver end with Málaga distribution using different atmospheric turbulence conditions in the presence of pointing error.

TABLE 4.11: Comparison of ABER for different FSO communication systems under Gamma-Gamma statistical distribution with pointing error ( $\xi = 0.5607$ ) for turbulence parameters  $\alpha_t = 4.20$  and  $\beta_t = 2.72$ .

System topology	ToD	Avg. SNR	No th	Fixed th	Optimal th
SISO FSO	--	90 dB	$1.4 \times 10^{-2}$	-	-
MISO FSO	STBC	90 dB	$3.0 \times 10^{-4}$	-	-
SIMO FSO	SEC	90 dB	-	$1.4 \times 10^{-6}$	$7.6 \times 10^{-7}$
ToD $\rightarrow$ Types of Diversity					

TABLE 4.12: Summary of the equations used for figures, Fig. 4.10 to Fig. 4.13.

Figure	Scenario	Equation
Fig. 4.10a	GG	Eq. 4.11 with Eq. 4.13 and Eq. 4.14
Fig. 4.10b	GG	Eq. 4.11 with Eq. 4.13 and Eq. 4.14
Fig. 4.10c	GG	Eq. 4.11 with Eq. 4.13 and Eq. 4.14
Fig. 4.10d	GG	Eq. 4.11 with Eq. 4.13 and Eq. 4.14
Fig. 4.11a	GG + pointing	Eq. 4.23 with Eq. 4.25 and Eq. 4.26
Fig. 4.11b	GG + pointing	Eq. 4.23 with Eq. 4.25 and Eq. 4.26
Fig. 4.11c	GG + pointing	Eq. 4.23 with Eq. 4.25 and Eq. 4.26
Fig. 4.11d	GG + pointing	Eq. 4.23 with Eq. 4.25 and Eq. 4.26
Fig. 4.12a	Málaga	Eq. 4.35 with Eq. 4.37 and Eq. 4.38
Fig. 4.12b	Málaga	Eq. 4.35 with Eq. 4.37 and Eq. 4.38
Fig. 4.12c	Málaga	Eq. 4.35 with Eq. 4.37 and Eq. 4.38
Fig. 4.12d	Málaga	Eq. 4.35 with Eq. 4.37 and Eq. 4.38
Fig. 4.13a	Málaga + pointing	Eq. 4.48 with Eq. 4.51 and Eq. 4.52
Fig. 4.13b	Málaga + pointing	Eq. 4.48 with Eq. 4.51 and Eq. 4.52
Fig. 4.13c	Málaga + pointing	Eq. 4.48 with Eq. 4.51 and Eq. 4.52
Fig. 4.13d	Málaga + pointing	Eq. 4.48 with Eq. 4.51 and Eq. 4.52

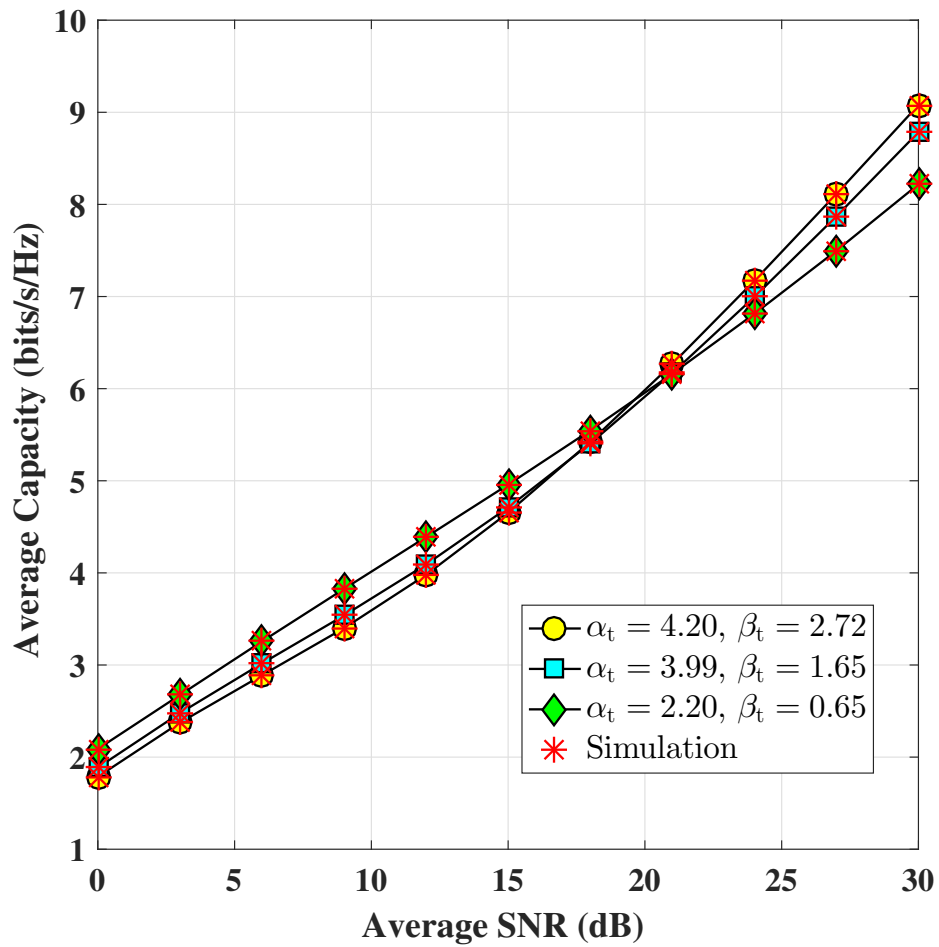
Table 4.11, indicates a comparison of ABER for various FSO communication systems in presence of a pointing error condition under the GG statistical distribution with turbulence parameters  $\alpha_t = 4.20$ ,  $\beta_t = 2.72$ . This comparison signifies that the ABER of the SIMO FSO link gets enhanced more than other FSO communication systems.

TABLE 4.13: Optimum switching threshold of  $1 \times N_r$  SIMO FSO system in the absence of pointing error with  $N_r = 2, 3, 4, 5$  and  $6$  for different average SNR with turbulence parameter  $\alpha_t = 2.20$  and  $\beta_t = 0.65$ .

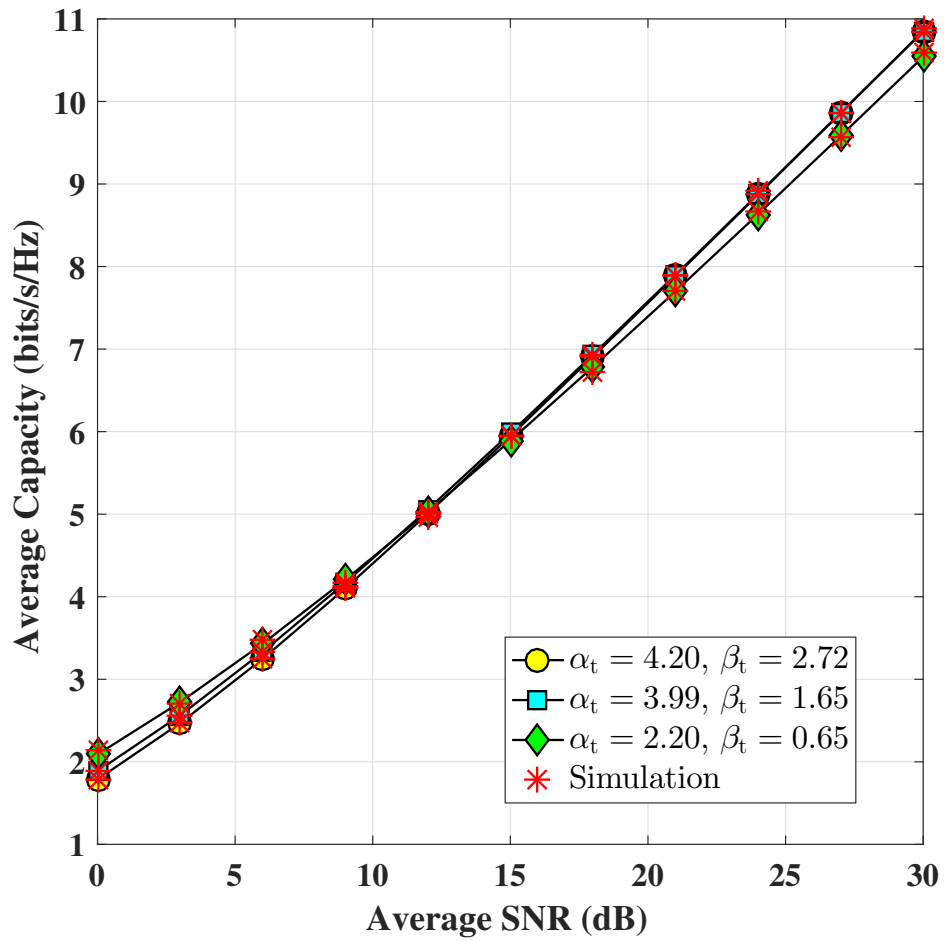
Avg. SNR (dB)	Optimum switching threshold ( $\gamma_0$ )				
	$N_r = 2$	$N_r = 3$	$N_r = 4$	$N_r = 5$	$N_r = 6$
0	0.51	1.17	2.37	3.31	4.07
3	1.42	3.23	4.53	5.53	6.35
6	3.38	5.33	6.73	7.81	8.69
9	5.37	7.49	9.01	10.17	11.12
12	7.42	9.73	11.36	12.62	13.62
15	9.54	12.05	13.81	15.14	16.20
18	11.76	14.47	16.34	17.74	18.86
21	14.07	16.90	18.94	20.42	21.57
24	16.47	19.55	21.62	23.15	24.34
27	18.97	22.21	24.35	25.93	27.16
30	21.55	24.92	27.14	28.76	30.01

TABLE 4.14: Optimum switching threshold of  $1 \times 4$  SIMO FSO system in the absence of pointing error with different average SNR for different turbulence parameters.

Avg. SNR (dB)	Optimum switching threshold ( $\gamma_0$ )		
	$\alpha_t = 4.20, \beta_t = 2.72$	$\alpha_t = 3.99, \beta_t = 1.65$	$\alpha_t = 2.20, \beta_t = 0.65$
0	1.99	2.17	2.37
3	4.56	4.64	4.53
6	7.19	7.17	6.73
9	9.88	9.77	9.01
12	12.65	12.44	11.36
15	15.48	15.20	13.81
18	18.37	18.02	16.34
21	21.29	20.89	18.94
24	24.25	23.80	21.62
27	27.22	26.74	24.35
30	30.20	29.70	27.14



**Figure 4.10 (a)** Average capacity of  $1 \times 4$  SIMO FSO link under Gamma-Gamma distribution in the absence of pointing error for different atmospheric turbulence condition using fixed switching threshold of 2dB.



**Figure 4.10 (b)** Average capacity of  $1 \times 4$  SIMO FSO link under Gamma-Gamma distribution in the absence of pointing error for different atmospheric turbulence condition using optimal switching threshold.

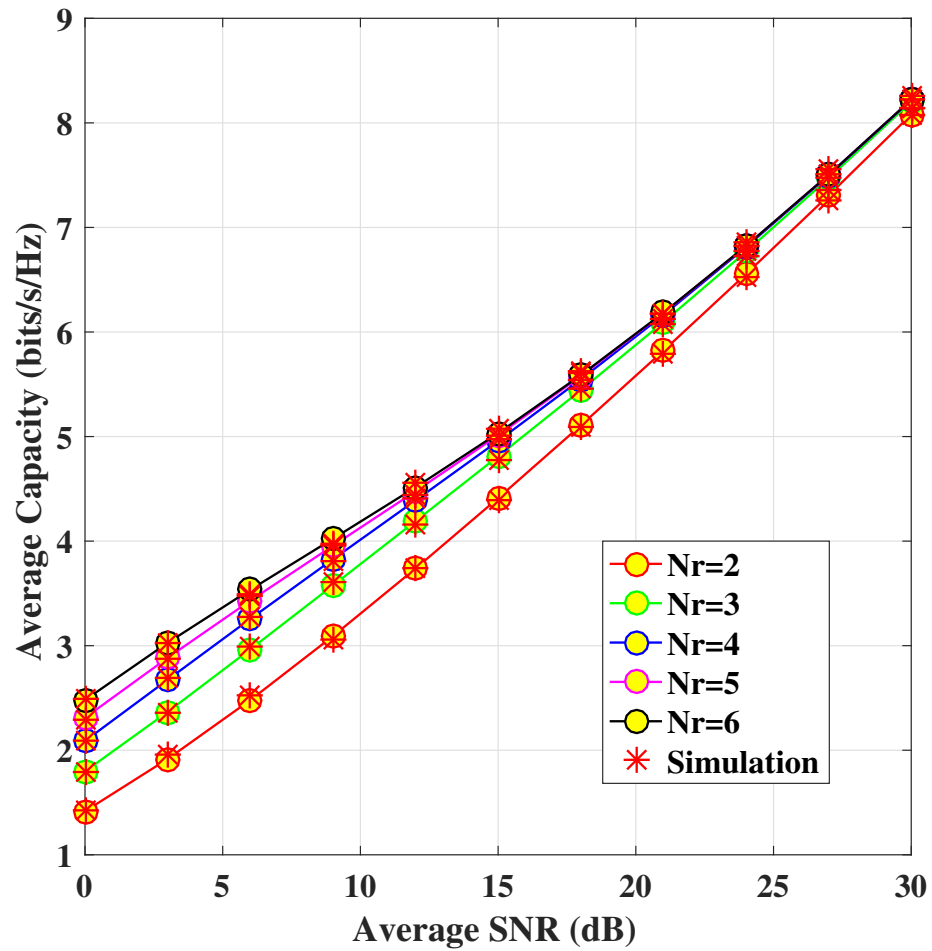


**Figure 4.10 (c)** Average capacity of  $1 \times N_r$  SIMO FSO link under Gamma-Gamma distribution in the absence of pointing error for  $\alpha_t = 2.20$  and  $\beta_t = 0.65$  with fixed switching threshold of 2 dB.

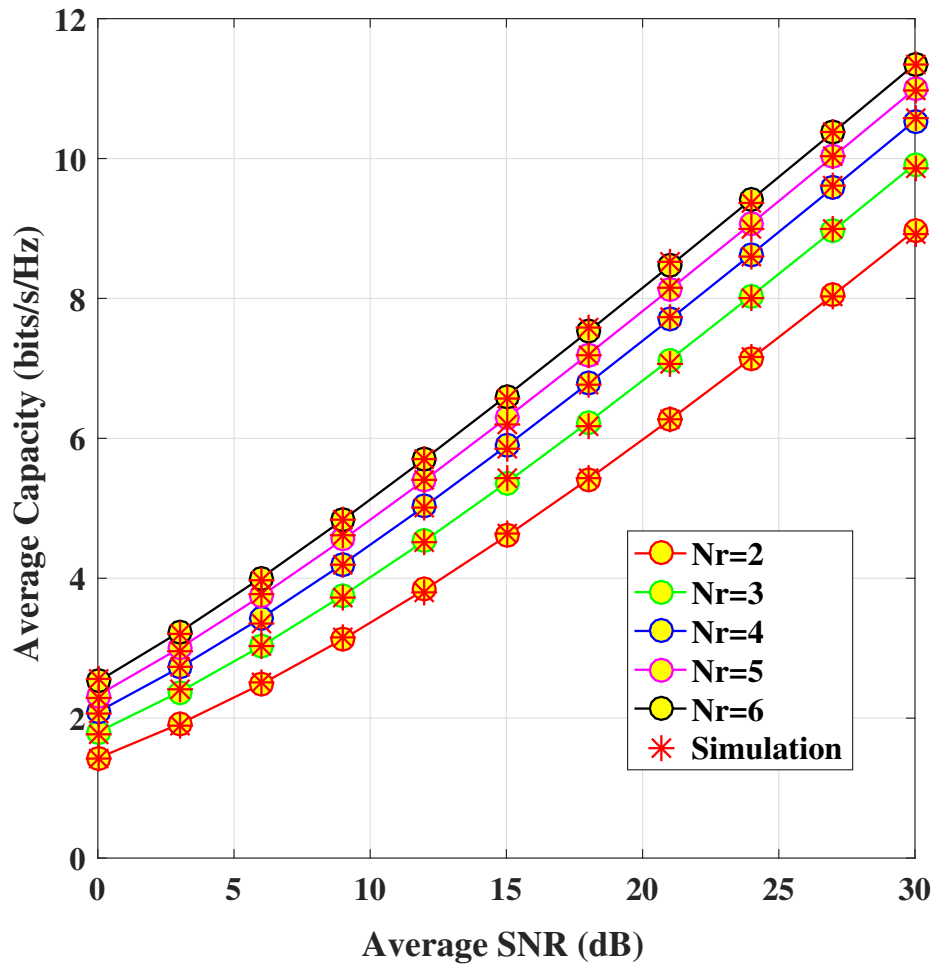


**Figure 4.10 (d)** Average capacity of  $1 \times N_r$  SIMO FSO link under Gamma-Gamma distribution in the absence of pointing error for  $\alpha_t = 2.20$  and  $\beta_t = 0.65$  with optimal switching threshold.

FIGURE 4.10: Average capacity of the SIMO FSO link employing switch and examine combining scheme at the receiver end with Gamma-Gamma distribution using different atmospheric turbulence condition in the absence of pointing error.

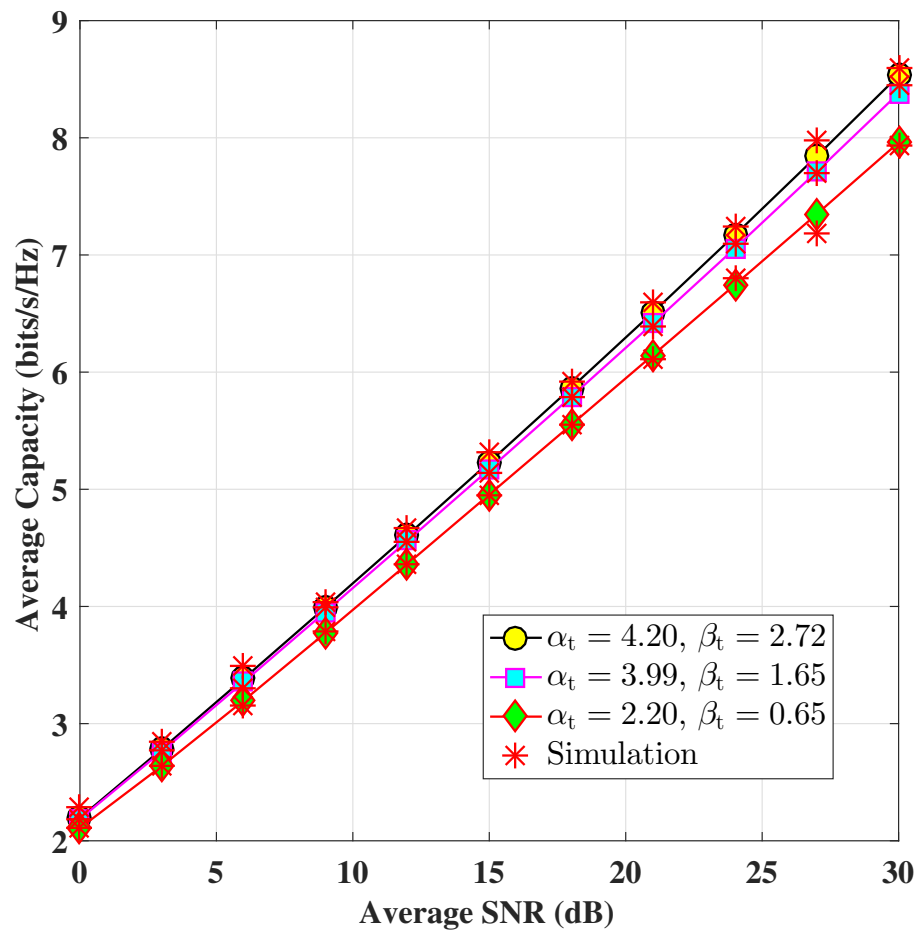


TABLE 4.15: Optimum switching threshold of  $1 \times N_r$  SIMO FSO system in the presence of pointing error ( $\xi = 0.5607$ ) with  $N_r = 2, 3, 4, 5$  and  $6$  for different average SNR with turbulence parameter  $\alpha_t = 2.20$  and  $\beta_t = 0.65$ .

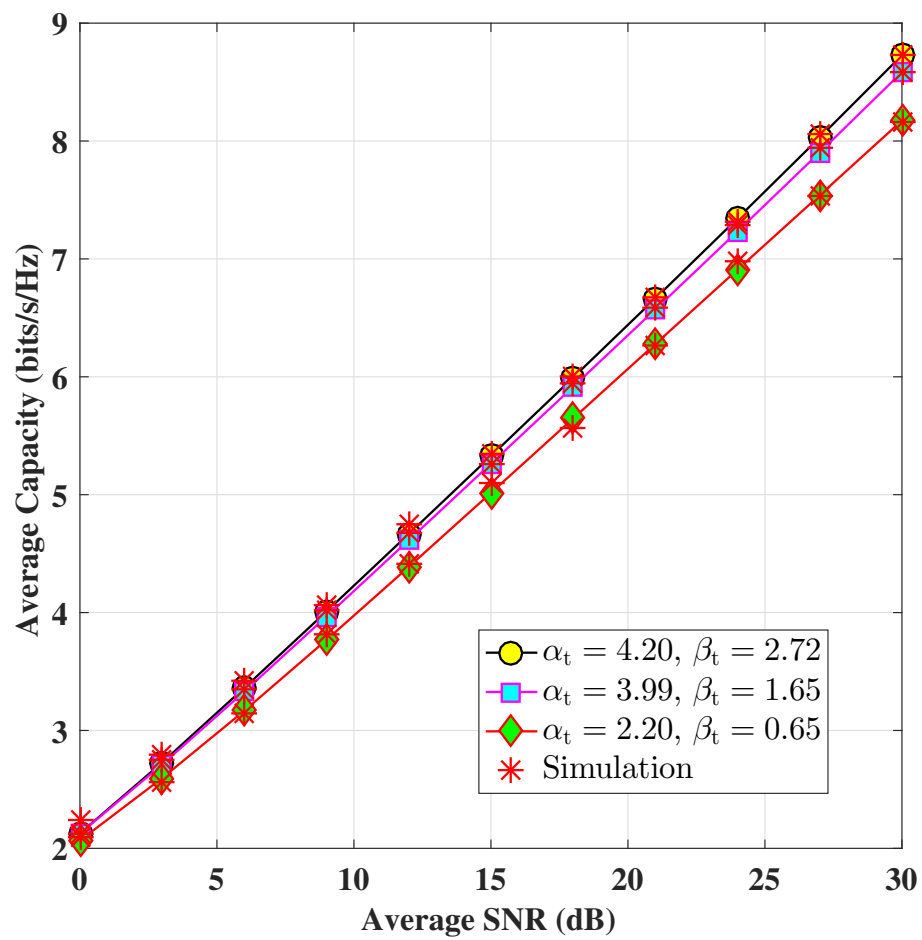
Avg. SNR (dB)	Optimum switching threshold ( $\gamma_0$ )				
	$N_r = 2$	$N_r = 3$	$N_r = 4$	$N_r = 5$	$N_r = 6$
0	1.70	2.17	2.47	2.68	2.85
3	2.08	2.50	2.78	2.98	3.14
6	2.39	2.78	3.05	3.25	3.40
9	2.66	3.04	3.30	3.49	3.64
12	2.90	3.28	3.53	3.72	3.85
15	3.13	3.50	3.75	3.92	4.05
18	3.34	3.71	3.95	4.11	4.22
21	3.54	4.90	4.13	4.28	4.38
24	3.73	4.08	4.30	4.44	4.53
27	3.91	4.26	4.46	4.59	4.66
30	4.08	4.42	4.61	4.72	4.78

TABLE 4.16: Optimum switching threshold of  $1 \times 4$  SIMO FSO system in the presence of pointing error ( $\xi = 0.5607$ ) with different average SNR for different turbulence parameter.

Avg. SNR (dB)	Optimum switching threshold ( $\gamma_0$ )		
	$\alpha_t = 4.20, \beta_t = 2.72$	$\alpha_t = 3.99, \beta_t = 1.65$	$\alpha_t = 2.20, \beta_t = 0.65$
0	2.62	2.59	2.47
3	2.96	2.92	2.78
6	3.25	3.21	3.05
9	3.51	3.47	3.30
12	3.75	3.71	3.53
15	3.97	3.92	3.75
18	4.16	4.12	3.95
21	4.34	4.30	4.13
24	4.50	4.47	4.30
27	4.66	4.62	4.46
30	4.80	4.76	4.61



**Figure 4.11 (a)** Average capacity of  $1 \times 4$  SIMO FSO link under Gamma-Gamma distribution in the presence of pointing error ( $\xi = 0.5607$ ) for different atmospheric turbulence using fixed switching threshold of 2dB.



**Figure 4.11 (b)** Average capacity of  $1 \times 4$  SIMO FSO link under Gamma-Gamma distribution in the presence of pointing error ( $\xi = 0.5607$ ) for different atmospheric turbulence using optimal switching threshold.

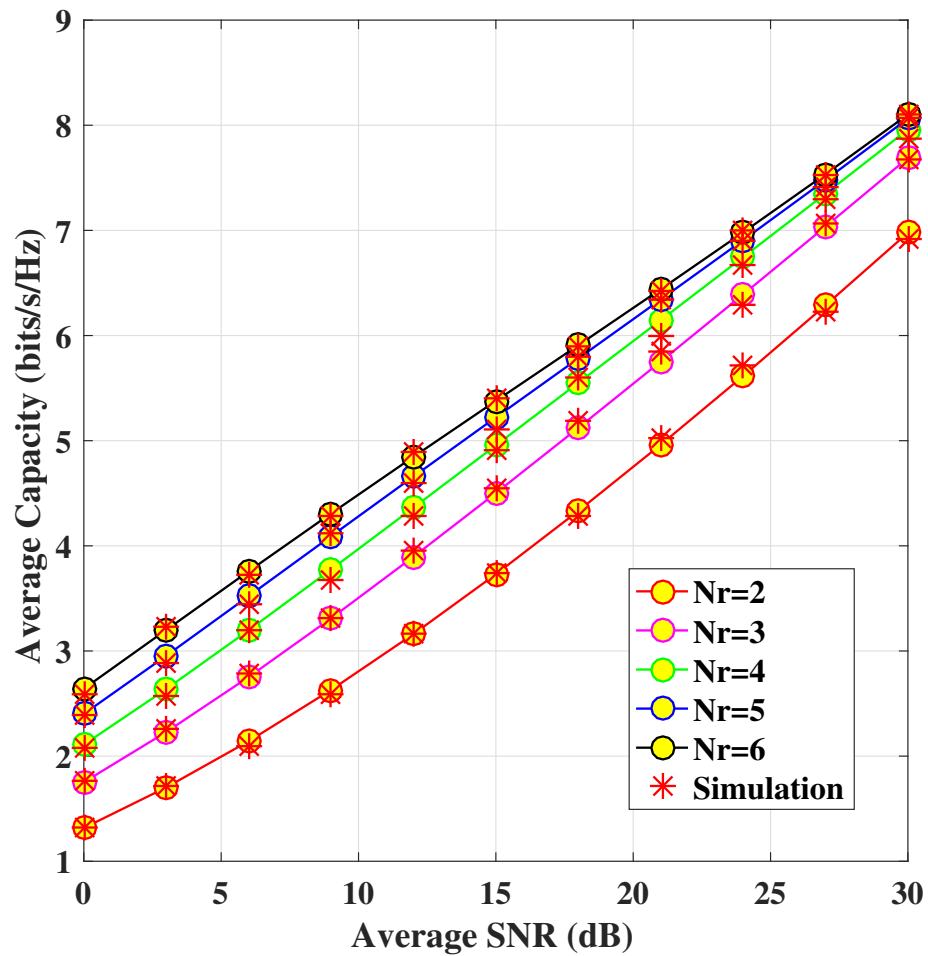


**Figure 4.11 (c)** Average capacity of  $1 \times N_r$  SIMO FSO link under Gamma-Gamma distribution in the presence of pointing error ( $\xi = 0.5607$ ) for  $\alpha_t = 2.20$  and  $\beta_t = 0.65$  with fixed switching threshold of 2 dB.

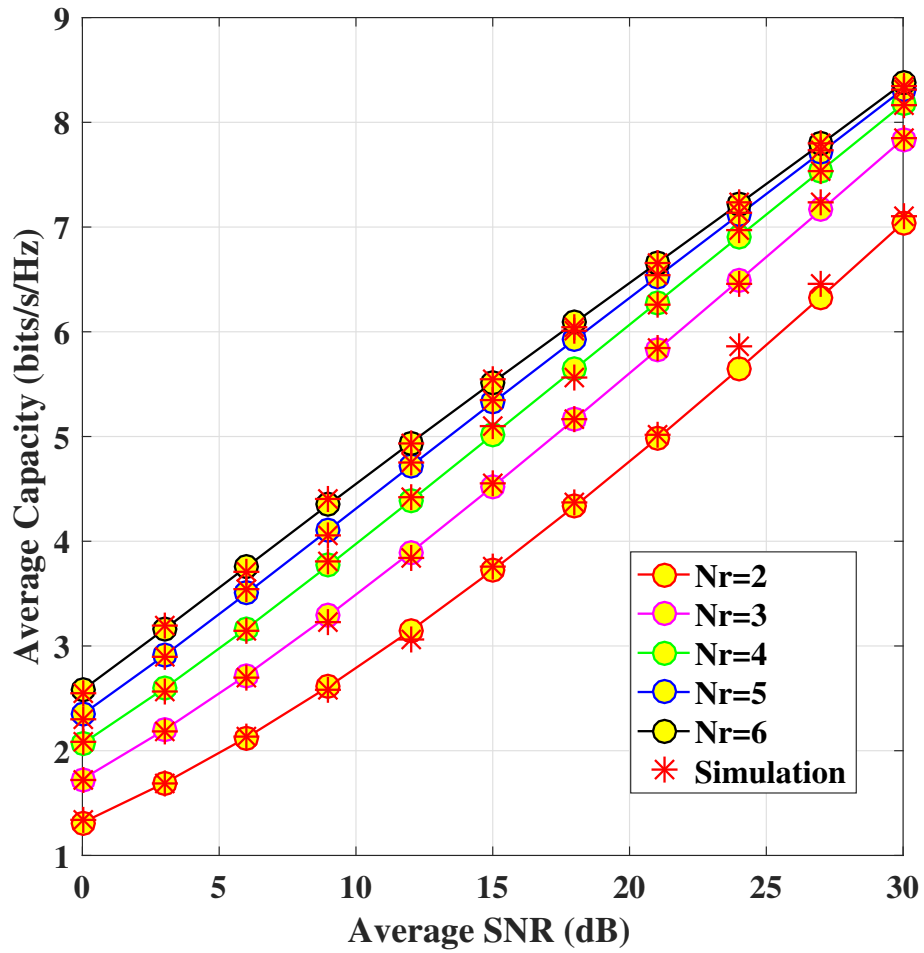


**Figure 4.11 (d)** Average capacity of  $1 \times N_r$  SIMO FSO link under Gamma-Gamma distribution in the presence of pointing error ( $\xi = 0.5607$ ) for  $\alpha_t = 2.20$  and  $\beta_t = 0.65$  with optimal switching threshold.

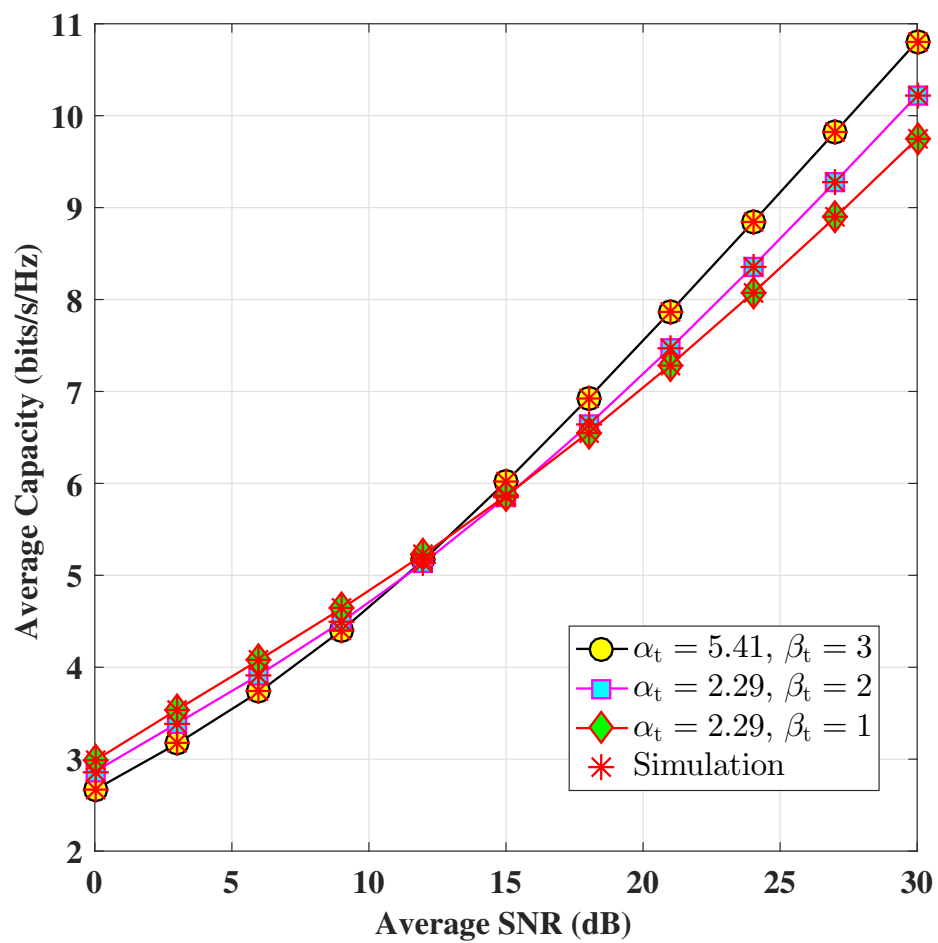
FIGURE 4.11: Average capacity of the SIMO FSO link employing switch and examine combining scheme at the receiver end with Gamma-Gamma distribution using different atmospheric turbulence condition in the presence of pointing error.

TABLE 4.17: Optimum switching threshold of  $1 \times N_r$  SIMO FSO system in the absence of pointing error with  $N_r = 2, 3, 4, 5$  and  $6$  for different average SNR with turbulence parameter  $\alpha_t = 2.29$  and  $\beta_t = 1$ .

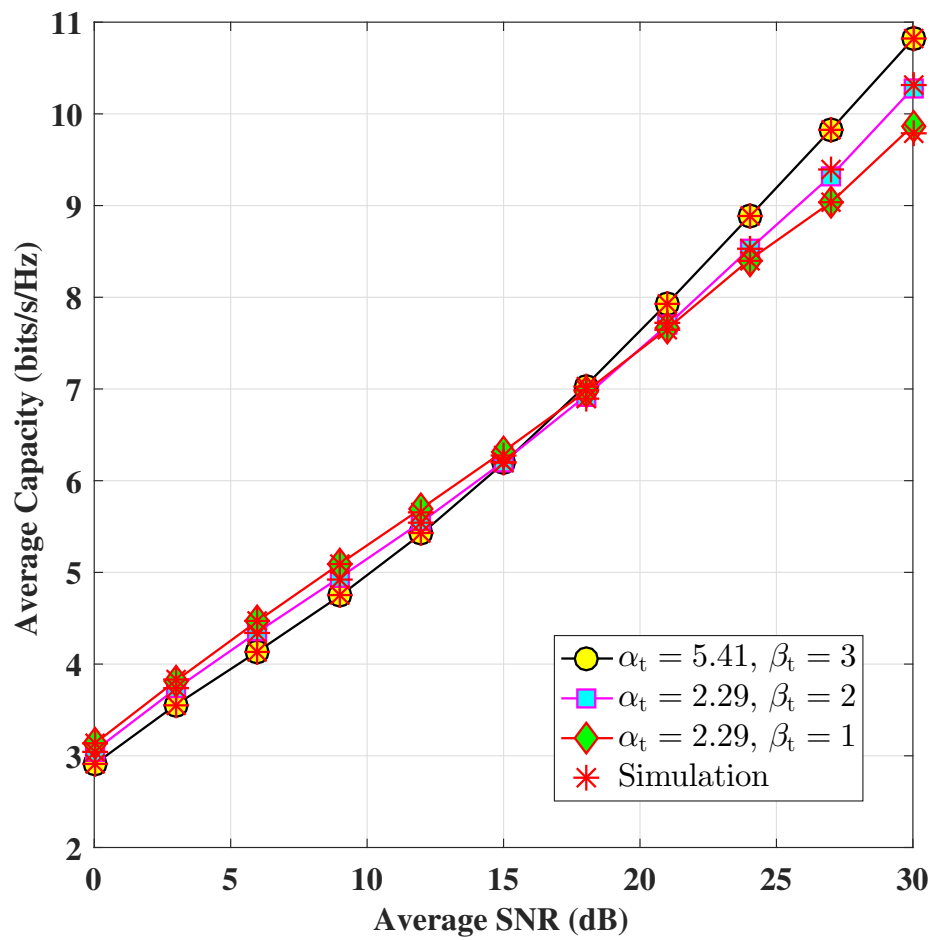
Avg. SNR (dB)	Optimum switching threshold ( $\gamma_0$ )				
	$N_r = 2$	$N_r = 3$	$N_r = 4$	$N_r = 5$	$N_r = 6$
0	3.19	2.97	3.19	3.35	3.47
3	3.49	3.29	3.49	3.63	3.72
6	3.74	3.56	3.74	3.85	3.92
9	3.96	3.81	3.96	4.05	4.09
12	4.16	4.04	4.16	4.21	4.24
15	4.33	4.24	4.33	4.36	4.37
18	4.48	4.41	4.48	4.49	4.52
21	4.63	4.60	4.63	4.63	4.63
24	5.00	5.00	5.00	5.00	5.00
27	3.04	3.04	3.04	3.04	3.04
30	3.14	3.14	3.14	3.14	3.14

TABLE 4.18: Optimum switching threshold of  $1 \times 4$  SIMO FSO system in the absence of pointing error with different average SNR for different turbulence parameters.

Avg. SNR (dB)	Optimum switching threshold ( $\gamma_0$ )		
	$\alpha_t = 5.41, \beta_t = 3$	$\alpha_t = 2.29, \beta_t = 2$	$\alpha_t = 2.29, \beta_t = 1$
0	3.25	3.23	3.19
3	3.54	3.52	3.49
6	3.77	3.77	3.74
9	3.97	3.98	3.96
12	4.15	4.16	4.16
15	4.33	4.33	4.33
18	4.52	4.48	4.48
21	4.69	4.66	4.63
24	5.11	4.80	5.00
27	3.19	2.73	3.04
30	3.51	3.80	3.14



**Figure 4.12 (a)** Average capacity of  $1 \times 4$  SIMO FSO link under Málaga distribution in the absence of pointing error for different atmospheric turbulence using fixed switching threshold of 2dB.



**Figure 4.12 (b)** Average capacity of  $1 \times 4$  SIMO FSO link under Málaga distribution in the absence of pointing error for different atmospheric turbulence using optimal switching threshold.



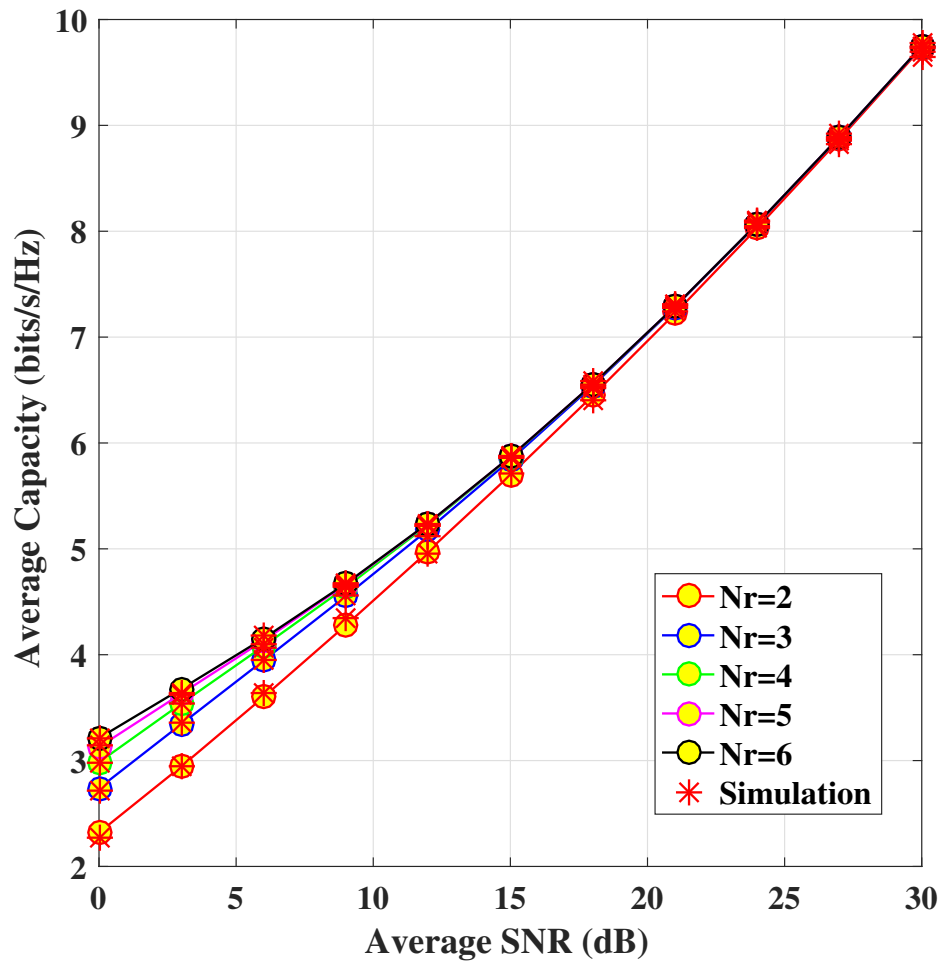


**Figure 4.12 (c)** Average capacity of  $1 \times N_r$  SIMO FSO link under Málaga distribution in the absence of pointing error for  $\alpha_t = 2.29$  and  $\beta_t = 1$  with fixed switching threshold of 2 dB.

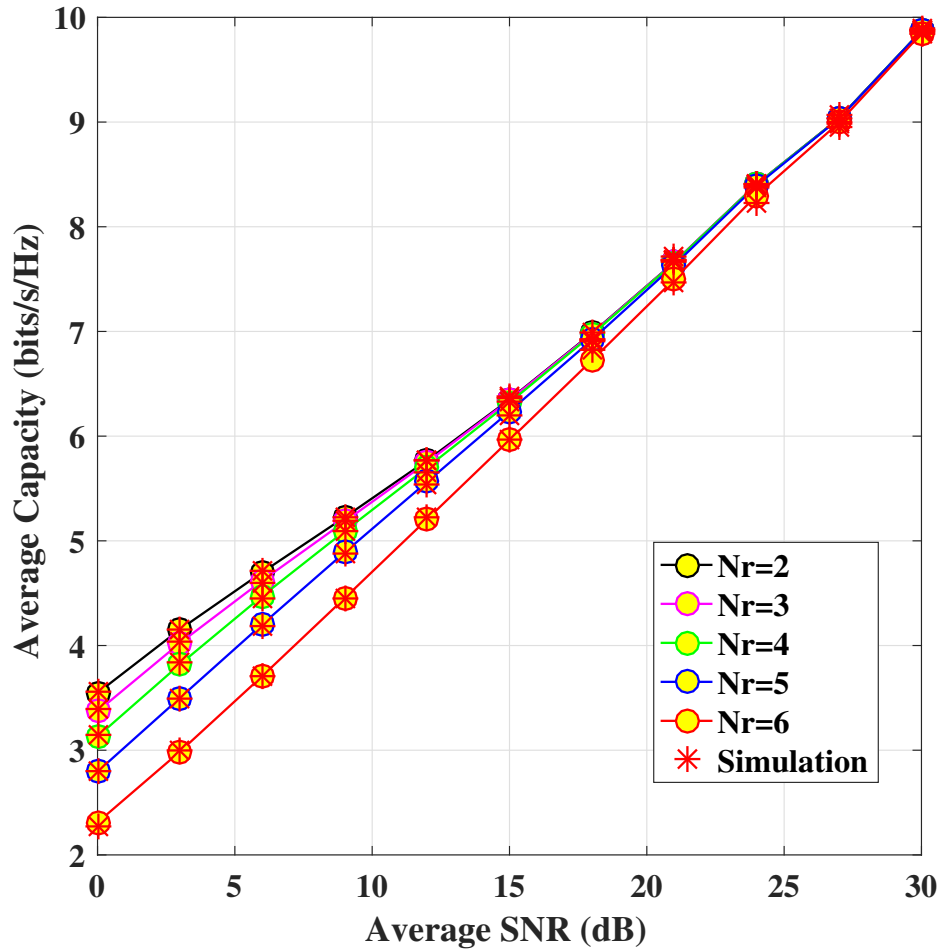


**Figure 4.12 (d)** Average capacity of  $1 \times N_r$  SIMO FSO link under Málaga distribution in the absence of pointing error for  $\alpha_t = 2.29$  and  $\beta_t = 1$  with optimal switching threshold.

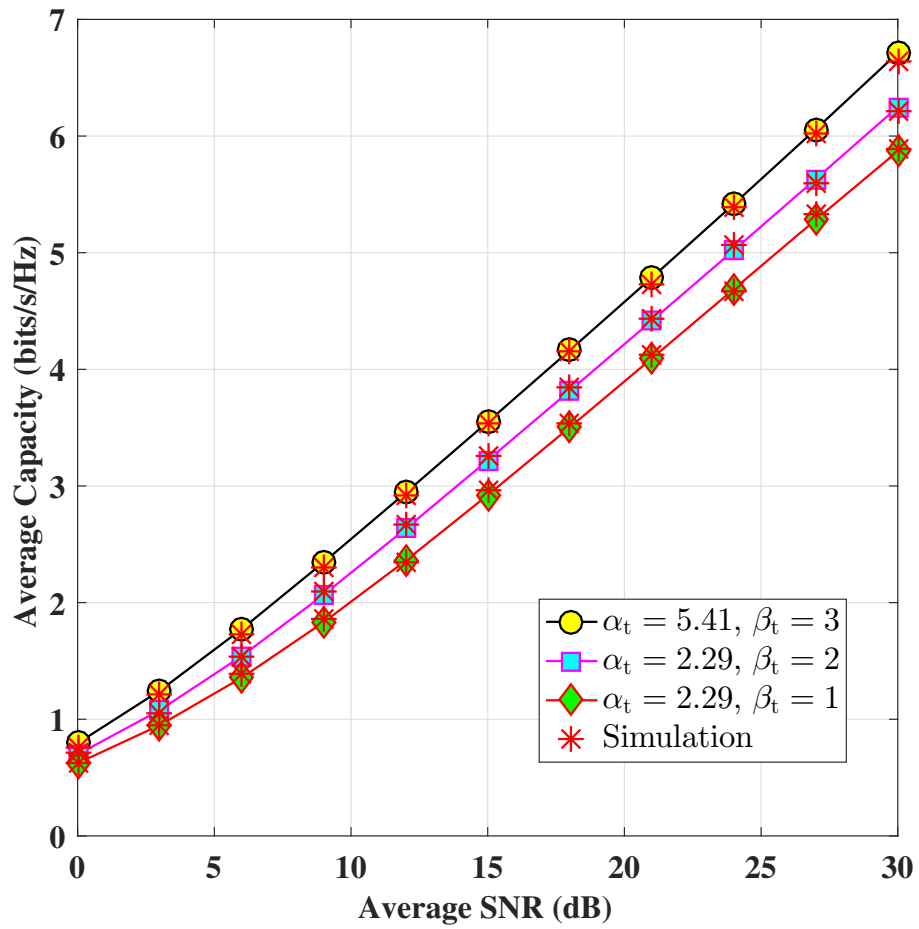
FIGURE 4.12: Average capacity of the SIMO FSO link employing switch and examine combining scheme in the receiver end with Málaga distribution using different atmospheric turbulence condition in the absence of pointing error.

TABLE 4.19: Optimum switching threshold of  $1 \times N_r$  SIMO FSO system in the presence of pointing error ( $\xi = 0.5607$ ) with  $N_r = 2, 3, 4, 5$  and  $6$  for different average SNR with turbulence parameter  $\alpha_t = 2.29$  and  $\beta_t = 1$ .

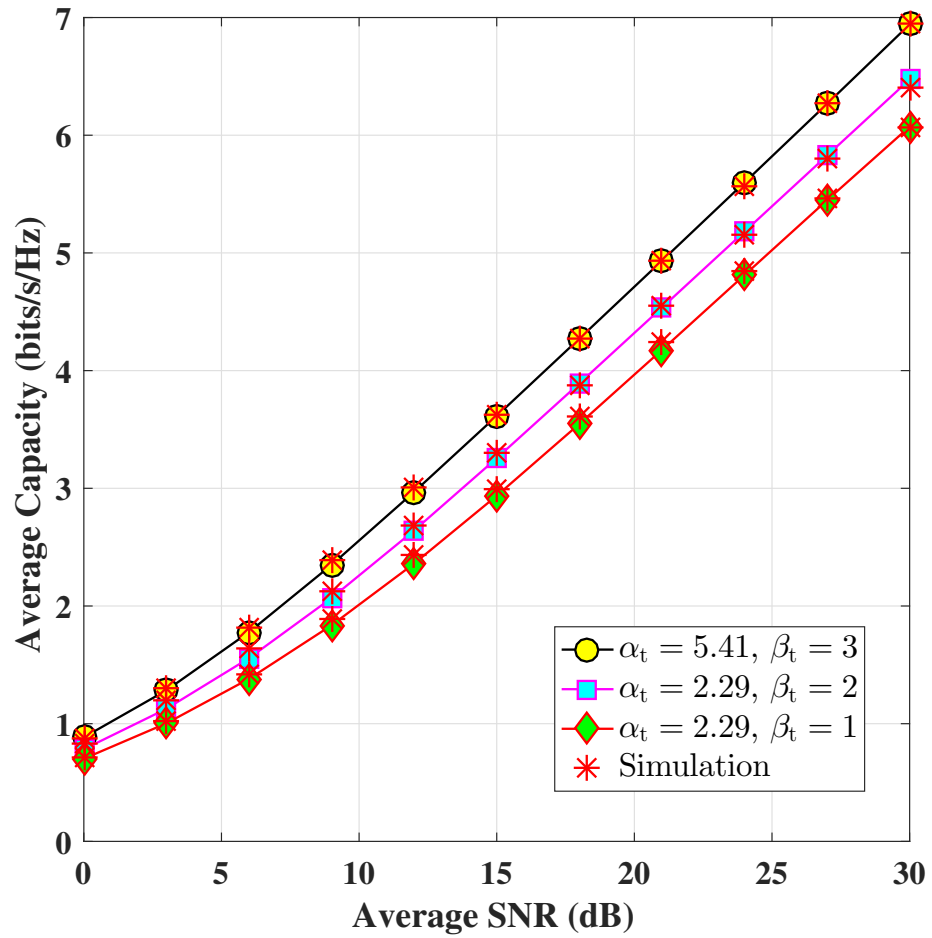
Avg. SNR (dB)	Optimum switching threshold ( $\gamma_0$ )				
	$N_r = 2$	$N_r = 3$	$N_r = 4$	$N_r = 5$	$N_r = 6$
0	0.18	0.26	0.34	0.42	0.50
3	0.28	0.41	0.55	0.68	0.82
6	0.42	0.64	0.86	1.08	1.27
9	0.64	0.98	1.29	1.53	1.72
12	0.95	1.40	1.71	1.93	2.09
15	1.33	1.78	2.06	2.25	2.39
18	1.69	2.10	2.35	2.52	2.65
21	1.99	2.37	2.59	2.75	2.87
24	2.26	2.61	2.82	2.97	3.05
27	2.55	2.82	2.95	3.17	3.21
30	2.76	3.12	3.12	3.21	3.36

TABLE 4.20: Optimum switching threshold of  $1 \times 4$  SIMO FSO system in the presence of pointing error ( $\xi = 0.5607$ ) with different average SNR for different turbulence parameter.

Avg. SNR (dB)	Optimum switching threshold ( $\gamma_0$ )		
	$\alpha_t = 5.41, \beta_t = 3$	$\alpha_t = 2.29, \beta_t = 2$	$\alpha_t = 2.29, \beta_t = 1$
0	0.49	0.40	0.34
3	0.83	0.66	0.55
6	1.31	1.06	0.86
9	1.78	1.52	1.29
12	2.15	1.93	1.71
15	2.45	2.25	2.06
18	2.71	2.53	2.35
21	2.93	2.77	2.59
24	3.12	2.97	2.82
27	3.27	3.16	2.95
30	3.48	3.31	3.12



**Figure 4.13 (a)** Average capacity of  $1 \times 4$  SIMO FSO link under Málaga distribution in the presence of pointing error ( $\xi = 0.5607$ ) for different atmospheric turbulence using fixed switching threshold of 2dB.



**Figure 4.13 (b)** Average capacity of  $1 \times 4$  SIMO FSO link under Málaga distribution in the presence of pointing error ( $\xi = 0.5607$ ) for different atmospheric turbulence using optimal switching threshold.

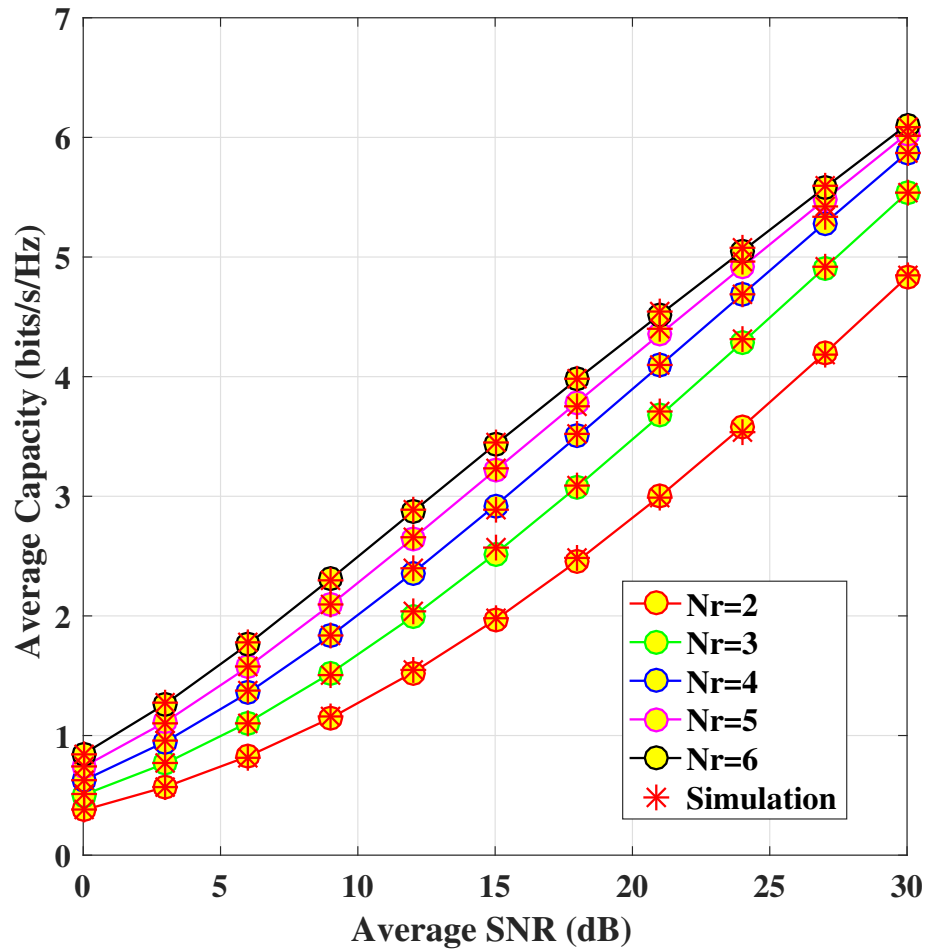


**Figure 4.13 (c)** Average capacity of  $1 \times N_r$  SIMO FSO link under Málaga distribution in the presence of pointing error ( $\xi = 0.5607$ ) for  $\alpha_t = 2.29$  and  $\beta_t = 1$  with fixed switching threshold of 2 dB.

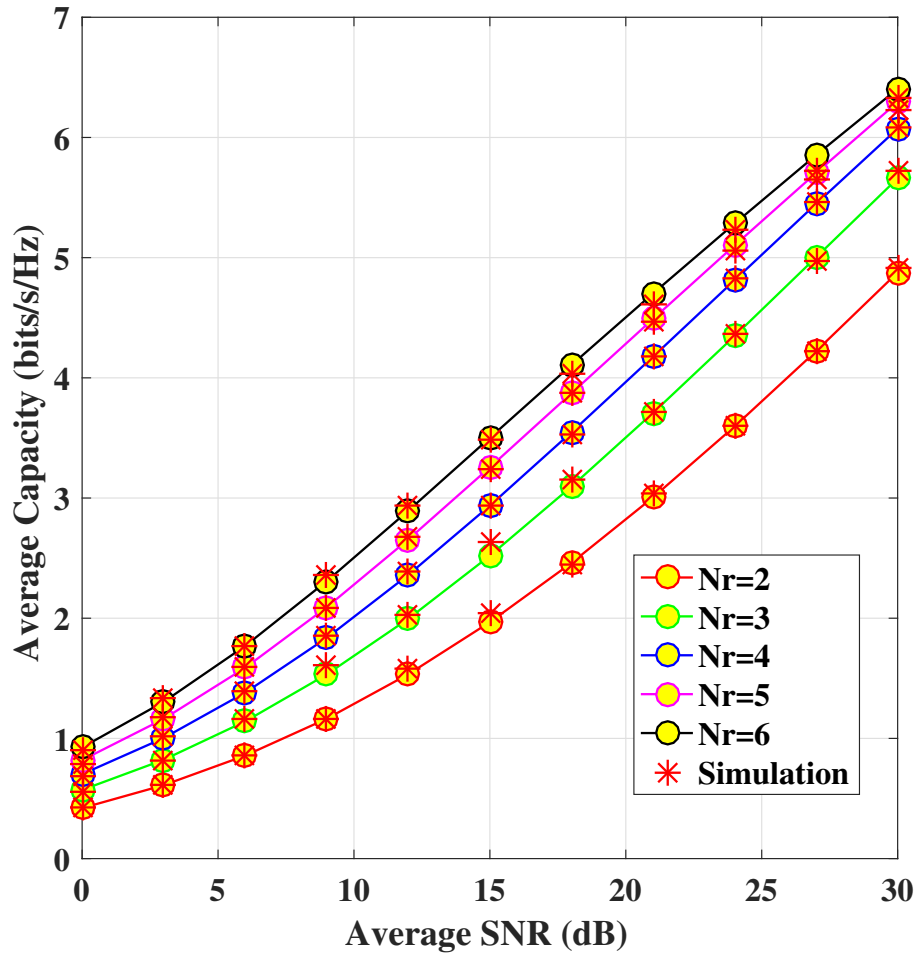


**Figure 4.13 (d)** Average capacity of  $1 \times N_r$  SIMO FSO link under Málaga distribution in the presence of pointing error ( $\xi = 0.5607$ ) for  $\alpha_t = 2.29$  and  $\beta_t = 1$  with optimal switching threshold.

FIGURE 4.13: Average capacity of the SIMO FSO link employing switch and examine combining scheme at the receiver end with Málaga distribution using different atmospheric turbulence conditions in the presence of pointing error.

TABLE 4.21: Comparison of Average capacity for different FSO communication systems under Gamma-Gamma statistical distribution without pointing error for turbulence parameters  $\alpha_t = 4.20$  and  $\beta_t = 2.72$ .

System topology	ToD	Avg. SNR	No th	Fixed th	Optimal th
SISO FSO	--	30 dB	9.06b/s/Hz	-	-
MISO FSO	STBC	30 dB	11.5b/s/Hz	-	-
SIMO FSO	SEC	30 dB	-	9.07b/s/Hz	10.85b/s/Hz
ToD $\rightarrow$ Types of Diversity					

TABLE 4.22: Comparison of Average capacity for different FSO communication systems under Gamma-Gamma statistical distribution with pointing error ( $\xi = 0.5607$ ) for turbulence parameters  $\alpha_t = 4.20$  and  $\beta_t = 2.72$ .

System topology	ToD	Avg. SNR	No th	Fixed th	Optimal th
SISO FSO	--	30 dB	4.91b/s/Hz	-	-
MISO FSO	STBC	30 dB	6.31b/s/Hz	-	-
SIMO FSO	SEC	30 dB	-	8.39b/s/Hz	8.72b/s/Hz
ToD $\rightarrow$ Types of Diversity					

The comparison of the average capacity of the systems has been provided in Table 4.21 and Table 4.22 under GG statistical distribution in the absence and presence of a pointing error. We have considered the turbulence parameters  $\alpha_t = 4.20$ ,  $\beta_t = 2.72$  for this comparison, and a single average SNR of 30 dB. This comparison indicates that in the presence of a pointing error, the average capacity of any FSO links severely decreases than the absence of a pointing error condition. Also, this comparison ensures that a SIMO FSO link is a useful technique to achieve higher channel capacity than the rest of the other FSO links under a pointing error condition, but in the absence of a pointing error, the MISO FSO link is a little better than SIMO FSO link. However, it is ensured that any diversity assists FSO communication systems can mitigate the effect of atmospheric turbulence and influence of pointing errors more than the primary FSO communication system.



## 4.8 Chapter summary

In this chapter, a SIMO FSO link has been characterized by employing the SEC receiver diversity scheme at the receiver end of the FSO communication system. Analytical derivations of the measuring metrics, such as OP, ABER, and average capacity, have been presented without and with the consideration of misalignment fading into the system. Two statistical distributions, GG and the generalised Málaga, have been considered in the above derivation to characterize the channel harshness. The numerical results have been presented as a 2D graphical plot to examine the nature of measuring metrics with the increase in the average SNR under various AT conditions. As per the numerical analysis, a MISO FSO communication system provides 28% more capacity than a simple SISO configuration, whereas a SIMO FSO system delivers 70.87% and 77.59% higher capacity than the baseline SISO system under fixed and optimal switching threshold conditions, respectively. All the values are calculated for a GG fading scenario under the pointing error regime.

Thus, results indicate that the system performs better when it attends the optimum switching threshold rather than the fixed switching threshold. It has been further noticed that the quality indices of all measurable metrics are associated with the number of branches present in the system. The investigation presented in this chapter established that an SEC-added SIMO FSO communication system yields superior outcomes than a typical SISO FSO system under all weather conditions, and like transmit diversity, receiver diversity also improves the performance of the primary FSO link.

## Chapter 5

# Performance Analysis of FSO Communication Channel with Alamouti Transmit and SEC Receive Diversity

**Chapter contributions:** A  $2 \times 4$  MIMO FSO system has been developed by integrating the Alamouti transmitter and SEC receiver diversity technique in the fundamental SISO FSO system. The performance of the MIMO FSO system has been compared in terms of ABER with MISO FSO, SIMO FSO, and SISO FSO communication systems in the absence and presence of misalignment.

---

The work of this chapter is published in:

*Photonic Network Communications*, 36(3), 350-360, Aug. 2018 [\[link\]](#)

---

## 5.1 Introduction

In this chapter, one more FSO network topology will be introduced to mitigate the effect of atmospheric turbulence in the propagation medium. A MIMO configuration will be developed by employing both transmit and receive diversity techniques at the transceiver terminals of the FSO communication system. The Alamouti STBC, a classical two beam transmit diversity scheme, will be considered at the transmitter terminal, and the SEC technique will be utilized to achieve the  $N_r$  diversity order at the receiver end of the MIMO FSO system. Moreover, to characterize the atmospheric turbulence in the propagation path, we employ the GG and the Málaga statistical distribution model. We will examine the performance metric of the MIMO FSO communication system in terms of an average BER of the system under different weather conditions in different pointing error regimes. Here, the OOK modulation scheme is considered to modulate the baseband signal.

The ABER of the proposed  $2 \times N_r$  MIMO FSO system will be determined for each average SNR with fixed and optimal switching threshold conditions. Furthermore, detailed performance comparisons will be presented for the above system using the optimum switching threshold instead of the fixed one. The performance comparisons of a MIMO FSO network with a single FSO link and other FSO configurations will also be discussed here.

## 5.2 Organization

After the introduction, this chapter is organized in the following way. In Section 5.3, we will present the channel characterization of a  $2 \times N_r$  MIMO FSO link employing the Alamouti STBC as a transmitter diversity scheme and the SEC as a receiver diversity scheme in the FSO communication system. Analytical derivation based on the severity of turbulence in the propagation path will be made by considering two

types of statistical distributions. The mathematical framework of measuring metrics under the GG distribution will be placed in Section 5.3.1 without pointing error and in Section 5.3.2 with pointing error. Section 5.3.3 and Section 5.3.4, will present similar analytical derivation for the general Málaga statistical distribution without and with pointing error. Next, the analytical and simulation results characterizing the MIMO FSO link will appear in Section 5.4. The chapter ends with the summary in Section 5.5.

### 5.3 Performance analysis with Alamouti STBC and SEC

Fig. 5.1 schematically shows a  $2 \times N_r$  MIMO FSO communication system using the Alamouti STBC and SEC.

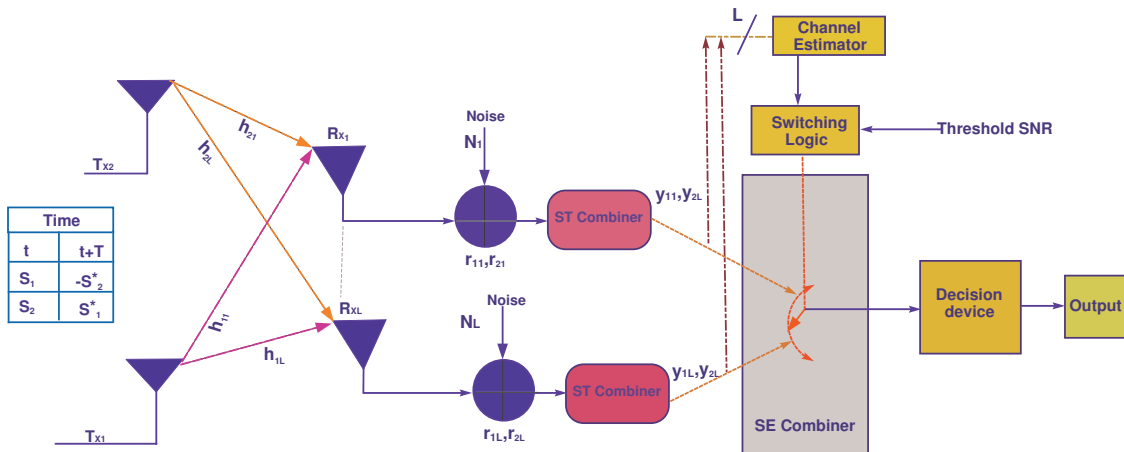


FIGURE 5.1: A  $2 \times N_r$  MIMO FSO system with Alamouti STBC and SEC.

Let  $\{s_1, s_2\}$  be two successive baseband message symbols to be transmitted. According to the Alamouti STBC scheme, During the first time slot, TX1 transmits signal  $s_1$  and TX2 transmits  $s_2$ , and during the second time slot, TX1 transmits  $-s_2^*$ , whereas TX2 transmits  $s_1^*$ , where  $(\cdot)^*$  indicates complex conjugate.

At the receiver end, the signals appearing at  $RX_j$  over these two-time intervals can be expressed as follows: [113]

$$r_{1j} = h_{1j}s_1 + h_{2j}s_2 + N_{1j} \quad (5.1a)$$

$$r_{2j} = -h_{1j}s_2^* + h_{2j}s_1^* + N_{2j} \quad (5.1b)$$

where,  $h_{ij}$ ;  $i \in \{1, 2\}, j \in \{1, 2, \dots, N_r\}$ , is the channel gain between TX $i$  and RX $j$ . Each copy of the signal is affected by zero-mean Gaussian noise,  $N_{ij}$ , with variance  $N_0$ , the noise being assumed to be statistically independent. The received signals are processed by a bank of  $N_r$  space-time (ST) combiners attached to each RX antenna branch. Basically, the ST combiners act as Alamouti decoders. The ST combiner attached to RX $j$  produces an output pair

$$y_{1j} = \hat{h}_{1j}^* r_{1j} + \hat{h}_{2j} r_{2j}^* \quad (5.2a)$$

$$y_{2j} = -\hat{h}_{2j} r_{2j}^* + \hat{h}_{1j}^* r_{1j} \quad (5.2b)$$

where,  $\hat{h}_{ij}$  is an estimate values of  $h_{ij}$ . Next, the output of the ST combiner is fed to the SEC. The channel estimators help ST combiners in decoding, and the SE combiner chooses one of the decoded outputs. In SEC a random branch (say,  $j$ ) is chosen for retrieving the message, and the branch is retained unless the average branch SNR falls below a threshold value  $\gamma_{th}$ , required to maintain link reliability. If  $\gamma_j < \gamma_{th}$ , the combiner switches to the next available branch for examining its quality. This process continues until a path is found within a tolerable condition or all available diversity paths are examined.

### 5.3.1 Gamma-Gamma turbulence in absence of pointing error

To derive the expression of BER of the system in the absence of pointing error, may use the following equation

$$BER = \frac{1}{\pi} \int_0^{\frac{\pi}{2}} \mathcal{M}_{\gamma Ala/SEC} \left( -\frac{1}{2 \sin^2 \theta} \right) d\theta \quad (5.3)$$

where,  $\mathcal{M}_{\gamma Ala/SEC}(\cdot)$  is expressed using (3.7) and (3.4) as

$$\mathcal{M}_{\gamma Ala/SEC}(s) = [F_{\gamma}(\gamma_{th})]^{N_r-1} \mathcal{M}_{\gamma Ala}(s) + \sum_{j=0}^{N_r-2} [F_{\gamma}(\gamma_{th})]^j \tilde{\Psi}(s) \quad (5.4)$$

where,  $\mathcal{M}_{\gamma Ala}(s)$  is the resultant MGF of the diversity branches, and  $\tilde{\Psi}(s) = \Psi(s) \times \Psi(s)$ , with,  $\Psi(s) = \int_{\gamma_{th}}^{\infty} \exp(s\gamma) F_{\gamma}(\gamma) d\gamma$ ,  $F_{\gamma}(\gamma)$  being the PDF of the individual diversity branch. For GG fading without pointing error environment the  $\mathcal{M}_{\gamma Ala}(s)$  has been already defined in (3.1), and the analytical closed-form of the other factor ( $\Psi(s)$ ) has been derived in (4.10).

### 5.3.2 Gamma-Gamma turbulence in presence of pointing error

In presence of pointing error  $\mathcal{M}_{\gamma Ala/SEC}^p(s)$  can be expressed, based on (5.4), as

$$\mathcal{M}_{\gamma Ala/SEC}^p(s) = [F_{\gamma}(\gamma_{th})]^{N_r-1} \mathcal{M}_{\gamma Ala}^p(s) + \sum_{j=0}^{N_r-2} [F_{\gamma}(\gamma_{th})]^j \tilde{\Psi}^p(s) \quad (5.5)$$

The resultant MGF  $\mathcal{M}_{\gamma Ala}^p(s)$  has been derived in (3.8), and  $\tilde{\Psi}^p(s) = \Psi^p(s) \times \Psi^p(s)$ , the closed-form expression of the other factor  $\Psi^p(s)$  has been derived in (4.22).

### 5.3.3 Málaga turbulence in absence of pointing error

In the absence of pointing error, we derive the BER of the system using the following equation as

$$\mathcal{M}_{\gamma_{Ala}/SEC}(s) = [F_{\gamma}(\gamma_{th})]^{N_r-1} \mathcal{M}_{\gamma_{Ala}}(s) + \sum_{j=0}^{N_r-2} [F_{\gamma}(\gamma_{th})]^j \tilde{\Psi}_M(s) \quad (5.6)$$

where,  $\mathcal{M}_{\gamma_{Ala}}(s)$  is the resultant MGF of the diversity branches,  $\tilde{\Psi}_M(s) = \Psi_M(s) \times \Psi_M(s)$ , and,  $\Psi_M(s) = \int_{\gamma_{th}}^{\infty} \exp(s\gamma) F_{\gamma}(\gamma) d\gamma$ , and,  $F_{\gamma}(\gamma)$  being the PDF of the individual diversity branch. Under Málaga fading without pointing error, the  $\mathcal{M}_{\gamma_{Ala}}(s)$  is already defined in (3.10). Next, to calculate the analytical closed-form of the other factor ( $\Psi_M(s)$ ), with the help of (2.26) and the mathematical definition of  $\Psi_M(s)$ , we may get

$$\Psi_M(s) = \frac{\mathcal{A}}{4} \sum_{k_t=1}^{\beta_t} \frac{a_k}{(\bar{\gamma})^{\frac{\alpha_t+k_t}{4}}} \int_{\gamma_{th}}^{\infty} \exp(s\gamma) (\gamma)^{\left(\frac{\alpha_t+k_t}{4}\right)-1} G_{0\ 2}^{2\ 0} \left[ \frac{\mathcal{B}^2 \alpha_t \beta_t}{4} \sqrt{\frac{\gamma}{\bar{\gamma}}} \middle| \begin{matrix} - \\ \frac{\alpha_t-k_t}{2}, \frac{k_t-\alpha_t}{2} \end{matrix} \right] d\gamma \quad (5.7)$$

. With the help of [95, Eq.(1.211.1)], the above equation can be written as

$$\Psi_M(s) = \frac{\mathcal{A}}{4} \sum_{k_t=1}^{\beta_t} \frac{a_k}{(\bar{\gamma})^{\frac{\alpha_t+k_t}{4}}} \sum_{k=0}^{\infty} \frac{s^k}{k!} \int_{\gamma_{th}}^{\infty} (\gamma)^{k+\left(\frac{\alpha_t+k_t}{4}\right)-1} G_{0\ 2}^{2\ 0} \left[ \frac{\mathcal{B}^2 \alpha_t \beta_t}{4} \sqrt{\frac{\gamma}{\bar{\gamma}}} \middle| \begin{matrix} - \\ \frac{\alpha_t-k_t}{2}, \frac{k_t-\alpha_t}{2} \end{matrix} \right] d\gamma \quad (5.8)$$

and further, utilizing [115, eq. (07.34.21.0085.01)], (4.9) can be written as follows

$$\Psi_M(s) = \frac{\mathcal{A}}{4} \sum_{k_t=1}^{\beta_t} \frac{a_k}{(\bar{\gamma})^{\frac{\alpha_t+k_t}{4}}} \sum_{k=0}^{\infty} \frac{s^k}{k!} \frac{1}{(\gamma_{th})^{1-k-\left(\frac{\alpha_t+k_t}{4}\right)}} G_{1\ 5}^{5\ 0} \left[ \frac{(\mathcal{B}^2 \alpha_t \beta_t)^2 \gamma_{th}}{64 \bar{\gamma}} \middle| \begin{matrix} 1-k-\left(\frac{\alpha_t+k_t}{4}\right) \\ 1-k-\left(\frac{\alpha_t+k_t}{4}\right), p \end{matrix} \right] \quad (5.9)$$

where,  $p \in \left\{ \frac{(\alpha_t-k_t)}{4}, \frac{(\alpha_t-k_t+2)}{4}, \frac{(k_t-\alpha_t)}{4}, \frac{(k_t-\alpha_t+2)}{4} \right\}$

### 5.3.4 Málaga turbulence in presence of pointing error

In presence of pointing error,  $\mathcal{M}_{\gamma_{Ala}/SEC}(s)$  can be represented as

$$\mathcal{M}_{\gamma_{Ala}/SEC}(s) = [F_{\gamma}(\gamma_{th})]^{N_r-1} \mathcal{M}_{\gamma_{Ala}}^p(s) + \sum_{j=0}^{N_r-2} [F_{\gamma}(\gamma_{th})]^j \tilde{\Psi}_M^p(s) \quad (5.10)$$

where,  $\mathcal{M}_{\gamma_{Ala}}^p(s)$  is defined in (3.12), and  $\tilde{\Psi}_M^p(s) = \Psi_M^p(s) \times \Psi_M^p(s)$ . Next,  $\Psi_M^p(s)$  can be further derived using (2.44) and (5.8) and finally expressed as

$$\Psi^p(s) = \frac{\xi^2 \mathcal{A}}{4} \sum_{k_t=1}^{\beta_t} b_k \sum_{k=0}^{\infty} \frac{s^k}{k!} (\gamma_{th})^k G_{3 \ 7}^{7 \ 0} \left[ \frac{(\mathcal{B})^2 \gamma_{th}}{16 \bar{\gamma}} \left| \begin{array}{c} \frac{\xi^2+1}{2}, \frac{\xi^2+2}{2}, 1-k \\ -k, \frac{\xi^2}{2}, \frac{\xi^2+1}{2}, \frac{\alpha_t}{2}, \frac{\alpha_t+1}{2}, \frac{k_t}{2}, \frac{k_t+1}{2} \end{array} \right. \right] \quad (5.11)$$

## 5.4 Numerical results and discussion for MIMO FSO link

In this section, we have explained the numerical results of the MIMO FSO link for the ABER under different AT conditions. Table 5.1 summarized the equation used for Fig. 5.2 to Fig. 5.5.

The ABER of  $2 \times 4$  MIMO FSO communication system under GG statistical distribution without pointing error is shown in Fig. 5.2 (a). Here, the system uses fixed switching threshold of 10 dB against each average SNR. In this figure, three sets of atmospheric turbulence parameters are considered in order to characterize the severity of the turbulence. Accordingly, the chosen value of the AT parameters are  $\alpha_t = 4.20$  and  $\beta_t = 2.72$  to model weak turbulence,  $\alpha_t = 3.99$  and  $\beta_t = 1.65$  for moderate and  $\alpha_t = 2.20$  and  $\beta_t = 0.65$  for strong turbulence. This figure shows that the decay lines bend after a certain dB of average SNR. This unusual pattern can be eliminated by using an optimal switching threshold.



TABLE 5.1: Summary of the equations used for figures, Fig. 5.2 to Fig. 5.5.

Figure	Scenario	Equation
Fig. 5.2a	GG	Eq. 5.3 with Eq. 5.4 and Eq. 4.10
Fig. 5.2b	GG	Eq. 5.3 with Eq. 5.4 and Eq. 4.10
Fig. 5.2c	GG	Eq. 5.3 with Eq. 5.4 and Eq. 4.10
Fig. 5.2d	GG	Eq. 5.3 with Eq. 5.4 and Eq. 4.10
Fig. 5.3a	GG + pointing	Eq. 5.3 with Eq. 5.5 and Eq. 4.22
Fig. 5.3b	GG + pointing	Eq. 5.3 with Eq. 5.5 and Eq. 4.22
Fig. 5.3c	GG + pointing	Eq. 5.3 with Eq. 5.5 and Eq. 4.22
Fig. 5.3d	GG + pointing	Eq. 5.3 with Eq. 5.5 and Eq. 4.22
Fig. 5.4a	Málaga	Eq. 5.3 with Eq. 5.6 and Eq. 5.9
Fig. 5.4b	Málaga	Eq. 5.3 with Eq. 5.6 and Eq. 5.9
Fig. 5.4c	Málaga	Eq. 5.3 with Eq. 5.6 and Eq. 5.9
Fig. 5.4d	Málaga	Eq. 5.3 with Eq. 5.6 and Eq. 5.9
Fig. 5.5a	Málaga + pointing	Eq. 5.3 with Eq. 5.10 and Eq. 5.11
Fig. 5.5b	Málaga + pointing	Eq. 5.3 with Eq. 5.10 and Eq. 5.11
Fig. 5.5c	Málaga + pointing	Eq. 5.3 with Eq. 5.10 and Eq. 5.11
Fig. 5.5d	Málaga + pointing	Eq. 5.3 with Eq. 5.10 and Eq. 5.11

Fig. 5.2 (b) shows the ABER of the MIMO FSO link when the system works with optimal switching threshold [Table 5.2] instead of a fixed switching threshold. This figure shows a significant change, where no unusual pattern is present for the higher SNR region. Also, Fig. 5.2 (a) and Fig. 5.2 (b) show that the ABER has been getting better for weak turbulence than strong and moderate turbulence.

Next, Fig. 5.2 (c) and Fig. 5.2 (d) depicts the ABER of  $2 \times N_r$  MIMO FSO system under fixed switching threshold and optimal switching threshold respectively.

TABLE 5.2: Optimum switching threshold of  $2 \times N_r$  SIMO FSO system in the absence of pointing error with  $N_r = 2, 3, 4, 5$  and  $6$  for different average SNR with turbulence parameter  $\alpha_t = 2.20$  and  $\beta_t = 0.65$  .

Avg. SNR (dB)	Optimum switching threshold ( $\gamma_0$ )				
	$N_r = 2$	$N_r = 3$	$N_r = 4$	$N_r = 5$	$N_r = 6$
0	0.39	0.61	0.82	1.01	1.21
3	0.55	0.85	1.14	1.42	1.68
6	0.74	1.14	1.53	1.91	2.27
9	0.96	1.49	2.00	2.49	2.97
12	1.21	1.88	2.53	3.17	3.79
15	1.48	2.32	3.14	3.94	4.72
18	1.78	2.80	3.81	4.81	5.78
21	2.09	3.32	4.55	5.76	6.94
24	2.42	3.88	5.35	6.80	8.22
27	2.77	4.47	6.20	7.91	9.60
30	3.12	5.10	4.10	9.10	11.07
33	3.49	5.74	8.05	10.15	12.64
36	3.86	6.42	8.91	11.40	14.26
39	4.23	7.11	10.15	12.64	15.96
42	4.62	7.67	11.40	14.43	17.71
45	5.01	8.55	12.64	15.87	20.09
48	5.40	9.29	13.32	17.35	21.36
51	5.81	10.15	14.44	20.09	23.24
54	6.12	10.81	15.12	20.09	30.02
57	6.59	11.40	16.75	21.94	30.02
60	6.99	12.64	17.93	23.51	30.02

TABLE 5.3: Optimum switching threshold of  $2 \times 4$  MIMO FSO system in the absence of pointing error with different average SNR for different turbulence parameter  $(\alpha_t, \beta_t)$ .

Avg. SNR (dB)	Optimum switching threshold ( $\gamma_0$ )		
	$\alpha_t = 4.20, \beta_t = 2.72$	$\alpha_t = 3.99, \beta_t = 1.65$	$\alpha_t = 2.20, \beta_t = 0.65$
0	1.16	1.09	0.82
3	1.82	1.66	1.14
6	2.73	2.40	1.53
9	3.91	3.33	2.00
12	5.39	4.46	2.53
15	7.19	5.81	3.14
18	9.33	7.36	3.81
21	11.81	9.12	4.55
24	15.12	11.07	5.35
27	17.74	12.64	6.20
30	20.09	15.12	7.10
33	24.84	17.96	8.05
36	30.02	20.09	8.91
39	32.88	23.22	10.15
42	39.95	30.02	11.40
45	39.95	30.02	12.64
48	46.27	30.02	13.32
51	51.00	39.95	14.44
54	55.83	39.95	15.12
57	60.74	39.95	16.75
60	65.71	43.85	17.93

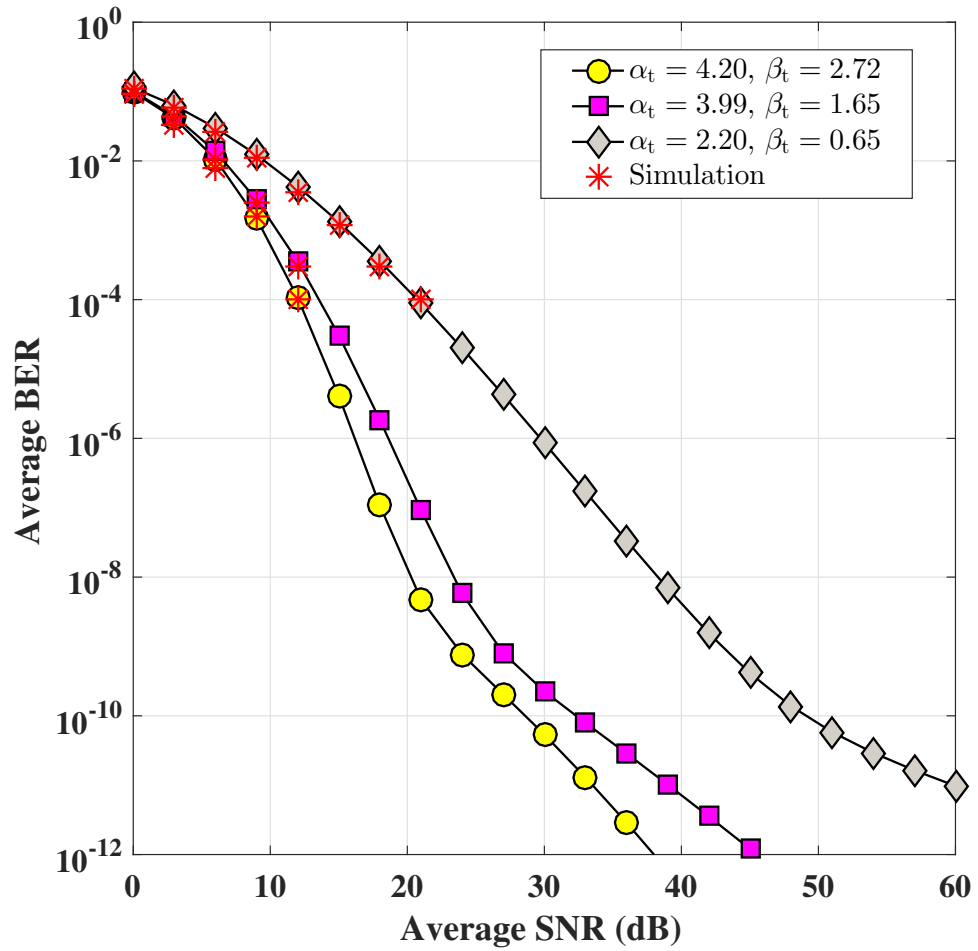
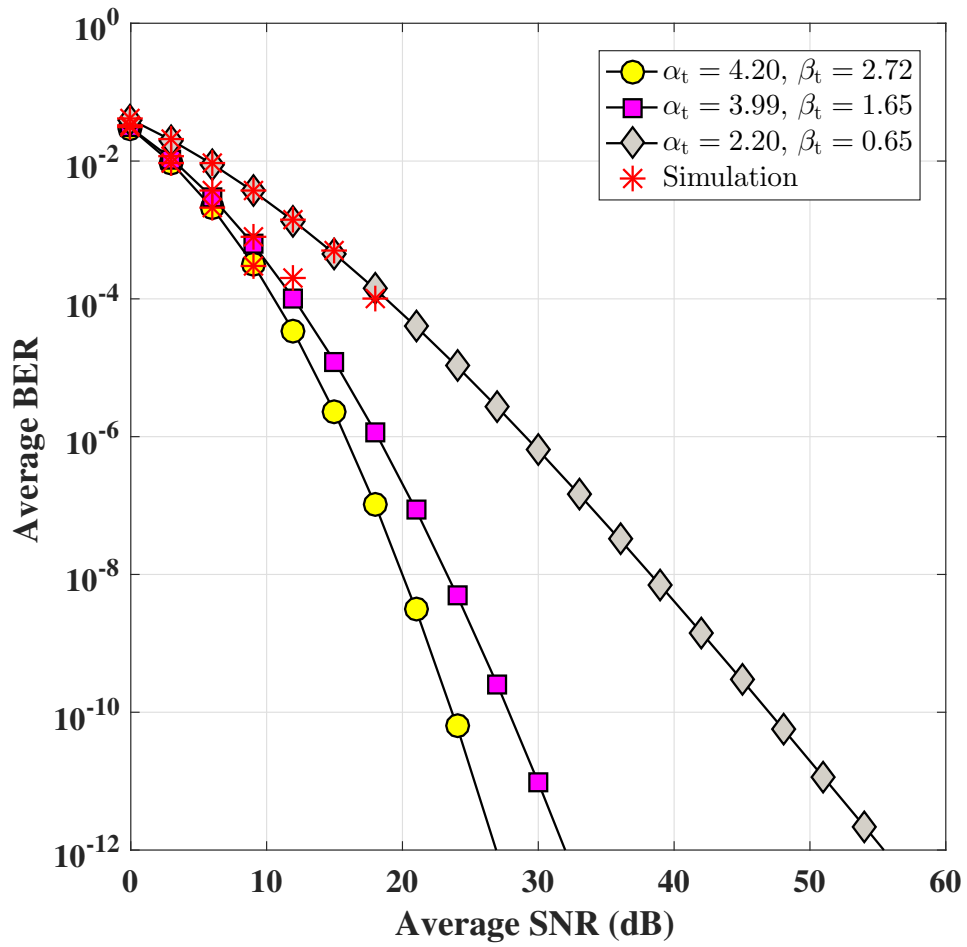


Figure 5.2 (a) Average bit error rate of  $2 \times 4$  MIMO FSO system under Gamma-Gamma distribution in the absence of pointing error for different atmospheric turbulence with fixed switching threshold of 10 dB



**Figure 5.2 (b)** Average bit error rate of  $2 \times 4$  MIMO FSO system under Gamma-Gamma distribution in the absence of pointing error for different atmospheric turbulence with optimal switching threshold.

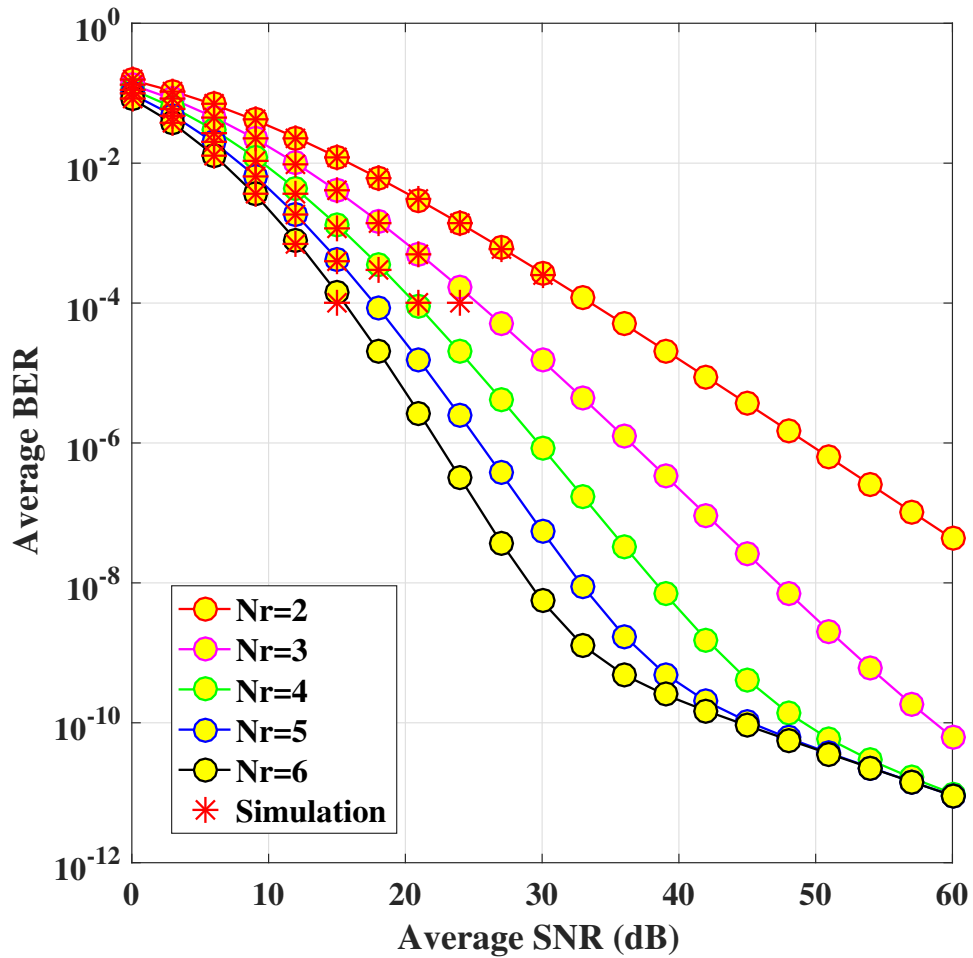


Figure 5.2 (c) Average bit error rate of  $2 \times N_r$  MIMO FSO system under Gamma-Gamma distribution in the absence of pointing error for  $\alpha_t = 2.20$  and  $\beta_t = 0.65$  with fixed switching threshold of 10 dB.

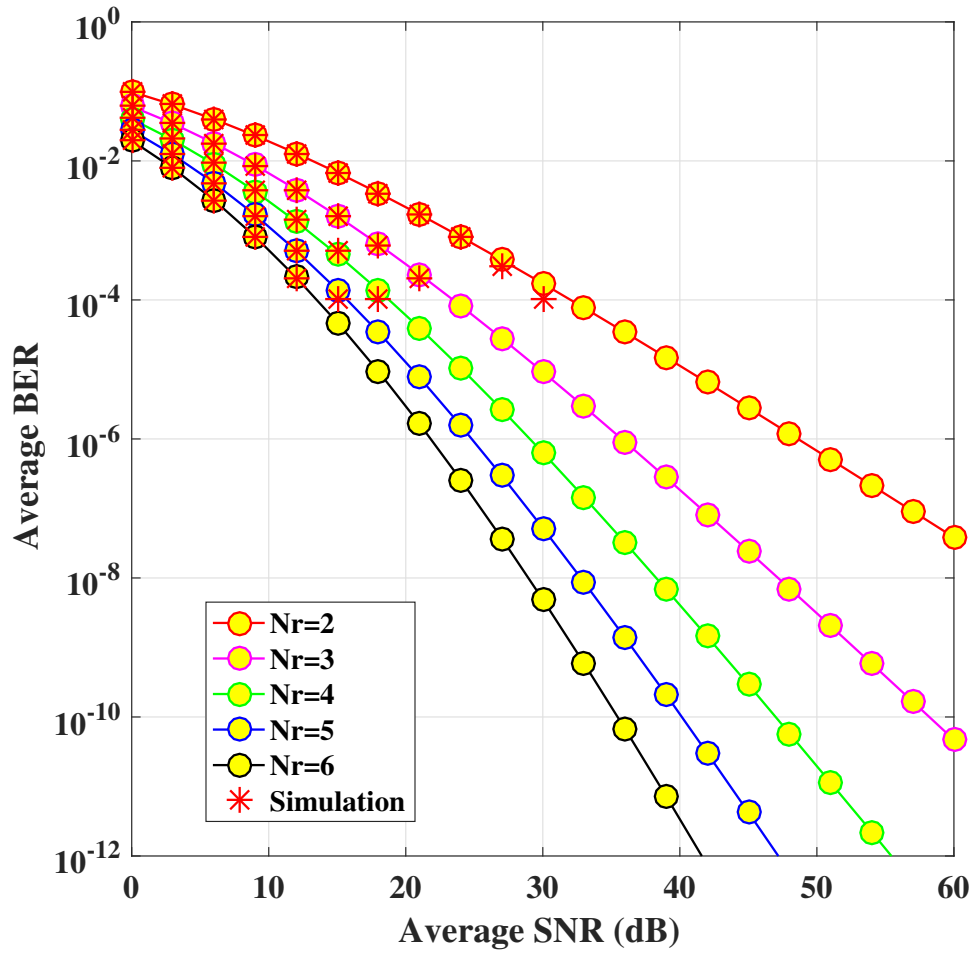


Figure 5.2 (d) Average bit error rate of  $2 \times N_r$  MIMO FSO system under Gamma-Gamma distribution in the absence of pointing error for  $\alpha_t = 2.20$  and  $\beta_t = 0.65$  with optimal switching threshold.

FIGURE 5.2: Average bit error rate of the MIMO FSO link employing Alamouti STBC at the transmitter end and switch and examine combining scheme at the receiver end, with Gamma-Gamma distribution using different atmospheric turbulence conditions in the absence of pointing error.

In Fig. 5.2 (c), decay lines for  $N_r = 4, 5$  and 6 merge for an average SNR large than 50 dB, implying no further improvement with the increase of branch diversity. Such phenomenon can be eliminated using the optimal switching threshold provided in Table 5.6 rather than a fixed switching threshold. Fig. 5.2 (d) also indicates drastic improvement in ABER with a higher order of receiver diversity, especially in the range of higher average SNR.

To examine the impact of misalignment fading into the propagation channel, the above investigations are repeated in the presence of pointing error ( $\xi = 0.5607$ ), and the results are presented in Fig. 5.3 (c) and Fig. 5.3 (d). Figures support more-or-less similar findings as above, where the optimal switching threshold against each average SNR point is provided in Table 5.6. Comparison of Fig. 5.2 (d) and Fig. 5.3 (d) reveals that the misalignment fading into the system makes an arduous propagation link yielding low-quality outcomes. Furthermore, a comparison of ABER for propagation link of different configurations, under fixed and optimum switching threshold conditions, leads to the conclusion that the quality indices of a MIMO FSO system are much better than those for SIMO FSO, MISO FSO and SISO FSO communication systems. Tabulated comparisons of the ABER under the STBC-SEC-added MIMO FSO link and the STBC-added SIMO FSO link are presented in Table 5.10 and Table 5.11 with strong AT modeled under Málaga statistical distribution without and with pointing error. The result sheet of this table also indicates that a MIMO FSO link performs better than all of the other configurations of FSO link under any weather condition in the absence and presence of pointing error.

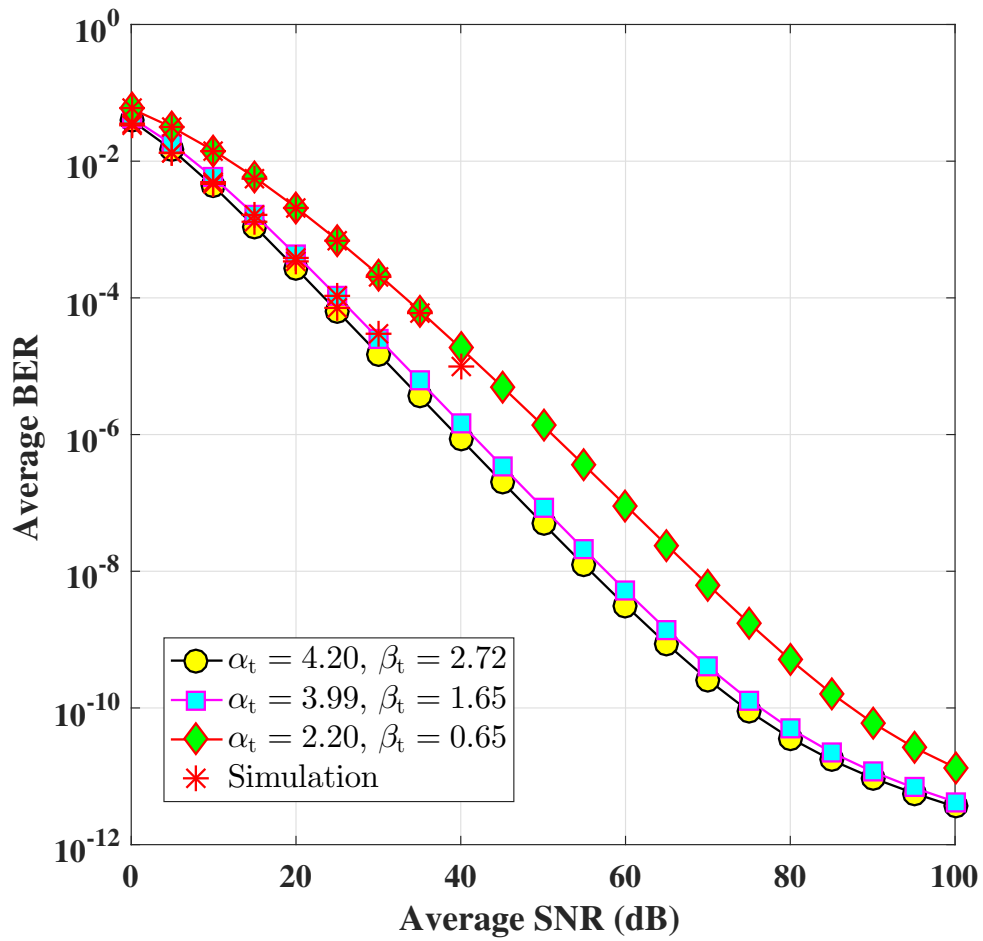


TABLE 5.4: Optimum switching threshold of  $2 \times N_r$  MIMO FSO system in the presence of pointing error ( $\xi = 0.5607$ ) with  $N_r = 2, 3, 4, 5$  and 6 for different average SNR with turbulence parameter  $\alpha_t = 2.20$  and  $\beta_t = 0.65$ .

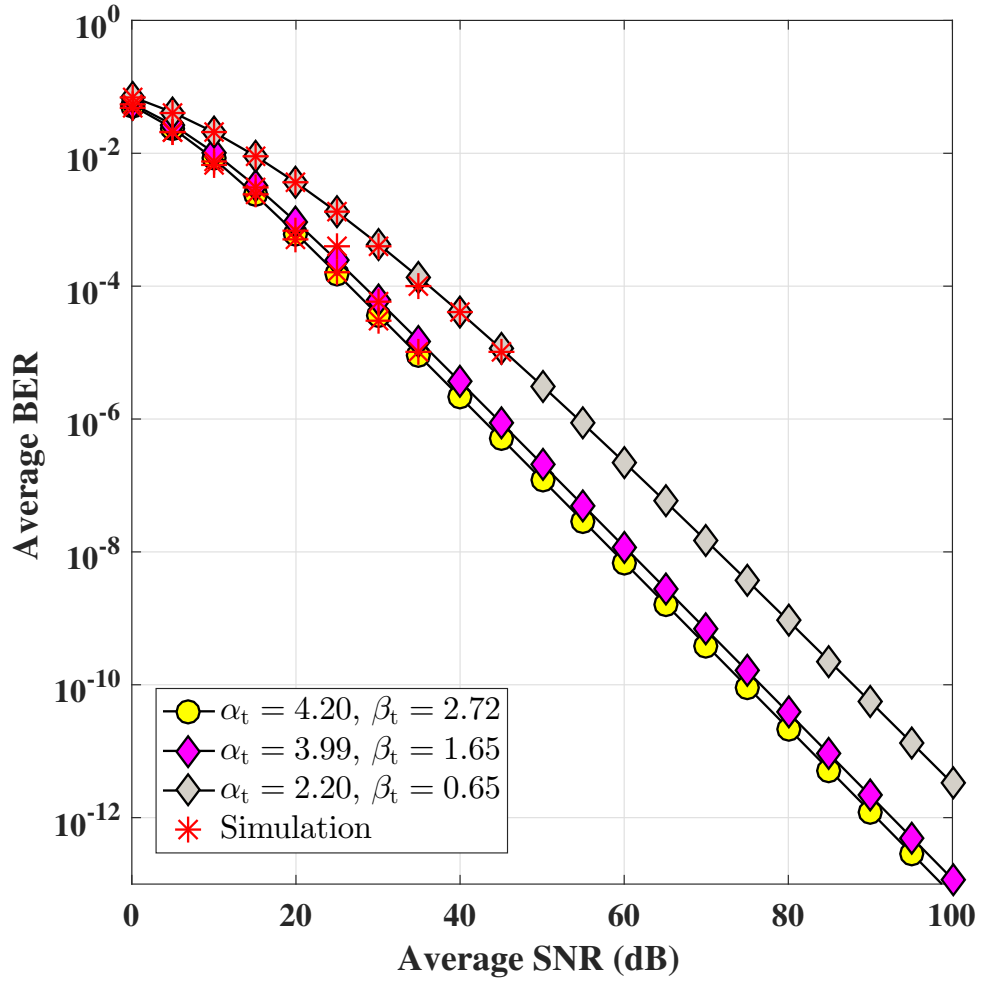
Avg. SNR (dB)	Optimum switching threshold ( $\gamma_0$ )				
	$N_r = 2$	$N_r = 3$	$N_r = 4$	$N_r = 5$	$N_r = 6$
0	21.83	21.83	21.83	21.83	21.83
5	22.33	22.33	22.33	22.33	22.33
10	22.88	22.88	22.88	22.88	22.88
15	23.46	23.46	23.46	23.46	23.46
20	24.07	24.07	24.07	24.07	24.07
25	24.69	24.69	24.69	24.69	24.69
30	25.33	25.33	25.33	25.33	25.33
35	25.97	25.97	25.97	25.97	25.97
40	26.61	26.61	26.61	26.61	26.61
45	27.25	27.25	27.25	27.25	27.25
50	27.87	27.87	27.87	27.87	27.87
55	28.48	28.48	28.48	28.48	28.48
60	29.07	29.07	29.07	29.07	29.07
65	29.65	29.65	29.65	29.65	29.65
70	30.19	30.19	30.19	30.19	30.19
75	30.71	30.71	30.71	30.71	30.71
80	31.20	31.20	31.20	31.20	31.20
85	31.65	31.65	31.65	31.65	31.65
90	32.06	32.06	32.06	32.06	32.06
95	32.45	32.45	32.45	32.45	32.45
100	32.79	32.79	32.79	32.79	32.79

TABLE 5.5: Optimum switching threshold of  $2 \times 4$  MIMO FSO system in the presence of pointing error ( $\xi = 0.5607$ ) with different average SNR for different turbulence parameter.

Avg. SNR (dB)	Optimum switching threshold ( $\gamma_0$ )		
	$\alpha_t = 4.20, \beta_t = 2.72$	$\alpha_t = 3.99, \beta_t = 1.65$	$\alpha_t = 2.20, \beta_t = 0.65$
0	22.18	22.03	21.83
5	22.96	22.74	22.33
10	23.68	23.46	22.88
15	24.36	24.15	23.46
20	25.01	24.82	24.07
25	25.64	25.46	24.69
30	26.23	26.08	25.33
35	26.80	26.66	25.97
40	27.34	27.22	26.61
45	27.84	27.75	27.25
50	28.31	28.24	27.87
55	28.74	28.70	28.48
60	29.13	29.12	29.07
65	29.48	29.50	29.65
70	29.80	29.85	30.19
75	30.08	30.15	30.71
80	30.33	30.43	31.20
85	30.55	30.67	31.65
90	30.74	30.87	32.06
95	30.90	31.06	32.45
100	31.04	31.21	32.79



**Figure 5.3 (a)** Average bit error rate of  $2 \times 4$  MIMO FSO system under Gamma-Gamma distribution in the presence of pointing error ( $\xi = 0.5607$ ) for different atmospheric turbulence with fixed switching threshold of 10 dB.



**Figure 5.3 (b)** Average bit error rate of  $2 \times 4$  MIMO FSO system under Gamma-Gamma distribution in the presence of pointing error ( $\xi = 0.5607$ ) for different atmospheric turbulence with optimal switching threshold.

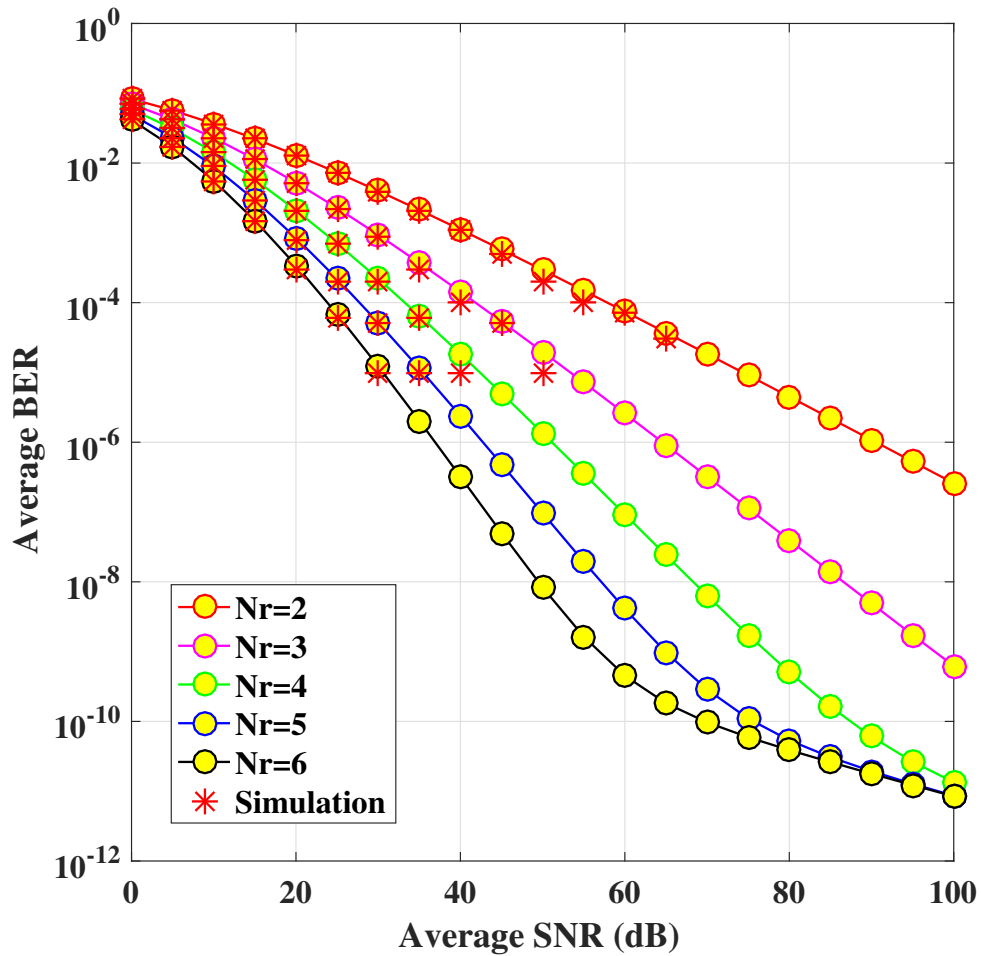


**Figure 5.3 (c)** Average bit error rate of  $2 \times N_r$  MIMO FSO system under Gamma-Gamma distribution in the presence of pointing error ( $\xi = 0.5607$ ) for  $\alpha_t = 2.20$  and  $\beta_t = 0.65$  with fixed switching threshold of 10 dB.

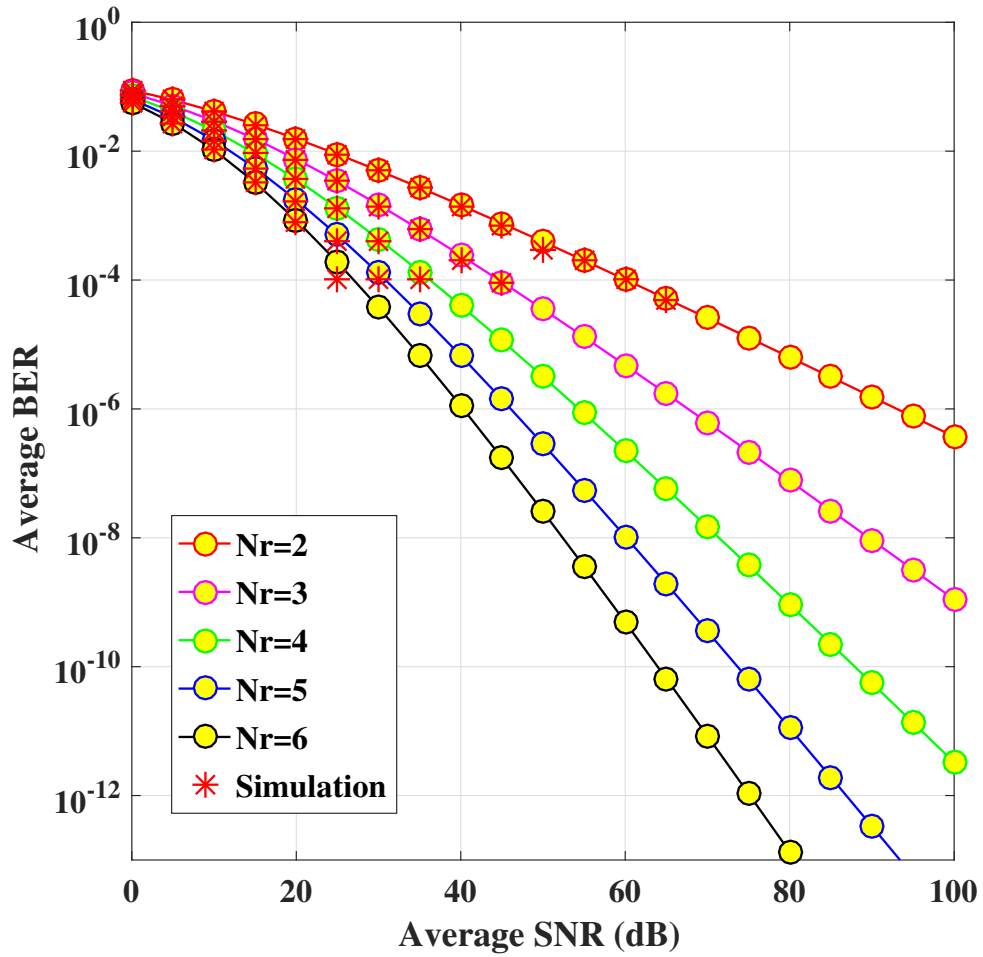


**Figure 5.3 (d)** Average bit error rate of  $2 \times N_r$  MIMO FSO system under Gamma-Gamma distribution in the presence of pointing error ( $\xi = 0.5607$ ) for  $\alpha_t = 2.20$  and  $\beta_t = 0.65$  with optimal switching threshold.

FIGURE 5.3: Average bit error rate of the MIMO FSO link employing Alamouti STBC at the transmitter end and switch and examine combining scheme at the receiver end with Gamma-Gamma distribution using different atmospheric turbulence condition in the presence of pointing error.

TABLE 5.6: Optimum switching threshold of  $2 \times N_r$  MIMO FSO system in the absence of pointing error with  $N_r = 2, 3, 4, 5$  and  $6$  for different average SNR with turbulence parameter  $\alpha_t = 2.29$  and  $\beta_t = 1$ .

Avg. SNR (dB)	Optimum switching threshold ( $\gamma_0$ )				
	$N_r = 2$	$N_r = 3$	$N_r = 4$	$N_r = 5$	$N_r = 6$
0	30.84	30.84	30.84	30.84	30.84
3	25.33	25.33	25.33	25.33	25.33
6	27.14	27.14	27.14	27.14	27.14
9	28.78	28.78	28.78	28.78	28.78
12	29.29	29.29	29.29	29.29	29.29
15	29.04	29.04	29.04	29.04	29.04
18	35.31	35.31	35.31	35.31	35.31
21	36.08	36.08	36.08	36.08	36.08
24	30.99	30.99	30.99	30.99	30.99
27	33.81	33.81	33.81	33.81	33.81
30	29.60	29.60	29.60	29.60	29.60
33	31.88	31.88	31.88	31.88	31.88
36	30.26	30.26	30.26	30.26	30.26
39	36.03	36.03	36.03	36.03	36.03
42	31.52	31.52	31.52	31.52	31.52
45	31.08	31.08	31.08	31.08	31.08
48	33.82	33.82	33.82	33.82	33.82
51	36.88	36.88	36.88	36.88	36.88
54	31.06	31.06	31.06	31.06	31.06
57	31.36	31.36	31.36	31.36	31.36
60	37.00	37.00	37.00	37.00	37.00

TABLE 5.7: Optimum switching threshold of  $2 \times 4$  MIMO FSO system in the absence of pointing error with different average SNR for different turbulence parameters.

Avg. SNR (dB)	Optimum switching threshold ( $\gamma_0$ )		
	$\alpha_t = 5.41, \beta_t = 3$	$\alpha_t = 2.29, \beta_t = 2$	$\alpha_t = 2.29, \beta_t = 1$
0	2.75	19.75	30.84
3	6.56	17.56	25.33
6	2.95	20.41	27.14
9	2.58	18.00	28.78
12	1.82	21.75	29.29
15	4.03	15.95	29.04
18	8.92	16.60	35.31
21	13.28	13.43	36.08
24	16.62	14.01	30.99
27	19.41	19.58	33.81
30	24.84	19.22	29.60
33	27.95	12.67	31.88
36	29.55	19.43	30.26
39	34.11	21.80	36.03
42	34.97	19.35	31.52
45	37.82	34.68	31.08
48	38.83	20.52	33.82
51	38.32	40.94	36.88
54	40.49	40.16	31.06
57	37.95	31.91	31.06
60	41.87	45.87	37.00



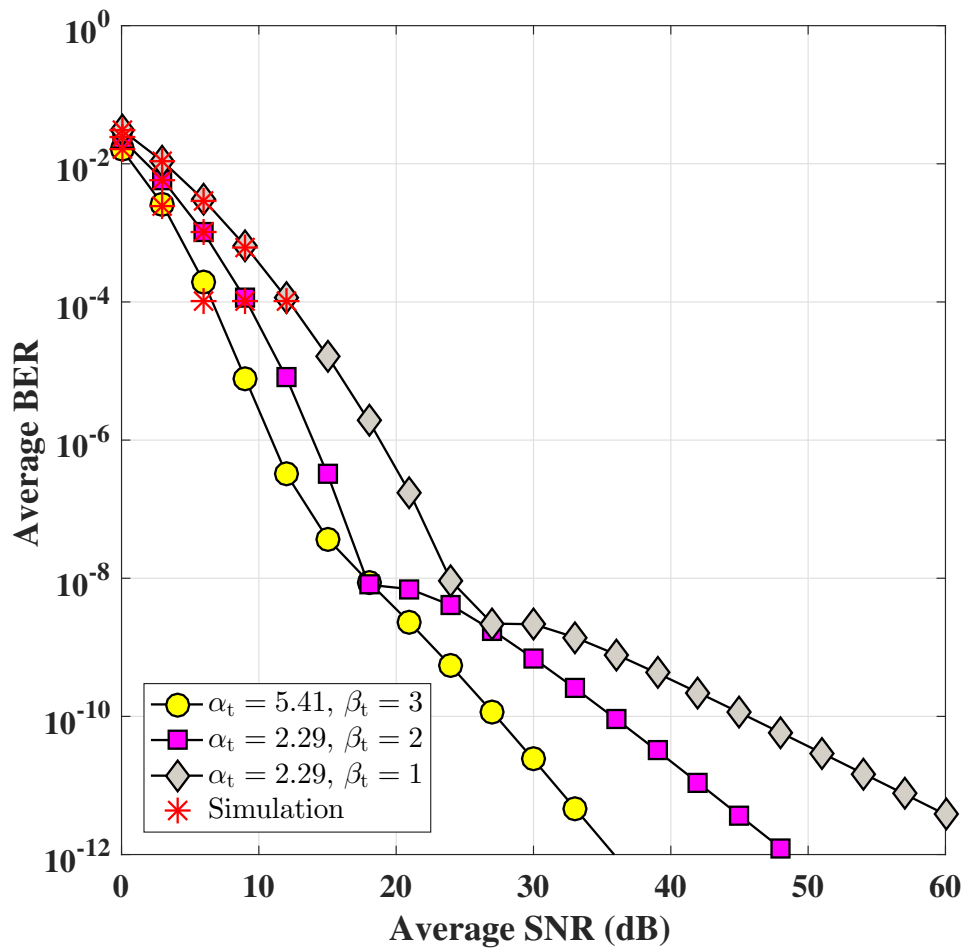


**Figure 5.4 (a)** Average bit error rate of  $2 \times 4$  MIMO FSO system under Málaga distribution in the absence of pointing error for different atmospheric turbulence with fixed switching threshold of 10 dB.

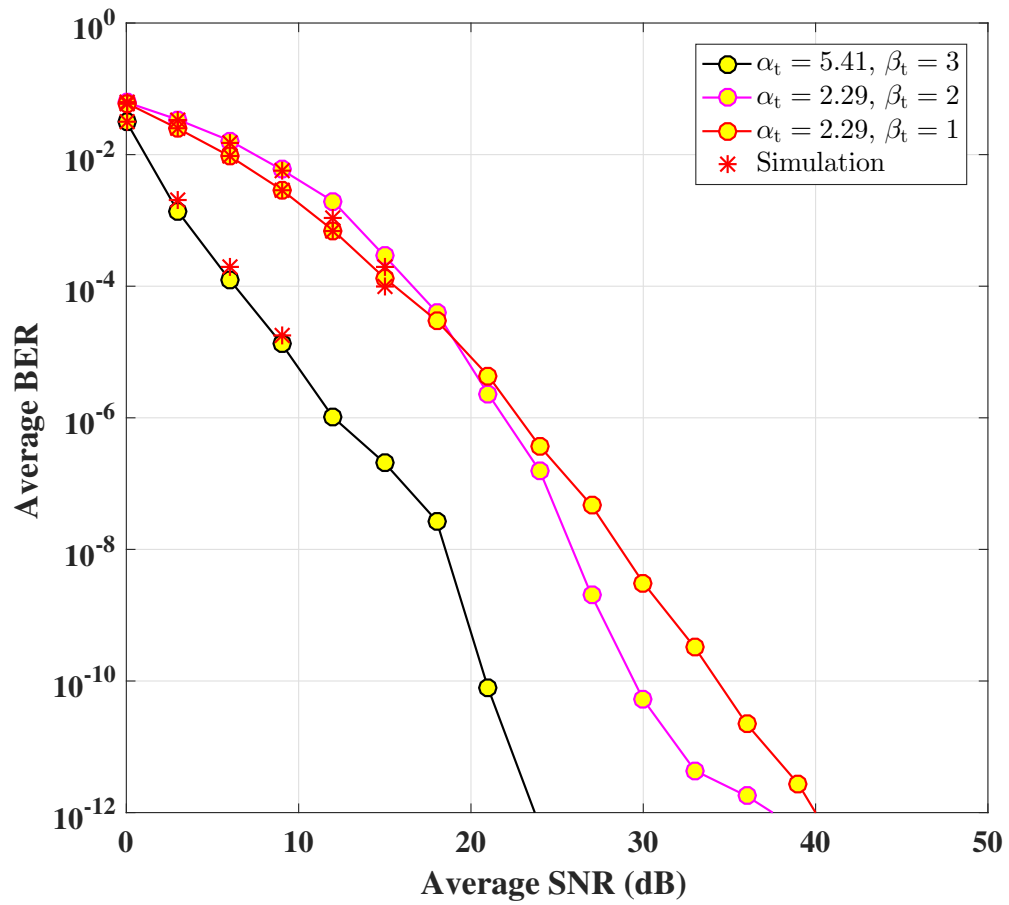


**Figure 5.4 (b)** Average bit error rate of  $2 \times 4$  MIMO FSO system under Málaga distribution in the absence of pointing error for different atmospheric turbulence with optimal switching threshold.

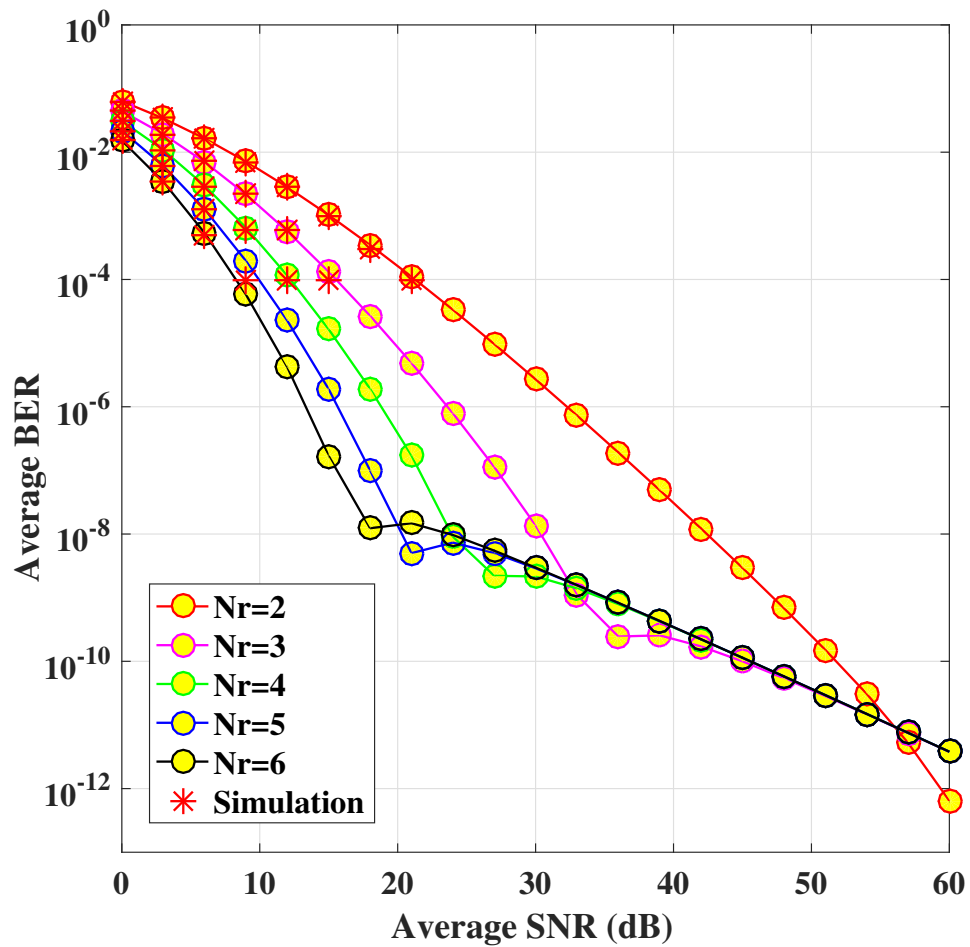
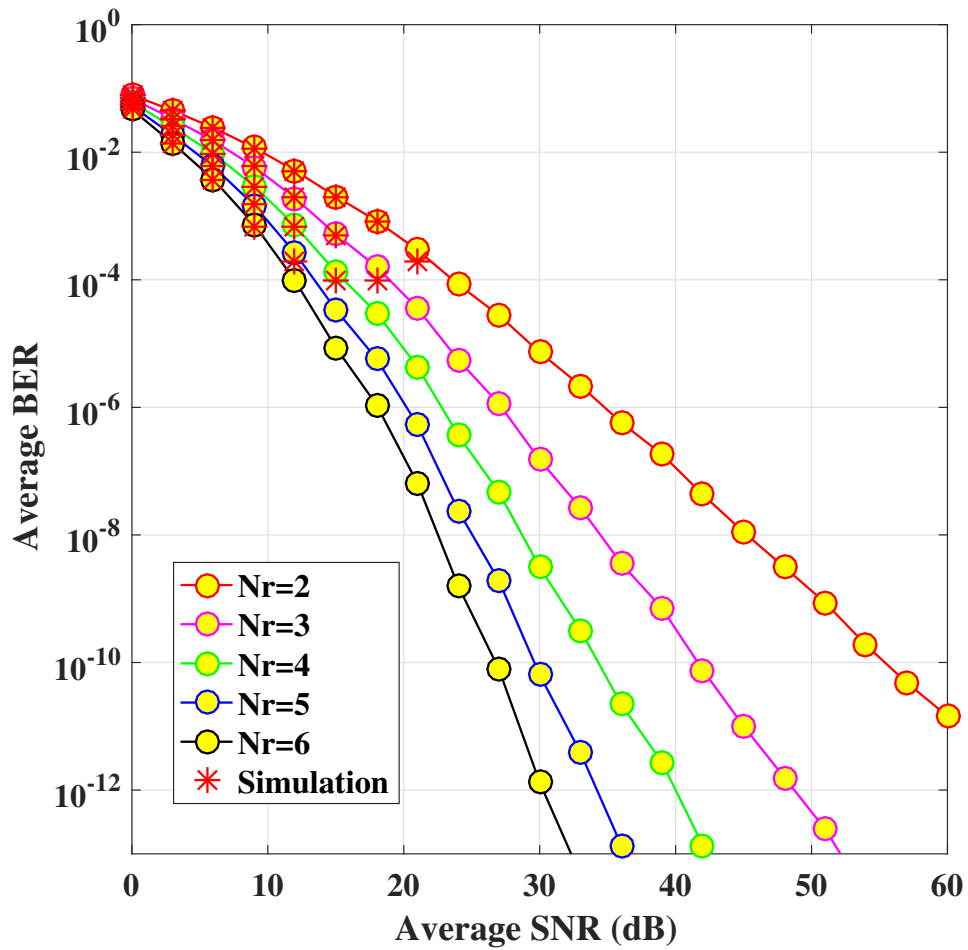


Figure 5.4 (c) Average bit error rate of  $2 \times N_r$  MIMO FSO system under Málaga distribution in the absence of pointing error for  $\alpha_t = 2.29$  and  $\beta_t = 1$  with fixed switching threshold of 10 dB.



**Figure 5.4 (d)** Average bit error rate of  $2 \times N_r$  MIMO FSO system under Málaga distribution in the absence of pointing error for  $\alpha_t = 2.29$  and  $\beta_t = 1$  with optimal switching threshold.

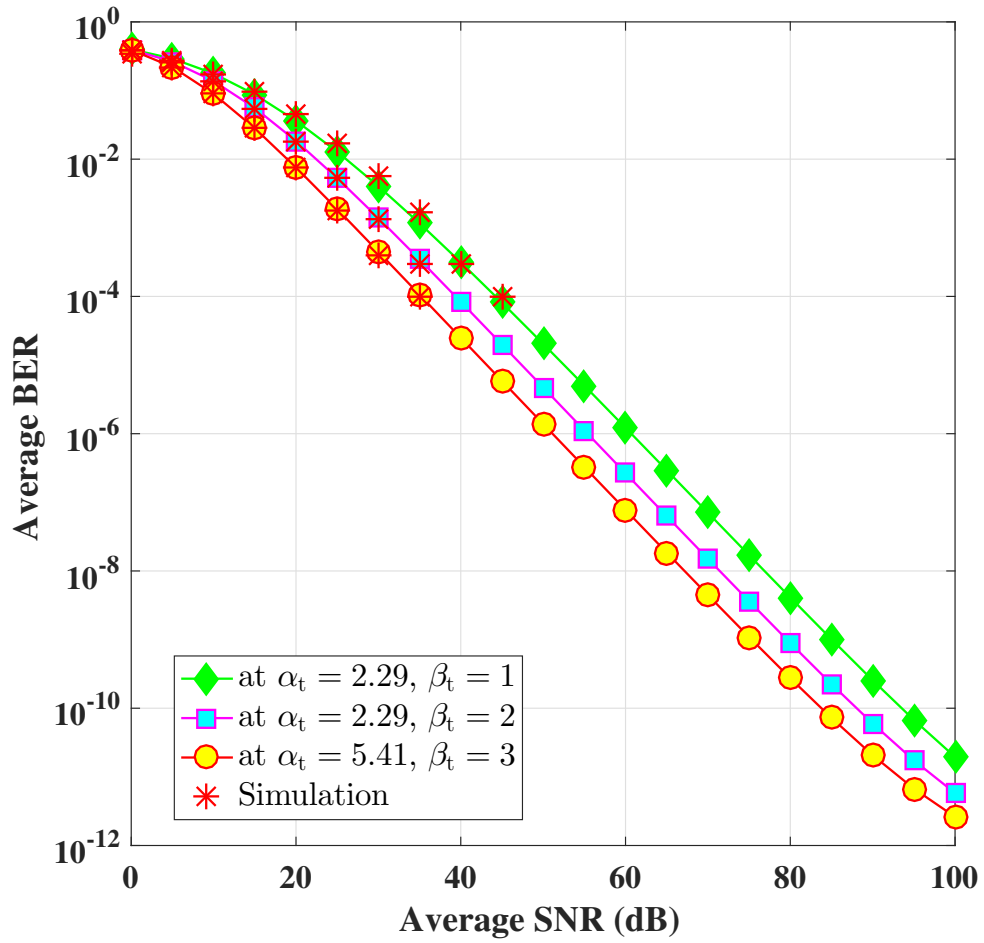
FIGURE 5.4: Average bit error rate of the MIMO FSO link employing Alamouti STBC at the transmitter end and switch and examine combining scheme at the receiver end with Málaga distribution using different atmospheric turbulence condition in the absence of pointing error.

TABLE 5.8: Optimum switching threshold of  $2 \times N_r$  MIMO FSO system in the presence of pointing error ( $\xi = 0.5607$ ) with  $N_r = 2, 3, 4, 5$  and 6 for different average SNR with turbulence parameter  $\alpha_t = 2.29$  and  $\beta_t = 1$ .

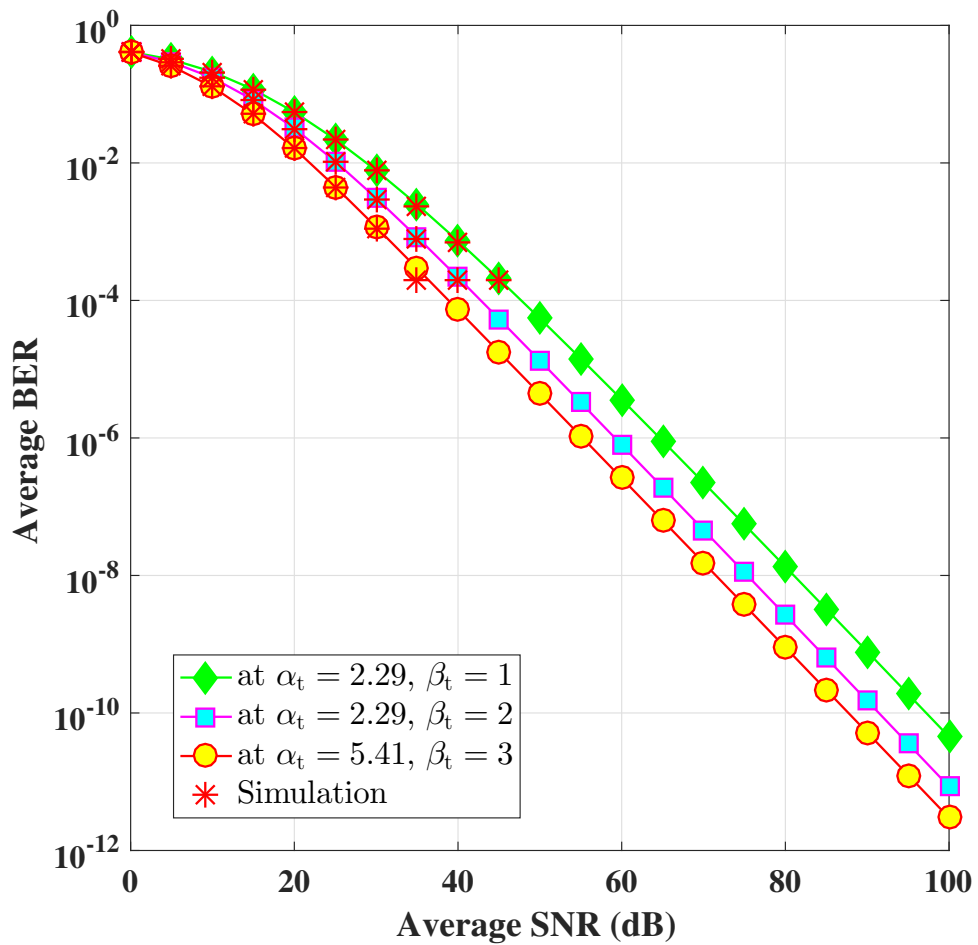
Avg. SNR (dB)	Optimum switching threshold ( $\gamma_0$ )				
	$N_r = 2$	$N_r = 3$	$N_r = 4$	$N_r = 5$	$N_r = 6$
0	18.14	18.14	18.14	18.14	18.14
5	18.87	18.87	18.87	18.87	18.87
10	19.84	19.84	19.84	19.84	19.84
15	21.00	21.00	21.00	21.00	21.00
20	22.26	22.26	22.26	22.26	22.26
25	23.60	23.60	23.60	23.60	23.60
30	24.97	24.97	24.97	24.97	24.97
35	26.35	26.35	26.35	26.35	26.35
40	27.73	27.73	27.73	27.73	27.73
45	29.09	29.09	29.09	29.09	29.09
50	30.43	30.43	30.43	30.43	30.43
55	31.73	31.73	31.73	31.73	31.73
60	33.00	33.00	33.00	33.00	33.00
65	34.21	34.21	34.21	34.21	34.21
70	35.37	35.37	35.37	35.37	35.37
75	36.47	36.47	36.47	36.47	36.47
80	37.50	37.50	37.50	37.50	37.50
85	38.45	38.45	38.45	38.45	38.45
90	39.33	39.33	39.33	39.33	39.33
95	40.12	40.12	40.12	40.12	40.12
100	40.84	40.84	40.84	40.84	40.84

TABLE 5.9: Optimum switching threshold of  $2 \times 4$  MIMO FSO system in the presence of pointing error ( $\xi = 0.5607$ ) with different average SNR for different turbulence parameter.

Avg. SNR (dB)	Optimum switching threshold ( $\gamma_0$ )		
	$\alpha_t = 5.41, \beta_t = 3$	$\alpha_t = 2.29, \beta_t = 2$	$\alpha_t = 2.29, \beta_t = 1$
0	18.46	17.89	18.14
5	20.03	18.83	18.87
10	21.83	20.08	19.84
15	23.52	21.46	21.00
20	25.09	22.88	22.26
25	26.61	24.26	23.60
30	28.12	25.60	24.97
35	29.61	26.88	26.35
40	31.08	28.11	27.73
45	32.53	29.28	29.09
50	33.96	30.39	30.43
55	35.36	31.43	31.73
60	36.73	32.39	33.00
65	38.07	33.28	34.21
70	39.36	34.09	35.37
75	40.61	34.81	36.47
80	41.80	35.46	37.50
85	42.93	36.03	38.45
90	44.00	36.53	39.33
95	44.99	36.96	40.12
100	45.91	37.34	40.84



**Figure 5.5 (a)** Average bit error rate of  $2 \times 4$  MIMO FSO system under Málaga distribution in the presence of pointing error ( $\xi = 0.5607$ ) for different atmospheric turbulence with fixed switching threshold of 10 dB.



**Figure 5.5 (b)** Average bit error rate of  $2 \times 4$  MIMO FSO system under Málaga distribution in the presence of pointing error ( $\xi = 0.5607$ ) for different atmospheric turbulence with optimal switching threshold.



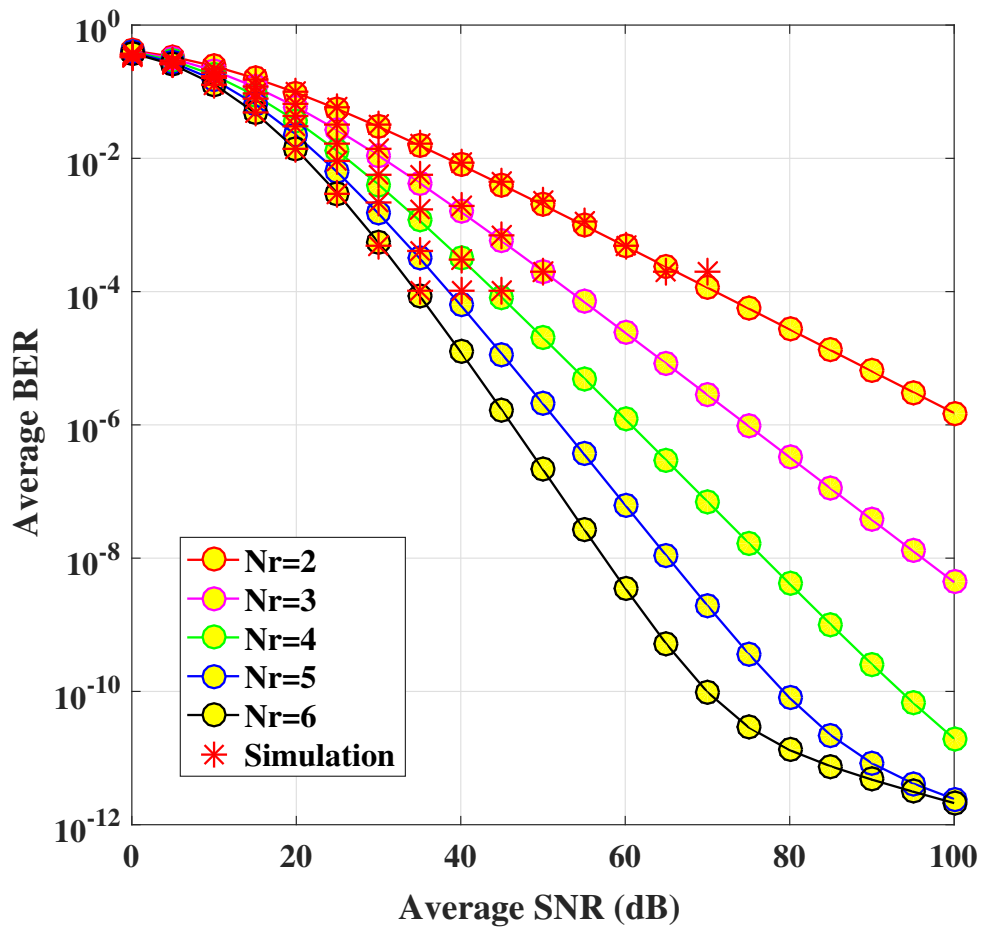


**Figure 5.5 (c)** Average bit error rate of  $2 \times N_r$  MIMO FSO system under Málaga distribution in the presence of pointing error ( $\xi = 0.5607$ ) for  $\alpha_t = 2.29$  and  $\beta_t = 1$  with fixed switching threshold of 10 dB.

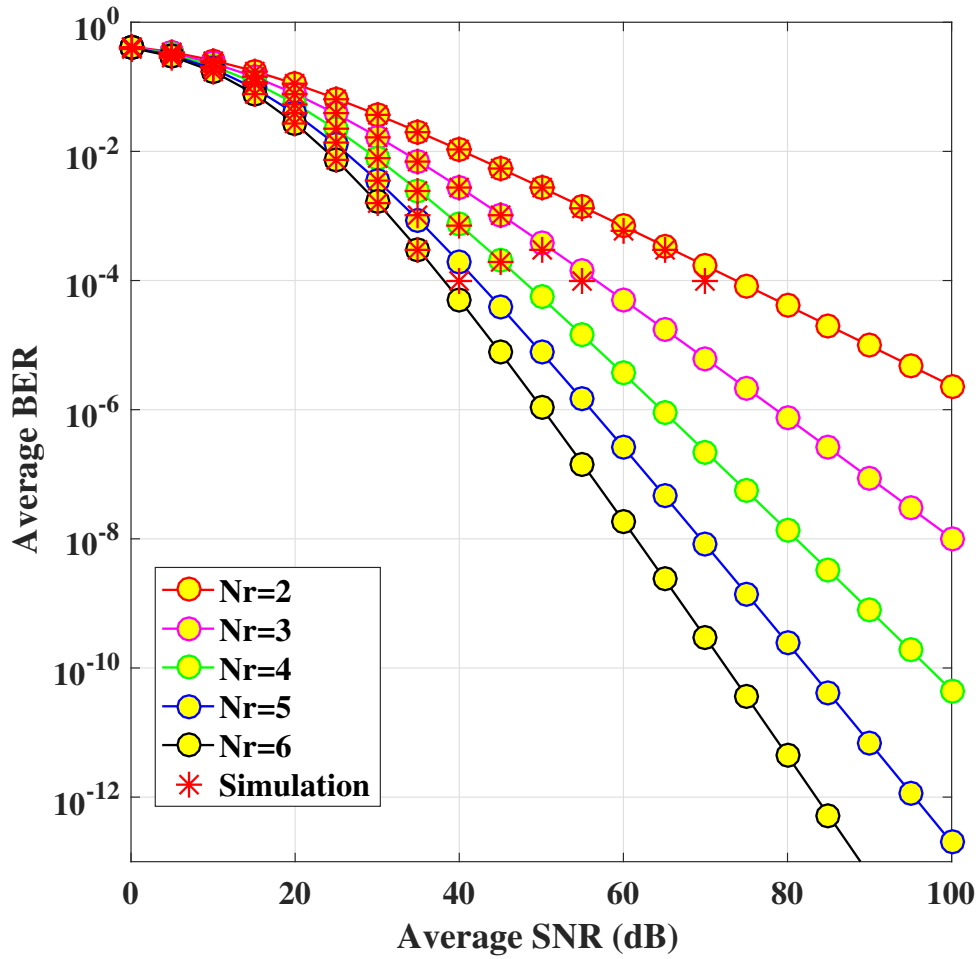


Figure 5.5 (d) Average bit error rate of  $2 \times N_r$  MIMO FSO system under Málaga distribution in the presence of pointing error ( $\xi = 0.5607$ ) for  $\alpha_t = 2.29$  and  $\beta_t = 1$  with optimal switching threshold.

FIGURE 5.5: Average bit error rate of the MIMO FSO link employing Alamouti STBC at the transmitter end and switch and examine combining scheme at the receiver end with Málaga distribution using different atmospheric turbulence condition in the presence of pointing error.

TABLE 5.10: Comparison of ABER for different FSO communication system under Málaga statistical distribution without pointing error for  $\alpha_t = 2.29$  and  $\beta_t = 1$ .

System topology	Avg.SNR	No th	Fixed th	Optimal th
SISO FSO	45 dB	$2.2 \times 10^{-3}$	-	
MISO FSO	45 dB	$1.2 \times 10^{-5}$	-	
SIMO FSO	45 dB	-	$4.2 \times 10^{-6}$	$5.6 \times 10^{-8}$
MIMO FSO	45 dB	-	$1.1 \times 10^{-10}$	$9.0 \times 10^{-15}$

TABLE 5.11: Comparison of ABER for different FSO communication system under Málaga statistical distribution with pointing error ( $\xi = 0.5607$ ) for turbulence parameters  $\alpha_t = 2.29$  and  $\beta_t = 1$ .

System topology	Avg.SNR	No th	Fixed th	Optimal th
SISO FSO	45 dB	$1.1 \times 10^{-1}$	-	-
MISO FSO	45 dB	$2.7 \times 10^{-2}$	-	-
SIMO FSO	45 dB	-	$6.2 \times 10^{-2}$	$9.0 \times 10^{-3}$
MIMO FSO	45 dB	-	$8.1 \times 10^{-5}$	$2.0 \times 10^{-5}$

## 5.5 Chapter summary

A MIMO FSO architectural setup has been developed in this chapter by introducing the transmitter and receiver diversity at the transceiver terminals of the FSO communication system. We have employed the Alamouti STBC scheme for transmitter diversity and the SEC technique for receiver diversity in the system. The performance analysis, in terms of the ABER, has been carried out for the above MIMO FSO link under various weather conditions, in the presence of misalignment fading into the channel, and also using fixed and optimal switching threshold of the system. The system performance is found to improve for an optimal switching threshold and degrade in the presence of pointing errors under any AT regime. A comparison of ABER under different network configurations of the FSO communication system proves that an STBC-SEC-added MIMO FSO link performs best.

# Chapter 6

## Performance Analysis of FSO Communication Channel with SSK Transmit diversity and SC Receive Diversity

**Chapter contributions:** In this contributory chapter, we analyzed the performance of the MISO FSO, SIMO FSO, and MIMO FSO systems by introducing spatial shift keying (SSK) and selection combining (SC) as transmitter and receiver diversity techniques. We have compared the outcomes with other FSO systems under all possible misalignment fading cases.

---

The work of this chapter is published in:

Proc. *2021 IEEE 93rd Vehicular Technology Conference (VTC2021-Spring)*, Helsinki, Finland, Apr. 2021, 1–5 [\[link\]](#)

---

## 6.1 Introduction

In this chapter, a non-traditional transmit diversity scheme called SSK [116, 117] will be adopted to develop a MISO FSO link. It is a special case of SM, where each antenna index is used to exchange information. The SM technique helps to reduce inter-channel interference and inter-antenna synchronization related problems. SSK offers some benefits over SM, like more straightforward detection protocol usable for both coherence and non-coherence detectors, simple transceiver hardware architecture, and easy implementation [102]. Thus, SSK modulation technique results in a low-complexity link configuration. For receive diversity, selection combining (SC) scheme will be used here to develop the MIMO FSO link. More complex receiver diversity schemes like MRC and EGC need all channel state information from all the receiver branches. An SC system deals with only the highest SNR branch among all available branches at the receiver end of the system, and therefore, the coherent addition of the individual branches is not essential. Thus, the scheme can be ideally used for both coherent and non-coherent modulation techniques, as it does not require any previous knowledge of the signal phases of the individual branches.

## 6.2 Organization

The rest of the chapter is organized as follows. The analytical derivation of the SSK-FSO link will be presented in Section 6.3. The mathematical derivation of ABER upper bound for SSK-FSO system under the GG turbulence will be provided in Section 6.3.1 in the absence of pointing error and in Section 6.3.2 in the presence of pointing error. Similar derivations appear in Section 6.3.3 and Section 6.3.4 for Málaga distribution. After the SSK-FSO, an architectural setup for the MIMO FSO link with SSK modulation and SC diversity technique will be developed. The channel characterization of SSK-SC-FSO or MIMO FSO will be placed in Section 6.4.

The analytical derivation of performance metric under GG and the Málaga distribution without pointing error will be provided in Section 6.4.1 and Section 6.4.3 respectively. Section 6.4.2 and Section 6.4.4 will provide an analytical derivation of the same measuring metric, taking pointing errors into consideration. The numerical results will be discussed in Section 6.5. Finally, Section 6.6 will bear a short chapter summary.

## 6.3 Performance analysis with SSK

In this section, a  $N_t \times 1$  MISO FSO link is developed as on Fig. 2.4 by employing the SSK modulation technique as a transmitting diversity scheme. At first, we express the PDF in terms of the end-to-end SNR of the system under atmospheric turbulence and misalignment fading. We also investigate the system's upper tight bound ABER.

### 6.3.1 Gamma-Gamma turbulence in absence of pointing error

We derive the PDF of a  $N_t \times 1$  MISO FSO system for GG atmospheric turbulence, neglecting the pointing error effect on it.

The PDF of the MISO FSO system with the GG fading channel under the SSK scheme can be written as [details in Appendix C]

$$f_\gamma(\gamma) = \frac{\alpha_t \beta_t}{(\Gamma(\alpha_t) \Gamma(\beta_t))^2 \sqrt{\gamma}} \left[ \sum_{p=0}^{\infty} \frac{\left( \frac{-\alpha_t \beta_t}{\sqrt{\gamma}} \right)^p}{p!} (\sqrt{\gamma})^{(p-1)} G_{3 \ 3}^{2 \ 3} \left[ 1 \left| \begin{matrix} 1 - \frac{\alpha_t + \beta_t}{2}, \frac{4+2p-3\alpha_t-\beta_t}{2}, \frac{4+2p-3\beta_t-\alpha_t}{2} \\ \frac{\alpha_t - \beta_t}{2}, \frac{\beta_t - \alpha_t}{2}, \frac{2+2p-\alpha_t-\beta_t}{2} \end{matrix} \right. \right] \right] \quad (6.1)$$

The average BER of the MISO FSO system for the GG fading channel in the absence of pointing error can be expressed as [48]

$$ABER_{SSK}^U \leq \frac{1}{N_t \log(N_t)} \sum_{i=1}^{N_t} \sum_{j=1}^{N_t} d_H(b_i, b_j) P(x_j \rightarrow x_{\hat{j}}) \quad (6.2)$$

where  $P(x_j \rightarrow x_{\hat{j}})$  is pairwise error probability of the system. In general, it can be defined in terms of  $Q(\cdot)$  function as [48]

$$P(x_j \rightarrow x_{\hat{j}}) = Q\left(\sqrt{\frac{\bar{\gamma}\gamma \log_2(N_t)}{2}}\right) \quad (6.3)$$

and the two-fold summation in (6.2) can be simplified as  $\frac{1}{N_t \log(N_t)} \sum_{i=1}^{N_t} \sum_{j=1}^{N_t} d_H(b_i, b_j) = \frac{N_t}{2}$ , using (6.2) and (6.3), the derived mathematical expression for the ABER of the proposed system can be expressed as follows:

$$ABER_{SSK}^U \leq \frac{N_t}{2} \int_0^\infty Q\left(\sqrt{\frac{\bar{\gamma}\gamma \log_2(N_t)}{2}}\right) f_\gamma(\gamma) d\gamma \quad (6.4)$$

where  $f_\gamma(\gamma)$  is the PDF of the given system. To find the closed-form expression of the resultant metric of the system in terms of ABER, we utilize a well known relationship between  $Q(\cdot)$  and error function as  $Q(y) = \frac{1}{2} \operatorname{erfc}\left(\frac{y}{\sqrt{2}}\right)$ . Using the above relation, and (6.1), we may re-write (6.4) as

$$ABER_{SSK}^U \leq \frac{N_t \Xi}{4} \int_0^\infty \operatorname{erfc}\left(\frac{\sqrt{\bar{\gamma}\gamma \log_2(N_t)}}{2}\right) (\sqrt{\gamma})^{p-1} d\gamma \quad (6.5)$$

where,  $\Xi = \frac{\alpha_t \beta_t}{(\Gamma(\alpha_t) \Gamma(\beta_t))^2 \sqrt{\bar{\gamma}}} \sum_{p=0}^\infty \frac{\left(\frac{-\alpha_t \beta_t}{\sqrt{\bar{\gamma}}}\right)^p}{p!} G_{3 \ 3}^{2 \ 3} \left[ 1 \left| \begin{matrix} 1 - \frac{\alpha_t + \beta_t}{2}, \frac{4+2p-3\alpha_t - \beta_t}{2}, \frac{4+2p-3\beta_t - \alpha_t}{2} \\ \frac{\alpha_t - \beta_t}{2}, \frac{\beta_t - \alpha_t}{2}, \frac{2+2p - \alpha_t - \beta_t}{2} \end{matrix} \right. \right]$ ,  $N_t$  is the number of transmitter link. Next, using [118, eq.(18)], the closed-form expression of ABER is given as

$$ABER_{SSK}^U \leq \frac{N_t \Xi (\Gamma(\frac{p}{2} + 1))}{4(p+1) \left(\frac{\sqrt{\bar{\gamma} \log_2 N_t}}{2}\right)^{p+1} \sqrt{\pi}} \quad (6.6)$$

### 6.3.2 Gamma-Gamma turbulence in presence of pointing error

In this subsection, we provide the performance metrics of the MISO FSO system under the combined effect of GG fading and pointing errors on the system. For this, we start with the corresponding PDF of the system.

The PDF under the combined effect of the misalignment fading and GG fading channel of the system can be written as [details in Appendix D]

$$f_{\gamma}(\gamma) = \frac{K^2}{\omega\sqrt{\bar{\gamma}}} \left[ \sum_{p=0}^{\infty} \frac{\left(\frac{-\omega}{\sqrt{\bar{\gamma}}}\right)^p}{p!} (\sqrt{\gamma})^{(p-1)} G_{5/5}^{3/4} \left[ 1 \left| \begin{matrix} 0, 1+p-\xi^2, 1+p-\alpha_t, 1+p-\beta_t, \xi^2 \\ \xi^2-1, \alpha_t-1, \beta_t-1, p-\xi^2, p \end{matrix} \right. \right] \right] \quad (6.7)$$

Following same steps in the previous subsection and using (6.7), the average BER for GG fading in the absence of pointing error, be expressed as

$$ABER_{SSK}^U \leq \frac{\Pi \left( \Gamma \left( \frac{p}{2} + 1 \right) \right)}{(p+1) \left( \frac{\sqrt{\bar{\gamma}} \log_2 N}{2} \right)^{p+1} \sqrt{\pi}} \quad (6.8)$$

$$\text{where, } \Pi = \frac{K^2}{\omega\sqrt{\bar{\gamma}}} \left[ \sum_{p=0}^{\infty} \frac{\left(\frac{-\omega}{\sqrt{\bar{\gamma}}}\right)^p}{p!} G_{5/5}^{3/4} \left[ 1 \left| \begin{matrix} 0, 1+p-\xi^2, 1+p-\alpha_t, 1+p-\beta_t, \xi^2 \\ \xi^2-1, \alpha_t-1, \beta_t-1, p-\xi^2, p \end{matrix} \right. \right] \right]$$

### 6.3.3 Málaga turbulence in absence of pointing error

In this subsection, The PDF and CDF of the MISO FSO system under Málaga turbulence channel are expressed in terms of instantaneous SNR ( $\gamma$ ) and end-to-end average SNR ( $\bar{\gamma}$ ). The performance of the system is examined in terms of the tight upper bound of the ABER.

Using the steps in the appendix (C) for finding the PDF under the GG fading channel in the absence of misalignment fading and (2.24), the PDF of the system in



terms of end-to-end SNR can be represented as

$$f_\gamma(\gamma) = \frac{\mathcal{A}^2}{4\sqrt{\gamma}} \sum_{k_t=1}^{\beta_t} a_k \sum_{k_t=1}^{\beta_t} a_k (\omega\alpha_t\beta_t)^{3-\alpha_t-k_t} \sum_{p=0}^{\infty} \frac{\left(\frac{-\omega\alpha_t\beta_t}{\sqrt{\gamma}}\right)^p}{p!} (\sqrt{\gamma})^{(p-1)} \times G_{3 \ 3}^{2 \ 3} \left[ 1 \left| \begin{matrix} 1-\frac{\alpha_t+k_t}{2}, \frac{4+2p-3\alpha_t-k_t}{2}, \frac{4+2p-3k_t-\alpha_t}{2} \\ \frac{\alpha_t-k_t}{2}, \frac{k_t-\alpha_t}{2}, \frac{2+2p-\alpha_t-k_t}{2} \end{matrix} \right. \right] \quad (6.9)$$

where,  $\omega = \frac{\mathcal{B}^2}{4}$ , and  $\mathcal{B} = \frac{2}{\sqrt{g_t\beta_t+\Omega_t}}$ . The parameters  $\mathcal{A}$  and  $a_k$  have been defined in (2.24). Following the same procedure as in Section 3.3.1.2, the average BER of this MISO FSO network under the Málaga fading without considering pointing error, and using (6.9) can be written as

$$ABER_{SSK}^U \leq \frac{N_t \mathcal{A}^2}{8\sqrt{\gamma}} \sum_{k_t=1}^{\beta_t} a_k \sum_{k_t=1}^{\beta_t} a_k (\omega\alpha_t\beta_t)^{3-\alpha_t-k_t} \sum_{p=0}^{\infty} \frac{\left(\frac{-\omega\alpha_t\beta_t}{\sqrt{\gamma}}\right)^p}{p!} \times \frac{\Gamma\left(\frac{p}{2}+1\right)}{(p+1) \left(\frac{\sqrt{\gamma} \log_2 N_t}{2}\right)^{p+1}} \frac{1}{\sqrt{\pi}} G_{3 \ 3}^{2 \ 3} \left[ 1 \left| \begin{matrix} 1-\frac{\alpha_t+k_t}{2}, \frac{4+2p-3\alpha_t-k_t}{2}, \frac{4+2p-3k_t-\alpha_t}{2} \\ \frac{\alpha_t-k_t}{2}, \frac{k_t-\alpha_t}{2}, \frac{2+2p-\alpha_t-k_t}{2} \end{matrix} \right. \right] \quad (6.10)$$

### 6.3.4 Málaga turbulence in presence of pointing error

In this subsection, we investigate the different performance metrics of a  $(N_t \times 1)$  MISO FSO system under the Málaga fading channel with pointing error effect on the system.

To express the closed-form equation for the PDF, we have followed the same procedure as given in the appendix (D). Using (2.43) and after some mathematical manipulation, we get the resultant PDF of the system as

$$f_\gamma(\gamma) = \frac{\gamma^4 \mathcal{A}^2 \omega}{4\sqrt{\gamma}} \sum_{k_t=1}^{\beta_t} b_{k_t} \sum_{k_t=1}^{\beta_t} b_{k_t} \sum_{p=0}^{\infty} \frac{(-\omega/\sqrt{\gamma})^p}{p!} (\sqrt{\gamma})^{p-1} \times G_{5 \ 5}^{3 \ 4} \left[ 1 \left| \begin{matrix} 1, 2+p-\xi^2, 2+p-\alpha_t, 2+p-k_t, \xi^2+1 \\ \xi^2, \alpha_t, k_t, 1+p-\xi^2, 1+p \end{matrix} \right. \right] \quad (6.11)$$

where,  $\omega = \frac{\alpha_t \beta_t}{A_0 I_l (g_t \beta_t + \Omega_t)}$ , and  $A_0$  and  $I_l$  are constant parameters related to misalignment fading and path loss component respectively.

We used the same steps for generating a closed-form mathematical equation for the tight upper bound of the average BER of an SSK-added MISO FSO communication system in the absence of pointing error. This is followed by (6.11) to get the average BER of the system in presence of pointing error, as

$$\begin{aligned}
 ABER_{SSK}^U &\leq \frac{\gamma^4 \mathcal{A}^2 \omega}{4\sqrt{\gamma}} \sum_{k_t=1}^{\beta_t} b_{k_t} \sum_{k_t=1}^{\beta_t} b_{k_t} \sum_{p=0}^{\infty} \frac{(-\omega/\sqrt{\gamma})^p}{p!} \\
 &\times \frac{(\Gamma(\frac{p}{2} + 1))}{(p+1) \left(\frac{\sqrt{\gamma} \log_2 N_t}{2}\right)^{p+1}} \frac{G_{5 \ 5}^{3 \ 4}}{\sqrt{\pi}} \left[ 1 \middle| \begin{matrix} 1, 2+p-\xi^2, 2+p-\alpha_t, 2+p-k_t, \xi^2+1 \\ \xi^2, \alpha_t, k_t, 1+p-\xi^2, 1+p \end{matrix} \right]
 \end{aligned} \tag{6.12}$$

## 6.4 Performance analysis with SSK and SC

In this section, we will develop the MIMO FSO link using the SSK transmit diversity technique at the transmitting terminal and the SC receiver diversity techniques. Fig. 6.1 represents a  $2 \times N_r$  schematic of the proposed switched MIMO FSO system. The transmitter antenna selection is accomplished by SSK transmit diversity technique, and the SC strategy controls the receiver diversity of the MIMO FSO link.

### 6.4.1 Gamma-Gamma turbulence in absence of pointing error

Here, we derive the PDF of the proposed MIMO FSO link under GG statistical distribution without a pointing error. Assuming that all coefficients are i.i.d., the overall PDF of the system is written, in terms of a RV ( $x$ ) as [119, 120]

$$f_Z(z) = \frac{N_r!}{(N_r - 1)!} f_X(x) [1 - F_X(x)]^{N_r - 1} \tag{6.13}$$

where  $f_X(\cdot)$  is the PDF of the given system,  $F_X(\cdot)$  is the symbolic representation of CDF of the system, and  $N_r$  is the receiver diversity order.

The required PDF has already been provided in Eq.(2.13). Now, with the help of the mathematical definition of the CDF and [96, eq. (26)], the CDF of this particular system can be expressed as

$$F_{I_a}(I_a)\Big|_{wop} = \frac{(\alpha_t\beta_t)^{\frac{\alpha_t+\beta_t}{2}}}{\Gamma(\alpha_t)\Gamma(\beta_t)} (I_a)^{\frac{\alpha_t+\beta_t}{2}} G_{1\ 3}^{2\ 1} \left[ \omega I_a \left| \begin{matrix} 1 - \frac{\alpha_t+\beta_t}{2} \\ \frac{\alpha_t-\beta_t}{2}, \frac{\beta_t-\alpha_t}{2}, -\frac{\alpha_t+\beta_t}{2} \end{matrix} \right. \right] \quad (6.14)$$

where,  $\omega = \alpha_t\beta_t$ , Next, using Eq.(2.13) and Eq.(6.14) into Eq.(6.13), the overall PDF of the proposed MIMO FSO link is expressed in terms of intensity ( $I_a$ ), as follows

$$f_{I_a}(I_a)\Big|_{wop}^{MIMOFSO} = \frac{N_r!}{(N_r - 1)!} \frac{2(\alpha_t\beta_t)^{\frac{(\alpha_t+\beta_t)}{2}}}{\Gamma(\alpha_t)\Gamma(\beta_t)} (I_a)^{\frac{(\alpha_t+\beta_t)}{2}-1} K_{\alpha_t-\beta_t} \left( 2\sqrt{\alpha_t\beta_t I_a} \right) \left[ 1 - \frac{(\alpha_t\beta_t)^{\frac{\alpha_t+\beta_t}{2}}}{\Gamma(\alpha_t)\Gamma(\beta_t)} (I_a)^{\frac{\alpha_t+\beta_t}{2}} G_{1\ 3}^{2\ 1} \left[ \omega I_a \left| \begin{matrix} 1 - \frac{\alpha_t+\beta_t}{2} \\ \frac{\alpha_t-\beta_t}{2}, \frac{\beta_t-\alpha_t}{2}, -\frac{\alpha_t+\beta_t}{2} \end{matrix} \right. \right] \right]^{N_r-1} \quad (6.15)$$

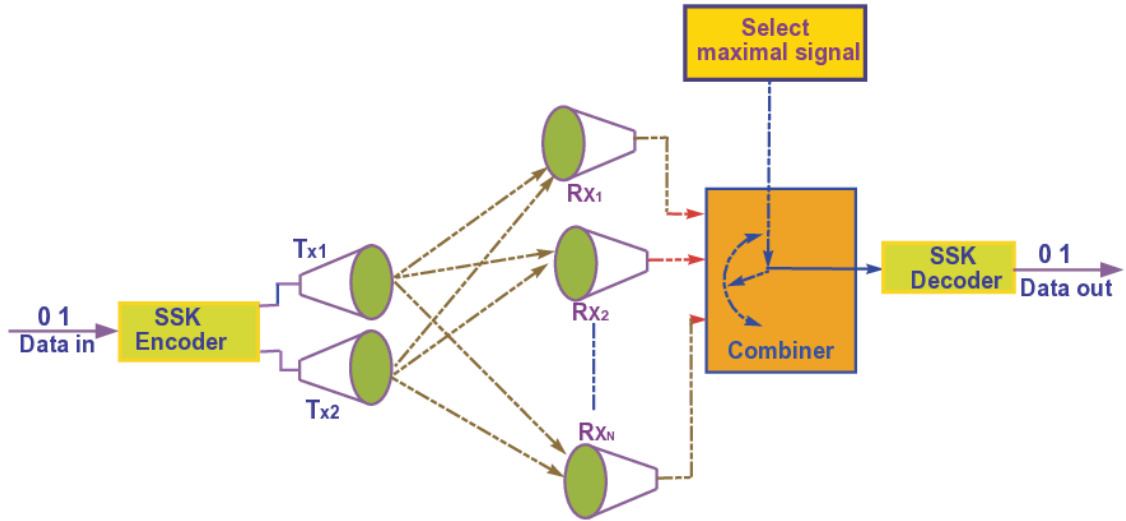


FIGURE 6.1: SSK-SC  $2 \times N_r$  MIMO FSO communication system.

Now, using the relation between 2<sup>nd</sup> order Bessel K function and Meijer'G function as on [95, Eq.(9.301)], the above equation becomes

$$f_{I_a}(I_a) \Big|_{wop}^{MIMOFSSO} = \frac{N_r!}{(N_r - 1)!} \frac{(\alpha_t \beta_t)^{\frac{\alpha_t + \beta_t}{2}}}{\Gamma(\alpha_t) \Gamma(\beta_t)} (I_a)^{\frac{\alpha_t + \beta_t}{2} - 1} G_{0 \ 2}^{2 \ 0} \left[ \omega I_a \Big|_{\frac{\alpha_t - \beta_t}{2}, \frac{\beta_t - \alpha_t}{2}}^{-} \right] \left[ 1 - \frac{(\alpha_t \beta_t)^{\frac{\alpha_t + \beta_t}{2}}}{\Gamma(\alpha_t) \Gamma(\beta_t)} (I_a)^{\frac{\alpha_t + \beta_t}{2}} G_{1 \ 3}^{2 \ 1} \left[ \omega I_a \Big|_{\frac{\alpha_t - \beta_t}{2}, \frac{\beta_t - \alpha_t}{2}, -\frac{\alpha_t + \beta_t}{2}}^{1 - \frac{\alpha_t + \beta_t}{2}} \right] \right]^{N_r - 1} \quad (6.16)$$

The power series representation of the Meijer'G function [121], gives  $G_{1 \ 3}^{2 \ 1}[\cdot]$  as

$$G_{1 \ 3}^{2 \ 1} \left[ \omega I_a \Big|_{\frac{\alpha_t - \beta_t}{2}, \frac{\beta_t - \alpha_t}{2}, -\frac{\alpha_t + \beta_t}{2}}^{1 - \frac{\alpha_t + \beta_t}{2}} \right] = \frac{\Gamma(\beta_t - \alpha_t) \Gamma(\alpha_t)}{\Gamma(\beta_t + 1)} (\omega)^{\frac{\alpha_t - \beta_t}{2}} (I_a)^{\frac{\alpha_t - \beta_t}{2}} + \frac{\Gamma(\alpha_t - \beta_t) \Gamma(\beta_t)}{\Gamma(\alpha_t + 1)} (\omega)^{\frac{\beta_t - \alpha_t}{2}} (I_a)^{\frac{\beta_t - \alpha_t}{2}} \quad (6.17)$$

Using Eq.(6.17), the term  $\left[ 1 - F_{I_a}(I_a) \Big|_{wop} \right]^{N_r - 1}$  may be expressed as

$$\left[ 1 - F_{I_a}(I_a) \Big|_{wop} \right]^{N_r - 1} = \left[ 1 - K(I_a)^{\frac{\alpha_t + \beta_t}{2}} \left[ S(a)^{\frac{\alpha_t - \beta_t}{2}} + T(\omega I_a)^{\frac{\beta_t - \alpha_t}{2}} \right] \right]^{N_r - 1} \quad (6.18)$$

where,  $K = \frac{(\alpha_t \beta_t)^{\frac{\alpha_t + \beta_t}{2}}}{\Gamma(\alpha_t) \Gamma(\beta_t)}$ ,  $S = \frac{\Gamma(\beta_t - \alpha_t) \Gamma(\alpha_t)}{\Gamma(\beta_t + 1)}$ , and  $T = \frac{\Gamma(\alpha_t - \beta_t) \Gamma(\beta_t)}{\Gamma(\alpha_t + 1)}$ . Employing the power series expansion using [122, Eq.(1.111)], Eq.(6.18) takes the form

$$\left[ 1 - F_{I_a}(I_a) \Big|_{wop} \right]^{N_r - 1} = \sum_{p=0}^{N_r - 1} \binom{N_r - 1}{p} (-1)^p \sum_{q=0}^p \binom{p}{q} \times \left[ KS (\omega I_a)^{\frac{\alpha_t - \beta_t}{2}} (I_a)^{\frac{\alpha_t + \beta_t}{2}} \right]^q \times \left[ KT (\omega I_a)^{\frac{\beta_t - \alpha_t}{2}} (I_a)^{\frac{\alpha_t + \beta_t}{2}} \right]^{p - q} \quad (6.19)$$

Next, using Eq.(6.19) in Eq.(6.16), the PDF of the system can be re-written as

$$f_{I_a}(I_a)\Big|_{wop}^{MIMOFSSO} = \frac{N_r!}{(N_r-1)!} \frac{(\alpha_t \beta_t)^{\frac{\alpha_t + \beta_t}{2}}}{\Gamma(\alpha_t) \Gamma(\beta_t)} (I_a)^{\frac{\alpha_t + \beta_t}{2} - 1} G_{0\ 2}^{2\ 0} \left[ \omega I_a \Big|_{\frac{\alpha_t - \beta_t}{2}, \frac{\beta_t - \alpha_t}{2}} \right] \\ \times \sum_{p=0}^{N_r-1} \binom{N_r-1}{p} (-1)^p \sum_{q=0}^p \binom{p}{q} \times \left[ KS(\omega I_a)^{\frac{\alpha_t - \beta_t}{2}} (I_a)^{\frac{\alpha_t + \beta_t}{2}} \right]^q \\ \times \left[ KT(\omega I_a)^{\frac{\beta_t - \alpha_t}{2}} (I_a)^{\frac{\alpha_t + \beta_t}{2}} \right]^{p-q} \quad (6.20)$$

Using the integral form of the Q-function [119, 110] the ABER of the proposed MIMO FSO system can be expressed as

$$ABER\Big|_{wop}^{MIMOFSSO} = \frac{1}{\pi} \int_0^{\pi/2} \int_0^\infty \exp\left(-\frac{\bar{\gamma} I_a}{4 \sin^2 \theta}\right) f_{I_a}(I_a)\Big|_{wop}^{MIMOFSSO} dI_a d\theta \quad (6.21)$$

Using Eq.(6.20), Eq.(6.21) is further written as

$$ABER\Big|_{wp}^{MIMOFSSO} = \frac{\mathcal{K}}{\pi} \int_0^{\pi/2} \int_0^\infty (I_a)^{R-1} \exp\left(-\frac{\bar{\gamma} I_a}{4 \sin^2 \theta}\right) \\ G_{0\ 2}^{2\ 0} \left[ \omega I_a \Big|_{\frac{\alpha_t - \beta_t}{2}, \frac{\beta_t - \alpha_t}{2}} \right] dI_a d\theta \quad (6.22)$$

where,  $R = \frac{\alpha_t + \beta_t}{2} + \alpha_t q + \beta_t p - \beta_t q$  and  $\mathcal{K} = \frac{N_r!}{(N_r-1)!} K \sum_{p=0}^{N_r-1} \binom{N_r-1}{p} (-1)^p \sum_{q=0}^p \binom{p}{q} \left[ KS(\omega)^{\frac{\alpha_t - \beta_t}{2}} \right]^q \left[ KT(\omega)^{\frac{\beta_t - \alpha_t}{2}} \right]^{p-q}$

With the help of [123, 07.34.21.0002.01] and [94, 2.24.3.1], the closed-form expression of the ABER for  $2 \times N_r$  MIMO FSO system under GG fading in absence of pointing error takes the final form as

$$ABER\Big|_{wop,GG}^{MIMOFSSO} = \frac{K}{\pi} \left(\frac{1}{\omega}\right)^R G_{2\ 3}^{2\ 2} \left[ \frac{4\omega}{\bar{\gamma}} \Big|_{R+1+\frac{\alpha_t - \beta_t}{2}, R+1+\frac{\beta_t - \alpha_t}{2}, 0}^{1,2} \right] \quad (6.23)$$

### 6.4.2 Gamma-Gamma turbulence in presence of pointing error

Using the mathematical definition of CDF, Eq. (2.36) and [96, eq.(26)], the CDF of the corresponding statistical distribution under influence of pointing error is derived as

$$F_{I_a}(I_a) \Big|_{wp} = \frac{\xi^2 \alpha_t \beta_t}{A_0 I_l \Gamma(\alpha_t) \Gamma(\beta_t)} I_a G_{2 \ 4}^3 \left[ \omega I_a \Big|_{\xi^2-1, \alpha_t-1, \beta_t-1, -1}^{0, \xi^2} \right] \quad (6.24)$$

where,  $\omega = \frac{\alpha_t \beta_t}{A_0 I_l}$ , Using the same procedure as discussed in the previous subsection to derive the closed-form of the resultant ABER, the modified ABER under the presence of the pointing error becomes

$$ABER \Big|_{wp, GG}^{MIMOFSSO} = \frac{\mathcal{K}}{\pi} \left( \frac{1}{\omega} \right)^R G_{3 \ 4}^3 \left[ \frac{4\omega}{\bar{\gamma}} \Big|_{R+1+\xi^2, R+1+\alpha_t, R+1+\beta_t, 0}^{1, 2, \xi^2+R} \right] \quad (6.25)$$

where,  $R = 1 + \beta_t q + \alpha_t m - p + \xi^2(p - q - m)$ ,  $\mathcal{K} = \frac{N_r!}{(N_r-1)!} \sum_{p=0}^{N_r-1} \binom{N_r-1}{p} (-1)^p \sum_{q=0}^p \binom{p}{q} [\mathcal{A} U \omega^{\beta_t-1}]^q \sum_{m=0}^{p-q} [\mathcal{A} T \omega^{\alpha_t-1}]^m \times [\mathcal{A} S \omega^{\xi^2-1}]^{p-q-m}$  where,  $\mathcal{A} = \frac{\xi^2 \alpha_t \beta_t}{A_0 I_l \Gamma(\alpha_t) \Gamma(\beta_t)}$ ,  $S = \frac{\Gamma(\alpha_t - \xi^2) \Gamma(\beta_t - \xi^2) \Gamma(\xi^2)}{\Gamma(1 + \xi^2)}$ ,  $T = \frac{\Gamma(\xi^2 - \alpha_t) \Gamma(\beta_t - \alpha_t) \Gamma(\alpha_t)}{\Gamma(1 + \xi^2 - \alpha_t) \Gamma(1 + \alpha_t)}$  and  $U = \frac{\Gamma(\xi^2 - \beta_t) \Gamma(\alpha_t - \beta_t) \Gamma(\beta_t)}{\Gamma(1 + \xi^2 - \beta_t) \Gamma(1 + \beta_t)}$

### 6.4.3 Málaga turbulence in absence of pointing error

The corresponding CDF of the generalized Málaga distribution in the absence of a pointing error, is obtained, using the Eq. (2.24) and [96, eq.(26)] as

$$F_{I_a}(I_a) \Big|_{wp} = \mathcal{A} \sum_{k_t=1}^{\beta_t} a_{k_t}(I_a)^{\frac{\alpha_t+k_t}{2}} G_{1 \ 3}^2 \left[ \omega I_a \Big|_{\frac{\alpha_t-k_t}{2}, \frac{k_t-\alpha_t}{2}, -\frac{\alpha_t+k_t}{2}}^{1-\frac{\alpha_t+k_t}{2}} \right] \quad (6.26)$$

where,  $\omega = \frac{\alpha_t k_t}{g_t \beta_t + \Omega_t}$ . Following the same steps as explained in subsection [3.4.1], we express the ABER, in absence of the pointing error, as

$$ABER \Big|_{wop, M\acute{a}laga}^{MIMOFSSO} = \frac{\mathcal{K}}{\pi} \left( \frac{1}{\omega} \right)^R G_{2 \ 3}^{2 \ 2} \left[ \frac{4\omega}{\bar{\gamma}} \Big|_{R+1+\frac{\alpha_t-k_t}{2}, R+1+\frac{k_t-\alpha_t}{2}, 0}^{1,2} \right] \quad (6.27)$$

where,  $R = \frac{\alpha_t+k_t}{2} + \alpha_t q + k_t p - k_t q$  and  $\mathcal{K} = \frac{N_r!}{(N_r-1)!} \frac{\mathcal{A}}{2} \sum_{k_t=1}^{\beta_t} a_{k_t} \sum_{p=0}^{N_r-1} \binom{N_r-1}{p} (-1)^p \sum_{q=0}^p \binom{p}{q} \left[ \frac{\mathcal{A}}{2} \sum_{k_t=1}^{\beta_t} a_{k_t} U(\omega)^{\frac{\alpha_t-k_t}{2}} \right]^q \left[ \frac{\mathcal{A}}{2} \sum_{k_t=1}^{\beta_t} a_{k_t} T(\omega)^{\frac{k_t-\alpha_t}{2}} \right]^{p-q}$ , where,  $U = \frac{\Gamma(k_t-\alpha_t)\Gamma(\alpha_t)}{\Gamma(1+k_t)}$  and  $T = \frac{\Gamma(\alpha_t-k_t)\Gamma(k_t)}{\Gamma(1+\alpha_t)}$ .

#### 6.4.4 M\acute{a}laga turbulence in presence of pointing error

The CDF of the generalized M\acute{a}laga distribution in the presence of pointing error is derived, using the Eq. (2.43) and [96, eq.(26)], as

$$F_{I_a}(I_a) \Big|_{wp} = \frac{\xi^2 \mathcal{A}}{2} \sum_{k_t=1}^{\beta_t} b_{k_t} G_{2 \ 4}^{3 \ 1} \left[ \omega I_a \Big|_{\xi^2, \alpha_t, k_t, 0}^{1, \xi^2+1} \right] \quad (6.28)$$

where,  $\omega = \frac{\mathcal{B}}{A_0 I_{pl}}$ , and  $\mathcal{B} = \frac{\alpha_t \beta_t}{g_t \beta_t + \Omega_t}$ . Next, following the same process in subsection [3.4.1], the analytical expression of the resultant ABER in the presence of the pointing error, appear as

$$ABER \Big|_{wp, M\acute{a}laga}^{MIMOFSSO} = \frac{\mathcal{K}}{\pi} \left( \frac{1}{\omega} \right)^R G_{3 \ 4}^{3 \ 2} \left[ \frac{4\omega}{\bar{\gamma}} \Big|_{R+1+\xi^2, R+1+\alpha_t, R+1+k_t, 0}^{1,2, \xi^2+2+R} \right] \quad (6.29)$$

where,  $R = k_t q + \alpha_t m + \xi^2(p-q-m)$  and  $\mathcal{K} = \frac{N_r!}{(N_r-1)!} \frac{\xi^2 \mathcal{A}}{2} \sum_{k_t=1}^{\beta_t} b_{k_t} \sum_{p=0}^{N_r-1} \binom{N_r-1}{p} (-1)^p \sum_{q=0}^p \binom{p}{q} \left[ \frac{\xi^2 \mathcal{A}}{2} \sum_{k_t=1}^{\beta_t} b_{k_t} U \omega^{k_t} \right]^q \sum_{m=0}^{p-q} \left[ \frac{\xi^2 \mathcal{A}}{2} \sum_{k_t=1}^{\beta_t} b_{k_t} T \omega^{\alpha_t} \right]^m \times \left[ \frac{\xi^2 \mathcal{A}}{2} \sum_{k_t=1}^{\beta_t} b_{k_t} S \omega^{\xi^2} \right]^{p-q-m}$ .

TABLE 6.1: Summary of the equations used for figures, Fig. 6.2 to Fig. 6.3.

Figure	Scenario	Equation
Fig. 6.2a	GG	Eq. 6.6
Fig. 6.2b	GG + pointing	Eq. 6.8
Fig. 6.2c	GG	Eq. 6.10
Fig. 6.2d	GG + pointing	Eq. 6.12
Fig. 6.3a	Málaga	Eq. 6.23
Fig. 6.3b	Málaga + pointing	Eq. 6.25
Fig. 6.3c	Málaga	Eq. 6.27
Fig. 6.3d	Málaga + pointing	Eq. 6.29

## 6.5 Numerical results and discussion for SSK based MIMO FSO link

This section examines the numerical results of SSK-FSO and SSK-SC-FSO links under different weather conditions. As we agree to find the tight upper bound of the ABER for all possible cases, our analytical outcomes will be matched with the higher SNR region instead of the lower SNR; due to system limitations, occasionally at very high SNR regions, the decay curves with asterisks symbol tend to deviate. Table 6.1 summarized the equation used for Fig. 6.2 to Fig. 6.3. The graphical plot in Fig. 6.2 (a) demonstrated a tight upper bound of ABER with GG distribution of SSK-FSO system without considering pointing error. This figure shows that at higher average SNRs, the analytical ABER solid lines match with the Monte Carlo simulation results for  $2 \times 1$  and  $4 \times 1$  SSK-FSO systems. This figure also signifies that under weak ( $\alpha_t = 4.20$  and  $\beta_t = 2.72$ ) atmospheric turbulence, the system yields a better output than under strong ( $\alpha_t = 2.20$  and  $\beta_t = 0.65$ ) atmospheric turbulence. Another important observation from the above figure is that the outcomes of the system become poorer with an increase in the number of transmitter arrays present in the system. Besides, we have furnished a comparison of the current measuring metric between the SSK-FSO link and STBC-FSO (MISO FSO in Chapter 3) link. Under strong atmospheric turbulence,  $2 \times 1$  SSK-FSO system gives  $1.29 \times 10^{-2}$



ABER (see Fig. 6.2 (a)), while STBC-FSO system produced  $1.33 \times 10^{-3}$  ABER (see Fig. 3.2 (a)). Hence, the previous MISO FSO link performance is better in terms of ABER than the current MISO FSO (SSK-FSO) link. Next, Fig. 6.2 (b) manifests a tight upper bound ABER of the SSK-FSO system in the presence of a pointing error. After examining Fig. 6.2 (b) and Fig. 3.2 (b), it is found that with pointing error ( $\xi = 0.8565$ ) and under strong turbulence, an STBC-FSO link performs significantly better than SSK-FSO link.

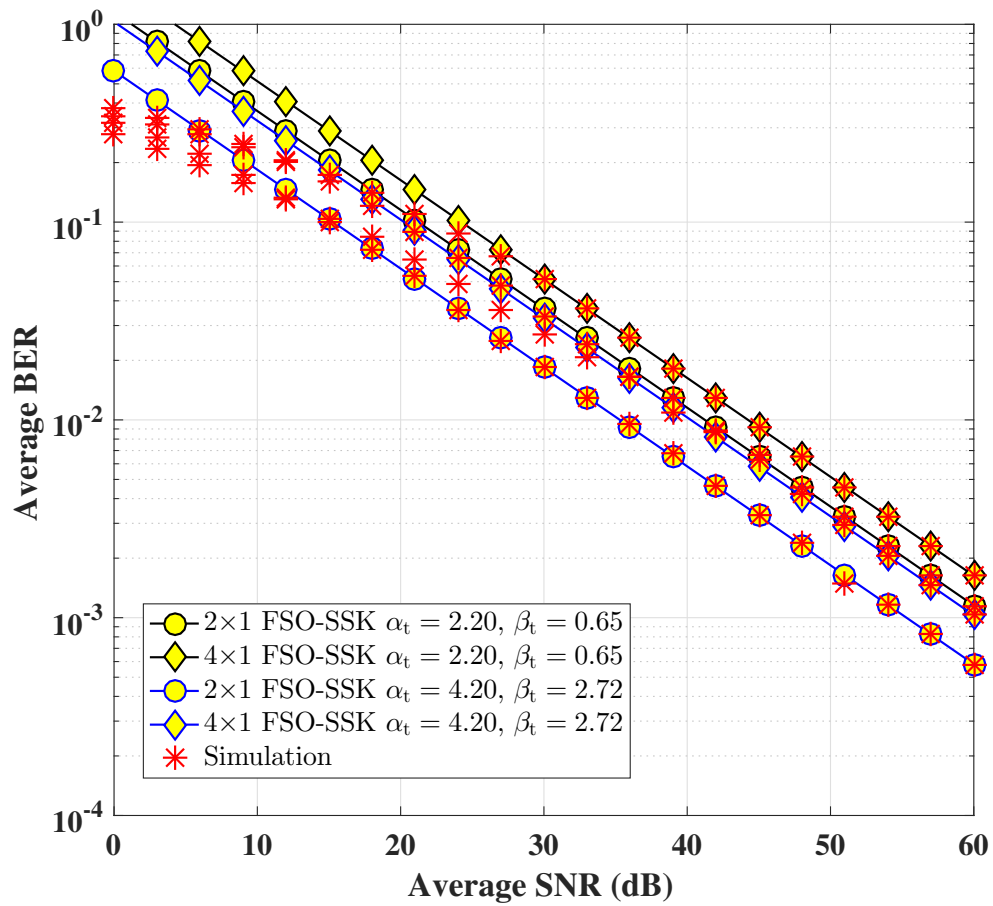


**Figure 6.2 (a)** Average bit error rate of MISO FSO link under Gamma-Gamma distribution and SSK transmit diversity scheme in the absence of pointing error.

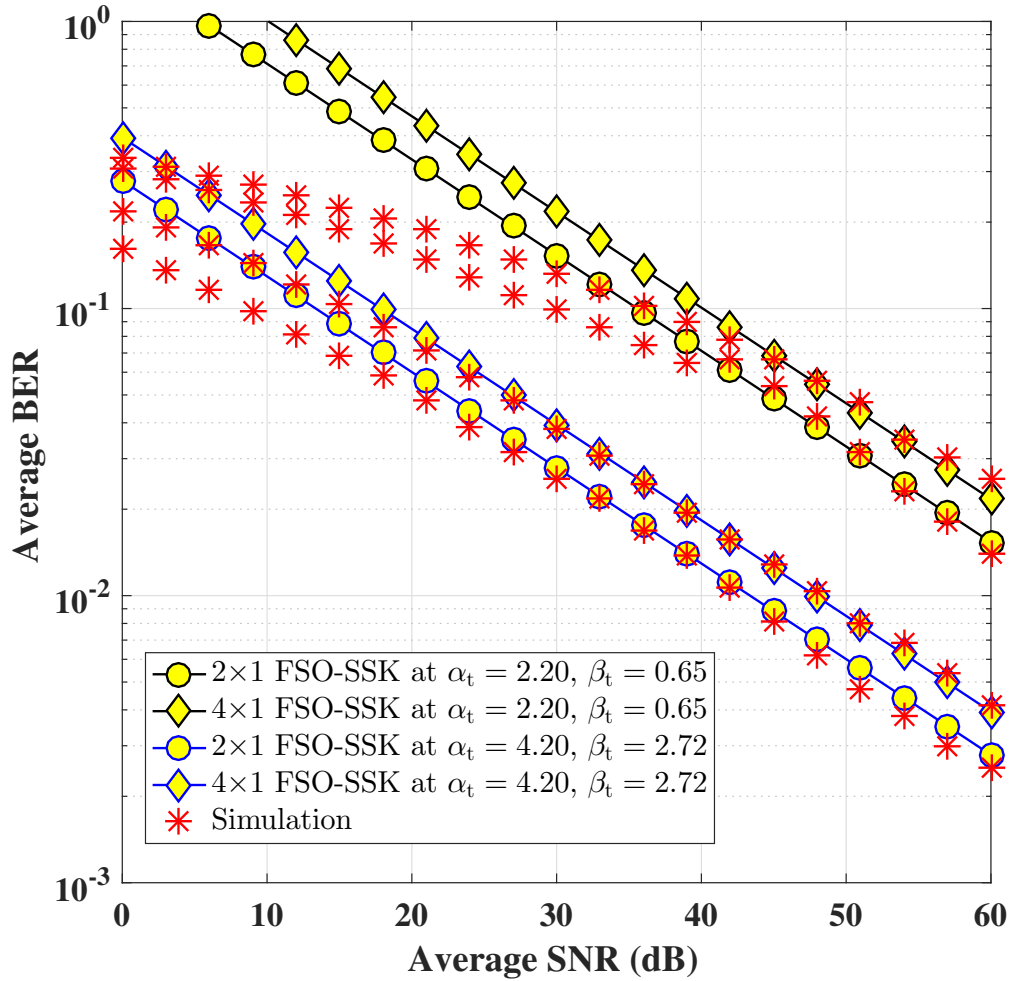
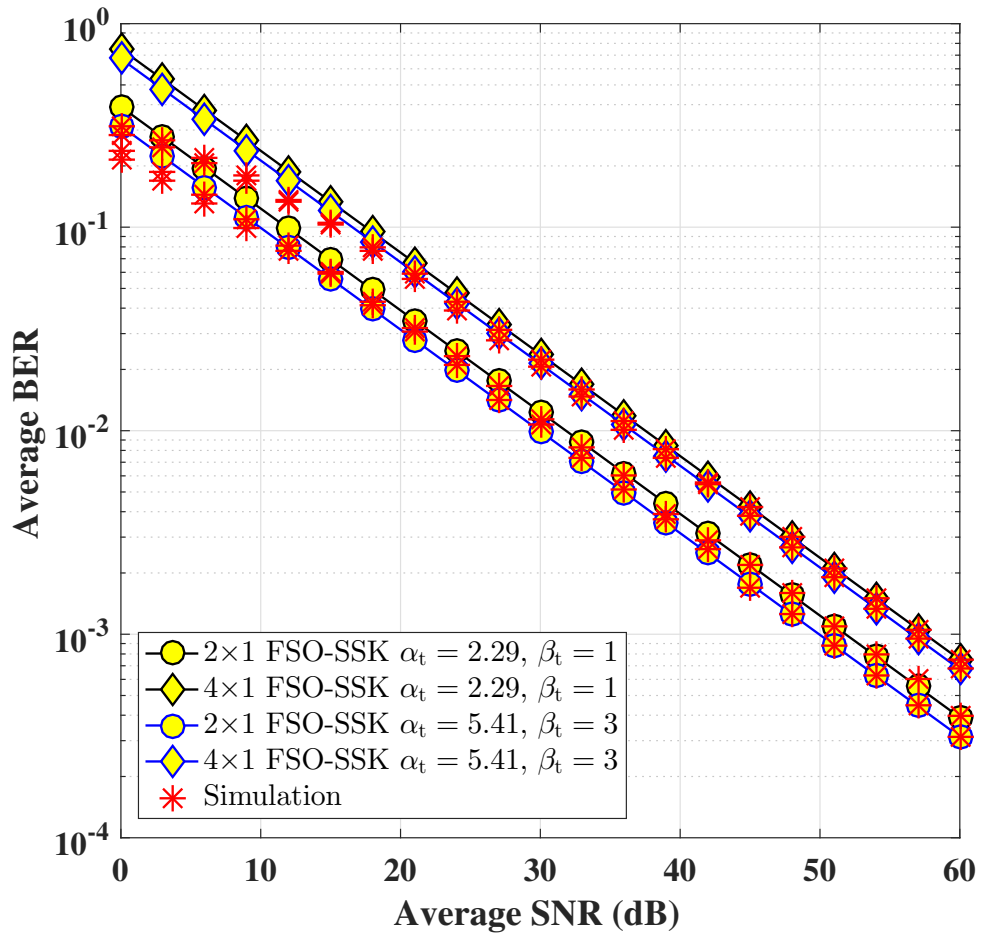
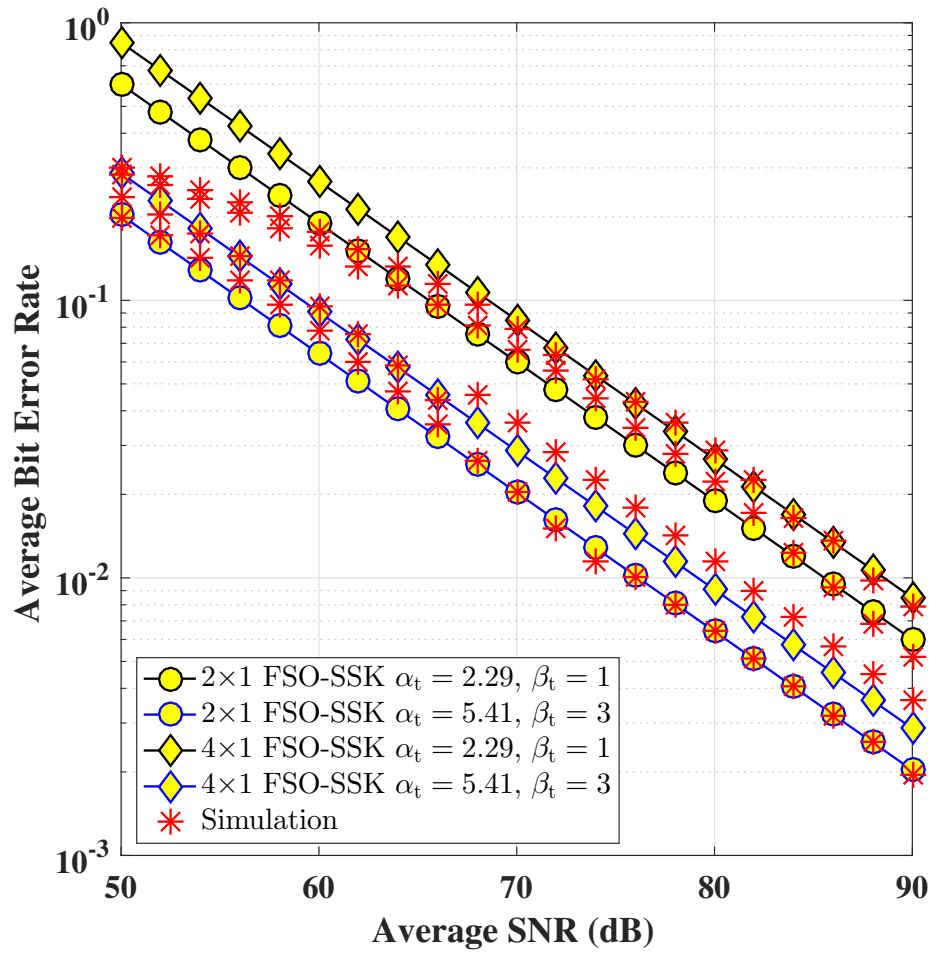


Figure 6.2 (b) Average bit error rate of MISO FSO link under Gamma-Gamma distribution and SSK transmit diversity scheme in the presence of pointing error  $\xi = 0.8565$



**Figure 6.2 (c)** Average bit error rate of MISO FSO link under Málaga distribution and SSK transmit diversity scheme in the absence of pointing error.



**Figure 6.2 (d)** Average bit error rate MISO FSO link under Málaga distribution and SSK transmit diversity scheme in the presence of pointing error  $\xi = 0.8565$

FIGURE 6.2: Average bit error rate of the MISO FSO link employing SSK scheme at the transmitter end with different atmospheric turbulence conditions in the absence and presence of pointing error regime.

The ABER under the Málaga statistical distribution without and with pointing error is presented in Fig. 6.2 (c) and Fig. 6.2 (d), respectively. Here, the values of turbulence parameters are taken as  $\alpha_t = 5.41$  and  $\beta_t = 3$  to signify weak turbulence, and  $\alpha_t = 2.29$  and  $\beta_t = 1$  for strong turbulence. From Fig. 6.2 (d), it is observed that under Málaga statistical distribution with pointing error, the system yields an acceptable outcome, especially at a higher average SNR region. Subsequently, from Fig. 3.2 (d) and Fig. 6.2 (d), in the presence of pointing error ( $\xi = 0.5607$ ) and strong atmospheric turbulence condition, an SSK-FSO link required  $\approx 27$  dB more average SNR than an STBC-FSO link to produce an ABER of  $10^{-2}$ .

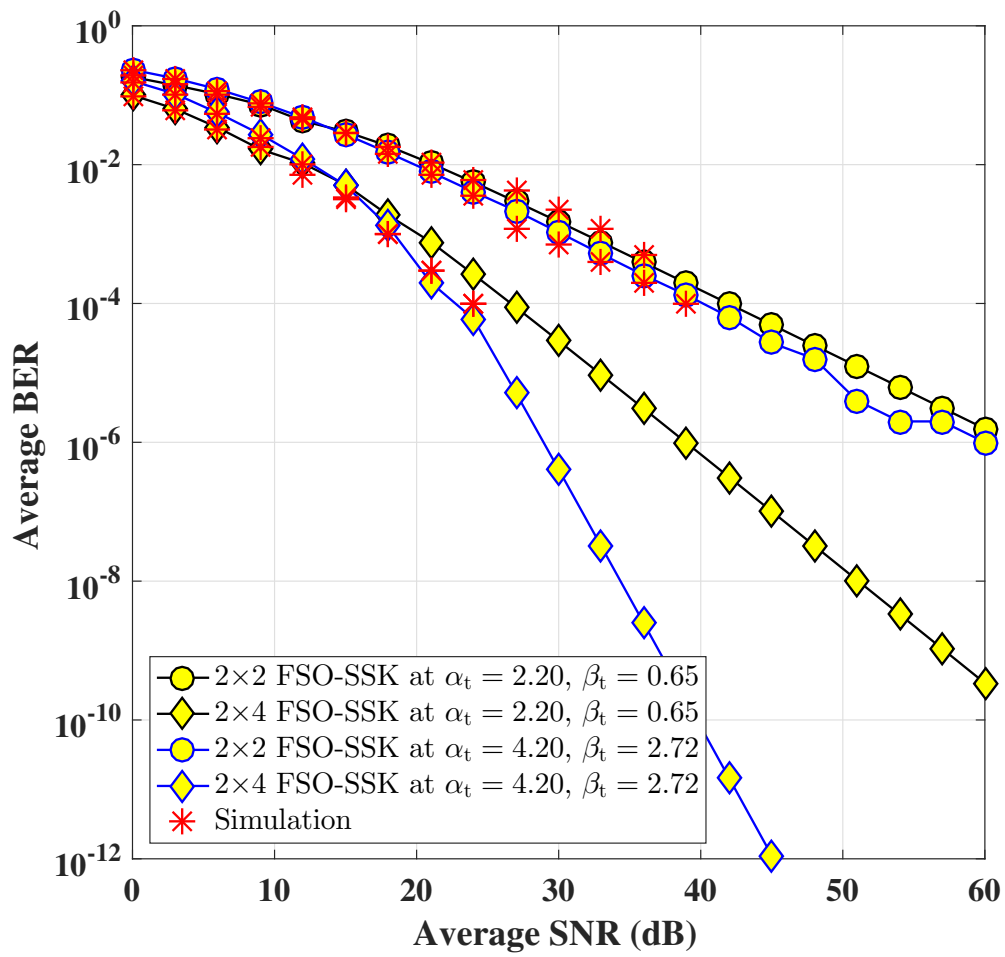
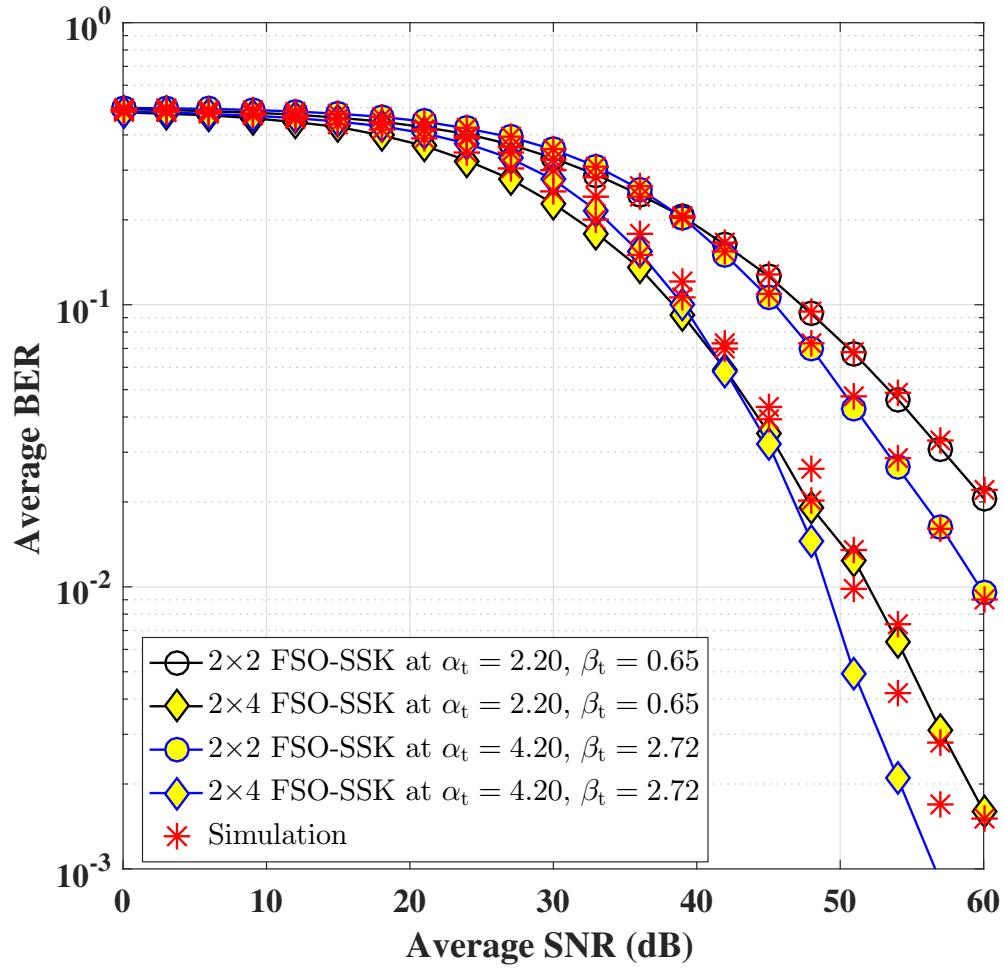


Figure 6.3 (a) Average bit error rate of MIMO FSO link under Gamma-Gamma distribution in the absence of pointing error.



**Figure 6.3 (b)** Average bit error rate of MIMO FSO link under Gamma-Gamma distribution in the presence of pointing error ( $\xi = 0.8565$ )



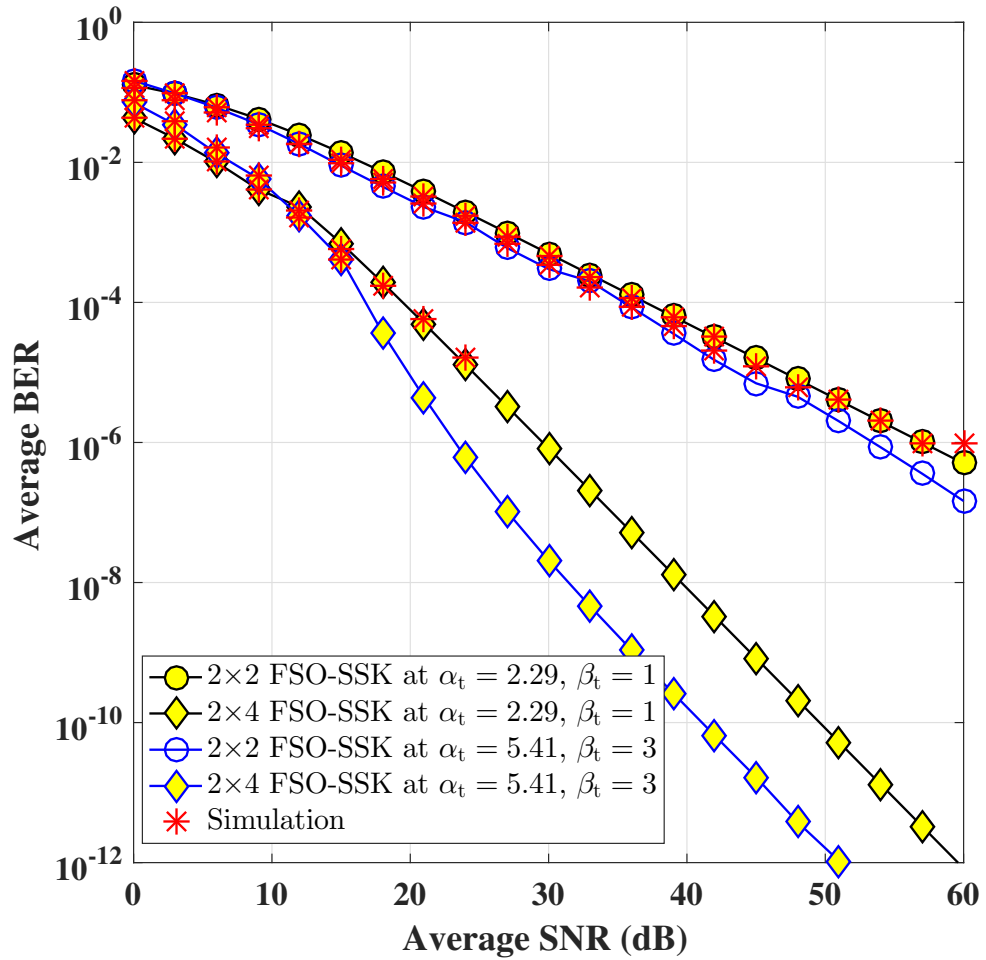


Figure 6.3 (c) Average bit error rate of MIMO FSO link under Málaga distribution in the absence of pointing error.

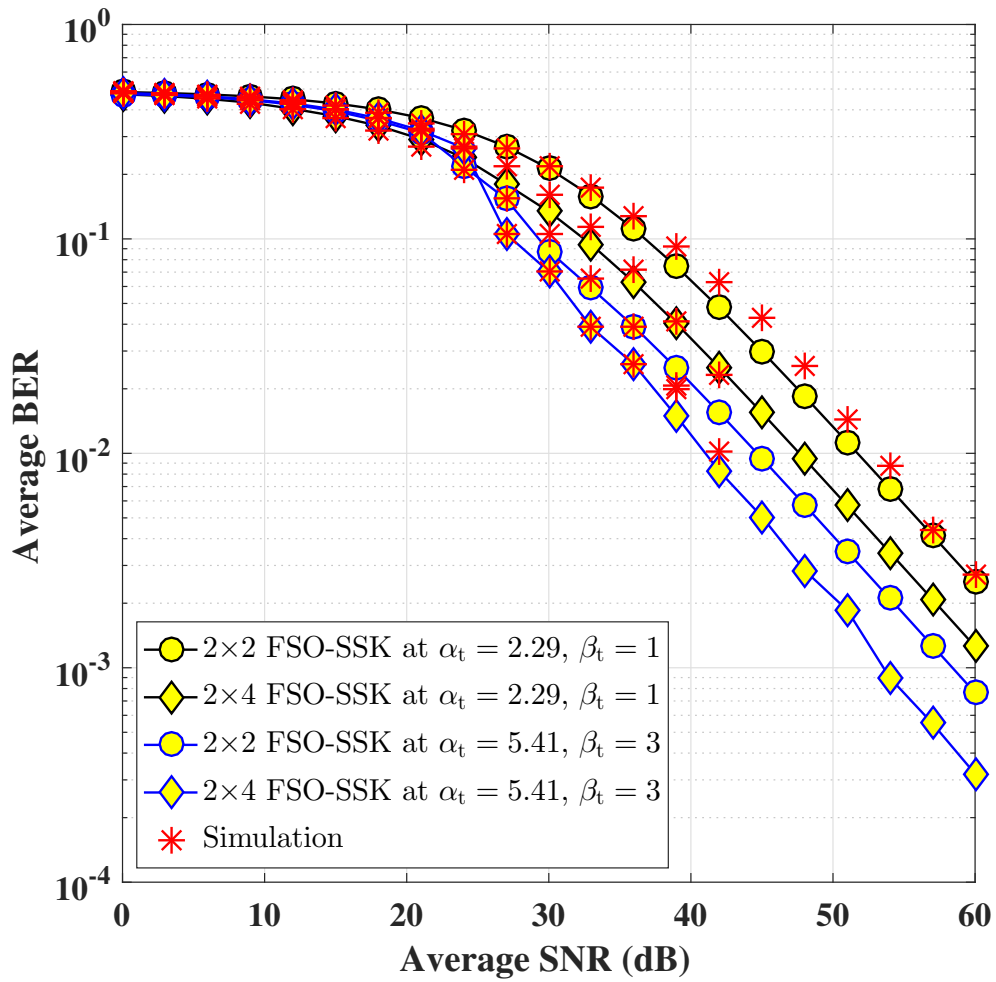


Figure 6.3 (d) Average bit error rate of MIMO FSO link under Málaga distribution in presence of pointing error ( $\xi = 0.8565$ )

FIGURE 6.3: Average bit error rate of the SSK-SC-FSO based MIMO FSO link employing SSK scheme at the transmitter end and selection combining at the receiver end with different atmospheric turbulence conditions in the absence and presence of pointing error regime.

TABLE 6.2: Comparison of ABER for different FSO communication system under Gamma-Gamma statistical distribution with pointing error ( $\xi = 0.8565$ ) for turbulence parameters  $\alpha_t = 2.20$  and  $\beta_t = 0.65$ .

System topology	ToD	Avg. SNR	No th	Fixed th	Optimal th
SISO FSO	--	60 dB	$1.8 \times 10^{-2}$	-	-
MISO FSO	STBC	60 dB	$3.6 \times 10^{-4}$	-	-
MISO FSO	SSK	60 dB	$9.2 \times 10^{-2}$	-	-
SIMO FSO	SEC	60 dB	-	$4.5 \times 10^{-6}$	$4.3 \times 10^{-6}$
MIMO FSO	STBC-SEC	60 dB	-	$8.0 \times 10^{-11}$	$7.0 \times 10^{-11}$
MIMO FSO	SSK-SC	60 dB	$1.6 \times 10^{-3}$	-	-
ToD: Type of Diversity					

TABLE 6.3: Comparison of ABER for different FSO communication system under Málaga statistical distribution with pointing error ( $\xi = 0.8565$ ) for turbulence parameters  $\alpha_t = 2.29$  and  $\beta_t = 1$ .

System topology	ToD	Avg. SNR	No th	Fixed th	Optimal th
SISO FSO	--	60 dB	$1.1 \times 10^{-2}$	-	-
MISO FSO	STBC	60 dB	$1.6 \times 10^{-4}$	-	-
MISO FSO	SSK	60 dB	$1.7 \times 10^{-1}$	-	-
SIMO FSO	SEC	60 dB	-	$3.2 \times 10^{-6}$	$1.6 \times 10^{-6}$
MIMO FSO	STBC-SEC	60 dB	-	$1.6 \times 10^{-6}$	$4.6 \times 10^{-7}$
MIMO FSO	SSK-SC	60 dB	$1.2 \times 10^{-3}$	-	-
ToD: Type of Diversity					

Finally, we have provided a comparison of ABER for different FSO links under the presence of pointing error in Table 6.2 and Table 6.3, respectively. For this comparison, we have considered all estimated FSO links are experiencing both strong atmospheric turbulence and pointing error. We have also considered a single average SNR of 60 dB for this comparison. This comparison signifies that an STBC-SEC-based MIMO FSO link produces the best outcome in presence of pointing error.

## 6.6 Chapter summary

In this chapter, an SSK-FSO link has been set up and the analytical expression of ABER has been derived. Next, an architectural setup of a MIMO FSO link has been investigated which employs SSK modulation as transmit diversity and the SC as receive diversity. The analytical framework of an upper tight bound ABER of the SSK-SC-FSO system has also been derived in this chapter. For the numerical analysis of two links, we have considered the GG and the general Málaga statistical distribution. The effect of misalignment fading has also been incorporated into the analysis. Besides the mathematical framework of the performance metric, we have presented the numerical results by 2D graphical representation for both statistical distributions. Next, we have compared our resultant metric with the numerical results of Chapter 3 and Chapter 5 for the SSK-FSO link and SSK-SC-FSO link, respectively. From this comparison, it can be stated that an STBC-FSO type MISO FSO system yields a better output than an SSK-FSO type MISO FSO communication system under any weather regime. Also, an STBC-SEC-FSO system is more advantageous than an SSK-SC-FSO system. The prime difference between the SSK and STBC type transmitting systems is that in the case of an SSK type system, only one transmitter is in ON condition during the transfer of message signal from the transmitter to the destination end, and the rest of the transmitter remains in OFF state;. In contrast, in the case of STBC, all transmitting antennas are kept ON at the time of signal sharing between the transmitter and receiver terminal.

# Chapter 7

## Summary of Results and Future Works

### 7.1 Summary of results

In this thesis, we have investigated the performance of a terrestrial FSO communication system to improve the QoS by employing the transmitter and receiver diversity scheme in the fundamental FSO link. Our discussion begins with a simple FSO link with a SISO structure, where we have derived the basic performance metrics to assess the performance of a single FSO link without employing any diversity technique under different turbulence conditions. Throughout our investigation, we have considered the IM/DD technique for simple architecture and low cost. We have used GG statistical distribution, which perfectly models the moderate to strong atmospheric turbulence condition. Further, in constructing a more generalized analytical model, Málaga distribution has been adopted for the same.

Next, diversity techniques have been employed in an FSO system. It starts with the Alamouti STBC technique to achieve the transmitter diversity in the resulting MISO FSO system. The investigation has been extended for the SIMO FSO system

TABLE 7.1: Comparison of performance metrics for different diversity aided FSO communication systems under Gamma-Gamma turbulence ( $\alpha_t = 4.20$ ,  $\beta_t = 2.72$ ) in the absence and presence of pointing error ( $\xi = 0.5607$ ) for SNR = 30 dB

System topology	Tx /Rx diversity	Outage probability		Bit error rate		Capacity (b/s/Hz)	
		NP	WP	NP	WP	NP	WP
SISO	--	$2.1 \times 10^{-3}$	$2.6 \times 10^{-1}$	$7.0 \times 10^{-4}$	$1.2 \times 10^{-1}$	9.05	4.91
MISO	STBC	$5.3 \times 10^{-7}$	$4.4 \times 10^{-2}$	$1.5 \times 10^{-6}$	$2.3 \times 10^{-2}$	11.56	6.31
SIMO	SEC	$6.8 \times 10^{-4}$	$1.8 \times 10^{-2}$	$2.8 \times 10^{-6}$	$1.8 \times 10^{-3}$	9.07	8.53
SIMO*	SEC	$6.2 \times 10^{-11}$	$5.7 \times 10^{-3}$	$4.7 \times 10^{-8}$	$2.4 \times 10^{-4}$	10.85	8.72

NP: No Pointing , WP: With Pointing, SIMO\*: SIMO with optimal threshold.

employing the SEC scheme as a receiver diversity technique. The further extension involves employing both the Alamouti STBC and SEC as transmitter and receiver diversity techniques to construct a MIMO FSO system. Lastly, we have used SSK, a relatively unexplored transmit diversity scheme and the SC receiver diversity technique to develop the MIMO FSO link, and compared the performance of both of the systems.

We analyzed the performances of FSO communication systems of different network topologies (SISO, SIMO, MISO, and MIMO) under different atmospheric turbulence conditions and pointing errors. For this, we first derived the closed-form expressions for the overall PDF, CDF or MGF (where relevant) of the FSO link. Next, we derived the closed-form expressions for the different performance metrics related to the FSO communication system, such as OP, ABER, and average capacity. Analytical results of the measuring metrics for all the cases, as mentioned above have been validated, through Monte Carlo simulation results.

In Table 7.1, we provide typical results for the different performance metrics under various FSO systems in the absence and presence of pointing errors. Here, the system is assumed to experience weak atmospheric turbulence conditions with  $\alpha_t = 4.20$ ,  $\beta_t = 2.72$ , and high pointing error with  $\xi = 0.5607$ . Also, a single average SNR of 30 dB is considered.

**OP:** When the SISO FSO link works under a pointing error condition, the OP of the link is  $10^{-2}$  times deteriorates than the absence of a pointing error condition. After employing the transmitter diversity scheme, the OP of the MISO FSO link improves  $10^{-4}$  order less that of a SISO FSO link without a pointing error condition and becomes  $10^{-1}$  order less in the presence of pointing error. Here, it also observed that the OP of the MISO FSO link again deteriorates  $10^{-5}$  order less in the presence of pointing error conditions than in the absence of pointing error conditions. The OP improves significantly in the presence of pointing error condition for SIMO FSO link than MISO and SISO FSO system under fixed and optimal switching threshold conditions. Also, in the absence of a pointing error, when the MISO FSO system works under the optimum switching threshold, the OP of the system improves  $10^{-8}$  order less that of a SISO FSO link. But, under pointing error conditions, the OP of the SIMO FSO system deteriorates under fixed and optimum switching threshold conditions as SIOS and MISO link. Results clearly indicate performance degradation of all the systems in the presence of pointing errors.

**ABER:** Under the pointing error condition, the ABER of the SISO FSO link deteriorates  $10^{-3}$  times than in the absence of a pointing error. On the other side, in the absence of a pointing error condition, the resultant ABER improves more than  $10^{-3}$  order less by the Alamouti STBC-based MISO FSO system than a single FSO link, and in the presence of a pointing error condition, it becomes  $10^{-1}$  times. Still, the resultant ABER is significantly low in the presence of pointing error conditions under the MISO FSO link, and it deteriorates nearly  $10^{-4}$  order than the absence of pointing error condition. Although, a MISO FSO communication system produces good quality outcomes than a SISO FSO system under the absence and presence of pointing error conditions. Next, after incorporating the receiver diversity in the primary FSO system, the ABER of the SIMO FSO link significantly improved than the SISO and MISO FSO link under optimum switching threshold conditions for both the absence and presence of pointing error regime. The resultant ABER gets improved by  $10^{-2}$  order less when the system attends the optimum switching

threshold rather than a fixed switching threshold in the absence of pointing error conditions, and it becomes nearly  $10^{-1}$  times in the presence of pointing error. So, the ABER of the SIMO FSO communication system significantly improved under the optimum switching threshold condition for both cases of pointing error scenarios. Next, we investigate when a SIMO FSO link works with a fixed switching threshold condition, that provides little bit poor output than a MISO FSO link under absence of a pointing error condition. It is become reverse when the system attends the optimum switching threshold condition. In the presence of pointing error conditions SIMO FSO system gives  $10^{-1}$  order less and  $10^{-2}$  order less better outcomes than MISO FSO link under fixed and optimum switching threshold condition, respectively. Hence, it may state that a MISO FSO link produces better outcomes than a SISO FSO link as well as a MISO FSO link too. Thus, the receiver diversity scheme may be more beneficial to produce the ABER of the system than a transmitter diversity scheme in the FSO communication system for all the cases of pointing error conditions.

**Average capacity:** In presence of a pointing error, the average capacity of the SISO FSO link drops 4.14 bits than in the absence of a pointing error condition. The average capacity increases under the MISO FSO link by 2.51 bits than a SISO FSO link without a pointing error condition; it also increases by 1.4 bits in the presence of a pointing error. So, it ensures that in the presence of a pointing error condition, the rate of changes of the average capacity is better than in the absence of pointing error conditions when the system employs transmit diversity scheme. On the other side, for the MISO FSO link, the average capacity decreases by 5.25 bits in the presence of a pointing error than in the absence of a pointing error condition. After incorporating the receiver diversity scheme in the primary FSO link, the average capacity of the SIMO FSO link changes a very minimal to the SISO FSO link with a fixed switching threshold in the absence of pointing error conditions. The average capacity of the SIMO FSO link gets enhanced from 9.07 b/s/Hz to 10.85 b/s/Hz under the optimum switching threshold, which is much better than a SISO FSO



communication system. In the presence of a pointing error, the average capacity significantly improved than a SISO FSO link. The MISO FSO system provides 8.53 b/s/Hz and 8.72 b/s/Hz average capacity under a fixed switching threshold and optimum switching conditions, respectively. In the presence of a pointing error condition, the average capacity of the SIMO FSO system is enhanced by 3.62 bits than a SISO FSO link, while in the MISO FSO link, it was just 1.4 bits. So, the receiver diversity scheme is more beneficial than a transmit diversity scheme for this particular parameter in the presence of a pointing error condition. On the other hand, it is vice versa in the absence of pointing error conditions.

**Comparison of MIMO configurations:** The results are presented in Table 7.2, where both transmitter and receiver diversity schemes are employed in the fundamental FSO communication system. The ABER of the STBC-SEC-based MIMO FSO system rapidly deteriorates in the presence of pointing errors for both switching threshold conditions. The ABER deteriorates  $10^{-6}$  and  $10^{-8}$  times under 10 dB of fixed and optimum switching threshold conditions, respectively. Next, the SSK-SC-based MIMO FSO system gives poor outcomes than the STBC-SEC-based MIMO FSO system for both the absence and presence of pointing error conditions. The SSK-SC-based MIMO FSO system provides  $10^{-4}$  and  $10^{-8}$  times poor outcomes than the STBC-SEC-based MIMO FSO communication system in the absence of pointing error under fixed and optimum switching threshold, and it becomes  $10^{-4}$  and  $10^{-6}$  times in the presence of a pointing error condition. Besides, it also observed that under the pointing error condition, all systems produce comparatively poor quality outcomes than without the pointing error condition.

However, in the same atmospheric turbulence scenario, SISO FSO, MISO FSO, and SIMO FSO communication systems [Table 7.1] provide less ABER than STBC-SEC-based MIMO FSO systems in the absence and presence of pointing error conditions. In the presence of pointing error conditions, it examined that the SSK-SC-based MIMO FSO system provides unsatisfactory outcomes than all of the other types of MIMO FSO systems, while in the absence of pointing error conditions, it is better

TABLE 7.2: Comparison of ABER for different MIMO FSO communication systems under Gamma-Gamma statistical distribution without and with ( $\xi = 0.5607$ ) pointing error for  $\alpha_t = 4.20$ ,  $\beta_t = 2.72$ , and average SNR = 30 dB

System topology	Tx /Rx diversity	NP	WP
MIMO	STBC-SEC	$5.3 \times 10^{-11}$	$1.5 \times 10^{-5}$
MIMO*	STBC-SEC	$9.3 \times 10^{-15}$	$1.2 \times 10^{-7}$
MIMO	SSK-SC	$4.0 \times 10^{-7}$	$2.3 \times 10^{-1}$
MIMO*: MIMO with optimal threshold.			

than the SISO FSO and MISO FSO link. From this observation, it was noticed that the performance of an STBC-SEC-based MIMO FSO system is much better than the SSK-SC-based MIMO FSO communication system under all weather conditions. We may finally conclude that the QoS of the FSO communication system gets enhanced when the fundamental FSO communication system utilizes a transmitter or receiver diversity scheme. Furthermore, atmospheric turbulence and pointing error can be mitigated most efficiently by incorporating the transmitter and receiver diversity techniques in the FSO system.

## 7.2 Future works

FSO communication is one of the key technology for upcoming B5G or 6G wireless standards. The work presented in this thesis is meant to improve the physical layer performance of the FSO communication system. As performance improvement is realized through employing diversity, a direct extension of the work is to explore other possible transmit and receive diversity combinations. For example, the generalized selective combining (GSC) is a low-complexity diversity scheme but is useful if a higher number of branches are available to exploit. GSC may be incorporated into the fundamental FSO link to improve the system's physical layer performance.

The links considered in this thesis are uncoded. First, no channel coding is considered for error mitigation. It is interesting to study the benefits of different MIMO

configurations of a coded FSO system, especially how these benefits are translated to the upper layer, changing the figure of merits such as frame error rates. Precoding schemes are also another possible extension. Researchers can incorporate zero-forcing beamforming (ZFB) or random unitary beamforming (RUB) type linear precoding strategies into the FSO system.

The work in this thesis is also useful when the FSO links are applied across different verticals. We consider two of them here, intelligent reflecting surface (IRS) and visible light communication (VLC).

Mirrors or shiny building surfaces can act as a reflector to an incident FSO beam. An array of such reflectors can overcome the shadowing issue in fixed FSO wireless links. Simultaneous transmission and reflection (STAR) type FSO IRS nodes have been considered recently, which can broaden the coverage area further. Unmanned aerial vehicles (UAVs) can also act as IRS nodes. Performance analysis of all these novel FSO IRS-based applications with MIMO possibilities may be carried out using the framework laid out in this thesis.

Light as a data carrier has been investigated for short-range indoor wireless scenarios, and one such popular implementation is light fidelity (LiFi). LiFi uses VLC technology, and its throughput will be immensely benefitted with the introduction of MIMO. Vehicular VLC is already a hot research topic in the domain of intelligent transportation system development. The performance of a MIMO VLC link is definitely worthy of research.

# Appendix A

## Channel Characterisation with Alamouti STBC

Let us consider the system transmit a couple of symbol  $s_1$  and  $s_2$  by two transmitter antennas based on Alamouti-STBC scheme. Over the GG fading channel two transmit antennas are transmitted the symbol as follows

$$S = \begin{pmatrix} s_1 & -s_2^* \\ s_2 & s_1^* \end{pmatrix} \quad (\text{A.1})$$

where,  $(\cdot)^*$  indicates the complex conjugate of the symbol. At the receiver terminal receiver aperture received the electrical signal in the form of

$$[y_1, y_2] = \eta \begin{pmatrix} h_1 & h_2^* \\ h_2 & -h_1^* \end{pmatrix} [s_1, s_2] + [n_1, n_2] \quad (\text{A.2})$$

where,  $\eta$  is known as optical-to-electrical conversation rate, and  $h_i$  is the channel gain co-efficient of each path. After some mathematical manipulation the input-output relation for detection the transmitted beam as follows

$$r_i = \eta h^2 s_i + n_i \quad (\text{A.3})$$

where,  $r_1 = y_1 h_1 + y_2^* h_2$ ,  $r_2 = y_1 h_2 + y_2^* h_1$ ,  $h^2 = h_1^2 + h_2^2$ , and  $n_i$  is the AWGN element with zero-mean and variance is  $\sigma^2$ . The received SNR of per symbol can be written as

$$\gamma = \frac{\eta^2 E_s^2 h}{\sigma^2} \quad (\text{A.4})$$

where,  $E_s$  is the energy of the each transmitted symbol. If the average SNR of the system is  $\bar{\gamma} = \frac{\eta^2 E_s}{\sigma^2}$ , then the overall received SNR can be expressed as

$$\begin{aligned} \gamma &= \bar{\gamma} h_1^2 + \bar{\gamma} h_2^2 \\ &= \gamma_1 + \gamma_2 \end{aligned} \quad (\text{A.5})$$

Thus, the overall MGF of the system in terms of received SNR can be represented as

$$\begin{aligned} \mathcal{M}_{\gamma_i}(s) &= E\{\exp(-s\gamma_i)\} \\ &= \mathcal{M}_{\gamma_1}(s) \times \mathcal{M}_{\gamma_2}(s) \end{aligned} \quad (\text{A.6})$$

where,  $E\{\cdot\}$  is the expectation operator.

# Appendix B

## Closed-form Expression of BER using MGF

We derive a closed-form expression for (3.4). The standard integral form of the equation for average BER is given by

$$P_e = \int_0^\infty P_e(x) f_x(X) dx \quad (\text{B.1})$$

where,  $f_x(X)$  is the PDF of the turbulence channel, and the probability of error function is indicate by the symbol  $P_e(x)$ . The probability of error function can be represented by the integral form of the Gaussian-Q function as [40]

$$P_e(x) = Q(X) = \frac{1}{\pi} \int_0^{\frac{\pi}{2}} \exp\left(-\frac{X^2}{2 \sin^2 \theta}\right) d\theta \quad (\text{B.2})$$

Henceforth, the probability of error function for OOK modulation scheme under AWGN channel may be written as

$$P_e^{OOK}(X) = \frac{1}{\pi} \int_0^{\frac{\pi}{2}} \exp\left(-\frac{x}{2 \sin^2 \theta}\right) d\theta \quad (\text{B.3})$$

Inserting (B.3) in (B.1), we can rewritten the (B.1) as

$$P_e^{OOK} = \int_0^\infty \left[ \frac{1}{\pi} \int_0^{\frac{\pi}{2}} \exp\left(-\frac{x}{2\sin^2\theta}\right) d\theta \right] f_x(X) dx \quad (\text{B.4})$$

Next, by changing the order of integral of the above equation, (B.4) may be rewritten as

$$P_e^{OOK} = \frac{1}{\pi} \int_0^{\frac{\pi}{2}} \left[ \int_0^\infty \exp\left(-\frac{x}{2\sin^2\theta}\right) f_x(X) dx \right] d\theta \quad (\text{B.5})$$

On the other hand, from the mathematical definition of MGF, we have

$$\mathcal{M}_x(s) = \int_0^\infty \exp(-xs) f_x(X) dx \quad (\text{B.6})$$

Now, established the link between (B.5) and (B.6) we can derived the a closed-form equation as follows

$$P_e^{OOK} = \frac{1}{\pi} \int_0^{\frac{\pi}{2}} \mathcal{M}_x\left(-\frac{1}{2\sin^2\theta}\right) d\theta \quad (\text{B.7})$$

# Appendix C

## Closed-form PDF for GG Turbulence with SSK

The probability density function for the irradiance ( $I$ ) of the travelling optical beam can be represented by GG statistical distribution with the help of (2.13) and [94, Eq.(8.4.23.1)]

$$f_I(I) = \frac{(\alpha_t \beta_t)^{\frac{(\alpha_t + \beta_t)}{2}}}{\Gamma(\alpha_t) \Gamma(\beta_t)} (I)^{\frac{(\alpha_t + \beta_t)}{2} - 1} G_{0\ 2}^{2\ 0} \left[ \alpha_t \beta_t I \left| \begin{matrix} - \\ \frac{\alpha_t - \beta_t}{2}, \frac{\beta_t - \alpha_t}{2} \end{matrix} \right. \right] \quad (\text{C.1})$$

Consider,  $X$  and  $Y$  are the two i.i.d. RVs, and a new variable  $U$  related as  $U = X - Y$ , then the PDF of new variable  $U$  is the cross correlation between the PDF of RVs. Assume link between irradiance and the RV [48] as  $X \triangleq I_j$  and  $Y \triangleq I_i$ , and  $Z \triangleq I_j - I_i = X - Y$ ; thus,  $|Z| = U$ . Hence, the pdf of  $Z$  can be defined as



$$f_Z(z) = \begin{cases} \int_0^\infty f_X(z+y)f_Y(y)dy, & z \geq 0 \\ \int_{-z}^\infty f_X(z+y)f_Y(y)dy, & z < 0 \end{cases} \quad (\text{C.2})$$

while we have consider only positive sided RV, where  $f_Z(u) = f_Z(z)$  for  $z \geq 0$  and  $f_Z(-u) = f_Z(z)$  for  $z < 0$  shown in (C.2). Using the (C.1) and (C.2) we may be defined following couple of equation as

$$f_Y(y) = \frac{(\alpha_t \beta_t)^{\frac{(\alpha_t + \beta_t)}{2}}}{\Gamma(\alpha_t) \Gamma(\beta_t)} (y)^{\frac{(\alpha_t + \beta_t)}{2} - 1} G_{0 \ 2}^{2 \ 0} \left[ \alpha_t \beta_t y \left| \frac{\alpha_t - \beta_t}{2}, \frac{\beta_t - \alpha_t}{2} \right. \right] \quad (\text{C.3})$$

$$f_X(z+y) = \frac{(\alpha_t \beta_t)^{\frac{(\alpha_t + \beta_t)}{2}}}{\Gamma(\alpha_t) \Gamma(\beta_t)} (z+y)^{\frac{(\alpha_t + \beta_t)}{2} - 1} G_{0 \ 2}^{2 \ 0} \left[ \alpha_t \beta_t (z+y) \left| \frac{\alpha_t - \beta_t}{2}, \frac{\beta_t - \alpha_t}{2} \right. \right] \quad (\text{C.4})$$

Plugin (C.3) and (C.4) into (C.2), can be written the pdf of  $Z$  as follows [48]

$$f_Z(z) = \left( \frac{(\alpha_t \beta_t)^{\frac{(\alpha_t + \beta_t)}{2}}}{\Gamma(\alpha_t) \Gamma(\beta_t)} \right)^2 \int_0^\infty (z+y)^{\frac{(\alpha_t + \beta_t)}{2} - 1} G_{0 \ 2}^{2 \ 0} \left[ \alpha_t \beta_t (z+y) \left| \frac{\alpha_t - \beta_t}{2}, \frac{\beta_t - \alpha_t}{2} \right. \right] \times (y)^{\frac{(\alpha_t + \beta_t)}{2} - 1} G_{0 \ 2}^{2 \ 0} \left[ \alpha_t \beta_t y \left| \frac{\alpha_t - \beta_t}{2}, \frac{\beta_t - \alpha_t}{2} \right. \right] dy \quad (\text{C.5})$$

with the help of [94, Eq.(8.2.2.15, 2.24.1.3)] (C.5) can be rewritten as

$$f_Z(z) = \frac{\alpha_t \beta_t}{(\Gamma(\alpha_t)\Gamma(\beta_t))^2} \left[ \sum_{p=0}^{\infty} \frac{(-\alpha_t \beta_t z)^p}{p!} G_{3 \ 3}^{2 \ 3} \left[ 1 \left| \begin{matrix} 1 - \frac{\alpha_t + \beta_t}{2}, \frac{4+2p-3\alpha_t - \beta_t}{2}, \frac{4+2p-3\beta_t - \alpha_t}{2} \\ \frac{\alpha_t - \beta_t}{2}, \frac{\beta_t - \alpha_t}{2}, \frac{2+2p - \alpha_t - \beta_t}{2} \end{matrix} \right. \right] \right] \quad (\text{C.6})$$

By following the same way we also find the mathematical equation for  $f_Z(-z)$ . So, the corresponding PDF for 'U' may be expressed  $f_U(u) = f_Z(z) + f_Z(-z)$  as

$$f_Z(z) = \frac{2\alpha_t \beta_t}{(\Gamma(\alpha_t)\Gamma(\beta_t))^2} \left[ \sum_{p=0}^{\infty} \frac{(-\alpha_t \beta_t z)^p}{p!} G_{3 \ 3}^{2 \ 3} \left[ 1 \left| \begin{matrix} 1 - \frac{\alpha_t + \beta_t}{2}, \frac{4+2p-3\alpha_t - \beta_t}{2}, \frac{4+2p-3\beta_t - \alpha_t}{2} \\ \frac{\alpha_t - \beta_t}{2}, \frac{\beta_t - \alpha_t}{2}, \frac{2+2p - \alpha_t - \beta_t}{2} \end{matrix} \right. \right] \right] \quad (\text{C.7})$$

Next, the overall PDF of the system in terms of ene-to-end instantaneous SNR ( $\gamma$ ) and average SNR ( $\bar{\gamma}$ ) can be expressed as

$$f_\gamma(\gamma) = \frac{\alpha_t \beta_t}{(\Gamma(\alpha_t)\Gamma(\beta_t))^2 \sqrt{\bar{\gamma}}} \left[ \sum_{p=0}^{\infty} \frac{\left(\frac{-\alpha_t \beta_t}{\sqrt{\bar{\gamma}}}\right)^p}{p!} (\sqrt{\bar{\gamma}})^{(p-1)} G_{3 \ 3}^{2 \ 3} \left[ 1 \left| \begin{matrix} 1 - \frac{\alpha_t + \beta_t}{2}, \frac{4+2p-3\alpha_t - \beta_t}{2}, \frac{4+2p-3\beta_t - \alpha_t}{2} \\ \frac{\alpha_t - \beta_t}{2}, \frac{\beta_t - \alpha_t}{2}, \frac{2+2p - \alpha_t - \beta_t}{2} \end{matrix} \right. \right] \right] \quad (\text{C.8})$$

## Appendix D

# PDF of GG Turbulence with SSK in Presence of Pointing Error

To expressed the PDF of the MISO-FSO with the effect of pointing error and GG fading turbulence under SSK transmit diversity scheme, we can develop following two equation with the help of (2.36) and (C.2) as follows

$$f_Y(y) = KG_1^3 \left[ \omega y \Big|_{\xi^2-1, \alpha_t-1, \beta_t-1}^{\xi^2} \right] \quad (\text{D.1})$$

$$f_X(z + y) = KG_1^3 \left[ \omega(z + y) \Big|_{\xi^2-1, \alpha_t-1, \beta_t-1}^{\xi^2} \right] \quad (\text{D.2})$$

where,  $K = \frac{\xi^2 \alpha_t \beta_t}{A_0 h_l \Gamma(\alpha_t) \Gamma(\beta_t)}$ , and  $\omega = \frac{\alpha_t \beta_t}{A_0 I_l}$ , where,  $A_0$  is the constant parameter related with pointing error of the system and  $I_l$  is known as amount of power level losses due to atmospheric turbulence, some time it is called the path loss.

Plugin (D.1) and (D.2) into (C.2), can be written the pdf of  $Z$  as follows

$$f_Z(z) = K^2 \int_0^\infty G_{1\ 3}^{3\ 0} \left[ \omega(z+y) \middle|_{\xi^2-1, \alpha_t-1, \beta_t-1}^{\xi^2} \right] G_{1\ 3}^{3\ 0} \left[ \omega y \middle|_{\xi^2-1, \alpha_t-1, \beta_t-1}^{\xi^2} \right] dy \quad (\text{D.3})$$

with the help of [94, Eq.(2.24.1.3)], the above equation can be written as

$$f_Z(z) = \frac{K^2}{\omega} \left[ \sum_{p=0}^{\infty} \frac{(-\omega z)^p}{p!} G_{5\ 5}^{3\ 4} \left[ 1 \middle|_{\xi^2-1, \alpha_t-1, \beta_t-1, p-\xi^2, p}^{0, 1+p-\xi^2, 1+p-\alpha_t, 1+p-\beta_t, \xi^2} \right] \right] \quad (\text{D.4})$$

and after some mathematical manipulation the PDF of the system in terms of end-to-end SNR can be expressed with the help of (D.4) as follows

$$f_\gamma(\gamma) = \frac{K^2}{\omega \sqrt{\gamma}} \left[ \sum_{p=0}^{\infty} \frac{\left(\frac{-\omega}{\sqrt{\gamma}}\right)^p}{p!} (\sqrt{\gamma})^{(p-1)} G_{5\ 5}^{3\ 4} \left[ 1 \middle|_{\xi^2-1, \alpha_t-1, \beta_t-1, p-\xi^2, p}^{0, 1+p-\xi^2, 1+p-\alpha_t, 1+p-\beta_t, \xi^2} \right] \right] \quad (\text{D.5})$$

# Appendix E

## Closed-form Expression for $\mathcal{J}_1$ and $\mathcal{J}_2$

Closed-form equation for  $\mathcal{J}_1$ : we have,

$$\mathcal{J}_1 = \frac{(\alpha_t \beta_t)^{\frac{(\alpha_t + \beta_t)}{2}}}{2\Gamma(\alpha_t)\Gamma(\beta_t)(\bar{\gamma})^{\frac{(\alpha_t + \beta_t)}{4}}} \int_0^{\gamma_{th}} (\gamma)^{\frac{(\alpha_t + \beta_t)}{4} - 1} \ln(1 + \gamma) G_{0 \ 2}^{2 \ 0} \left[ \alpha_t \beta_t \sqrt{\frac{\gamma}{\bar{\gamma}}} \middle| \begin{matrix} \cdot \\ \frac{\alpha_t - \beta_t}{2}, \frac{\beta_t - \alpha_t}{2} \end{matrix} \right] d\gamma \quad (\text{E.1})$$

Using [95, eq. (1.511)] the Taylor series expansion of  $\ln(1 + \gamma)$ , can be derived as the following

$$\ln(1 + \gamma) = \sum_{p=1}^{\infty} \frac{(-1)^{p+1}}{p} \gamma^p = \gamma - \frac{\gamma^2}{2} + \frac{\gamma^3}{3} + O(\gamma^4). \quad (\text{E.2})$$

with the help of (E.2), (E.1) can be rewritten as

$$\mathcal{J}_1 = \frac{(\alpha_t \beta_t)^{\frac{(\alpha_t + \beta_t)}{2}}}{2\Gamma(\alpha_t)\Gamma(\beta_t)(\bar{\gamma})^{\frac{(\alpha_t + \beta_t)}{4}}} \sum_{p=1}^{\infty} \frac{(-1)^{p+1}}{p} \int_0^{\gamma_{th}} (\gamma)^{2p + \left(\frac{\alpha_t + \beta_t}{4}\right) - 1} \times G_{0\ 2}^{2\ 0} \left[ \alpha_t \beta_t \sqrt{\frac{\gamma}{\bar{\gamma}}} \middle| \frac{\alpha_t - \beta_t}{2}, \frac{\beta_t - \alpha_t}{2} \right] d\gamma \quad (\text{E.3})$$

further, using [96, eq. (26)] the closed-form equation of (E.3) can be expressed as

$$\mathcal{J}_1 = \frac{(\alpha_t \beta_t)^{\frac{(\alpha_t + \beta_t)}{2}}}{\Gamma(\alpha_t)\Gamma(\beta_t)(\bar{\gamma})^{\frac{(\alpha_t + \beta_t)}{4}}} \sum_{p=1}^{\infty} \frac{(-1)^{p+1}}{p} (\sqrt{\gamma_{th}})^{2p + \left(\frac{\alpha_t + \beta_t}{2}\right)} \times G_{1\ 3}^{2\ 1} \left[ \alpha_t \beta_t \sqrt{\frac{\gamma_{th}}{\bar{\gamma}}} \middle| \frac{\alpha_t - \beta_t}{2}, \frac{\beta_t - \alpha_t}{2}, -2p - \left(\frac{\alpha_t + \beta_t}{2}\right) \right] \quad (\text{E.4})$$

**Closed-form equation for  $\mathcal{J}_2$ :** we have,

$$\mathcal{J}_2 = \frac{(\alpha_t \beta_t)^{\frac{(\alpha_t + \beta_t)}{2}}}{2\Gamma(\alpha_t)\Gamma(\beta_t)(\bar{\gamma})^{\frac{(\alpha_t + \beta_t)}{4}}} \int_0^{\infty} (\gamma)^{\left(\frac{\alpha_t + \beta_t}{4}\right) - 1} \ln(1 + \gamma) G_{0\ 2}^{2\ 0} \left[ \alpha_t \beta_t \sqrt{\frac{\gamma}{\bar{\gamma}}} \middle| \frac{\alpha_t - \beta_t}{2}, \frac{\beta_t - \alpha_t}{2} \right] d\gamma \quad (\text{E.5})$$

utilises the link between Meijer's  $G$  function  $G[\cdot]$  and  $\ln(\cdot)$  in [94, eq. (8.4.6.5)] as

$$\ln(1 + \gamma) = G_{2\ 1}^{1\ 2} \left[ \gamma \middle| \begin{matrix} 1, 1 \\ 1, 0 \end{matrix} \right] \quad (\text{E.6})$$

the equation (E.5) may be presented as

$$\mathcal{J}_2 = \frac{(\alpha_t \beta_t)^{\frac{(\alpha_t + \beta_t)}{2}}}{2\Gamma(\alpha_t)\Gamma(\beta_t)(\tilde{\gamma})^{\frac{(\alpha_t + \beta_t)}{4}}} \int_0^\infty (\gamma)^{\frac{(\alpha_t + \beta_t)}{4} - 1} G_{2 \ 1}^{1 \ 2} \left[ \gamma \middle| \begin{matrix} 1,1 \\ 1,0 \end{matrix} \right] G_{0 \ 2}^{2 \ 0} \left[ \alpha_t \beta_t \sqrt{\frac{\gamma}{\tilde{\gamma}}} \middle| \begin{matrix} \cdot \\ \frac{\alpha_t - \beta_t}{2}, \frac{\beta_t - \alpha_t}{2} \end{matrix} \right] d\gamma \quad (\text{E.7})$$

Now, with the help of [94, eq. (2.24.1.1)], the closed-form equation of (E.7) can be written as follows

$$\mathcal{J}_2 = \frac{(\alpha_t \beta_t)^{\frac{(\alpha_t + \beta_t)}{2}}}{4\pi\Gamma(\alpha_t)\Gamma(\beta_t)(\tilde{\gamma})^{\frac{(\alpha_t + \beta_t)}{4}}} G_{2 \ 6}^{6 \ 1} \left[ \frac{(\alpha_t \beta_t)^2}{16\tilde{\gamma}} \middle| \begin{matrix} -\frac{\alpha_t + \beta_t}{4}, 1 - \frac{\alpha_t + \beta_t}{4} \\ P, -\frac{\alpha_t + \beta_t}{4}, -\frac{\alpha_t + \beta_t}{4} \end{matrix} \right] \quad (\text{E.8})$$

where,  $P \in \left\{ \frac{(\alpha_t - \beta_t)}{4}, \frac{(\alpha_t - \beta_t + 2)}{4}, \frac{(\beta_t - \alpha_t)}{4}, \frac{(\beta_t - \alpha_t + 2)}{4} \right\}$ .

# Appendix F

## Closed-form Expression for $\mathcal{P}_1$ and $\mathcal{P}_2$

Closed-form equation for  $\mathcal{P}_1$ : we have,

$$\mathcal{P}_1 = \frac{\mathcal{A}}{8} \sum_{k_t=1}^{\beta_t} \frac{a_k}{(\tilde{\gamma})^{\frac{\alpha_t+k_t}{4}}} \int_0^{\gamma_{th}} (\gamma)^{\frac{\alpha_t+k_t}{4}-1} \operatorname{erfc} \left( \sqrt{\frac{\gamma}{2}} \right) G_{0 \ 2}^{2 \ 0} \left[ \frac{\mathcal{B}^2 \alpha_t \beta_t}{4} \sqrt{\frac{\gamma}{\tilde{\gamma}}} \middle| \frac{\alpha_t-k_t}{2}, \frac{k_t-\alpha_t}{2} \right] d\gamma \quad (\text{F.1})$$

Using the link between  $\operatorname{erfc}(\cdot)$  and  $\exp(\cdot)$ , can be written with the following equation as [124]

$$\operatorname{erfc} \left( \sqrt{\frac{\gamma}{2}} \right) \approx \frac{1}{6} \exp \left( -\frac{\gamma}{2} \right) + \frac{1}{2} \exp \left( -\frac{2\gamma}{3} \right), \gamma > 0 \quad (\text{F.2})$$

Next, with the help of [95, Eq.(1.211.1)] the exponential term of the above equation can be represented as



$$\begin{aligned}\frac{1}{6} \exp\left(-\frac{\gamma}{2}\right) &= \frac{1}{6} \sum_{m=0}^{\infty} (-1)^m \frac{\gamma^m}{(2)^m (m!)} \\ \frac{1}{2} \exp\left(-\frac{2\gamma}{3}\right) &= \frac{1}{2} \sum_{m=0}^{\infty} (-1)^m \frac{\gamma^m}{(m!)} \left(\frac{2}{3}\right)^m\end{aligned}$$

Next, by plugin (F.2) in (F.1), we can derived  $\mathcal{P}_1$  in the form of  $\mathcal{P}_1 = \mathcal{P}_1^{(1)} + \mathcal{P}_1^{(2)}$ , and  $\mathcal{P}_1^{(1)}$ ,  $\mathcal{P}_1^{(2)}$  can be expressed as follows

$$\mathcal{P}_1^{(1)} = \frac{\mathcal{A}}{48} \sum_{k_t=1}^{\beta_t} \frac{a_k}{(\bar{\gamma})^{\frac{\alpha_t+k_t}{4}}} \int_0^{\gamma_{th}} (\gamma)^{\frac{\alpha_t+k_t}{4}-1} \exp\left(-\frac{\gamma}{2}\right) G_{0\ 2}^{2\ 0} \left[ \frac{\mathcal{B}^2 \alpha_t \beta_t}{4} \sqrt{\frac{\gamma}{\bar{\gamma}}} \middle| \frac{\alpha_t-k_t}{2}, \frac{k_t-\alpha_t}{2} \right] d\gamma \quad (\text{F.3})$$

and,

$$\mathcal{P}_1^{(2)} = \frac{\mathcal{A}}{16} \sum_{k_t=1}^{\beta_t} \frac{a_k}{(\bar{\gamma})^{\frac{\alpha_t+k_t}{4}}} \int_0^{\gamma_{th}} (\gamma)^{\frac{\alpha_t+k_t}{4}-1} \exp\left(-\frac{2\gamma}{3}\right) G_{0\ 2}^{2\ 0} \left[ \frac{\mathcal{B}^2 \alpha_t \beta_t}{4} \sqrt{\frac{\gamma}{\bar{\gamma}}} \middle| \frac{\alpha_t-k_t}{2}, \frac{k_t-\alpha_t}{2} \right] d\gamma \quad (\text{F.4})$$

Now, using the relation between power series with  $\exp(\cdot)$ , and with the help of [96, eq. (26)], the closed-form of  $\mathcal{P}_1^{(1)}$  and  $\mathcal{P}_1^{(2)}$  can presented as

$$\begin{aligned}\mathcal{P}_1^{(1)} &= \frac{\mathcal{A}}{24} \sum_{k_t=1}^{\beta_t} \frac{a_k}{(\bar{\gamma})^{\frac{\alpha_t+k_t}{4}}} \sum_{m=0}^{\infty} \frac{(-1)^m}{(2)^m (m!)} (\sqrt{\gamma_{th}})^{\frac{\alpha_t+k_t}{4}+2m} \times \\ &\quad G_{1\ 3}^{2\ 1} \left[ \frac{\mathcal{B}^2 \alpha_t \beta_t}{4} \sqrt{\frac{\gamma_{th}}{\bar{\gamma}}} \middle| \frac{\alpha_t-k_t}{2}, \frac{k_t-\alpha_t}{2}, -2m-\frac{\alpha_t+k_t}{2} \right]\end{aligned} \quad (\text{F.5})$$

and,

$$\mathcal{P}_1^{(1)} = \frac{\mathcal{A}}{8} \sum_{k_t=1}^{\beta_t} \frac{a_k}{(\tilde{\gamma})^{\frac{\alpha_t+k_t}{4}}} \sum_{m=0}^{\infty} \frac{(-1)^m (2)^m}{(3)^m (m!)} (\sqrt{\gamma th})^{\frac{\alpha_t+k_t}{4}+2m} \times \quad (\text{F.6})$$

$$G_{1 \ 3}^{2 \ 1} \left[ \frac{\mathcal{B}^2 \alpha_t \beta_t}{4} \sqrt{\frac{\gamma th}{\tilde{\gamma}}} \middle| \begin{matrix} 1-2m-\frac{\alpha_t+k_t}{2} \\ \frac{\alpha_t-k_t}{2}, \frac{k_t-\alpha_t}{2}, -2m-\frac{\alpha_t+k_t}{2} \end{matrix} \right]$$

**Closed-form equation for  $\mathcal{P}_1$ :** we have,

$$\mathcal{P}_2 = \frac{\mathcal{A}}{8} \sum_{k_t=1}^{\beta_t} \frac{a_k}{(\tilde{\gamma})^{\frac{\alpha_t+k_t}{4}}} \int_0^{\infty} (\gamma)^{\frac{\alpha_t+k_t}{4}-1} \text{erfc} \left( \sqrt{\frac{\gamma}{2}} \right) G_{0 \ 2}^{2 \ 0} \left[ \frac{\mathcal{B}^2 \alpha_t \beta_t}{4} \sqrt{\frac{\gamma}{\tilde{\gamma}}} \middle| \begin{matrix} \cdot \\ \frac{\alpha_t-k_t}{2}, \frac{k_t-\alpha_t}{2} \end{matrix} \right] d\gamma \quad (\text{F.7})$$

We have the relationship between  $\text{erfc}(\cdot)$  and  $G[\cdot]$  as [94, eq. (8.4.14.2)]

$$\text{erfc} \left( \sqrt{\frac{\gamma}{2}} \right) = \frac{1}{\sqrt{\pi}} G_{1 \ 2}^{2 \ 0} \left[ \frac{\gamma}{2} \middle| \begin{matrix} 1 \\ 0, \frac{1}{2} \end{matrix} \right] \quad (\text{F.8})$$

Plugin (F.8) in (F.7), can be written the following equation as

$$\mathcal{P}_2 = \frac{\mathcal{A}}{8\sqrt{\pi}} \sum_{k_t=1}^{\beta_t} \frac{a_k}{(\tilde{\gamma})^{\frac{\alpha_t+k_t}{4}}} \int_0^{\infty} (\gamma)^{\frac{\alpha_t+k_t}{4}-1} G_{1 \ 2}^{2 \ 0} \left[ \frac{\gamma}{2} \middle| \begin{matrix} 1 \\ 0, \frac{1}{2} \end{matrix} \right] G_{0 \ 2}^{2 \ 0} \left[ \frac{\mathcal{B}^2 \alpha_t \beta_t}{4} \sqrt{\frac{\gamma}{\tilde{\gamma}}} \middle| \begin{matrix} \cdot \\ \frac{\alpha_t-k_t}{2}, \frac{k_t-\alpha_t}{2} \end{matrix} \right] d\gamma \quad (\text{F.9})$$

Now, with the help of [94, eq. (2.24.1.1)], the closed-form equation of the above equation as follows

$$\mathcal{P}_2 = \frac{\mathcal{A}}{16\pi\sqrt{\pi}} \sum_{k_t=1}^{\beta_t} \frac{a_k}{(\tilde{\gamma})^{\frac{\alpha_t+k_t}{4}}} \left(\frac{1}{2}\right)^{-\frac{\alpha_t+k_t}{4}} G_{2\ 5}^{4\ 2} \left[ \frac{\mathcal{B}^4 \alpha_t^2 \beta_t^2}{128\tilde{\gamma}} \middle| \begin{matrix} 1-\frac{\alpha_t+k_t}{4}, \frac{1}{2}-\frac{\alpha_t+k_t}{4} \\ \frac{\alpha_t-k_t}{4}, \frac{\alpha_t-k_t+2}{4}, \frac{k_t-\alpha_t}{4}, \frac{k_t-\alpha_t+2}{4}, -\frac{\alpha_t+k_t}{4} \end{matrix} \right]$$

(F.10)

## Appendix G

# MATLAB Code for Monte Carlo simulation of a turbulent channel

**Turbulent Channel simulation for Gamma-Gamma fading:**

```
clear all; close all; clc;
numbits = 104;
alpha = any numerical value;
beta = any numerical value;
X = gamrnd(alpha, 1/alpha, 1, numbits);
Y = gamrnd(beta, 1/beta, 1, numbits);
H = abs(X.*Y);
```

**Turbulent Channel simulation for Málaga fading:**

```
clear all; close all; clc;
numbits = 104;
alpha = any numerical value;
beta = any numerical value [integer only];
b0 = 0.6525;
rho = 0.988;
Omega = 0.4618;
phiAB = pi/2;
phiA = pi + 2*pi.*rand(1,numbits);
phiB = phiA-phiAB;
X = gamrnd(alpha,1/alpha,1,numbits);
G = gamrnd(beta,1/beta,1,numbits);
UsD = raylrnd(1/sqrt(2),1,numbits);
Rs = sqrt(G).* sqrt(Omega)*exp(1i*phiA)+sqrt(rho*2*b0)*exp(1i*phiB))+sqrt(1-
rho)*UsD;
H =(abs(Rs.2)).*X;
```

# Bibliography

- [1] S. Bloom, E. Korevaar, J. Schuster, and H. Willebrand, “Understanding the performance of free-space optics,” *Journal of optical networking*, vol. 2, no. 6, pp. 178–200, Jun. 2003.
- [2] A. K. Majumdar, “Chapter 4 - fundamentals of free-space optical communications systems, optical channels, characterization, and network/access technology,” in *Optical Wireless Communications for Broadband Global Internet Connectivity*. Elsevier, 2019, pp. 55–116. [Online]. Available: <https://www.sciencedirect.com/science/article/pii/B9780128133651000047>
- [3] E. Soleimani-Nasab and Z. Ghassemlooy, “Multihop radio and optical wireless relaying systems over EGK, DGG, and CU fading channels,” *Journal of Optical Communications and Networking*, vol. 14, no. 5, pp. 426–438, May 2022.
- [4] H. Kaushal and G. Kaddoum, “Optical communication in space: Challenges and mitigation techniques,” *IEEE Communications Surveys Tutorials*, vol. 19, no. 1, pp. 57–96, Aug. 2017.
- [5] H. Manor and S. Arnon, “Performance of an optical wireless communication system as a function of wavelength,” in *The 22nd Convention on Electrical and Electronics Engineers in Israel, 2002.*, Tel-Aviv, Israel, Israel , Feb. 2003, pp. 4285–4294.

- 
- [6] J. Singh and N. Kumar, "Performance analysis of different modulation format on free space optical communication system," *Elsevier Optik Optics*, vol. 124, no. 120, pp. 4651–4654, Oct. 2013.
- [7] A. Mansour, R. Mesleh, and M. Abaza, "New challenges in wireless and free space optical communications," *Optics and Lasers in Engineering*, vol. 89, pp. 95–108, Feb. 2017.
- [8] P. Kaur, V. K. Jain, and S. Kar, "Performance Analysis of FSO Array Receivers in Presence of Atmospheric Turbulence," *IEEE Photon. Technol. Lett.*, vol. 26, no. 12, pp. 1165–1168, Jun. 2014.
- [9] E. Wainright, H. H. Refai, and J. James J. Sluss, "Wavelength diversity in free-space optics to alleviate fog effects," *Proceedings of SPIE*, vol. 5712, pp. 110–118, Apr. 2005.
- [10] M. Mushtaq, S. Yasir, M. Khan, A. Wahid, and M. Iqbal, "Analysis of internal design parameters to minimize geometrical losses in free-space optical communication link," in *Special Issue of the 7th International Advances in Applied Physics and Materials Science (APMAS 2017)*, Mugla, Turkey, Apr. 2017, pp. 275–277.
- [11] W. R. Leeb, "Degradation of signal to noise ratio in optical free space data links due to background illumination," *Appl. Opt.*, vol. 28, no. 15, pp. 3443–3449, Apr. 1989.
- [12] Z. Sodnik, B. Furch, and H. Lutz, "Free-space laser communication activities in europe: Silex and beyond," in *LEOS 2006 - 19th Annual Meeting of the IEEE Lasers and Electro-Optics Society*, Montreal, Que., Canada, Oct. 2006, pp. 78–79.
- [13] Elizabeth Landau, "OPALS: Light Beams Let Data Rates Soar," Last Accessed on 08/07/2020. [Online]. Available: [https://www.nasa.gov/mission\\_pages/station/research/news/opals\\_data\\_rates\\_soar](https://www.nasa.gov/mission_pages/station/research/news/opals_data_rates_soar)

- 
- [14] Andrew Williams , “Free-space Optics Beginning to Achieve Real-World Value,” Last Accessed on 08/07/2022. [Online]. Available: <https://spie.org/news/free-space-optics-beginning-to-achieve-real-world-value?SSO=1>
- [15] A. K. Majumdar, *Advanced Free Space Optics (FSO): A Systems Approach*. New York, USA: Springer Series in Optical Sciences, 2015, vol. 186.
- [16] X. Zhu and J. M. Kahn, “Free-space optical communication through atmospheric turbulence channels,” *IEEE Trans. Commun.*, vol. 50, no. 8, pp. 1293–1300, Aug. 2002.
- [17] ———, “Performance bounds for coded free-space optical communication through atmospheric turbulence channels,” *IEEE Trans. Commun.*, vol. 51, no. 8, pp. 1233–1239, Aug. 2003.
- [18] X. Zhu and J. Kahn, “Pairwise codeword error probability for coded free-space optical communication through atmospheric turbulence channels,” in *ICC 2001. IEEE International Conference on Communications. Conference Record (Cat. No.01CH37240)*, Helsinki, Finland, Finland , Jun. 2001, pp. 161 – 164.
- [19] D. A. Luong and A. T. Pham, “Average capacity of mimo free-space optical gamma-gamma fading channel,” in *2014 IEEE International Conference on Communications (ICC)*, Sydney, NSW, Australia , Aug. 2014, pp. 3354–3358.
- [20] M. Uysal, ing(Tiffany)L, and M. Yu, “Error rate performance analysis of coded free-space optical links over gamma-gamma atmospheric turbulence channels,” *IEEE Trans. Wireless Commun.*, vol. 5, no. 6, pp. 1229–1233, Jun. 2006.
- [21] K. P. Peppas and C. K. Datsikas, “Average symbol error probability of general-order rectangular quadrature amplitude modulation of optical wireless communication systems over atmospheric turbulence channels,” *J. OPT. COMMUN. NETW.*, vol. 2, no. 2, pp. 102–110, Feb. 2010.



- [22] P. J. Awrejcewicz, *Numerical Simulations of Physical and Engineering Processes*. InTech, 2011.
- [23] A. Jurado-Navas, J. M. Garrido-Balsells, J. F. Paris, M. Castillo-Vázquez, and A. Puerta-Notario, “Further insights on Málaga distribution for atmospheric optical communications,” in *2012 International Workshop on Optical Wireless Communications (IWOW)*, Pisa, Italy, Nov. 2012, pp. 1–3.
- [24] A. A. Farid and S. Hranilovic, “Outage capacity optimization for free-space optical links with pointing errors,” *J. Lightw. Technol.*, vol. 25, no. 7, pp. 1702–1710, Jul. 2007.
- [25] —, “Outage Capacity for MISO Intensity-Modulated Free-Space Optical Links With Misalignment,” *J. Opt. Commun. Netw.*, vol. 3, no. 10, pp. 780–789, Oct. 2011.
- [26] G. T. Djordjevic, M. I. Petkovic, M. Spasic, and D. S. Antic, “Outage capacity of FSO link with pointing errors and link blockage,” *Optics Express*, vol. 24, no. 1, pp. 219–230, Jan. 2016.
- [27] A. Jurado-Navas, J. M. Garrido-Balsells, J. F. Paris, M. Castillo-Vázquez, and A. Puerta-Notario, “Impact of pointing errors on the performance of generalized atmospheric optical channels,” *Optics Express*, vol. 20, no. 11, pp. 2730–2742, May 2012.
- [28] I. S. Ansari, F. Yilmaz, and M.-S. Alouini, “Performance Analysis of Free-Space Optical Links Over Malaga Turbulence Channels With Pointing Errors,” *IEEE Trans. Wireless Commun.*, vol. 15, no. 1, pp. 91–102, Jan. 2016.
- [29] J. M. Garrido-Balsells, A. Jurado-Navas, J. F. Paris, M. Castillo-Vázquez, and A. Puerta-Notario, “Novel formulation of the  $\mu$  model through the Generalized-K distribution for atmospheric optical channels,” *Optics Express*, vol. 23, no. 5, pp. 6345–6358, Mar. 2015.

- 
- [30] Antonio Gracia-Zambrana and Carmen Castillo-Vazquez and Beatriz Castillo-Vazquez, “On the Capacity of FSO Links over Gamma-Gamma Atmospheric Turbulence Channels Using OOK Signaling,” *EURASIP Journal on Wireless Communications and Networking*, vol. 2010, no. 127657, pp. 1–9, Mar. 2010.
- [31] S. M. Alamouti, “A Simple Transmit Diversity Technique for Wireless Communications,” *IEEE J. Sel. Areas Commun.*, vol. 16, no. 8, pp. 1451–1458, Oct. 1998.
- [32] M. K. Simon and V. A. Vilmrotter, “Alamouti-Type Space–Time Coding for Free-Space Optical Communication With Direct Detection,” *IEEE Trans. Wireless Commun.*, vol. 4, no. 1, pp. 35–39, Jan. 2005.
- [33] E. Bayaki and R. Schober, “On Space–Time Coding for Free–Space Optical Systems,” *IEEE Trans. Commun.*, vol. 58, no. 1, pp. 58–62, Jan. 2010.
- [34] —, “Performance and Design of Coherent and Differential Space-Time Coded FSO Systems,” *J. Lightw. Technol.*, vol. 30, no. 11, pp. 1569–1577, Jun. 2012.
- [35] C. Abou-Rjeily and W. Fawaz, “Space-Time Codes for MIMO Ultra-Wideband Communications and MIMO Free-Space Optical Communications with PPM,” *IEEE J. Sel. Areas Commun.*, vol. 26, no. 6, pp. 938–947, Aug. 2008.
- [36] A. García-Zambrana, C. Castillo-Vázquez, B. Castillo-Vázquez, and A. Hiniesta-Gómez, “Selection Transmit Diversity for FSO Links Over Strong Atmospheric Turbulence Channels,” *IEEE Photon. Technol. Lett.*, vol. 21, no. 14, pp. 1017–1019, Jul. 2009.
- [37] M. R. Abaza, R. Mesleh, A. Mansour, and E.-H. M. Aggoune, “Diversity techniques for a free-space optical communication system in correlated log-normal channels,” *Optical Engineering*, vol. 53, no. 1, pp. 1–7, Jan. 2014.

- [38] Z. Hajjarian and J. Fadlullah, "MIMO Free Space Optical Communications in Turbid and Turbulent Atmosphere (Invited Paper)," *JOURNAL OF COMMUNICATIONS*, vol. 4, no. 8, pp. 524–532, Sep. 2009.
- [39] J. Zhang, L. Dai, Y. Han, Y. Zhang, and Z. Wang, "On the Ergodic Capacity of MIMO Free-Space Optical Systems Over Turbulence Channels," *IEEE J. Sel. Areas Commun.*, vol. 33, no. 9, pp. 1925–1934, Sep. 2015.
- [40] E. Bayaki, R. Schober, and R. K. Mallik, "Performance Analysis of MIMO Free-Space Optical Systems in Gamma-Gamma Fading," *IEEE Trans. Commun.*, vol. 57, no. 11, pp. 3415–3424, Nov. 2009.
- [41] T. A. Tsiftsis, H. G. Sandalidis, and G. K. Karagiannidis, "Optical Wireless Links with Spatial Diversity over Strong Atmospheric Turbulence Channels," *IEEE Trans. Wireless Commun.*, vol. 8, no. 2, pp. 951–956, Feb. 2009.
- [42] R. Tian-Peng, C. Yuen, Y. L. Guan, and T. Ge-Shi, "High-Order Intensity Modulations for OSTBC in Free-Space Optical MIMO Communications," *IEEE Wireless Commun. Lett.*, vol. 2, no. 6, pp. 607–610, Dec. 2013.
- [43] W. Gappmair, "Further results on the capacity of free-space optical channels in turbulent atmosphere," *IET Communications*, vol. 5, no. 9, pp. 1262–1367, Jul. 2011.
- [44] M. R. Bhatnagar and Z. Ghassemlooy, "Performance Analysis of Gamma-Gamma Fading FSO MIMO Links With Pointing Errors," *J. Lightw. Technol.*, vol. 34, no. 9, pp. 2158–2169, May. 2016.
- [45] Milica I. Petkovic and Nemanja M. Zdravkovic and Goran T. Dordevic, "Outage performance of switch-and-examine combining receiver over FSO Gamma-Gamma atmospheric turbulence with pointing errors," in *2014 22<sup>nd</sup> Telecommunications Forum Telfor (TELFOR)*, Belgrade, Serbia, Feb. 2015, pp. 383–386.

- [46] H. G. Sandalidis, T. A. Tsiftsis, and G. K. Karagiannidis, "Optical Wireless Communications With Heterodyne Detection Over Turbulence Channels With Pointing Errors," *J. Lightw. Technol.*, vol. 27, no. 20, pp. 4440–4445, Oct. 2015.
- [47] R. Mesleh, H. Haas, C. W. Ahn, and S. Yun, "Spatial modulation - a new low complexity spectral efficiency enhancing technique," in *2006 First International Conference on Communications and Networking in China*, Beijing, China, Apr. 2007.
- [48] M. Abaza, R. Mesleh, A. Mansour, and E.-H. M. Aggoune, "The performance of space shift keying for free-space optical communications over turbulent channels," in *Broadband Access Communication Technologies IX*, San Francisco, California, United States, Feb. 2015, pp. 184–191.
- [49] A. Salehiomran and J. A. Salehi, "Spatial Heterodyning Optical Code Division Multiple Access Technique for Near-Field Free-Space Optical Communication Systems," *J. Opt. Commun. Netw.*, vol. 1, no. 5, pp. 498–511, Oct. 2009.
- [50] T. Fath and H. Haas, "Performance Comparison of MIMO Techniques for Optical Wireless Communications in Indoor Environments," *IEEE Trans. Commun.*, vol. 61, no. 2, pp. 733–742, Feb. 2013.
- [51] R. Mesleh, H. Elgala, and H. Haas, "Optical Spatial Modulation," *J. Opt. Commun. Netw.*, vol. 3, no. 3, pp. 234–244, Mar. 2011.
- [52] G. Keiser, *Optical fiber communications*. Tata Mc Graw Hill, 2013.
- [53] I. I. Kim and E. J. Korevaar, "Availability of free-space optics (fso) and hybrid fso/rf systems," in *Optical Wireless Communications IV*, Denver, CO, United States, Nov. 2001, pp. 84 – 95.
- [54] I. I. Kim, R. Stieger, J. Koontz, C. Moursund, M. Barclay, P. Adhikari, J. J. Schuster, E. J. Korevaar, R. Ruigrok, and C. M. DeCusatis, "Wireless optical

- transmission of fast ethernet, FDDI, ATM, and ESCON protocol data using the TerraLink laser communication system,” *Optical Engineering*, vol. 37, no. 12, pp. 3143 – 3155, Dec. 1998.
- [55] P. Kaur, V. K. Jain, and S. Kar, “Ber performance improvement of fso links with aperture averaging and receiver diversity technique under various atmospheric conditions,” in *2014 9th International Conference on Industrial and Information Systems (ICIIS)*, Gwalior, India , Dec. 2014, pp. 1–6.
- [56] A. Viswanath, V. K. Jain, and S. Kar, “Aperture averaging and receiver diversity for FSO downlink in presence of atmospheric turbulence and weather conditions for OOK, M-PPM and M-DPPM schemes,” *Optical and Quantum Electronics*, vol. 48, no. 9, pp. 1 – 20, Aug. 2016.
- [57] P. Nicolas and F. Daniel, “Aperture averaging: theory and measurements,” *Free-Space Laser Communication Technologies XVI*, vol. 5338, pp. 233–242, Jun. 2004.
- [58] M.-A. Khalighi, N. Schwartz, N. Aitamer, and S. Bourennane, “Fading Reduction by Aperture Averaging and Spatial Diversity in Optical Wireless Systems,” *J. Opt. Commun. Netw.*, vol. 1, no. 6, pp. 580 – 593, Nov. 2009.
- [59] P. K. Sharma, A. Bansal, P. Garg, T. Tsiftsis, and R. Barrios, “Relayed fso communication with aperture averaging receivers and misalignment errors,” *IET Communications*, vol. 11, pp. 45–52(7), Jan. 2017.
- [60] F. S. Vetelino, C. Young, L. Andrews, and J. Reclons, “Aperture averaging effects on the probability density of irradiance fluctuations in moderate-to-strong turbulence ,” *Appl. Opt.*, vol. 46, no. 11, pp. 2099–2108, Apr. 2007.
- [61] Jack L. Green, Bryan W. Welch, and Robert M. Manning, “Optical Communication Link Atmospheric Attenuation Model,” Last Accessed on 20/07/2022. [Online]. Available: <https://ntrs.nasa.gov/search.jsp?R=201900010122020-07-20T02:05:49+00:00Z>

- [62] D. Killinger, “Free Space Optics for Laser Communication Through the Air,” *Opt. Photon. News*, vol. 10, no. 13, pp. 36 – 42, Oct. 2002.
- [63] S. A. Fares and F. Adachi, *Mobile and Wireless Communications Network Layer and Circuit Level Design*. InTech, 2010.
- [64] M. C. A. Naboulsi, H. Sizun, and F. de Fornel, “Fog attenuation prediction for optical and infrared waves,” *Optical Engineering*, vol. 43, no. 2, pp. 319 – 329, Feb. 2004.
- [65] I. I. Kim, J. Koontz, H. Hakakha, P. Adhikari, R. Stieger, C. Moursund, M. Barclay, A. Stanford, R. Ruigrok, J. J. Schuster, and E. J. Korevaar, “Measurement of scintillation and link margin for the terralink laser communication system,” in *Wireless Technologies and Systems: Millimeter-Wave and Optical*, Dallas, TX, United States , Jan. 1998, pp. 100 – 118.
- [66] Z. Jia, Q. Zhu, and F. Ao, “Atmospheric attenuation analysis in the fso link,” in *2006 International Conference on Communication Technology*, Guilin, China , Nov. 2006, pp. 1–4.
- [67] J. R. Meyer-Arendt and C. B. Emmanuel, *OPTICAL SCINTILLATION; A SURVEY OF THE LITERATURE*. NATIONAL BUREAU OF STANDARDS, U.S. Government Printing Office, 1965.
- [68] M. Abtahi, P. Lemieux, W. Mathlouthi, and L. A. Rusch, “Suppression of Turbulence-Induced Scintillation in Free-Space Optical Communication Systems Using Saturated Optical Amplifiers,” *J. Lightw. Technol.*, vol. 24, no. 12, pp. 4966 – 4973, Dec. 2006.
- [69] O. J. Famoriji, A. Fadamiro, and F. Lin, “Impact study of turbulence-induced scintillation on fso link design,” in *2017 IEEE International Conference on Microwaves, Antennas, Communications and Electronic Systems (COMCAS)*, Tel-Aviv, Israel , Nov. 2017, pp. 1 – 4.

- 
- [70] C. Y. Y. Larry C. Andrews, Ronald L. Phillips, *Laser Beam Scintillation with Applications*. SPIE, 2001.
- [71] I. I. Kim, M. Mitchell, and E. J. Korevaar, “Measurement of scintillation for free-space laser communication at 785 nm and 1550 nm,” in *Optical Wireless Communications II*, Boston, MA, United States, Dec. 1999, pp. 49 – 62.
- [72] M. Uysal, J. T. Li, and M. Yu, “Error Rate Performance Analysis of Coded Free-Space Optical Links over Gamma-Gamma Atmospheric Turbulence Channels,” *IEEE Trans. Wireless Commun.*, vol. 5, no. 6, pp. 1229 – 1233, Jun. 2006.
- [73] D. Kedar and S. Arnon, “Optical wireless communication through fog in the presence of pointing errors,” *Appl. Opt.*, vol. 42, no. 24, pp. 4946–4954, Aug. 2003.
- [74] S. Arnon, “Effects of atmospheric turbulence and building sway on optical wireless-communication systems,” *Opt. Lett.*, vol. 28, no. 2, pp. 129 – 131, Jan. 2003.
- [75] D. K. Borah, D. Voelz, and S. Basu, “Maximum-likelihood estimation of a laser system pointing parameters by use of return photon counts,” *Appl. Opt.*, vol. 45, no. 11, pp. 2504–2509, Apr. 2006.
- [76] F. Yang, J. Cheng, and T. A. Tsiftsis, “Free-Space Optical Communication with Nonzero Boresight Pointing Errors,” *IEEE Trans. Commun.*, vol. 62, no. 2, pp. 713–725, Feb. 2014.
- [77] D. K. Borah and D. G. Voelz, “Estimation of laser beam pointing parameters in the presence of atmospheric turbulence,” *Appl. Opt.*, vol. 23, no. 46, pp. 6010–6018, Aug. 2007.
- [78] J. C. Ricklin and F. M. Davidson, “Atmospheric turbulence effects on a partially coherent Gaussian beam: implications for free-space laser communication,” *J. Opt. Soc. Am. A*, vol. 19, no. 9, pp. 1794–1802, Sep. 2002.

- [79] L. Yang, X. Gao, and M.-S. Alouini, "Performance Analysis of Free-Space Optical Communication Systems With Multiuser Diversity Over Atmospheric Turbulence Channels," *IEEE Photonics Journal*, vol. 6, no. 2, pp. 1–17, Apr. 2014.
- [80] H. E. Nistazakis, E. A. Karagianni, A. D. Tsigopoulos, M. E. Fafalios, and G. S. Tombras, "Average Capacity of Optical Wireless Communication Systems Over Atmospheric Turbulence Channels," *J. Lightw. Technol.*, vol. 27, no. 8, pp. 974–979, Apr. 2009.
- [81] H. Nistazakis, G. Tombras, A. Tsigopoulos, E. Karagianni, and M. Fafalios, "Average capacity of wireless optical communication systems over gamma gamma atmospheric turbulence channels," in *2008 IEEE MTT-S International Microwave Symposium Digest*, Atlanta, GA, USA, USA, Sep. 2008, pp. 1561 – 1564.
- [82] M. A. Kashani and M. Uysal, "Outage Performance and Diversity Gain Analysis of Free-Space Optical Multi-hop Parallel Relaying," *J. Opt. Commun. Netw.*, vol. 5, no. 8, pp. 901–909, Aug. 2013.
- [83] M. Elamassie and M. Uysal, "Incremental Diversity Order for Characterization of FSO Communication Systems Over Lognormal Fading Channels," *IEEE Commun. Lett.*, vol. 24, no. 4, pp. 825–829, Jan. 2020.
- [84] H. Moradi, M. Falahpour, H. H. Refai, P. G. LoPresti, and M. Atiquzzaman, "BER analysis of optical wireless signals through lognormal fading channels with perfect CSI," in *2010 17th International Conference on Telecommunications*, Doha, Qatar, Jun. 2010, pp. 493–497.
- [85] M. T. Dabiri and S. M. S. Sadough, "Performance analysis of all-optical amplify and forward relaying over log-normal FSO channels," *IEEE J. Opt. Commun. Netw.*, vol. 10, no. 2, pp. 79–89, Jan. 2018.



- [86] Z. Ghassemlooy, W. Popoola, and E. Leitgeb, "Free-space optical communication using subcarrier modulation in gamma-gamma atmospheric turbulence," in *2007 9th International Conference on Transparent Optical Networks*, Rome, Italy, Aug. 2007, pp. 156–160.
- [87] R. A. Saeed and E. B. Abbas, "Performance evaluation of mimo fso communication with gamma-gamma turbulence channel using diversity techniques," in *2018 International Conference on Computer, Control, Electrical, and Electronics Engineering (ICCCEEE)*, Khartoum, Sudan, Nov. 2018, pp. 1 – 5.
- [88] N. Cherif, I. Trigui, and S. Affes, "Dual-hop Málaga M FSO systems with pointing errors," in *2017 IEEE 28th Annual International Symposium on Personal, Indoor, and Mobile Radio Communications (PIMRC)*, Montreal, QC, Canada, Oct. 2017, pp. 1 – 5.
- [89] I. S. Ansari, M. M. Abdallah, M.-S. Alouini, and K. A. Qaraqe, "Outage analysis of asymmetric rf-fso systems," in *2016 IEEE 84th Vehicular Technology Conference (VTC-Fall)*, Montreal, QC, Canada, Sep. 2016, pp. 1 – 6.
- [90] G. Marsaglia and W. W. Tsang, "A simple method for generating gamma variables," *ACM Transactions on Mathematical Software*, vol. 26, no. 3, pp. 363–372, Sep. 2000.
- [91] D. Kundu and R. D. Gupta, "A convenient way of generating gamma random variables using generalized exponential distribution," *Computational Statistics & Data Analysis*, vol. 51, no. 6, pp. 2796–2802, Mar. 2007.
- [92] W. O. Popoola and Z. Ghassemlooy, "BPSK Subcarrier Intensity Modulated Free-Space Optical Communications in Atmospheric Turbulence," *J. Lightw. Technol.*, vol. 27, no. 8, pp. 967–973, Apr. 2009.
- [93] T. A. Tsiftsis, H. G. Sandalidis, G. K. Karagiannidis, and N. C. Sagias, "Multihop free-space optical communications over strong turbulence channels," in

- 2006 *IEEE International Conference on Communications*, Istanbul, Turkey , Dec. 2006, pp. 2755–2759.
- [94] A. P. Prudnikov, Y. A. Brychkov, and O. I. Marichev, *Integrals and Series Volume 3 : More Special Functions*. Gordon and Breach Science, 1990.
- [95] I. Gradshteyn and I. Ryzhik, *Table of Integrals, Series, and Products Seventh Edition*. Elsevier Academic Press, 2007.
- [96] V. S. Adamchik and O. I. Marichev, “The algorithm for calculating integrals of hypergeometric type functions and its realization in REDUCE system,” in *Proc. of the international symposium on Symbolic and algebraic computation*. Tokyo, Japan: ACM, Aug. 1990, pp. 212–224.
- [97] M. D. Renzo, F. Graziosi, and F. Santucci, “Channel Capacity Over Generalized Fading Channels: A Novel MGF-Based Approach for Performance Analysis and Design of Wireless Communication Systems,” *IEEE Trans. Veh. Technol.*, vol. 59, no. 1, pp. 127–149, Jan. 2010.
- [98] M. Khalighi and M. Uysal, “Survey on free space optical communication: A communication theory perspective,” *IEEE Commun. Surveys*, vol. 16, no. 4, pp. 2231—2258, Jun. 2014.
- [99] H. G. Sandalidis, T. A. Tsiftsis, and G. K. Karagiannidis, “Optical Wireless Communications With Heterodyne Detection Over Turbulence Channels With Pointing Errors,” *J. Lightw. Technol.*, vol. 27, no. 20, pp. 4440—4445, Oct. 2009.
- [100] M. Elamassie, S. M. Sait, and M. Uysal, “Finite-SNR Diversity Gain Analysis of FSO Systems over Gamma-Gamma Fading Channels With Pointing Errors,” *IEEE Commun. Lett.*, vol. 25, June 2021, doi: 10.1109/LCOMM.2021.3061775.

- 
- [101] J. A. Anguita, M. A. Neifeld, and B. V. Vasic, "Spatial correlation and irradiance statistics in a multiple-beam terrestrial free-space optical communication link," *Appl. Opt.*, vol. 46, no. 26, pp. 6561–6571, Sep. 2007.
- [102] J. Jeganathan, A. Ghrayeb, L. Szczecinski, and A. Ceron, "Space Shift Keying Modulation for MIMO Channels," *IEEE Trans. Wireless Commun.*, vol. 8, no. 7, pp. 3692–3703, Jul. 2009.
- [103] E. J. Lee and V. W. S. Chan, "Part 1: Optical Communication Over the Clear Turbulent Atmospheric Channel Using Diversity," *IEEE J. Sel. Areas Commun.*, vol. 22, no. 9, pp. 1896–1906, Nov. 2004.
- [104] S. M. Navidpou, M. Uysal, and M. Kavehrad, "BER Performance of Free-Space Optical Transmission with Spatial Diversity," *IEEE Trans. Wireless Commun.*, vol. 6, no. 8, pp. 2813–2819, Aug. 2007.
- [105] Y. Fu, J. Ma, S. Yu, and L. Tan, "BER performance analysis of coherent SIMO FSO systems over correlated non-Kolmogorov turbulence fading with nonzero boresight pointing errors," *IEEE Commun. Surveys*, vol. 430, pp. 31–38, Jan. 2019.
- [106] A. K. M. N. Islam and S. P. Majumder, "Performance analysis of an fso link in presence of pointing error using multiple pin photodetectors with equal gain combiner," in *2015 18th International Conference on Computer and Information Technology (ICCIT)*, Dhaka, Bangladesh, Dec. 2015, pp. 341–346.
- [107] N. T. Dang, L. H. Nguyen, and H. T. T. Pham, "Performance of multi-hop m-ary ppm fso systems with simo links over strong atmospheric turbulence channel and pointing errors," in *2013 Third World Congress on Information and Communication Technologies (WICT 2013)*, Hanoi, Vietnam, Dec. 2013, pp. 121–126.

- 
- [108] H.-C. Yang and M.-S. Alouini, “Performance analysis of multibranch switched diversity systems,” *IEEE Trans. Commun.*, vol. 51, no. 5, pp. 782–794, May. 2003.
- [109] —, “Improving the Performance of Switched Diversity with Post-Examining Selection,” *IEEE Trans. Wireless Commun.*, vol. 5, no. 1, pp. 67–71, Jan. 2006.
- [110] M. K. Simon and M. S. Alouini, *Digital Communication over Fading Channels*, 2nd ed. New York, NY, USA: John Wiley & Sons, 2005.
- [111] B. B. Barrow, “Diversity combination of fading signals with unequal mean strengths,” *IEEE Trans. Commun. Syst.*, vol. CS-11, pp. 73–78, Mar. 1963.
- [112] M. Schwartz, W. R. Bennett, and S. Stein, *Communication Systems and Techniques*. NY: McGraw-Hill, 1966.
- [113] A. Das, B. Bag, C. Bose, and A. Chandra, “Performance analysis of MIMO FSO link with Alamouti coding and switch-and-examine combining,” *Photonic Network Communications*, vol. 36, no. 3, pp. 350–360, Aug. 2018.
- [114] —, “Free space optical links over Málaga turbulence channels with transmit and receive diversity,” *Optics Communications*, vol. 456, Feb. 2020.
- [115] Wolfram Research, “Meijer-G Hypergeometric Functions: Integrals for classical integral transforms,” <http://functions.wolfram.com/07.34.21.0085.01>.
- [116] M. Abazaa, R. Mesleha, A. Mansourb, and M. Aggoune, “The performance of space shift keying for free-space optical communications over turbulent channels,” in *Proc. SPIEe*, vol. 9387 93870 V, Feb. 2015.
- [117] J. Jeganathan, A. Ghayeb, and L. Szczecinski, “Spatial Modulation: Optimal Detection and Performance Analysis,” *IEEE Communications Letters*, vol. 12, no. 8, pp. 545–547, Aug. 2008.

- 
- [118] E. W. Ng and M. Geller, “A Table of Integrals of the Error Functions,” *J. Res. Natl. Inst. Stand. B*, vol. 37B, no. 1, pp. 1–20, Jan. 1969.
- [119] A. Ananth and M. D. Selvaraj, “Error Analysis of SSK With Euclidean Distance Based Selection Combining,” *IEEE Trans. Veh. Technol.*, vol. 67, Apr. 2018, doi: 10.1109/TVT.2017.2778753.
- [120] G. Casella and R. L. Berger, *Statistical Inference*, 2nd ed. Pacific Grove, CA, USA: Duxbury, 2002.
- [121] Wolfram Research, “Integrals for classical integral transforms,” Last Accessed on 12/07/2022. [Online]. Available: <http://functions.wolfram.com/07.34.06.0006.01>
- [122] I. Gradshteyn and I. Ryzhik, *Table of Integrals, Series, and Products Seventh Edition*. Elsevier Academic Press, 2007.
- [123] Wolfram Research, “Integrals for classical integral transforms,” Last Accessed on 12/07/2022. [Online]. Available: <http://functions.wolfram.com/07.34.21.0002.01>
- [124] M. Chiani, D. Dardari, and M. K. Simon, “New exponential bounds and approximations for the computation of error probability in fading channels,” *IEEE Transactions on Wireless Communications*, vol. 2, no. 4, pp. 840–845, Jul. 2003.
- [125] B. W. W. Jack L. Green and R. M. Manning, “Optical communication link atmospheric attenuation model,” *National Aeronautics and Space Administration*, Feb. 2019.
- [126] M. K. Simon and V. A. Vilnrotter, “Alamouti-type space-time coding for free-space optical communication with direct detection,” *IEEE Trans. Wireless Commun.*, vol. 4, no. 1, pp. 35–39, Jan. 2005.

- [127] M. A. Al-Habash, L. C. Andrews, and R. L. Phillips, "Mathematical model for the irradiance probability density function of a laser beam propagating through turbulent media," *Optical Engineering*, vol. 40, no. 5, pp. 1554–1562, Aug. 2001.
- [128] M. D. Renzo and H. Haas, "Space Shift Keying (SSK-) MIMO over Correlated Rician Fading Channels: Performance Analysis And a New Method for Transmit-Diversity," *IEEE Trans. Commun.*, vol. 59, no. 1, pp. 116–129, Jan. 2011.
- [129] I. S. Ansari, F. Yilmaz, and M. S. Alouini, "Impact of Pointing Errors on the Performance of Mixed RF/FSO Dual-Hop Transmission Systems," *IEEE Wireless Commun. Lett.*, vol. 2, no. 3, pp. 351–354, Jun. 2013.
- [130] J. Romba, Z. Sodnik, M. Reyes, A. Alonso, and A. Bird, "ESA's bidirectional space-to-ground laser communication experiments," *Proc. of SPIE*, vol. 5550, pp. 287–298, Oct. 2004.
- [131] H. Ivanov, E. Leitgeb, T. Plank, P. Bekhrad, and T. Mitsev, "Link budget optimization of free space optical systems in relation to the beam diverging angle," in *2015 13th International Conference on Telecommunications (ConTEL)*, Graz, Austria, Jul. 2015, pp. 1 – 5.
- [132] Z. Sodnik, H. Smit, M. Sans, I. Zayer, M. Lanucara, K.-J. Schulz, D. Giggenbach, P. Becker, R. Mata-Calvo, C. Fuchs, J. Widmer, F. Arnold, M. Mosberger, A. Alonso, and I. Montilla, "Results from a lunar laser communication experiment between nasa's ladee satellite and esa's optical ground station," in *International Conference on Space Optical Systems and Applications (ICSOS)*, Kobe, Japan, May 2014.
- [133] We Are Social and Hootsuite's, "Digital 2019: Global Internet Use Accelerates," Last Accessed on 29/06/2020. [Online]. Available: <https://wearesocial.com/blog/2019/01/digital-2019-global-internet-use-accelerates>

- 
- [134] University of Idaho., “Raindrops are Different Sizes,” Last Accessed on 05/07/2020. [Online]. Available: [https://www.usgs.gov/special-topic/water-science-school/science/raindrops-are-different-sizes?qt-science\\_center\\_objects=0#qt-science\\_center\\_objects](https://www.usgs.gov/special-topic/water-science-school/science/raindrops-are-different-sizes?qt-science_center_objects=0#qt-science_center_objects)
- [135] J.Allen Zak, “Drop Size Distributions and Related Properties of Fog for Five Locations Measured From Aircraft,” Last Accessed on 05/07/2020. [Online]. Available: <https://ntrs.nasa.gov/search.jsp?R=199400285592020-07-05T11:06:07+00:00Z>
- [136] I. Alimi, A. Shahpari, A. Sousa, R. Ferreira, P. Monteiro, and A. Teixeira, *Challenges and Opportunities of Optical Wireless Communication Technologies*. InTech, 2017.